ORNL/TM-12018

ornl

OAK RIDGE
NATIONAL
LABORATORY

MARTIN MARIETTA

Field Studies of Streamflow Generation Using Natural and Injected Tracers on Bickford and Walker Branch Watersheds

David Genereux
Harold Hemond
Patrick Mulholland

Environmental Sciences Division
Publication No. 3811

MANAGED BY
MARTIN MARIETTA ENERGY SYSTEMS, INC.
FOR THE UNITED STATES
DEPARTMENT OF ENERGY

ORNL/TM-12018

ENVIRONMENTAL SCIENCES DIVISION

FIELD STUDIES OF STREAMFLOW GENERATION USING NATURAL AND INJECTED TRACERS ON BICKFORD AND WALKER BRANCH WATERSHEDS

David Genereux[1], Harold Hemond[1], and Patrick Mulholland[2]

Environmental Sciences Division
Publication No. 3811

[1]Department of Civil Engineering, Building 48, Room 419, Massachusetts Institute of Technology, Cambridge, MA 02139
[2]Co-author on Chapters 3 and 4

Date Published: May 1992

Office of Health and Environmental Research
(Budget Activity KP 02 04 00 0)

Prepared by
OAK RIDGE NATIONAL LABORATORY
Oak Ridge, Tennessee 37831-6258
managed by
MARTIN MARIETTA ENERGY SYSTEMS, INC.
for the
U.S. DEPARTMENT OF ENERGY
under contract DE-AC05-84OR21400

Contents

Figures

Chapter 4

Appendix 1

Tables

Appendix 1

Acknowledgements

The early stages of the work at Bickford Watershed were funded by electric utilities: Empire State Electric Energy Research Corp., New England Power Service Co., and American Electric Power Service Co. The work at Bickford was also supported by the U.S. Geological Survey. The research at Walker Branch Watershed in Tennessee was supported by the National Science Foundation and the U.S. Department of Energy (DOE). The research was also sponsored by the Walker Branch Watershed Project, Environmental Sciences Division, Office of Health and Environmental Research, DOE.

Much of the field work at Bickford Watershed was made possible by the able-bodied assistance of two former MIT undergraduates (Aleks Franz and Jennifer Gauss) and former graduate student Monique Villars. At the Environmental Sciences Division (ESD), Oak Ridge National Laboratory, Amy Rosemond, Bonnie Lu, Amanda Hood, and Lisa Au provided enthusiastic help in the field. Jeff Riggs was a great help with electronic equipment (data loggers and pressure transducers) on Walker Branch, and Norm Farrow provided much help with subsurface sampling. Scott Gregory, Roger Clapp, Helga Van Miegroet, Tom Early, Linda Mann, Merilyn Gentry, Bob Luxmoore, Ranaye Dreier, and Dick Ketelle helped locate data of various kinds. Rich Norby and Tim Tschaplinski allowed the use of their gas chromatograph. I. Lauren Larsen offered much helpful advice on the use of the gamma counting equipment at ESD. Bonnie Lu analyzed several dozen Cl^- samples for this work

research. Major laboratory help at MIT was provided by Henry Spliethoff, who analyzed about 300 water samples on the ICP. The maps in this report were generated through the computer cartographic skills of Sidey Timmins, Rosemary Adams, and Kim Sneed at ESD. Major administrative support was provided by Shirley Lawson (ESD), and Tom Carlin and Vicki Murphy (both at the Parsons Lab). The insightful advice of Peter Eagleson and Phil Gschwend was greatly appreciated.

Abstract

GENEREUX, D., H. HEMOND, and P. MULHOLLAND. 1992. Field studies of streamflow generation using natural and injected tracers on Bickford and Walker Branch Watersheds. ORNL/TM-12018. Oak Ridge National Laboratory, Oak Ridge, Tennessee. 310 pp.

Field studies of streamflow generation were undertaken on two forested watersheds, the West Road subcatchment of Bickford Watershed in central Massachusetts and the West Fork of Walker Branch Watershed in eastern Tennessee. A major component of the research was development of a two-stage methodology for the use of naturally-occurring ^{222}Rn as a tracer. The first of the two stages was solving a mass-balance equation for ^{222}Rn around a stream reach of interest in order to calculate $[Rn]_q$, the ^{222}Rn content of the lateral inflow to the reach; a conservative tracer (chloride) and a volatile tracer (propane) were injected into the study stream to account for lateral inflow to, and ^{222}Rn volatilization from, the study reach. The second stage involved quantitative comparison of $[Rn]_q$ to the measured ^{222}Rn concentrations of different subsurface waters in order to assess how important these waters were in contributing lateral inflow to the stream reach. The method was first applied to a 34 m stream reach at Bickford during baseflow; results suggested that $\geq$70% of the lateral inflow could be considered "vadose zone water" (water which had been in a saturated zone for less than a few days), and the remainder "soil groundwater" or "saturated zone water" (which had a longer residence time in a soil saturated zone). The method was then applied to two stream reaches on the West Fork of Walker Branch over

a wide range of flow conditions; four springs were also investigated. It was found that springwater and inflow to the stream could be viewed as a mixture of water from three end members: the two defined at Bickford (vadose zone water and soil groundwater) and a third ("bedrock groundwater") to account for the movement of water through fractured dolomite bedrock. Calcium was used as a second naturally-occurring tracer to distinguish bedrock groundwater from the other two end members. The behavior indicated by the three-end-member mixing model (e.g., increased importance of the two soil end members with increasing flow, and the differences between the stream reaches and among some of the springs) were consistent with a wide variety of environmental observations, including temperature and flow variations at springs, water table responses, the general lack of saturated zones on hillslopes and even near the stream in some places, and the importance of water movement through bedrock.

Preface

The research reported here had two closely intertwined goals: explore the utility of naturally occurring ^{222}Rn as a tracer for streamflow generation, and describe (hopefully quantitatively) the processes important in streamflow generation at the two study sites, the West Road subcatchment of Bickford Watershed in central Massachusetts and the West Fork of Walker Branch Watershed in Oak Ridge, Tennessee.

The early stages of the work were done at Bickford. Appendix 1 gives the details of a new method for measuring ^{222}Rn in soil gas by liquid scintillation counting; this method was first applied at Bickford, and was used (with minor modification) at Walker Branch. Chapter 1 gives the background theory and mathematical derivations behind our method for use of ^{222}Rn as a streamflow generation tracer. Results from the application of this method at Bickford are also presented.

The bulk of the research, reported in chapters 2-4, was done on the West Fork of Walker Branch. The ^{222}Rn method used on the West Fork was the same as that used at Bickford, and involved injection of two artificial tracers (the conservative tracer Cl^- and the volatile tracer propane) into the study stream. Chapter 2 describes the use of propane in determining gas exchange rates for the stream. Chapter 3 gives the results of the Cl^- injections; this work was essentially chemical dilution stream gauging, and it demonstrated the spatial and temporal structure of streamflow generation on the West Fork, and helped identify the

controls on that structure. Chapter 4 describes the use of ^{222}Rn and a second naturally-occurring tracer, Ca, in formulating a three-end-member mixing model for streamflow generation on the West Fork.

CHAPTER 1

Naturally-Occurring Radon-222 as a Tracer for Streamflow Generation: Steady-State Methodology and Field Example

David Genereux and Harold Hemond

Published in Water Resources Research 26(12): 3065-3075, December 1990

Abstract

This paper presents a quantitative framework for the use of ^{222}Rn as a tracer for streamflow generation under conditions of steady streamflow. The methodology consists of two distinct parts, the first of which is the determination of $[Rn]_q$, the average ^{222}Rn content of the lateral inflow to a given stream reach. $[Rn]_q$ is determined by measuring the concentrations of ^{222}Rn and two injected tracers (one conservative, the other volatile) in the streamwater at the ends of the reach, and solving a mass balance equation for ^{222}Rn around the stream reach. The second part of the methodology involves using $[Rn]_q$ values to determine the sources of stream inflow (and, implicitly, the flowpaths important in streamflow generation). One means of accomplishing this, a simple "geographic-source" separation, is presented here. Both parts of the methodology were demonstrated with a field experiment at the Bickford watershed in central Massachusetts. The injected tracers were NaCl (conservative) and propane (volatile). The value of $[Rn]_q$ (700 dpm/L) was found to be closer to the ^{222}Rn content of vadose zone water (<500 dpm/L) than to that of saturated zone water (2000 dpm/L), suggesting that lateral unsaturated flow through the low-^{222}Rn environment of the vadose zone was important in supplying baseflow to the stream reach studied.

1. Introduction

Understanding hydrologic flowpaths and streamflow generation on forested watersheds has significance for a wide variety of water resource, contaminant transport, and biogeochemical issues. The past 25 years have seen publication of many studies aimed at elucidating the mechanisms by which water moves down hillslopes and into small streams [e.g., Weyman, 1973; Harr, 1977; Rodhe, 1981; Bonell et al., 1981; Mosely, 1979; Sklash et al., 1986]; the many mechanisms proposed as being potentially important include saturation overland flow, Hortonian overland flow, macropore flow, perched saturated flow, saturated flow at the base of the soil profile, and unsaturated flow. A wide range of methodologies has been developed for the field investigation of these streamflow generation mechanisms. Among the most important methodologies are those involving naturally-occurring tracers.

Tracer studies generally involve the separation of streamflow into two flow components, though other types of investigations have been reported (e.g., the use of mainly-anthropogenic tritium to calculate groundwater residence times; Dincer et al., 1970; Martinec et al., 1974; Maloszewski et al., 1983). Virtually all tracer studies have focused on stormflow, with the most common type of analysis being separation of a hydrograph into its "new" water (precipitation or snowmelt during the event of interest) and "old" water (water present on the watershed before the start of the storm, excluding snow and surface ice) components. Numerous studies have demonstrated the utility of stable hydrogen (deuterium, or D) and oxygen

(^{18}O) isotopes in old/new separations. D and ^{18}O are excellent tracers of water movement, largely because they are incorporated into water molecules (mainly $HD^{16}O$ and $H_2{}^{18}O$). Other tracers (such as tritium (^3H), Si, and various major ions) have been used for hydrograph separation. However, several studies have demonstrated that water of low ionic strength may rapidly acquire substantial amounts of Si and major ions from soil [e.g., Pilgrim et al., 1979; Mckeague and Cline, 1963], making old/new separation with these tracers problematic.

Though the stable isotope "old/new" tracers provide useful constraints in deciphering the mechanisms of streamflow generation, they have limitations. For example, as implied in the above discussion, old/new tracers are useful in the analysis of stormflow only. Furthermore, the criterion for use of D and ^{18}O is not met by every storm (D or ^{18}O may be used to separate a hydrograph into its old and new water components only if the difference in isotopic composition of the components is large relative to the sum of the analytical uncertainties associated with the isotopic analyses plus any isotopic variability which exists within the components). Indeed, it is unrealistic to expect that any one tracer or hydrometric methodology will provide all the answers to the important questions surrounding hydrologic flowpaths on forested watersheds. Streamflow generation processes may exhibit great variability in time and space, and field study of these processes is often complex and problematic. For these reasons, many researchers now recognize the importance of applying multiple field techniques in the study of streamflow generation.

In this paper, we suggest a means of using naturally occurring ^{222}Rn to elucidate the hydrologic flowpaths important in streamflow generation. Naturally-occurring ^{222}Rn has already seen limited application as a hydrologic tracer. Several authors [Rogers, 1958; Jacoby et al., 1979; Lee and Hollyday, 1987; Genereux, 1988] have used the ^{222}Rn content of streamwater to identify and (in some cases) quantify discrete spring inflows to streams. In this application, ^{222}Rn possesses a special capability that conservative tracers do not: ^{222}Rn could potentially be used to identify a seep even if the seep water did not have a higher ^{222}Rn content than the rest of the water feeding the stream. However, simple surveys of streamwater ^{222}Rn content ([Rn]) alone can not be used to infer the relative importance of hydrologic flowpaths responsible for distributed, non-point source stream inflows. Indeed, [Rn] measurements alone could fail to detect even a sizable seep. For example, if the volatilization rate over a particular stream reach is high, [Rn] could decrease over the reach even if the reach is receiving large groundwater inflows. This is because [Rn] is determined by the rates of both inflow and volatilization; strictly speaking, one must know one of these rates in order to draw any conclusions about the other ([Rn] measurements alone are not sufficient). Thus, a more general, quantitative framework for the use of ^{222}Rn is desirable, and possible.

The methodology described here extends the use of ^{222}Rn to providing information on flowpaths which generate distributed (non-point source) stream inflows, by capitalizing on the fact that water from the different "pools" contributing

to streamflow may differ in ^{222}Rn concentration. For example, vadose zone water may have a markedly different ^{222}Rn content than groundwater. In addition, streams may be fed by groundwaters of differing ^{222}Rn content (e.g., groundwater from saturated soil vs. that from fractures in the underlying bedrock). Differences in the ^{222}Rn content of subsurface waters arise from differences in ^{222}Rn emanation by porous media (e.g., bedrock vs. soil), and from differences in the degree of ventilation to the atmosphere (e.g., vadose-zone vs. saturated zone). The factors influencing the behavior of ^{222}Rn in the subsurface have been the subject of numerous investigations, among them Kraner et al. [1964], Clements and Wilkening [1974], Brutsaert et al. [1981], Kristiansson and Malmqvist [1982], Schery et al. [1984], Fukui [1985], Lanctot et al. [1985], and Hall et al. [1987]. What is important to the present discussion is that markedly different ^{222}Rn concentrations are expected, and found, in natural waters associated with different subsurface zones (especially those zones corresponding to unsaturated soils and saturated soils). Most importantly, these zones are involved in streamflow generation through different postulated subsurface pathways.

Our methodology consists of two distinct parts: solving a mass balance equation for ^{222}Rn around a given stream reach, in order to determine $[Rn]_q$, the average ^{222}Rn content of water feeding the reach from the adjacent hillslopes; and, subsequently, using $[Rn]_q$ to draw conclusions about hillslope hydrologic processes. The first part involves the steady injection of a conservative tracer and a volatile tracer into a small study stream. The conservative tracer allows determination of

the increase in streamflow over a given stream reach. Use of the volatile tracer allows determination of the amount of ^{222}Rn volatilizing from the stream (over the same reach). With this information, and knowledge of the ^{222}Rn content of the streamwater, one can calculate $[Rn]_q$.

The second part of the method involves extracting flowpath information from $[Rn]_q$. On some watersheds, it may be possible to use $[Rn]_q$ to separate the flow feeding a stream into components, in much the same way that ^{18}O is used to separate storm streamwater into its old and new water components. For example, if the water feeding a stream is a mixture of vadose-zone water with ^{222}Rn concentration $[Rn]_{vzw}$, and saturated-zone water with concentration $[Rn]_{szw}$, one may use a simple mixing calculation to separate $[Rn]_q$ into its $[Rn]_{vzw}$ and $[Rn]_{szw}$ components. This of course requires knowledge of $[Rn]_{vzw}$ and $[Rn]_{szw}$. If a third "pool" is important (e.g., groundwater from bedrock fractures, or overland flow during a storm), it is necessary to know the ^{222}Rn content of this third water; it is also necessary to have an additional equation (based on a different tracer or on hydrometric data), since introducing a third "pool" introduces a third unknown. The next section describes the methodology in greater detail (mathematical derivations and other supporting information are found in Appendixes A and B). Section 3 gives data from a field experiment at the Bickford Reservoir watershed in central Massachusetts.

2. Use of ^{222}Rn in Tracing Steady-State Distributed Lateral Inflows

2.1. Methodology

The methodology described here involves the discretization of a study stream into j reaches through the selection of j+1 stream measurement stations. Measurement of injected tracer and ^{222}Rn concentrations at the j+1 measurement stations will allow calculation of $[Rn]_q$ (for each of the j reaches), with Eqn. (1) (derived in Appendix 1; see Eqn. (A21)):

$$[Rn]_q = \frac{[Rn]_2}{1-\frac{S_2}{S_1}} - \frac{[Rn]_1}{\frac{S_1}{S_2}-1} + \frac{([Rn]_1+[Rn]_2)(\frac{S_2}{S_1}+1)F}{4(1-\frac{S_2}{S_1})} \qquad (1)$$

where $[Rn]_q$ = average ^{222}Rn content of lateral inflow to the stream reach

[Rn] = ^{222}Rn concentration of streamwater

F = $\ln(G_1S_2/G_2S_1)$, where G and S are the steady-state streamwater concentrations of the injected volatile and conservative tracers, respectively, with any natural, background concentrations of these tracers subtracted.

1, 2 = subscripts indicating upstream and downstream ends of reach, respectively.

As noted in Appendix A, Eqn. (1) is applicable to the steady-state situation.

The field experiment has the following steps:

1. divide the stream into j study reaches by choosing j+1 measurement stations

2. begin the steady injection of a conservative tracer and a volatile tracer

upstream of the measurement station which is farthest upstream

3. measure the steady-state concentration of the conservative tracer at each measurement station;

4. measure the steady-state concentration of the volatile tracer at each measurement station;

5. measure the streamwater ^{222}Rn concentration at each measurement station; calculate $[Rn]_q$.

Each of these five steps is discussed in turn below.

Step 1. This is the most subjective part of the entire procedure. The choice of reach length should depend somewhat on the characteristics of the particular study stream. If there are places where properties such as channel slope change substantially, it would be sensible to locate measurement stations at these points so that averaging is done over reaches which are relatively homogeneous. In addition, it would be best to avoid placing measurement stations at points of large lateral inflow, since incomplete transverse mixing at these points could lead to errors in the one-dimensional analysis. Points or areas of large inflow could easily be identified with a preliminary steady conservative tracer injection in which stream sampling is done at a finer scale than will eventually be used for the full dual-tracer-plus-^{222}Rn experiment.

Step 2. Chloride, bromide, and tritiated water have been used as conservative tracers. Considerations of cost, safety, and the difficulty in obtaining permission to release tritium into a stream combine to make Cl^- or Br^- salt tracers

more attractive than ^3H at most sites. An additional advantage of a salt tracer is the potential for in situ analysis with a conductivity meter. The use of a field conductivity meter allows one to easily and accurately determine the lateral inflow between measurement stations in the field (see Steps 3 and 4). One can also readily determine when the tracer concentrations have reached their steady-state values.

Step 3. The series of measurements proposed here is designed to take advantage of the ease of measuring specific conductance (γ) in the field. The data set needed consists of the following:

· the background γ (γ_b) at each measurement station

· the final, steady-state γ (γ_s) at each measurement station

· the temperature (T) of the streamwater at each measurement station.

Two important facts make it possible to use γ as a surrogate for S:

· at low S values (below ~0.05 M, which is in the range of values likely to be encountered in an experiment such as this one) the relationship between γ and S is highly linear, and

· the total γ of a mixture of salts (such as streamwater) is, at low total salt concentrations, very nearly equal to the linear sum of the conductivity contributions from each ion.

These two facts make it generally allowable to use in situ γ_s-γ_b values (perhaps with a temperature correction; see below) rather than S values in Eqn. (1).

Before the salt injection is begun, γ_b values should be measured at all the

stations; after the injection has started and γ has reached its steady-state value, γ_s should be recorded. Since γ is a function of T, the streamwater temperature at each measurement station should also be measured. If two adjacent stations differ in temperature, a correction should be applied to normalize the γ values to a single temperature. This correction is about 2% per °C between 5° and 45°C. So, for example, if $T_2 = 14°$ and $T_1 = 12°$ C, then:

$$\frac{S_1}{S_2} = \frac{(\gamma_s - \gamma_b)_1 (1.02)^2}{(\gamma_s - \gamma_b)_2} \qquad (2)$$

Step 4. If the injection of the volatile and conservative tracers is begun at about the same time, water samples for analysis of the volatile tracer may be collected from a particular measurement station after the conservative tracer concentration has reached steady-state at that station.

Step 5. Several authors have used purge-and-trap methods in combination with gas-phase alpha counting to measure the ^{222}Rn content of streamwater [e.g., Rogers, 1958; Lee and Hollyday, 1987; Wanninkhof et al., 1990]. This technique is quite sensitive, but relatively time and labor intensive. In many small streams, ^{222}Rn concentrations are sufficiently high to allow the use of simple liquid scintillation techniques originally developed for analyzing ^{222}Rn in groundwater [Prichard and Gesell, 1977; Wadach, 1983; Genereux, 1988]. Liquid scintillation techniques generally involve collection of a 10-15 ml water sample in a ground-glass syringe or other suitable container, followed by injection of the sample into a glass

scintillation vial which already contains a few ml of scintillation fluor. It has been found that ^{222}Rn leakage from such vials may be a problem [e.g., Genereux, 1988]; however, this leakage may be essentially eliminated by inverting the vials immediately after they are capped, and counting them in this upside-down position. $[Rn]_1$ and $[Rn]_2$ may be used along with the injected tracer concentrations to solve Eqn. (1) for $[Rn]_q$.

2.2. Use of $[Rn]_q$ in providing constraints on sources of streamwater

The information embodied in $[Rn]_q$ may be used, along with other constraints, to estimate the relative importance of the different hydrologic flowpaths contributing to streamflow generation. $[Rn]_q$ values may be used in more than one way. Some uses involve simple mixing calculations designed to separate the water feeding a stream into different components; other uses could involve hillslope or watershed models. We will discuss the former, beginning with the separation of vadose-zone water and saturated-zone water as an example.

As discussed earlier, the geochemistry of ^{222}Rn is such that $[Rn]_{vzw}$ is likely to be much less than $[Rn]_{szw}$ at a given study site. If we consider the water feeding a stream to be composed of water from the vadose zone and the saturated zone, then a simple mixing calculation can be performed to determine the relative importance of these two sources. In other words, $[Rn]_q$ may be separated into its $[Rn]_{vzw}$ and $[Rn]_{szw}$ components, using the following expression:

$$f_{vzw} = \frac{[Rn]_{szw} - [Rn]_q}{[Rn]_{szw} - [Rn]_{vzw}} \quad (3)$$

where f_{vzw} is the fraction of streamflow in a given reach which is due to water from the vadose zone.

As with any mixing calculation, it is necessary to know the tracer concentration in each component ($[Rn]_{vzw}$ and $[Rn]_{szw}$), and in the mixture ($[Rn]_q$). Simple liquid scintillation techniques for measuring ^{222}Rn in water samples (e.g., $[Rn]_{szw}$) are by now well established [e.g., Prichard and Gesell, 1977; Wadach, 1983; Genereux, 1988]. Direct measurement of $[Rn]_{vzw}$ may not be practical, since collecting water from unsaturated soil without allowing loss of volatile compounds is problematic. An alternative is to measure the ^{222}Rn content of the soil gas, $[Rn]_g$, and assume that $[Rn]_{vzw} = K_H[Rn]_g$, where K_H is the Henry's Law constant for radon. Since K_H is a function of temperature, it is necessary to have some estimate of the soil temperature at the depths from which soil gas samples are collected.

Naturally, there will be some variability in both $[Rn]_{vzw}$ and $[Rn]_{szw}$. For example, calculating an average $[Rn]_{vzw}$ to use in Eqn. (3) will certainly require vertical averaging over the vadose zone, since $[Rn]_{vzw}$ is a function of depth in the vadose zone. The same type of general guideline which applies to the separation of old and new water with ^{18}O also applies to the use of Eqn. (3): a separation may be performed if the difference between $[Rn]_{vzw}$ and $[Rn]_{szw}$ is large compared to the sum of the analytical uncertainty associated with the ^{222}Rn measurements

plus the variability within $[Rn]_{vzw}$ and $[Rn]_{szw}$. Since $[Rn]_{vzw}$ is a strong function of soil moisture, the difference between $[Rn]_{vzw}$ and $[Rn]_{szw}$ should be enhanced in coarse, well-drained soils.

The type of separation described above addresses the issue of where water was (i.e., in what "pool") before draining to the stream, as opposed to how it moved to the stream. Thus, in the terminology of Sklash et al. [1976], this is a "geographic source" separation rather than a "runoff mechanism" separation, and vadose-zone water and groundwater are "geographic source components". (Sklash et al. also recognized a third type of separation, that of old vs. new water, which they designated a "time-source" separation.) This distinction is important to keep in mind, since separation of streamwater using an incongruent set of components, such as old water (time source component) and overland flow (runoff mechanism component), can result in considerable confusion. Clearly there are relationships between the components of the different separation schemes (e.g., most overland flow may be new water). However, these relationships are of a secondary nature, and may vary in time and space.

This is perhaps an appropriate point for a brief digression concerning the definitions of the components in the separation schemes described above. The terms "vadose-zone water" and "saturated-zone water" (the latter being groundwater plus capillary-fringe water) are commonplace in hydrology; however, within the framework of a streamflow separation scheme, their meanings bear close scrutiny. Clearly, no water drains directly to a stream from unsaturated soil, since only water

at a pressure of ≥1 atm may drain from a porous medium into an open water body. Therefore, all vadose-zone water which finds its way to a stream must spend some time, however short, as groundwater (water in the saturated zone, below the water table). Furthermore, it is likely that, on most watersheds, nearly all the water in the saturated zone was at one time in the vadose zone. Thus, the definitions of the components involve complications, and these complications are not unique to this study.

With stable isotope studies, the most vexing component-definition problem seems to be that of the variability in the isotopic composition of the "old" and "new" water components [e.g., Sklash and Farvolden, 1979; Kennedy et al., 1986; Hooper and Shoemaker, 1986]. The isotopic composition of new water (precipitation or melt water) may change with time during a storm or snowmelt event. The isotopic composition of old water varies in space (vadose-zone water is typically isotopically heavier than the underlying groundwater), and may change over time (e.g., on a seasonal time scale) as well. Additional confusion can arise from using the word "groundwater" as a surrogate for old water [e.g., Sklash and Farvolden, 1979], since not all old water is groundwater and, during and after storms, not all groundwater is old water. All of these problems are part of the general issue of defining terms and components.

Studies involving hydrometric (as opposed to tracer) methods have not been immune to difficulties associated with the definitions of hydrologic terms. Several hydrometric studies have referred to baseflow maintenance by unsaturated flow

[e.g., Hewlett and Hibbert, 1963; Weyman, 1970, 1973; Mosely, 1979]. The authors of these studies have implicitly attached greater significance to the unsaturated flow processes which, they concluded, were occurring over the bulk of the hillslope, than to the flow (which must have been saturated) occurring in the near-channel area. This emphasis, while perhaps quite reasonable and appropriate, is worth stating explicitly, if only because it may not be universally accepted. For example, Dunne and Black [1970, p.1310] concluded that "In the upland watersheds of Vermont the major portion of storm runoff seems to be produced as overland flow on small saturated areas close to streams", and that "Runoff from these wet areas is [partially] supplied by water escaping from the ground surface to reach the channel as overland flow". Dunne and Black are clearly describing the phenomenon of "return flow", in which subsurface water flows upward out of saturated soil. However, Hewlett [1974, p.606] argued strongly that "subsurface stormflow is any water passing the [stream] gaging station that has, however briefly, entered the mineral soil surface and has traveled for some distance, however short, within the soil". Thus, while Dunne and Black [1970] described return flow as overland flow (emphasizing the near-channel flowpath), Hewlett [1974] clearly considers return flow to be subsurface flow (emphasizing the upland flowpath).

With regard to this study, the working definition of vadose-zone water must include some criterion for how long the water resides in the saturated zone before draining to the stream. This is because the ^{222}Rn content of vadose-zone water will begin to increase when the water enters the saturated zone. This increase takes

place with a time constant equivalent to the decay constant of ^{222}Rn (0.18 day^{-1}). Since changing $[Rn]_{vzw}$ by a factor of two or three will probably not greatly affect the conclusions drawn from this technique (e.g., see section 3.2.), we suggest that water which resides in the saturated zone for less than a few days be considered "vadose-zone water", and that "saturated-zone water" be defined as water with a long (several ^{222}Rn half-lives) residence time in the saturated zone.

3. Field Example: Bickford Watershed

3.1. Study site, materials, and methods

On June 20, 1989, the steady-state experiment described in section II was performed at the Bickford Reservoir watershed in central Massachusetts. The Bickford watershed has been described in detail elsewhere [e.g., Hemond and Eshleman, 1984; Eshleman and Hemond, 1985; Eshleman and Hemond, 1988], and is not unlike other forested watersheds in the Northeast. Soils are generally thin (1 m or less in most places). The small stream selected for study drains a 32 ha catchment on the east side of the watershed. The experiment focused on a single stream reach, 34 m long, at the downstream end of the stream. There were no visible inputs of water (such as springs or small tributaries) to the study reach. Conservative and volatile tracers were injected into the stream at a point 17 m upstream of the first (farthest upstream) measurement station.

NaCl was used as a conservative tracer. Though they are not needed for the calculation of $[Rn]_q$, the injection rate and concentration of the tracer solution were

determined, in order to allow calculation of the streamflow rate at each measurement station (Eqn. (A13)). The salt solution (with a concentration of 2.85 M) drained into the stream from a 20 L Marriotte bottle, at a constant rate of 290 ml/min. A steady injection rate was maintained for about 50 minutes. The conductivity of the streamwater at each measurement station was measured with a battery-operated conductivity meter. The meters used automatically corrected the conductivity values to 25°C. Conductivity measurements were made about once every minute during the course of the injection.

Propane was used as a volatile tracer. Propane was bubbled into the stream from a small tank, using a 3 m length of plastic tubing with a glass frit at the outlet. The propane and salt injections were started at the same time (12:37 P.M.). Propane gas flow was controlled with a single-stage regulator. The regulator outlet pressure remained constant at 18 kPa (above atmospheric) for the course of the injection. Five streamwater samples for propane analysis were collected at each measurement station. The 34 ml samples were collected in ground-glass syringes, 45 to 75 minutes after the conservative tracer concentration had reached steady-state (see section 3.2., and Fig. 1). In order to avoid damaging the ground-glass syringes with suspended sediment, all samples were filtered with 0.8 μm filters during collection. The samples were packed in ice in the field, and not removed until the next morning, about 3 hours before analysis.

All ten propane samples were analyzed in the early afternoon on June 21. A known amount (6-7 ml) of helium was introduced into each syringe. The helium

and water were allowed to equilibrate at room temperature (24.8°C) for about 3 hours; each syringe was shaken gently several times. Using a sample loop, 1.0 ml of the helium headspace in each syringe was injected into a Perkin-Elmer 3920B gas chromatograph equipped with an FID detector. Helium was used as the carrier gas, and a packed column (6 feet long, 2 mm I.D., packed with 80-100 mesh Porapak Super Q) was employed. Oven (column) temperature was 120°C, and retention time for propane was 1.3 minutes. Calibration was achieved with a series of standard helium:propane mixtures obtained from Scott Specialty Gases. These standards were used to verify that the gas chromatograph was responding linearly and consistently. In addition, they allowed calculation of the absolute propane concentration in each water sample, though only relative concentrations are needed for purposes of this experiment.

Streamwater samples were also collected for ^{222}Rn analysis. These samples, like those for propane analysis, were drawn through 0.8 μm filters into ground-glass syringes and packed in ice in the field. Two samples were collected at each measurement station: one before the start of the salt solution and propane injections, and the other after the last propane sample was collected. Back at the lab, 10.0 ml of water from each syringe was ejected into a glass liquid scintillation vial containing 6.0 ml of scintillation fluor. The vials were quickly and tightly capped, and allowed to stand (for purposes of equilibration) overnight. Beginning the next morning, the amount of ^{222}Rn in each vial was measured using 50 minute counts on a Beckman 1801 liquid scintillation counter. The calibration procedure

used was essentially that of Wadach [1983], and details are given elsewhere [Genereux, 1988].

The ^{222}Rn content of soil gas from two sampling tubes (tubes 141 and 142) was also measured. Sampling tubes 141 and 142 are 35 and 56 cm deep, respectively. These tubes are about 1 m apart (horizontally), and are located on the south slope (left side of the stream if one is facing downstream), about 10 m from the stream channel, at approximately the middle of the reach. Both tubes consist of ¼" copper tubing with a piece of stainless steel wellscreen (7 cm long, 2 cm in diameter) brazed onto the end. The soil gas samples were collected in ground-glass syringes. Back at the lab, about 10 ml of scintillation fluor was drawn into each syringe, the air and fluor were equilibrated (with most of the ^{222}Rn ending up in the fluor), and the fluor was then expelled into a glass scintillation vial. This novel method for analysis of ^{222}Rn in soil gas is very simple and gives highly reproducible results, with total uncertainty in the results being about 15%. The method is described in detail elsewhere [Genereux and Hemond, 1991].

The streamwater temperature at each station was measured several times during the experiment.

3.2. Results and discussion

The conductivity data are plotted in Fig. 1 and summarized in Table 1. For station 1, γ_s-γ_b was 343 ± 1 μS/cm; using the conductivity-concentration data of Jones (1912), one finds that this conductivity corresponds to 3.05×10^{-3} M NaCl

(25°C). Using this value for S_1, and the known S_0 and Q_0 values (2.85 M and 0.290 L/min, respectively), gives a value of 273 L/min for Q_1 (Eqn. (A13)). At station 2, γ_s-γ_b was 290 μS/cm, giving Q_2 = 323 L/min. The difference between Q_2 and Q_1 gives $q\Delta x$, 50 L/min.

The conductivity data was also used to calculate the travel time (τ) through the study reach. τ was calculated as τ'_2 - τ'_1 (see Table 1), where τ' is the time to "half-height" for the conductivity (i.e., the time, measured from when the salt injection was started, when $\gamma = \gamma_b + \frac{1}{2}[\gamma_s-\gamma_b]$). From the τ' values given in Table 1, τ was found to be 21.5 min (plus or minus 0.2 min).

The propane data are also given in Table 1. The five samples from station 1 had an average propane concentration (G) of 6.19 μM; the standard deviation (σ) for the five samples was 2.5%. The average G value for station 2 was 2.99 μM (σ = 4%). Using these values for G_1 and G_2, the γ_s-γ_b value for each station, and Eqn. (A19), the first-order volatilization rate constant (k, see Appendix B) was found to be 1.56 ± 0.08 hr^{-1} (justifying the decision to neglect radioactive decay of ^{22}Rn, which occurs with a time constant of 7.55 × 10^{-3} hr^{-1}).

The [Rn] values given in Table 1 are averages based on the two samples collected at each station. The two samples from station 1 had ^{222}Rn concentrations of 184 and 150 dpm/L, giving an average of 167 dpm/L. The two samples from station 2 had 164 and 166 dpm/L, giving an average of 165 dpm/L. The samples containing 184 and 164 dpm/L were collected before the start of the tracer injections, while the other two were collected ~2.5 hours later, after the injected

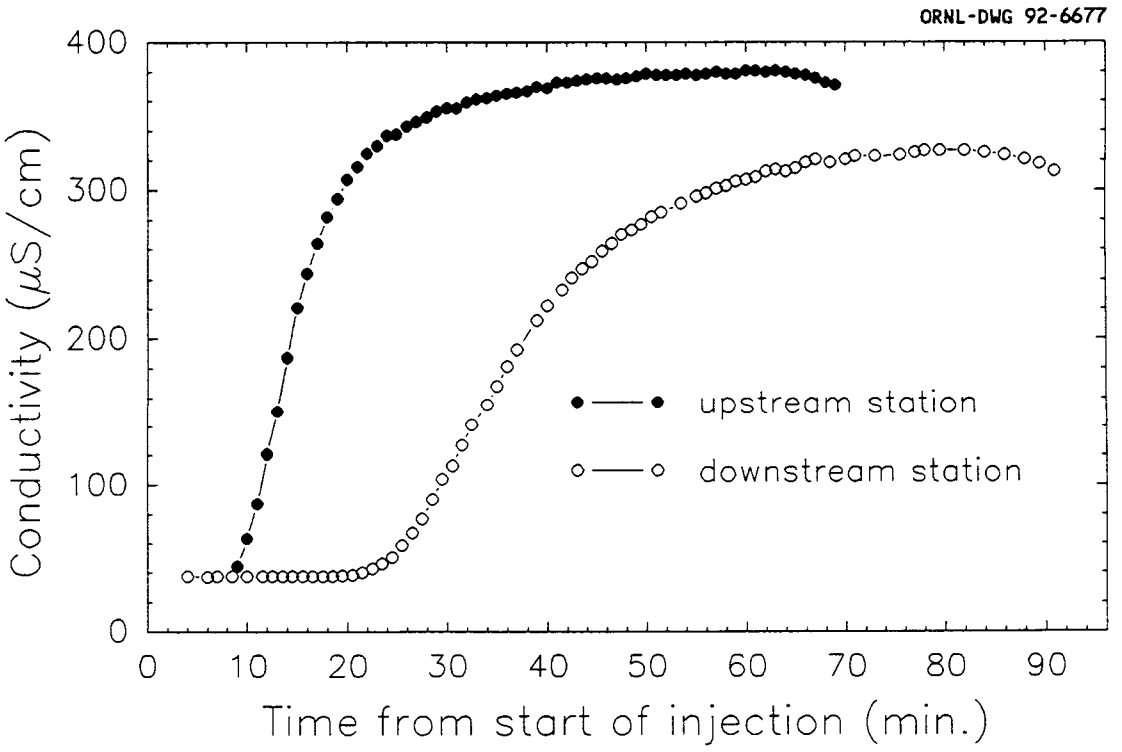

Figure 1. Streamwater conductivity vs. time at the two stream measurement stations during the field experiment of June 20, 1989.

Parameter	Station 1	Station 2	Reach
γ_s (μS/cm)	380	327	
γ_b (μS/cm)	37.5	37.4	
Q (L/min)	273	323	
τ' (min)	14.6	36.1	
τ (min)			21.5
G (μM)	6.19	2.99	
F			0.56
[Rn] (dpm/L)	167	165	
$[Rn]_q$ (dpm/L)			700

Table 1. Summary of results from the field experiment of June 20, 1989.

tracer portion of the experiment was over. Counting uncertainty (2σ) for these samples was 12-13%. With the data in Table 1, Eqn. (1) gives 700 dpm/L as the value of $[Rn]_q$. The uncertainty in this number is ~18%; the uncertainty analysis was based on equation B.4 of Kline [1985].

An appropriate starting point for interpreting this $[Rn]_q$ value is a two-component (vadose-zone water and saturated-zone water) separation. The two soil gas samples collected during the experiment may be used to estimate the $[Rn]_{vzw}$ value needed for the separation. The soil gas from tube 141 contained 730 dpm of ^{222}Rn per liter, that from tube 142 had 1580 dpm/L. Soil gas from these two near-channel tubes typically has a higher ^{222}Rn content (by 50-100%) than that from tubes of similar depth located farther up the hillslopes, 50-100 m from the study stream (data for the hillslope tubes are found in Genereux and Hemond [1991]). The values from tubes 141 and 142 are the most appropriate values for our purposes, since these tubes are on the lower portion of the hillslope and are clearly within the contributing area of our study reach. No direct measurements of the soil temperature are available. If a temperature of 15°C is assumed for the vadose-zone soil, the $[Rn]_g$ values given above correspond to $[Rn]_{vzw}$ values of 220 (tube 141) and 480 (tube 142) dpm/L. While the soil gas was being drawn from tube 142, some water was also pulled up the tube, indicating that the top of the saturated zone was about 50-55 cm below the ground surface. Thus, all vadose-zone water must have had between roughly zero (at the ground surface) and 500 (at the bottom of the vadose zone) dpm/L. Within this range, the choice

of a representative $[Rn]_{vzw}$ value for the two-component separation is somewhat subjective. One may simply use an average value for the vadose zone (~200 dpm/L); alternately, one may use the value for deep vadose-zone water (~500 dpm/L), in order to give greater weight to water which is nearer the saturated zone, and is therefore nearer (in space and time) to becoming streamwater. As is demonstrated below, the conclusions of this analysis are not very sensitive to which $[Rn]_{vzw}$ value (200 or 500 dpm/L) is used.

On the day of the experiment, the depth of the top of the saturated zone (as judged from tube 142) was almost exactly equal to the depth of the interface between loamy forest soil and a hard, dense, rocky "subsoil" containing no roots. Thus, the $[Rn]_{szw}$ value appropriate for our separation is that associated with this hard subsoil. An estimate of the subsoil $[Rn]_{szw}$ was obtained by digging a soil pit, collecting a subsoil sample, and sealing the sample in a container at the lab, to allow ^{222}Rn ingrowth. The container consisted of a piece of copper pipe (2" diameter, 77 cm long) with fittings soldered onto each end. Disaggregated subsoil was packed into the container, to a bulk density of 1.46 g/ml (~10% lower than the natural subsoil bulk density of 1.64 g/ml). The subsoil was saturated by setting up the container with its long axis vertical, flushing it with CO_2, and passing about 10 L of water up through it (i.e., in through the bottom and out through the top) over a period of about 5 hours. Once the container was saturated, brass valves at the ends were closed tightly to allow ^{222}Rn to build up to its secular equilibrium concentration. After waiting a conservatively long amount of time (>1 month),

three water samples were drawn from the container. The average $[Rn]_{szw}$ for the three samples was 2000 dpm/L (corrected for the 10% decrease in bulk density).

Assuming $[Rn]_{vzw}$ = 200 dpm/L and $[Rn]_{szw}$ = 2000, Eqn. (3) gives f_{vzw} = 0.72. Changing $[Rn]_{vzw}$ to 500 yields f_{vzw} = 0.87. Thus, choosing any reasonable value for $[Rn]_{vzw}$ leads to the same conclusion: much of the water (>70%) entering the stream over the 34 m study reach seems to be traveling to the stream via shallow, low-^{222}Rn pathways in the vadose zone. This result is consistent with the conclusions of several previous studies [e.g., Hewlett and Hibbert, 1963; Weyman, 1973; Mosely, 1979]; each of these studies found lateral unsaturated flow to be the dominant flowpath maintaining baseflow in small streams.

4. Summary, Conclusions, Future Work

In this paper, we have presented a specific, quantitative framework for the use of naturally- occurring ^{222}Rn as a hydrologic flowpath tracer. Our methodology builds on earlier work in the areas of ^{222}Rn geochemistry, hillslope hydrology, and volatilization in open-channel flow. The methodology consists of two distinct parts, the first of which is the calculation of $[Rn]_q$, the average ^{222}Rn content of the water feeding a given stream reach. $[Rn]_q$ is determined by measuring the concentrations of ^{222}Rn and two injected tracers (one conservative, one volatile) in the streamwater, and solving a mass-balance equation for ^{222}Rn around the reach of interest. The second part of the methodology involves using $[Rn]_q$ values to determine the sources of stream inflow (and, implicitly, the flowpaths important in

streamflow generation). One means of accomplishing this, simple "geographic-source" separations, was presented here; other means are certainly possible. For example, if one had a numerical watershed model incorporating ^{222}Rn geochemistry, one could compare model predictions and field determinations of $[Rn]_q$. This would provide a basis for judging whether the model generates streamflow in a physically realistic way, in addition to generating it in the right amount. While it seems likely that any quantitative use of ^{222}Rn as a streamflow generation tracer will require a method (such as that presented here) for determining $[Rn]_q$ at some spatial scale, conceptual models for the interpretation of $[Rn]_q$ values may differ from watershed to watershed, and we have certainly not exhausted all of the possibilities here.

The Bickford watershed experiment showed that the proposed field methodology is feasible. The entire experiment was completed by two people in about 4 hours; roughly the same amount of time was required in the laboratory for ^{222}Rn and propane analyses. The equipment required (portable conductivity meters, a liquid scintillation counter, a gas chromatograph) is standard in environmental science laboratories. The results from the Bickford experiment clearly suggest the possible importance of water flow through the low-^{222}Rn environment of the vadose zone, since the $[Rn]_q$ value for the study reach (700 dpm/L) was closer to that of vadose-zone water ($\leq$500 dpm/L) than to that of saturated-zone water (2000 dpm/L). This is consistent with the conclusions of several previous investigations of streamflow generation.

Though we have limited the scope of this paper to the steady-state, it is possible to extend the ^{222}Rn methodology to unsteady (i.e., stormflow) situations. Some extra measurements are required, mainly to account for changes in channel storage. Depending on the error one is willing to incur, it may be perfectly reasonable to apply a steady-state analysis to some "quasi-steady" cases. However, for those situations in which time variability is too important to ignore, the unsteady change-in-storage term must be determined to solve the ^{222}Rn mass balance for each stream reach. Work is currently underway to implement an integrated stormflow methodology which makes use of ^{222}Rn and other "tools" of the the hillslope hydrology trade (e.g., stable isotopes and automated piezometers). Our philosophy is that each of these tools has its own strengths and weaknesses, and no tracer or hydrometric technique alone is adequate for unraveling the mechanisms of streamflow generation. In the field study of streamflow generation, the best approach is the simultaneous application of multiple tracer and hydrometric methodologies. Thus, we view ^{222}Rn as one of several tools which, when properly used in concert, may provide much information about the hydrologic flowpaths important in streamflow generation.

Appendix A. Mathematical Derivations

The general, one-dimensional transport equation applicable to rivers and streams is:

$$\frac{\partial(AC)}{\partial t}+\frac{\partial(AUC)}{\partial x}=\frac{\partial}{\partial x}(AE_L\frac{\partial C}{\partial x})+Ar \qquad \text{(A1)}$$

where t = time

x = coordinate direction along the channel (positive downstream)

C = solute concentration

A = stream cross-sectional area, perpendicular to x

U = velocity of water flow along x

r = solute source/sink strength (moles per unit volume of water per unit time)

E_L = longitudinal dispersion coefficient.

In general, A, U, C, E_L, and r may all be functions of x and t. The one-dimensional continuity equation is:

$$\frac{\partial A}{\partial t}=q-\frac{\partial(AU)}{\partial x} \qquad \text{(A2)}$$

where q(x, t) is the lateral inflow function expressing how much water enters the stream per unit length of stream channel per unit time. After using the chain rule to expand (A1), substituting in (A2), and dividing through by A, the following expression is obtained:

$$\frac{\partial C}{\partial t}+U\frac{\partial C}{\partial x}+\frac{q}{A}C=\frac{1}{A}[\frac{\partial}{\partial x}(AE_L\frac{\partial C}{\partial x}]+r \qquad \text{(A3)}$$

Neglecting solute transport by longitudinal dispersion, the steady-state form of (A3) is:

$$U\frac{dC}{dx}+\frac{q}{A}C=r \tag{A4}$$

where A, U, C, q, and r may all be functions of x.

While a conservative solute has r=0, a solute undergoing first-order decay or loss has r = -kC, where k is the first order rate constant. Volatilization is often parameterized in this way (see Appendix B). A solute which is both volatile and radioactive has r = -(k + λ)C, where λ is the radioactive decay constant. Any solute which is present in the water feeding the stream requires an additional source term of the form $(q/A)C_q$, where $C_q(x, t)$ is the solute concentration in the lateral inflow. Thus, for ^{222}Rn, r = $(q/A)C_q$ - (k + λ)C, and (A4) may be written:

$$U\frac{dR}{dx}=\frac{q}{A}[Rn]_q-(\frac{q}{A}+k+\lambda)[Rn] \tag{A5}$$

where [Rn] is the ^{222}Rn concentration of the streamwater and $[Rn]_q$ is the ^{222}Rn concentration in the water feeding the stream. In general, U, A, q, k, $[Rn]_q$, and [Rn] may all be functions of x. This equation may be simplified by dividing through by U and introducing the expression:

$$Q(x)=A(x)U(x) \tag{A6}$$

If radioactive decay is neglected (λ << k; see Appendix B), (A6) becomes:

$$\frac{\partial[Rn]}{\partial x}=\frac{q}{Q}[Rn]_q-(\frac{q}{Q}+\frac{k}{U})[Rn] \tag{A7}$$

As indicated in the introduction, our goal is to solve for $[Rn]_q$. Once $[Rn]_q$ is

known, it may be used in separating the streamflow into hydrologically distinct components. The parameters needed to solve for $[Rn]_q$ are q, Q, U, k, and [Rn]. [Rn] comes from direct measurements of the ^{222}Rn content of streamwater; the other four parameters are obtained with the use of conservative and volatile tracers injected into the study stream. Putting (A7) in finite difference form and solving for $[Rn]_q$ gives:

$$[Rn]_q = \frac{Q_2[Rn]_2 - Q_1[Rn]_1 + Q_{avg}R_{avg}\tau k}{q\Delta x} \qquad \text{(A8)}$$

where $\tau = \Delta x/U$, $q\Delta x = Q_2 - Q_1$, $Q_{avg} = (Q_1 + Q_2)/2$, and $[Rn]_{avg} = ([Rn]_2 + [Rn]_1)/2$.

Q values for each measurement station, and q for each reach, may be determined from the steady-state conservative tracer (e.g., chloride) concentration at each station. This requires the use of the governing equation for Cl^- concentration. The form of (A4) appropriate for a conservative solute is:

$$U(x)\frac{dS}{dx} = \frac{-q(x)}{A(x)}S \qquad \text{(A9)}$$

This equation may be simplified by introducing Eqn. (A6):

$$\frac{dS}{dx} = \frac{-q(x)}{Q(x)}S \qquad \text{(A10)}$$

Since dQ/dx = q, Eqn. (A10) may be written:

$$-\frac{dS}{S}=\frac{dQ}{Q} \tag{A11}$$

the solution to which is:

$$-\int_{S_0}^{S_1}\frac{dS}{S}=\int_{Q_0}^{Q_1}\frac{dQ}{Q} \tag{A12}$$

$$S_0Q_0-S_1Q_1 \tag{A13}$$

where Q_0 and S_0 are the injection rate and Cl^- concentration, respectively, of the tracer solution; S_1 and Q_1 are the steady-state Cl^- concentration and streamflow rate, respectively, at station 1.

Calculation of k for a given reach requires τ for the reach, and S and G data from both ends of the reach (G is the concentration of the volatile tracer gas in the streamwater). The steady-state governing equation for a volatile (but otherwise non-reactive) tracer may be written:

$$\frac{dG}{dx}=-(\frac{q}{Q}+\frac{k}{U})G \tag{A14}$$

Integrating Eqns. (A10) and (A14) between x_1 and x_2 gives:

$$\int_{S_2}^{S_1}\frac{dS}{S}=\int_{x_1}^{x_2}\frac{q(x)}{Q(x)}dx \tag{A15}$$

$$\int_{G_2}^{G_1}\frac{dG}{G}=\int_{x_1}^{x_2}\frac{q(x)}{Q(x)}dx+\int_{x_1}^{x_2}\frac{k(x)}{U(x)}dx \qquad \text{(A16)}$$

Subtracting (A15) from (A16) gives:

$$\ln\frac{G_1}{G_2}-\ln\frac{S_1}{S_2}=\int_{x_1}^{x_2}\frac{k(x)}{U(x)}dx \qquad \text{(A17)}$$

Letting $U = U_{avg}$, and $k = k_{avg}$, (A17) yields:

$$\ln\frac{G_1S_2}{G_2S_1}=\frac{k_{avg}(x_2-x_1)}{U_{avg}}\equiv F \qquad \text{(A18)}$$

and since $(x_2 - x_1)/U_{avg} = \tau$,

$$k_{avg}=\frac{F}{\tau} \qquad \text{(A19)}$$

Eqn. (A19) may be used to calculate k_{avg} for each stream reach. However, this is not necessary for the determination of $[Rn]_q$. Substituting Eqn. (A19) into Eqn. (A8) gives:

$$[Rn]_q=\frac{Q_2[Rn]_2-Q_1[Rn]_1+Q_{avg}[Rn]_{avg}F}{q\Delta x} \qquad \text{(A20)}$$

In this formulation, the volatilization term is not separated into volatilization coefficient and travel time factors. Hence, the measurement of travel time becomes unnecessary, simplifying the field sampling procedure (only steady-state

γ values need be recorded). Each term in Eqn. (A20) may be expressed as a function of one or more of the six tracer concentrations measured for each reach (S_1, S_2, G_1, G_2, $[Rn]_1$, and $[Rn]_2$), allowing this equation to be written:

$$[Rn]_q = \frac{[Rn]_2}{1-\frac{S_2}{S_1}} - \frac{[Rn]_1}{\frac{S_1}{S_2}-1} + \frac{([Rn]_1+[Rn]_2)(\frac{S_2}{S_1}+1)F}{4(1-\frac{S_2}{S_1})} \qquad \text{(A21)}$$

Eqn. (A21) shows that it is not necessary to know the injection rate of either the conservative or the volatile tracer, or the absolute concentrations these tracers, one need determine only the ratio of their upstream to downstream concentrations.

Appendix B. Streamwater Volatilization Correction

For a hydrologic tracer to be useful, any in-stream processes which affect it must be well understood and readily quantified. The two processes which may affect the concentration of ^{222}Rn in streamwater are radioactive decay and volatilization (production is not important, since the concentration of ^{226}Ra in streamwater is typically a small fraction of the ^{222}Rn concentration). Experimentally determined volatilization rates for small streams [e.g., Parker and Gay, 1987; Wanninkhof, unpub. data, 1987; Genereux, unpub. data, 1989] indicate that ^{222}Rn loss by volatilization is much greater than loss by radioactive decay (volatilization rate constants (k) of 10-100 day^{-1} are not uncommon, while the decay constant for ^{222}Rn is only 0.18 day^{-1}). Thus, the only in-stream sink which need be

considered for ^{222}Rn is volatilization.

A simple and effective way of quantifying the volatilization of a trace gas from a stream is with the use of a first-order volatilization coefficient (k). A large number of empirical equations have been developed for predicting k from various combinations of hydraulic parameters (depth, width, slope, volumetric flow rate, velocity); Rathbun [1977] and Duran [1985] have compiled many of these equations. However, these equations are based on results from large streams and small rivers, and they typically do a very poor job of predicting k for small streams [e.g., Parker and Gay, 1987]. Indeed, some of the parameters on which the equations are based (e.g., average depth, width, or velocity) may be very difficult to estimate for a first order, pool-and-riffle type stream.

Fortunately, there are relatively simple methods available for measuring k. The simplest is probably the steady-state tracer-gas method. This technique involves the continuous injection of a tracer gas into a stream at a constant rate. The concentration of the tracer gas in the streamwater is then measured at two or more locations downstream [Wilcock, 1984; Duran and Hemond, 1984; Yotsukura et al., 1983]. The difference in tracer gas concentration between any two locations, along with the travel time and the amount of dilution by lateral inflow between the two (determined from an injection of a conservative tracer), allows calculation of k. (The k value determined by this technique is an average value for the stream reach, designated "k_{avg}" in Appendix A.) Several of these experiments at different flow rates are sufficient to characterize a particular stream reach.

k is a function of the aqueous diffusion coefficient (D) of the gas in question. Therefore, unless the injected tracer gas (propane was used in this work) and the volatile compound of interest (in this case, radon) have the same diffusion coefficient, a correction is needed to convert the tracer-gas k value to an equivalent value for the compound of interest. This correction could be made using measured values of D, but this approach has the added complication of requiring that one choose a particular conceptual model for volatilization. For example, the stagnant boundary layer (or two-film) conceptualization of volatilization predicts a linear dependence of k on D. In contrast, the surface-renewal theory predicts that k is proportional to $D^{0.5}$. Other models of volatilization give still other predictions of how k will depend on D [e.g., Bennett and Rathbun, 1972], and experimental data often does not fit one model much better than another [e.g., Duran, 1985].

The problem of selecting a particular conceptual model of volatilization is circumvented by making a correction based on direct determination of k for both the tracer gas and the compound of interest in the same water body. Several authors [e.g., Tsivoglou et al., 1965; Rathbun et al., 1978; Duran, 1984] have shown that the ratio of the k values for two gases is independent of temperature and the level of turbulence in a water body (over the range of conditions investigated). Thus, the ratio k(gas 1)/k(gas 2) should be the same for a natural stream and a stirred tank in the laboratory. Rathbun et al. [1978] demonstrated that $k(\text{propane})/k(O_2) = 0.72 \pm 0.02$ in laboratory experiments (uncertainty is the 95% confidence range of the slope of the data on a plot of k(propane) vs. $k(O_2)$).

Tsivoglou et al. [1965] found that k(radon)/k(O_2) = 0.70 ± 0.08 (again, uncertainty is the 95% confidence limits). These experimental results indicate that k(radon)/k(propane) = 0.97 ± 0.11; thus, only a very small correction (or, arguably, no correction) should be used to convert k(propane) values to k(radon) values.

There has been much discussion in the literature of the possible importance of chemical or biological sinks for hydrocarbon tracers [e.g., Rathbun et al., 1980; Tsivoglou, 1979; Rathbun et al., 1978]. Ethylene may have biological sources and sinks [e.g., Abeles, 1973], which could make it inappropriate as a tracer gas for determining k. Bopp et al. [1981] found degradation rate constants of about 0.01-0.1 day^{-1} for propane in model estuarine ecosystems containing water from Narragansett Bay in Rhode Island. These rate constants are a factor of 10^2-10^4 smaller than k values for small streams [Parker and Gay, 1987; Wanninkhof, unpub. data, 1987; Genereux, unpub. data, 1989; this paper, section 3]. Indeed, the biological uptake of propane would likely be slower in small streams draining forested areas than in the microcosms used by Bopp and coworkers, since the latter are similar to Narragansett Bay in "abundance, species composition, and seasonal succession of phytoplankton, zooplankton, bacterioplankton, and benthic macro- and meiofauna" [Bopp et al., 1981]. These results suggest that chemical and/or biological degradation of propane should not interfere with its use in determining k for small streams.

List of Symbols

A = cross-sectional area of a stream, perpendicular to the direction of flow

C = general symbol for the concentration of a solute in streamwater

E_L = longitudinal dispersion coefficient for a stream

G = concentration of an injected tracer gas in streamwater

k = first-order rate constant for volatilization from a water body

K_H = dimensionless Henry's Law constant, (mol/L air) per (mol/L water)

q = rate of inflow of water to a stream channel (volume per unit time per unit length of channel)

Q = volumetric streamflow

r = source or sink rate for a solute in streamwater

[Rn] = concentration of ^{222}Rn in streamwater

$[Rn]_z$ = concentration of ^{222}Rn in water "z" (see subscripts listed below)

S = concentration of Cl^- in streamwater

t = time

T = streamwater temperature

U = velocity of streamwater flow

x = coordinate direction along the stream channel (positive downstream)

γ = conductivity (=specific conductance) of water

λ = radioactive decay constant for ^{222}Rn, equal to $7.549 \times 10^{-3}\ hr^{-1}$

τ = travel time through a stream reach (i.e., average time it takes water to flow from the upstream end of a reach to the downstream end)

Subscripts:

avg = average value for a stream reach

b = background

q = the average for the lateral inflow to a stream reach

g = soil gas

s = steady-state

szw = saturated-zone water

vzw = vadose-zone water

1, 2 = indicate the upstream and downstream ends, respectively, of a stream reach

The letter "Δ" before a symbol (e.g., ΔQ) denotes the difference in the value of the variable (e.g., Q) between the two ends of a reach (i.e., $\Delta Q = Q_2 - Q_1$).

Acknowledgements

The authors wish to acknowledge the invaluable assistance of Jennifer Gauss and Monique T. Villars during the field work at the Bickford watershed. Our field work at Bickford was made possible through the cooperation of the Massachusetts Department of Environmental Management and the Water Registrar of the City of Fitchburg. We also thank Phil Gschwend, for his insightful comments on this manuscript. This work was supported by New England Power Service Co., Empire State Electric Energy Research Co., American Electric Power Service Co., the U.S. Geological Survey (contract # 14-08-0001-G1725), the National Institue of

Environmental Health Sciences (N.I.H contract # NIH5P42ESO4675-03), and the National Science Foundation (contract # BCS-8906032).

Bibliography

Abeles, F.B. 1973. Ethylene in Plant Biology. Academic Press, New York, NY.

Anderson, M.G., and T.P. Burt. 1978. The role of topography in controlling throughflow generation. Earth Surf. Processes Landforms 3: 331-344.

Bennett, J.P., and R.E. Rathbun. 1972. Reaeration in open-channel flow. USGS Professional Paper 737.

Bonell, M., D.A. Gilmour, and D.F. Sinclair. 1981. Soil hydraulic properties and their effect on surface and subsurface water transfer in a tropical rainforest catchment. Hydrol. Sci. Bull. 26: 1-18.

Bopp, R.P., P.H. Santschi, Y.H. Li, and B.L. Deck. 1981. Biodegradation and gas exchange of gaseous alkanes in model estuarine ecosystems. Organic Geochemistry 3: 9-14.

Brutsaert, W.F., S.A. Norton, C.T. Hess, and J.S. Williams. 1981. Geologic and hydrologic factors controlling radon-222 in ground water in Maine. Ground Water 19(4): 407-417.

Clements, W.E., and M.H. Wilkening. 1974. Atmospheric pressure effects on ^{222}Rn transport across the earth-air interface. J. Geophysical Research 79(33): 5025-5029.

Cronan, C.S., and G.R. Aiken. 1985. Chemistry and transport of soluble humic

substances in forested watersheds of the Adirondack Park, New York. Geochimica et Cosmochimica Acta 49: 1697-1705.

Dincer, T., B. Payne, T. Florkowski, J. Martinec, and E. Tongiorgi. 1970. Snow-melt runoff from measurements of tritium and oxygen-18. Water Resources Research 6: 110-124.

Dunne, T. and R. Black. 1970. Partial area contributions to storm runoff in a small New England watershed. Water Resources Research 6(5): 1296-1311.

Duran, A.P., and H.F. Hemond. 1984. Dichlorodifluoromethane (Freon-12) as a tracer for nitrous oxide release from a nitrogen-enriched river. In: Brutsaert, W., and G.H. Jirka (eds.), Gas Transfer at Water Surfaces, p.413-420.

Duran, Alexander. 1985. "Nitrous Oxide Production in Nitrogen-Rich River Sediments." Ph.D. Thesis, Massachusetts Institute of Technology, Department of Civil Engineering.

Eshleman, K.N., and H.F. Hemond. 1985. The role of organic acids in the acid-base status of surface waters at Bickford Watershed, Massachusetts. Water Resources Research 21(10): 1503-1510.

Eshleman, K.N., and H.F. Hemond. 1988. Alkalinity and major ion budgets for a Massachusetts reservoir and watershed. Limnology and Oceanography 33(2): 174-185.

Fukui, M. 1985. ^{222}Rn concentrations and variations in unconfined groundwater. J. Hydrology 79: 83-94.

Genereux, D. 1988. Hydrogeochemistry of ^{222}Rn on a forested watershed. M.S. Thesis, Massachusetts Institute of Technology.

Genereux, D., and H.F. Hemond. 1991. Measurement of the ^{222}Rn content of soil-gas by liquid scintillation counting. Isotope Geoscience, in press.

Hall, F.R., E.L. Boudette, and W.J. Olszewski Jr. 1987. Geologic controls and radon occurrence in New England. In: B. Graves (ed.), Radon, Radium, and Other Radioactivity in Ground Water, Lewis Publishers, Chelsea, Michigan, pp. 15-29.

Harr., R.D. 1977. Water flux in soil and subsoil on a steep forested slope. J. Hydrology 33: 37-58.

Hemond, H.F., and K.N. Eshleman. 1984. Nitrate processing and watershed acid sensitivity. Water Resources Research 20(11): 1718-1724.

Hewlett, J.D., and and A. Hibbert. 1963. Moisture and energy conditions within a sloping soil mass during drainage. J. Geophys. Res. 68(4): 1081-1087.

Hewlett, J.D. 1974. Comments on letters relating to "Role of subsurface flow in generating surface runoff, 2, upstream source areas", by R. Allen Freeze. Water Resource Research.

Hooper, R.P., and C. A. Shoemaker. 1986. A comparison of chemical and isotopic hydrograph separation. Water Resources Research 22(10): 1444-1454.

Jacoby, G.C., H.J. Simpson, G. Mathieu, and T.Torgersen. 1979. Analysis of groundwater and surface water supply interrelationships in the upper

Colorado River basin using natural radon-222 as a tracer. John Muir Institute, Napa, CA.

Jones, H.C. 1912. The Electrical Conductivity, Dissociation and Temperature Coefficients of Conductivity from Zero to Sixty-Five Degrees of Aqueous Solutions of a Number of Salts and Organic Acids, Carnegie Institution of Washington, Washington, D.C.

Kennedy, V.C., C. Kendall, G.W. Zellweger, T.A. Wyerman, and R.J. Avanzino. 1986. Determination of the components of stormflow using water chemistry and environmental isotopes, Mattole River Basin, California. J. Hydrol. 84: 107-140.

Kline, S.J. 1985. The purpose of uncertainty analysis. J. Fluids Eng. 107: 153-160.

Kraner, H.W., G.L. Schroeder, and R.D. Evans. 1964. Measurements of the effects of atmospheric variables on radon-222 flux and soil-gas concentrations. In: The Natural Radiation Environment, University of Chicago Press, Chicago, IL, pp. 191-215.

Kristainsson, K., and L. Malmqvist. 1982. Evidence for nondiffusive transport of ^{222}Rn in the ground and a new physical model for the transport. Geophys. 47(10): 1444-1452.

Lanctot, E.M., A.L. Tolman, and M. Loiselle. 1985. Hydrogeochemistry of radon in ground water. In: The Second Annual Eastern Regional Ground Water Conference, July 16-18, Portland, ME, pp. 66-85.

Lee, R.W., and E.F. Hollyday. 1987. Radon measurement in streams to determine

location and magnitude of groundwater seepage. In: B. Graves (ed.), Radon, Radium, and Other Radioactivity in Ground Water, Lewis Publishers, Chelsea, MI, pp. 241-249.

Maloszewski, P., W. Rauert, W. Stichler, and A. Herrmann. 1983. Application of flow models in an alpine catchment area using tritium and deuterium data. J. Hydrol. 66: 319-330.

Martinec, J., H. Siegenthaler, H. Oeschger, and E. Tongiorgi. 1974. New insight into the runoff mechanism by environmental isotopes. In: Proceedings of the Symposium on Isotope Techniques in Groundwater Hydrology, I.A.E.A., Vienna, Austria, 1:129-143.

McKeague, J.A., and M.G. Cline. 1963. Silica in soil solutions: 1. The form and concentration of dissolved silica in aqueous extracts of some soils. Canadian Journal of Soil Science 43: 70-82.

Mosley, M.P. 1979. Streamflow generation in a forested watershed, New Zealand. Water Resources Research 15(4): 795-806.

Mosley, M.P. 1982. Subsurface flow velocities through selected forest soils, South Island, New Zealand. J. Hydrol. 55: 65-92.

Osmond, J.K., and J.B. Cowart. 1976. The theory and uses of natural uranium isotopic variations in hydrology. Atomic Energy Review 144: 621-679.

Parker, G.W., and F.B. Gay. 1987. A procedure for estimating reaeration coefficients for Massachusetts streams. USGS Water Resources Investigations Report 86-4111.

Pilgrim, D.H., D.D. Huff, and T. Steele. 1979. Use of specific conductance and contact time relations for separating flow components in storm runoff. Water Resources Research 15(2): 329-339.

Prichard, H.M., and T.F. Gesell. 1977. Rapid measurements of ^{222}Rn concentrations in water with a commercial liquid scintillation counter. Health Physics 33: 577-581.

Rathbun, R.E. 1977. Reaeration coefficients of streams: State of the art. Journal of Hydraulics Division, Proceedings of the ASCE 103(HY4): 409-424.

Rathbun, R.E., D.W. Stephens, D.J. Shultz, and D.Y. Tai. 1978. Laboratory studies of gas tracers for reaeration. Journal of the Environmental Engineering Division, Proceedings of the ASCE 104(EE2): 215-229.

Rathbun, R.E., D.W. Stephens, D.J. Shultz, and D.Y. Tai. 1980. Laboratory studies of gas tracers for reaeration: Closure. Journal of the Environmental Engineering Division, Proceedings of the ASCE 106(EE3): 663-670.

Rodhe, A. 1981. Springflood: meltwater or groundwater? Nordic Hydrol. 12: 21-30.

Rogers, A. 1958. Physical behavior and geologic control of radon in mountain streams. USGS Bulletin 1052-E.

Schery, S.D., D.H. Gaeddert, and M.H. Wilkening. 1984. Factors affecting exhalation of radon from a gravelly sand loam. J. Geophys. Research 89: 7299-7309.

Sklash, M.G., R.N. Farvolden, and P. Fritz. 1976. A conceptual model of

watershed response to rainfall, developed through the use of oxygen-18 as a natural tracer. Canadian J. Earth Sci. 13: 271-283.

Sklash, M.G., and R.N. Farvolden. 1979. The role of groundwater in storm runoff. J. Hydrol. 43: 45-65.

Sklash, M.G., M.K. Stewart, and A.J. Pearce. 1986. Storm runoff generation in humid headwater catchments, 2. A case of hillslope and low-order stream response. Water Resources Research 22(8): 1273-1282.

Tsivoglou, E.C., R.L. O'Connell, C.M. Walter, P.J. Godsil, and G.S. Logsdon. 1965. Tracer measurements of atmospheric reaeration: 1. Laboratory studies. Journal of the Water Pollution Control Federation 37(10): 1343-1362.

Tsivoglou, E.C. 1967. Tracer measurement of stream reaeration. Federal Water Pollution Control Administration. Washington, D.C.

Tsivoglou, E.C. 1979. Laboratory studies of gas tracers for raeration: Discussion. Journal of the Environmental Engineering Division, Proceedings of the ASCE 105(EE2): 426-428.

Wadach, J.B. 1983. Detection of radon concentration in air, water, and soil using track etch detectors and liquid scintillation. M.S. Thesis, University of Maine, Orono, ME.

Wadach, J.B., and C.T. Hess. 1985. Radon-222 concentration measurements in soil using liquid scintillation and track etch. Health Physics 48: 805-808.

Weyman, D.R. 1970. Throughflow on hillslopes and its relation to the stream

hydrograph. Int. Assoc. Sci. Hydrol. Bull. 15: 25-33.

Weyman, D.R. 1973. Measurements of the downslope flow of water in a soil. Journal of Hydrology 20: 267-288.

Wilcock, R.J. 1984. Reaeration studies on some New Zealand rivers using methyl chloride as a gas tracer. In: Brutsaert, W., and G.H. Jirka (eds.), Gas Transfer at Water Surfaces, p. 413-420.

Yotsukura, N., D.A. Stedfast, R.E. Draper, and W.H. Brutsaert. 1983. An assessment of steady-state propane-gas tracer method for reaeration coefficients: Cowaselon Creek, New York. USGS Water Resources Investigations Report 83-4183.

Yotsukura, N., D.A. Stedfast, and G.H. Jirka. 1984. Assessment of steady-state propane gas tracer method for determining reaeration coefficients, Chenango River, New York. U.S. Geological Survey Water Resources Investigations Report 84-4368.

CHAPTER 2

Determination of Gas Exchange Rate Constants for a First Order Stream, Walker Branch Watershed, Tennessee

David P. Genereux and Harold F. Hemond

Abstract

The steady-state tracer gas method was used to determine gas exchange rate constants (k) for a first order stream draining the West Fork of Walker Branch Watershed in eastern Tennessee. Chloride was used as a conservative tracer to account for dilution by lateral inflow, and propane and ethane were used as volatile tracers. Gas exchange rate constants for propane (k_p) were about 100 day^{-1} over a wide range of flow conditions, while those for ethane (k_e) were about 117 day^{-1}; an equivalent rate constant for O_2 (k_{O2}) would be about 118-139 day^{-1}, depending on the method used for its calculation. These rate constants are much larger than those typically found in rivers and large streams. Much lower k_p values (about 50 day^{-1}) were found during one experiment conducted at low flow with much of the stream surface covered with floating leaves. Nineteen previously published empirical equations were used to predict k_{O2} values for one 72 m stream reach; agreement between the predicted and measured values was generally very poor. Because ethane and propane have similar gas exchange rates and similar aqueous diffusion coefficients (k_e/k_p and D_e/D_p are both close to 1, where D is the compound's diffusion coefficient), accurate determination of the exponent n in the relationship $k_e/k_p = (D_e/D_p)^n$ was not possible. The ratio k_e/k_p (1.17) is much closer to D_e/D_p (1.24) than to H_e/H_p (0.82, where H is the compound's Henry's Law constant), suggesting that stripping of dissolved volatiles by air bubbles was not a significant mode of gas exchange for the study stream.

1. Introduction

Small streams are the first places where much groundwater enters a surface drainage system, carrying what is often a large load of dissolved gases (CO_2, CH_4, radon, volatile pollutants, etc.). The combination of high gas content and potentially high gas exchange rates may make small streams important sites for fluxes of volatile compounds to the atmosphere. Knowledge of gas exchange rate constants (k) is essential to quantifying and ultimately predicting the transport and fate of both natural and pollutant gases in small streams. Studies in natural and artificial streams have produced many empirical equations for prediction of k from stream hydraulic characteristics (slope, depth, etc.). These equations were shown to be poor predictors of k values in many moderate and large natural streams in Massachusetts [Parker and Gay, 1987]. We suspected (and show in this paper) that the predictions for a small first-order stream are as inaccurate or even more so. Thus, determination of gas exchange rates for these streams must rely, at least at the present time, on direct measurement.

A convenient and widely used method of determining k values for flowing water bodies is the steady-state tracer gas method [Yotsukura et al., 1983; Duran and Hemond, 1984; Kilpatrick et al., 1987; Genereux and Hemond, 1990]. As the name suggests, the technique involves making a steady injection of a tracer gas into a stream. The concentration of the tracer gas in the streamwater (G) is then measured at two or more points downstream of the injection; the difference in G between the two measurement stations is used to estimate k. This technique has

been successfully applied to rivers and large streams, but studies of small first-order streams are lacking. We know of only two published measurements of k on first-order streams. Genereux and Hemond [1990] used propane to determine the gas exchange rate over a 34 m reach of a stream on Bickford Watershed in Massachusetts. Wanninkhof et al. [1990] used SF_6 to study gas exchange over a 282 m section of a stream on Walker Branch Watershed in Tennessee. With only one gas exchange experiment on each of two streams, and no studies covering a range of flow conditions on a single stream, little is known about gas exchange in first-order streams. For example, it is unclear which model of gas exchange (e.g., the surface renewal model or the stagnant boundary layer model) is most appropriate for first-order streams. Indeed, there may be as yet undescribed features controlling gas exchange in these streams. Little is known about the role bubbles may play in gas exchange in small streams, though the importance of bubbles has received much attention in studies of large open water bodies with breaking waves [Mémery and Merlivat, 1983; Jähne et al., 1984; Mémery and Merlivat, 1984]. Also, it is not known exactly how the various empirical equations for prediction of k perform on these streams.

For these reasons, and to provide supporting gas exchange data for the ^{222}Rn work described in Chapter 4, we used the steady-state tracer gas method to determine k values for four reaches of a first-order stream draining the West Fork of Walker Branch Watershed in eastern Tennessee (the same stream studied by Wanninkhof et al. [1990]).

2. Study Site

The West Fork of Walker Branch Watershed is a 38.4 ha forested catchment in Oak Ridge, Tennessee (Fig. 1). The forest cover is predominantly deciduous (oak, hickory, beech, tulip poplar). Mean annual air temperature is 14.5°C, and mean annual rainfall is 139 cm [Johnson and van Hook, 1989]. Watershed soils are mainly Ultisols (Paleudults, Hapludults) and Alfisols (Hapludalfs) [Lietzke, 1990], and bedrock consists of fractured dolomite with chert beds. The watershed is drained by a first-order "pool-and-riffle" stream. Streamflow is measured with a 120° V-notch weir at the basin outlet, and the upstream limit of perennial flow is about 350 m upstream of the weir. Positions in the stream are designated by their distance (in meters) upstream of the weir, preceded by the prefix "WB" (e.g., WB60 is the point 60 m upstream of the weir). The four stream reaches studied were WB300-WB242, WB242-WB170, WB170-WB100, and WB100-WB60. When streamflow at the weir (Q_{weir}) dropped below about 1000 L/min, the extremely low flow above WB242 precluded study of the uppermost reach.

Figure 2 shows an elevation profile for the stream. The stream flows directly over bedrock for most of the lower 200 m, while above WB200 the channel bottom is covered with gravel and coarse sand. Mean gradient between WB300 and WB0 is 0.038. The presence of rocks and woody debris of various sizes, and irregular weathering of exposed bedrock, make the channel geometry highly complex. Channel width is irregular, averaging about 3 m and varying between 1

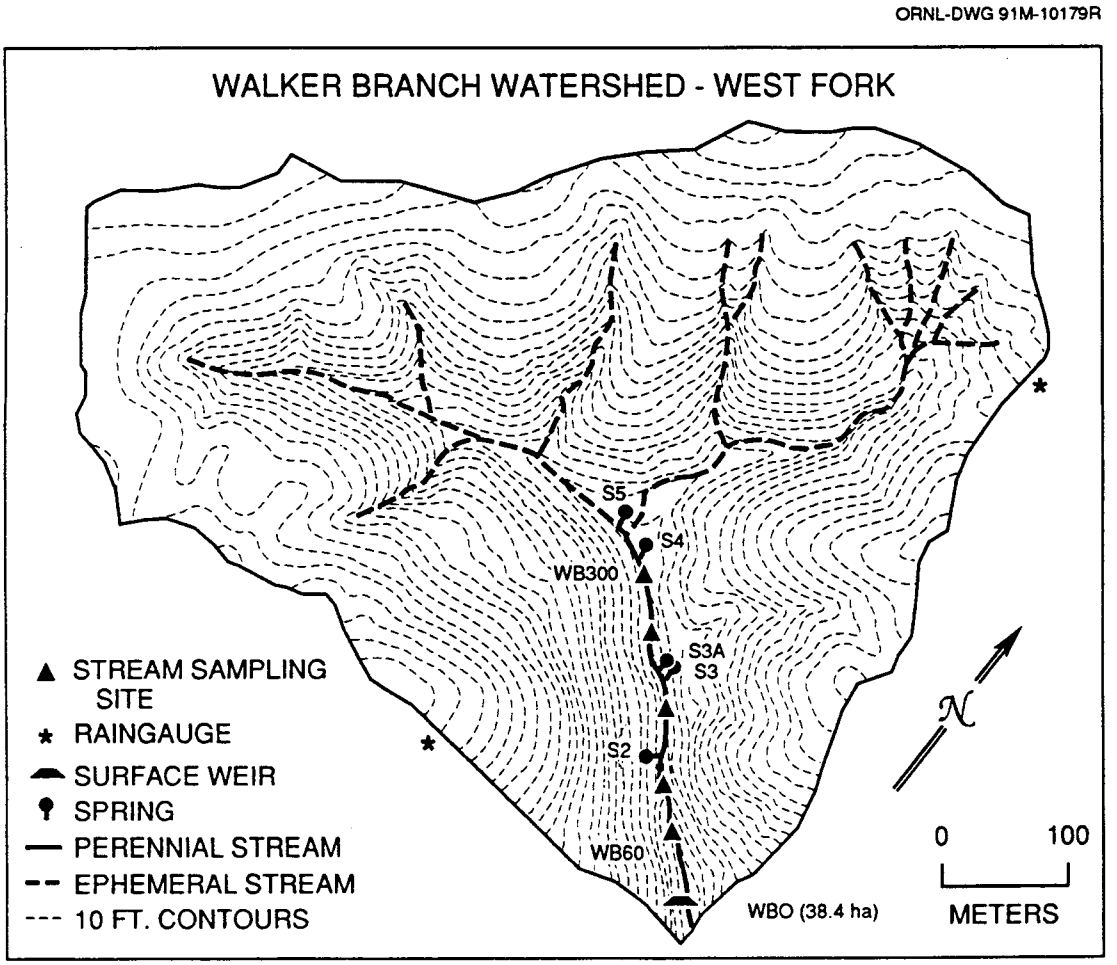

Figure 1. Contour map of the West Fork of Walker Branch Watershed. Triangles indicate the five stream sampling sites which served as the ends of the study reaches. Two of the triangles (WB60 and WB300) are labeled with the prefix "WB" followed by their distance upstream of the weir in meters. The other three triangles represent the sites WB100, WB170, and WB242.

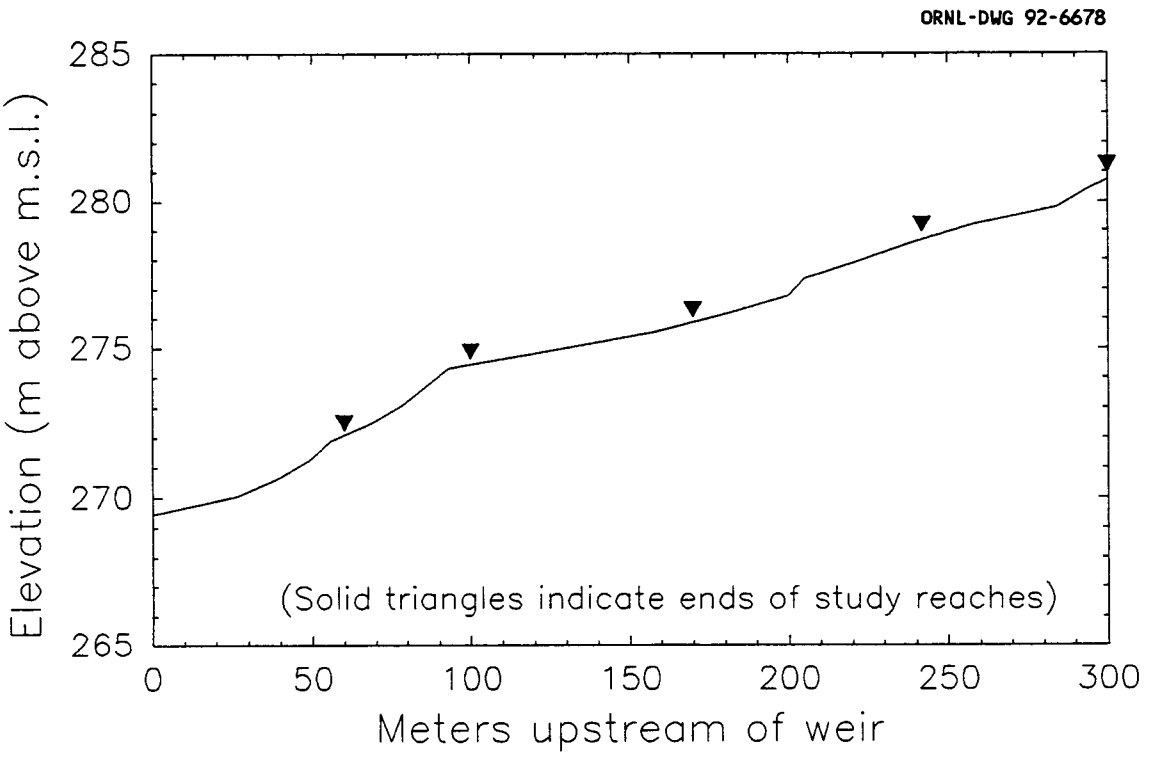

Figure 2. Elevation profile of the study stream.

and 6 m (Fig. 3). Streamwater depth varies from about 1 cm at some riffles and small waterfalls to about 30 cm in the largest pools; average depth is roughly 10 cm. Stream depth and width obviously change with streamflow, but the temporal variability in these parameters is considerably smaller than the spatial variability. Stream width may vary by a factor of 6 from place to place at a given time, and stream depth by a factor of 30; however, width and depth at a given stream site vary by factors of only about 1.2 and 3, respectively.

3. Field and Laboratory Methods

Nine experiments were done between September 1989 and August 1990. The tracer gas used was HD-5 liquified petroleum gas, which consists mainly of propane (about 95%). The relatively large ethane content of HD-5 (about 4%) allowed simultaneous determination of gas exchange rates for ethane and propane (k_e and k_p, respectively). A standard 20 lb (9 kg) HD-5 tank was used; 0.1-1 kg of gas was injected during each experiment. Tracer gas was bubbled into the stream through a circular glass frit having a diameter of 25 mm and a pore size of 5-15 μm. Gas pressure was set at 20-35 kPa with a single-stage regulator, and remained constant through the course of each injection.

For the experiments done at low flow (Q_{weir} < 1000 L/min), a flat piece of styrofoam (40 x 40 cm) was floated on the stream surface, with its upstream edge directly above the bubbling frit. A small branch was laid across the stream, just above the water surface, to keep the styrofoam in place. This styrofoam plate

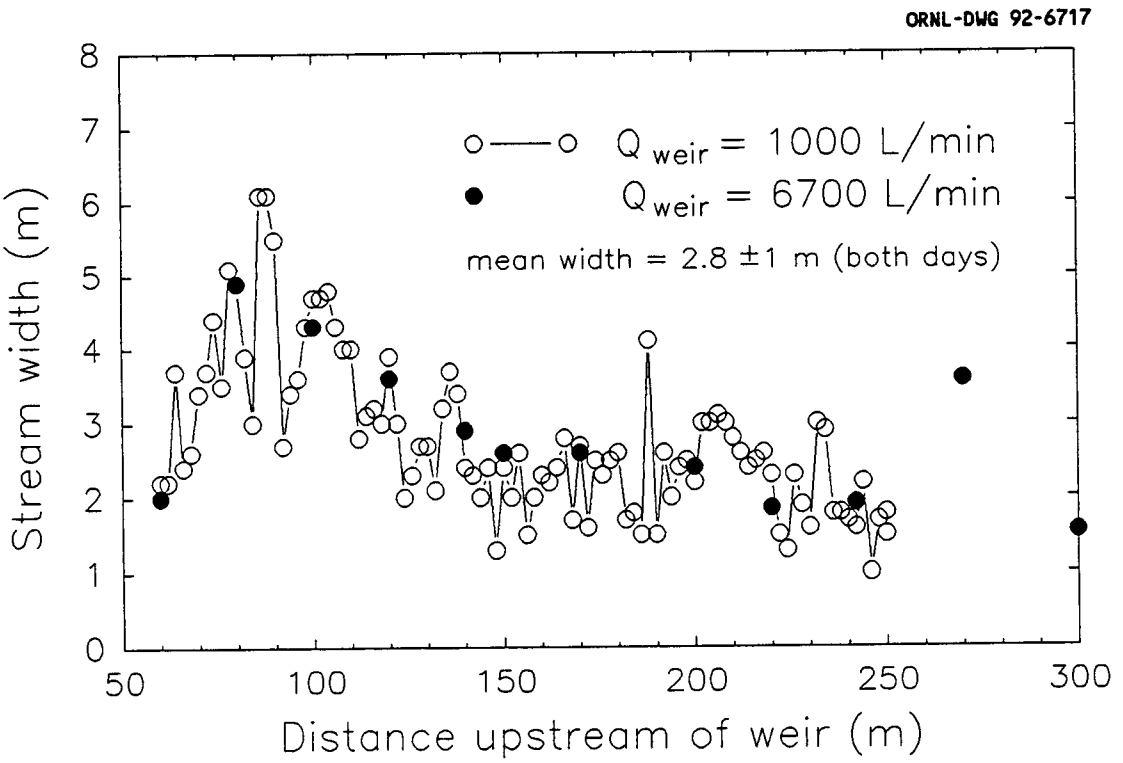

Figure 3. Width of the study stream on two different days with different streamflow rates.

acted as a barrier to delay the loss of tracer gas bubbles from the stream at the injection site. By holding these bubbles in the stream for an extra few seconds, it was possible to dissolve more tracer gas in the streamwater, making measurement of propane and ethane concentrations in the streamwater somewhat easier and more accurate.

Chloride was used as a conservative tracer to account for lateral inflow to the stream (e.g., Genereux and Hemond [1990]). Steady injections of Cl^- were made by dripping concentrated (about 3 M) NaCl solutions from a 50 liter Marriotte bottle. The tracer gas and Cl^- injections were generally made at the same site, about 15 m upstream of the nearest measurement station; this distance was more than adequate for thorough vertical and horizontal mixing of the tracers, allowing a one-dimensional data analysis to be used [Genereux and Hemond, 1990]. Twice (on 3/7/90 and 3/18/90) the tracer gas injection was made at WB317 (nearest measurement station WB300) and the Cl^- injection at WB254 (nearest station WB242). For these two experiments, the streamflow at WB300 (Q_{300}) was measured with a flume. An "equivalent conservative tracer concentration" at WB300, C_{300}, was then estimated as Q_oC_o/Q_{300}, where Q_o is the tracer solution injection rate (determined in the field with a stopwatch and graduated cylinder) and C_o is the tracer solution concentration (determined by knowing the quantity of water and NaCl used in preparing the solution).

Before the Cl^- and tracer gas injections were started, the background electrical conductivity (γ_b) of the streamwater was measured and streamwater

samples for Cl^- analysis were collected at each measurement station. The Cl^- and tracer gas injections were begun within a few minutes of each other, and γ was monitored to determine when the tracer concentrations reached steady-state. Once steady-state was achieved at a given measurement station (i.e., once a steady γ value, γ_s, was recorded for >10 minutes), three or four streamwater samples were collected for Cl^- analysis. Four 40 ml streamwater samples for propane and ethane analysis were then taken. (During the 3/7 and 3/18 experiments, when the tracer gas injection was made about 60 m upstream of the Cl^- injection, tracer gas samples were taken 30-40 minutes after γ reached steady-state. This period, 2-4 times the travel time through WB300-WB242, provided enough time for the tracer gas concentrations to reach steady-state.) These samples were collected in 50 ml wetted ground-glass syringes. To avoid damaging the syringes with suspended sediment, the samples were filtered with 0.8 μm filters during collection. Samples were packed in ice within a few minutes of collection, and were left on ice overnight.

Conservative tracer concentrations were estimated by two independent methods. The Cl^- concentration of streamwater samples (both steady-state, S_s, and background, S_b) was measured with an automated ferricyanide method (U.S. EPA [1983]), using a Technicon TRAACS 800 auto-analyzer. The steady-state samples were diluted with doubly distilled water prior to analysis, to bring their Cl^- contents into the range spanned by the calibration standards. Results were used to calculate the difference between steady-state and background Cl^- content (S_s-S_b). In addition,

since only relative determinations of the conservative tracer concentration were needed, γ_s-γ_b was used directly as an index of the concentration of injected tracer Cl^-. These two indices of tracer Cl^- (S_s-S_b and γ_s-γ_b) gave results which were not significantly different; each was used to calculate a value of the gas exchange rate constant for each reach on each experiment, and the two values were then averaged. Thus, each value of k reported in Table 1 is the average of a value based on γ_s-γ_b as a measure of conservative tracer concentration and a value based on S_s-S_b as a measure of conservative tracer concentration.

Propane and ethane analyses were done at about midday, the day after each field experiment. The samples were removed from ice and a known amount of helium (6-7 ml) was introduced into each syringe. The helium and water were allowed to equilibrate at room temperature for 2-3 hours; each syringe was shaken periodically during this time. Using a sample loop, 1.0 ml of the helium headspace in each syringe was injected into a Perkin Elmer 3920B gas chromatograph equipped with a flame ionization detector. Helium was used as the carrier gas, and a packed column (6 feet long, 2 mm I.D., packed with 80/100 mesh Porapak Q) was employed. Oven temperature was 120°C; retention times were 1.0 minutes for propane and 0.5 minutes for ethane. Peak areas were integrated with a Hewlett-Packard 3390A electronic integrator. Standard literature data on the partitioning of propane and ethane between water and air [Hayduk, 1982; Hayduk, 1986] were used to relate measured peak areas to aqueous (streamwater) concentrations. A standard helium:propane mixture from Scott Specialty Gases

was used to verify that the gas chromatograph was responding consistently.

The gas exchange rate constant k (units of time^{-1}) is calculated from the steady-state tracer gas concentration (G) and conservative tracer concentration (C, equal to γ_s-γ_b or S_s-S_b) as follows:

$$k=(\frac{1}{\tau})\ln(\frac{G_1C_2}{G_2C_1}) \quad (1)$$

where τ is the travel time through the stream reach of interest, and the subscripts 1 and 2 designate the upstream and downstream ends, respectively, of the reach [Genereux and Hemond, 1990]. τ values were determined by measuring the increase in γ with time during the Cl^- injections. The "time to half height" is defined as the time at which $\gamma = \gamma_b + \frac{1}{2}(\gamma_s-\gamma_b)$, and τ for a given reach was determined as the difference in the time to half height for the two ends of the reach. For three experiments (WB170-WB100 on 4/13/90 and 5/7/90, and WB242-WB170 on 5/7/90) during which the rising portions of the γ vs. time curves were not recorded, τ was estimated from an empirical curve of τ vs. Q_{avg} (Fig. 4) based on results from other experiments ($Q_{avg} = (Q_1+Q_2)/2$).

4. Ethane Gas Exchange Rates

Simultaneous determination of gas exchange rate for two gaseous tracers could be useful in revealing how k depends on D, the aqueous diffusion coefficient of the tracer gas (e.g., whether $k \propto D$, as the stagnant boundary layer model of gas

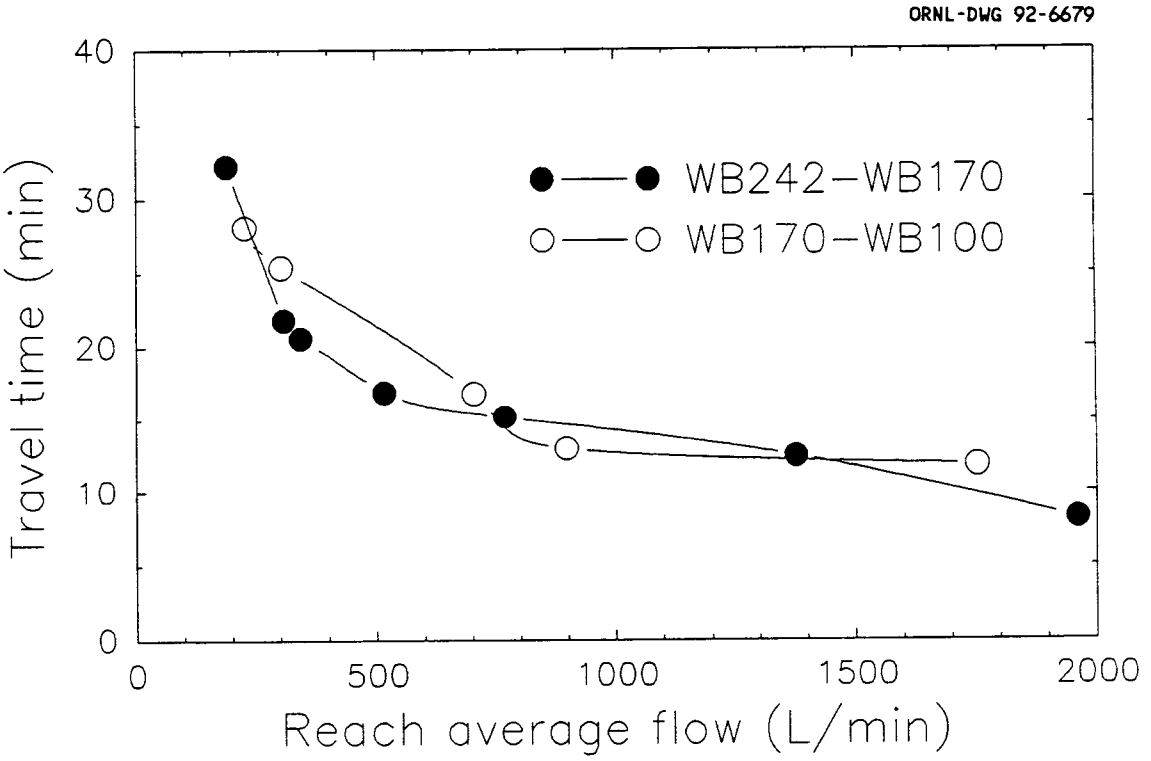

Figure 4. Travel time as a function of reach-average flow for the reaches WB170-WB100 and WB242-WB170. Reach-average flow is the average of the flow values determined (by Cl^- dilution) at the two ends of the reach.

exchange predicts, or $k \propto D^{0.5}$, as the surface renewal theory predicts [Bennett and Rathbun, 1972]). The ethane content of the injected gas was sufficient to produce measurable ethane concentrations in most of the samples analyzed for propane. However, determination of gas exchange rates for ethane was complicated somewhat by the slightly unsteady nature of the ethane injections.

Liquid ethane has a significantly higher vapor pressure than liquid propane (about 4 times as high at 25°C [Weast, 1976]). As a result, the mole fraction of ethane in the gas in equilibrium with the HD-5 liquid (y_e) is about 4 times the mole fraction of ethane in the HD-5 liquid (x_e). Thus as gas is removed from the tank, ethane is preferentially volatilized from the remaining liquid, and the injection rate of ethane decreases with time (even though the total gas injection rate remains constant). Gas evolution from the tank may be thought of as essentially a Rayleigh distillation in which increments of vapor are formed and immediately removed from contact with the original liquid. Fig. 5 shows how x_e would theoretically vary with the amount of residual HD-5 liquid in the tank; the figure is based on the standard Rayleigh distillation equation [e.g., King, 1980, p. 117] and vapor pressure data from Weast [1976] at about room temperature.

Of course, if the total gas injection rate remains constant and x_e continually decreases, x_p (mole fraction of propane in the residual liquid) must continually increase. While this unsteadiness may be important for ethane, since there may be large relative changes in x_e, it is not important for propane, because x_p is large (0.96-1.0) and undergoes very small relative changes.

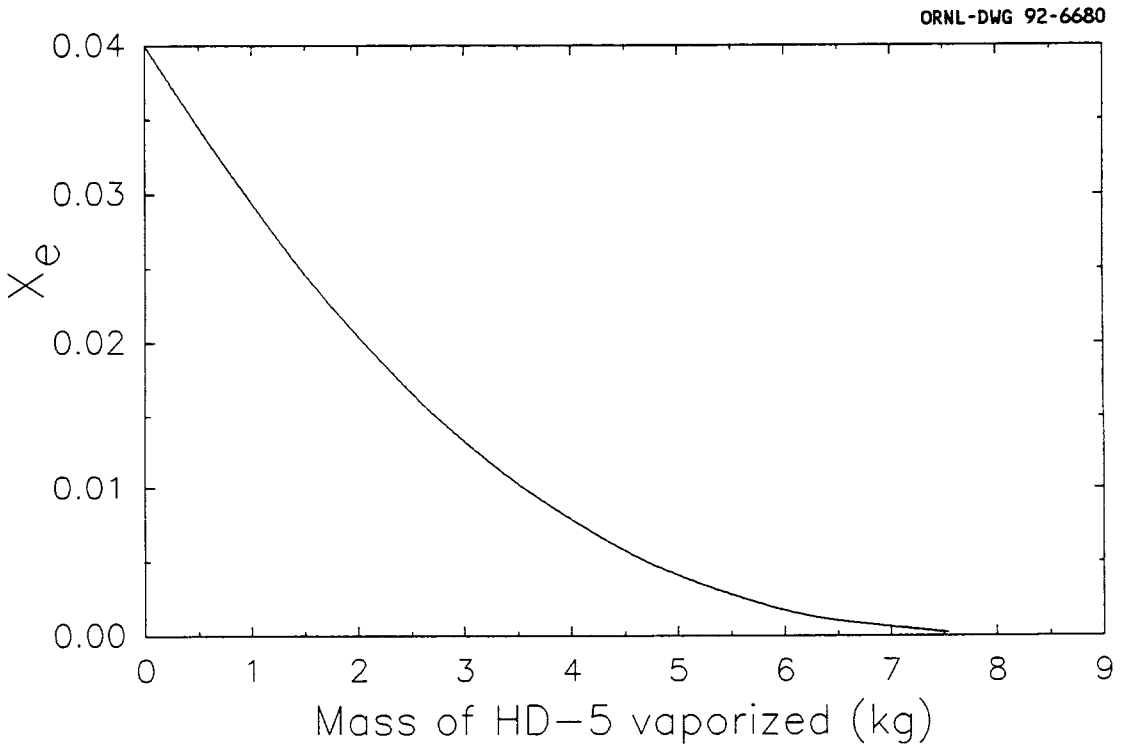

Figure 5. Mole fraction of ethane in HD-5 liquefied petroleum gas (x_e) as a function of mass of HD-5 vaporized. The curve is based on an initial x_e of 0.04, an initial x_p (mole fraction of propane in the HD-5 liquid) of 0.96, and an initial mass of HD-5 of 9 kg (roughly the capacity of the small tank used in this study). The curve was calculated using the Rayleigh distillation equation (e.g., King [1980], p.117). A value of 4 was used for the selectivity coefficient (ethane/propane mole ratio in the gas phase divided by ethane/propane ratio in the residual HD-5 liquid phase); this value is based on vapor pressure data at about 25°C in Weast [1976].

There are two conceptually different problems which arise in trying to determine the ethane gas exchange rate given the slowly decreasing ethane injection rate: each element or parcel of streamwater passing the injection point receives a slightly smaller injection of ethane than the parcel before, and because of this there is at least the possibility that transport by longitudinal dispersion (unimportant in a truly steady-state analysis) may not be insignificant.

The first issue was addressed by limiting determination of k_e values to those experiments during which ≥3 kg of liquid remained in the tank, thus avoiding that portion of the distillation curve (see Fig. 5) where relative changes in x_e are large. Experiments excluded by this criterion would generally not have yielded useful k_e data even in the absence of unsteadiness, since the low x_e (and hence low ethane injection rate) resulted in streamwater ethane concentrations near the limit of detection. The set of experiments for k_e determination was further limited by excluding those for which the gas tracer sampling times at the ends of the reach were not within $\tau \pm 15$ minutes of each other. This guaranteed that the parcel of streamwater sampled at the downstream end of the reach received essentially the same input of ethane as the parcel sampled at the upstream end (Fig. 5 shows that at a typical injection rate of 0.05 kg of HD-5 per hour, with ≥3 kg of residual liquid, x_e can change by no more than 1% in 15 minutes).

The second issue, the importance of ethane transport by longitudinal dispersion, was evaluated by estimating the magnitude of the terms on the left-hand side of the following one-dimensional transport equation:

$$\frac{\partial E}{\partial t} + u\frac{\partial E}{\partial x} + kE - D_L\frac{\partial^2 E}{\partial x^2} \qquad (2)$$

or, in finite difference form:

$$\frac{\Delta E_{avg}}{\Delta t} + u_{avg}\frac{\Delta E}{\Delta x} + kE_{avg} - D_L\frac{\Delta(\Delta E)}{\Delta(\Delta x)} \qquad (3)$$

where E = ethane content of streamwater

E_{avg} = average of E at the two ends of the reach

t = time

x = distance along channel (positive downstream)

u_{avg} = average velocity of streamflow

k = gas exchange rate constant

D_L = longitudinal dispersion coefficient

For experiments meeting the criteria given in the previous paragraph, it was found that the advection and gas exchange terms approximately canceled each other; each was about 10x larger than $\Delta E_{avg}/\Delta t$, and about 20x larger than the sum of the left-hand side terms (i.e., the dispersion term). Thus, ethane transport by longitudinal dispersion is unimportant for experiments meeting the criteria of the previous paragraph.

5. Results and Discussion

The results from the Cl^- injections are themselves of hydrologic interest,

since they demonstrate the variability in stream inflow. These results are discussed in detail in Chapter 3.

In order to more directly assess the spatial variability in gas exchange rate and its possible relation to streamflow rate, temperature effects were accounted for by correcting k values to 20°C. The following equation was used for temperature correction:

$$k(20°) = k(T_{avg})\,\Theta^{(20-T_{avg})} \qquad (4)$$

[Elmore and West, 1961; Metzger, 1968] where T_{avg}, the average temperature of streamwater in the reach of interest, was set equal to $(T_1+T_2)/2$. The value of Θ was determined using the method suggested by Metzger [1968]. Using a typical $k(T_{avg})$ of 100 day^{-1} for propane (see below) and an approximate stream depth of 10 cm, Fig. 2 of Metzger [1968] gives $\Theta=1.005$. The same value of Θ was used for ethane, since the small difference in propane and ethane gas exchange rates (about 10%; see below) would lead to a negligible difference (<1%) in Θ values for the two gases, based on Fig. 2 of Metzger [1968]. Since all experiments were done at stream temperatures of 10°-20° C, the temperature correction was small (a few percent, at most).

Since only relative changes in tracer concentrations (G_1/G_2, C_2/C_1) are needed to determine k, the only relevant uncertainty issues for the tracer measurements are those concerning linearity and precision (absolute accuracy is unimportant). Of the two relevant concerns, precision is by far the largest source

of uncertainty (the flame ionization detector of the gas chromatograph has a linear dynamic range of 10^5-10^8 [Peters et al., 1974, p.576], while propane concentrations spanned a range of about 5 x 10^2; the response of the TRAACS instrument, and the relationship between γ and Cl^- concentration, are both highly linear over the ranges encountered in this study). While precision varied somewhat from site to site, and from experiment to experiment, the typical relative standard deviation of propane and ethane replicates was about 4%, while that of Cl^- estimates (from both of the methods described earlier) was about 2%. While unimportant with regard to tracer concentrations, accuracy was important in estimating travel time. Closely spaced (usually 30 seconds, sometimes 60 seconds) measurements on the rising limbs of the conductivity curves allowed accurate ($\pm$0.2 min) determination of time-to-half-height values. The total uncertainty in the travel time values was about 0.5 minutes. Using standard methods (Kline [1985], Eqn. B.4) to propagate this uncertainty and that in the tracer concentrations lead to typical uncertainties (95% confidence) of about $\pm$13% for the k values. The most uncertain k value ($\pm$26%) was that for propane in reach WB100-WB60 on 3/18/90, while the least uncertain (6%) was that for propane in reach WB242-WB170 on 8/28/90.

With the exception of the 11/1/89 data, the k values (either ambient or temperature corrected) show very little variability, spatial or temporal (Table 1). The average of all temperature corrected values is 100 ± 18 day^{-1} for propane, 117 ± 8 for ethane (uncertainty is the standard deviation of the values in Table 1). While the stream may be more turbulent at higher flows, this does not result in

Table 1. Gas exchange rate constants. The first column gives the streamflow rate at the weir (L/min). The reaches are defined as follows: 1=WB300-WB242; 2=WB242-WB170; 3=WB170-WB100; 4=WB100-WB60; 5=WB242-WB60; 6=WB300-WB100. Q_{avg} and T_{avg} are the reach average streamflow (L/min) and water temperature (°C), respectively; they are simply averages of values measured at the ends of the reach. τ is the travel time through the reach in minutes. F is defined as $\ln(G_1C_2/G_2C_1)$ (G and C are defined in the text). $k(T_{avg})$ is the rate constant determined at the ambient temperature, k(20) is the $k(T_{avg})$ value corrected to 20°C; all k values are in day^{-1}. R_k is the ratio $k_e(20)/k_p(20)$ (the ratio of the ethane to propane rate constants at 20°C).

						Propane			Ethane			
Q_{weir}	Date	Reach	Q_{avg}	T_{avg}	τ	F	$k(T_{avg})$	k(20)	F	$k(T_{avg})$	k(20)	R_k
302	9/8/89	3	213	16.9	28.1	1.958	100	102	2.245	115	117	1.15
354	11/1/89	2	178	13.6	47.8	1.825	55.0	56.8				
		3	306	13.4	38.6	1.255	46.8	48.4				
		4	312	13.1	23.7	0.906	55.0	57.0				
		5	194	13.4	110	3.986	52.1	53.9				
411	8/28/90	2	192	17.6	32.2	2.296	103	104				
		3	309	17.6	25.4	1.689	95.7	96.9				
		4	326	18.1	15.2	1.278	121	122				
		5	210	17.8	72.8	5.263	104	105				
680	4/13/90	2	322	14.2	21.8	1.526	101	104				
		3	475	15.3	21.2	1.268	86.1	88.2	1.540	105	107	1.21
1050	3/7/90	2	548	13.0	16.9	1.144	97.5	101				
		3	743	13.4	16.8	0.874	74.9	77.3				

Table 1 (cont.)

1368	10/4/89	1	578	16.4	13.3	0.845	91.5	93.2	1.017	110	112	1.20
		2	760	16.1	15.2	1.056	100	102	1.250	118	121	1.18
		3	892	15.8	12.9	0.934	104	106	0.975	109	111	1.05
		6	709	16.1	41.4	2.835	98.6	101	3.242	113	115	1.14
1447	5/7/90	1	573	14.1	12.4	0.849	98.5	101				
		2	774	14.4	15.1	0.911	86.9	89.4	1.129	108	111	1.24
		3	962	14.5	12.9	0.998	111	114	1.131	126	130	1.13
		6	761	14.3	40.4	2.752	98.3	101				
2749	11/17/89	1	1134	13.3	9.3	0.922	143	148				
		2	1357	13.2	12.4	0.710	82.4	85.3				
		3	1539	12.9	11.8	0.490	59.8	62.0				
		6	1330	13.1	33.5	2.122	91.2	94.4				
3457	3/18/90	2	1980	14.0	8.2	0.545	95.7	98.6				

higher gas exchange rates. The increase in stream depth may offset the effects of increased turbulence.

Propane gas exchange rate constants measured on 11/1/89 were about half the magnitude of those determined on other days. On 11/1/89, a large portion of the stream surface was covered with floating leaves from the recent leaf fall. A crude visual estimate of the fraction of stream surface covered was 0.5±0.2. This floating leaf cover seems the most likely reason for the lowered gas exchange rates. Floating leaves could act as a direct diffusive barrier, decreasing the surface area available for gas exchange. In addition, floating leaves may dampen surface turbulence, thus increasing the thickness of the stream's stagnant surface boundary layer and slowing gas exchange.

Most models of gas exchange predict that $k_1/k_2 = (D_1/D_2)^n$, with $0.5 \leq n \leq 1$ [Bennett and Rathbun, 1972]. As noted earlier, the surface renewal and stagnant boundary layer models predict n=0.5 and n=1, respectively. Based on the data of Witherspoon and Bonoli [1969], $D_e/D_p = 1.24 \pm 0.07$ (error is the one s.d. precision of replicates). The few available measurements of k_e from this study suggest that $k_e/k_p = 1.16 \pm 0.06$ (one s.d.), giving n=0.7. However, given the uncertainty in k_e/k_p (5.2%) and D_e/D_p (5.6%), and the fact that both ratios are very close to 1, the estimate of n has a very large uncertainty (±0.9). Hence, these results can not be used to assess whether the surface renewal or stagnant boundary layer model is more appropriate for the study stream.

Studies of gas exchange in rivers and large streams generally report k_{O2}, the

gas exchange rate constant for O_2 (this is often designated "K_2"). To facilitate comparison with these other studies, we used two independent ways of relating the k_p values measured in this study to k_{O2} values:

Method 1: Laboratory experiments have shown that $k_p/k_{O2} = 0.72$ over a wide range of mixing conditions [Rathbun et al., 1978]. Applying the common assumption that rate constant ratios are the same in different water bodies (e.g., laboratory apparatus and natural streams) gives an average k_{O2} value of 139 day^{-1} for the study stream.

Method 2: The equation $k_{O2} = k_p(D_{O2}/D_p)^n$ was used to estimate k_{O2}. There is substantial variability among literature values of D_p ($0.68x10^{-5}$ to $1.81x10^{-5}$ cm^2/sec) and D_{O2} ($1.76x10^{-5}$ to $2.3x10^{-5}$ cm^2/sec) at 20-25°C [Baird and Davidson, 1962; Unver and Himmelblau, 1964; Wise and Houghton, 1966; Witherspoon and Bonoli, 1969]. Only the ratio D_{O2}/D_p is needed, and the best way of obtaining an accurate estimate of this ratio is by using D_{O2} and D_p values measured with the same technique in the same study. For this reason, data from Wise and Houghton [1966] ($D_{O2} = 2.3x10^{-5}$, $D_p = 1.81x10^{-5}$) were used. If 0.7 is accepted as the best estimate of n, average k_{O2} is estimated to be 118 day^{-1} (n values of 0.5 and 1 lead to k_{O2} values of 113 and 127 day^{-1}, respectively).

Given the present state of knowledge concerning gas exchange in streams, we consider both of these methods to be reasonable. Though there is a large uncertainty in n, the estimate of k_{O2} obtained by the second method is reasonably

insensitive to n over the range of most reasonable values ($0.5 \leq n \leq 1$). As Wanninkhof et al. [1990] point out in their Table 1, rate constants of 110-140 day^{-1} are much higher than the k_{O2} values that have been found for rivers and large streams (0.3-15 day^{-1}). As noted in the introduction, these high rate constants make small streams important sites for gas exchange.

In applying the steady-state tracer gas method to a reach (WB332-WB50) of the same stream studied here, Wanninkhof et al. [1990] determined a gas exchange rate constant of 70 day^{-1} for SF_6 at 13.5°C (72 day^{-1} corrected to 20°C with the method described earlier). They went on to estimate a value of 134 day^{-1} for k_{O2} (at 25°C), in apparent close agreement with the k_{O2} estimates from this study. However, Wanninkhof et al. [1990] derived their k_{O2} estimate by assuming that $k_{O2} = k_{SF6}(D_{O2}/D_{SF6})^{0.5}$ (data in their paper suggest that a value of 3.74 was used for D_{O2}/D_{SF6}, though this was not stated and no citation is given for the diffusivities). As noted earlier, n=0.5 can not be ruled out by our k_e/k_p data. However, using n=0.7, k_{SF6}=72 day^{-1}, and D_{O2}/D_{SF6} =3.74 gives k_{O2}=176 day^{-1}. This estimate of k_{O2} must be seen as highly uncertain, since the large D_{O2}/D_{SF6} ratio makes the estimated k_{O2} value highly sensitive to n, which has a large uncertainty. Thus results from this study are not necessarily inconsistent with the measurement reported by Wanninkhof et al. [1990].

Predictive empirical equations for k_{O2} have been generated by many experimental studies of gas exchange in natural and artificial streams. These predictive equations generally express k_{O2} as a function of water velocity (u), water

depth (d), and channel slope (w). In order to see how well these equations could predict the results from our study stream, we used the 19 equations compiled by Parker and Gay [1987] to predict k_{O2} for reach 2 (WB242-WB170) for seven of the eight days on which experiments were done in this reach (11/1/89 was excluded because of the complications with leaves mentioned earlier). The 19 equations are listed below; in addition to u, d, and w, some also contain the Froude number (N), friction velocity (u^*), the difference in elevation between the ends of the reach (ΔH), and the travel time (τ). The equations as transcribed from Parker and Gay [1987] require u and u^* in ft/s, d and ΔH in ft, and τ in hours, and give k_{O2} in day^{-1}.

Dobbins [1965]:

$$k_{O2} = \frac{116.6(1+N^2)(uw)^{0.375}}{d\sqrt{(0.9+N)}} \coth \frac{4.1(uw)^{0.125}}{\sqrt{(0.9+N)}} \tag{5}$$

O'Connor and Dobbins [1958]:

$$k_{O2} = \frac{12.81\sqrt{u}}{d^{1.5}} \tag{6}$$

Krenkel and Orlob [1963]:

$$k_{O2} = \frac{234.5(uw)^{0.404}}{d^{0.66}} \tag{7}$$

Cadwallader and McDonnell [1969]:

$$k_{O2}=\frac{336.8\sqrt{uw}}{d} \tag{8}$$

Parkhurst and Pomeroy [1972]:

$$k_{O2}=\frac{48.39(1+0.17N^2)(uw)^{0.375}}{d} \tag{9}$$

Bennett and Rathbun [1972]:

$$k_{O2}=\frac{106.16u^{0.413}w^{0.273}}{d^{1.408}} \tag{10}$$

Churchhill et al. [1962]:

$$k_{O2}=\frac{0.03453u^{2.695}}{d^{3.085}w^{0.823}} \tag{11}$$

Lau [1972]:

$$k_{O2}=\frac{2515(u^*)^3}{u^2d} \tag{12}$$

Thackston and Krenkel [1969]:

$$k_{O2}=\frac{24.94(1+\sqrt{N})u^*}{d} \tag{13}$$

Langbein and Durum [1967]:

$$k_{O2} = \frac{7.61u}{d^{1.33}} \tag{14}$$

Owens et al. [1964]:

$$k_{O2} = \frac{23.23u^{0.73}}{d^{1.75}} \tag{15}$$

Owens et al. [1964]:

$$k_{O2} = \frac{21.74u^{0.67}}{d^{1.85}} \tag{16}$$

Churchill et al. [1962]:

$$k_{O2} = \frac{11.57u^{0.969}}{d^{1.673}} \tag{17}$$

Isaac and Gaudy [1968]:

$$k_{O2} = \frac{8.62u}{d^{1.5}} \tag{18}$$

Negulescu and Rojanski [1969]:

$$k_{O2} = 10.92(u/d)^{0.85} \tag{19}$$

Padden and Gloyna [1971]:

$$k_{O2} = \frac{6.87u^{0.703}}{d^{1.054}} \tag{20}$$

Bansal [1973]:

$$k_{O2} = \frac{4.67u^{0.6}}{d^{1.4}} \tag{21}$$

Bennett and Rathbun [1972]:

$$k_{O2} = \frac{20.19u^{0.607}}{d^{1.689}} \tag{22}$$

Tsivoglou and Neal [1976]:

$$k_{O2} = \frac{1.296\Delta H}{\tau} \tag{23}$$

ΔH (2.9 m) was determined from a topographic map; the value of channel slope (w) was 2.9/72=0.04. Water velocity (u) for the reach during each experiment was calculated as the reach length (72 m) divided by the travel time (given in Table 1). Average water depth (d) was estimated as average volumetric flow (Q_{avg}; Table 1) divided by the product ub, where b is the average width of the reach (about 2.2 m, assumed to be constant; see Fig. 3). Froude number (N) and friction velocity (u^*) were calculated as in Parker and Gay [1987]: $N = u/(gd)^{0.5}$ and $u^* = (gdf)^{0.5}$ (g = acceleration due to gravity). Each "true" k_{O2} value plotted

in Fig. 6 is an average of two values; the two values were obtained by using the two methods described earlier to convert the measured k_p value to an equivalent k_{O2}.

Results (Fig. 6) show that none of the predictive equations reproduces the observed behavior (i.e., the nearly constant k_{O2}). Many of the equations predict that k_{O2} should change substantially with flow; others predict small changes with flow, but most of these equations show large negative offsets from the experimental results. In general, k_{O2} values are underpredicted, the exceptions being Eqns. 8, 15, 16, and 22 at low flow and Eqns. 10 and 12 under all conditions (results from Eqn. 12 are not shown in Fig. 6, as the numbers are 60-600 times larger than the true values). It appears that direct measurement is necessary for accurate determination (e.g., ±20% or better) of gas exchange rates for our stream.

The k_e/k_p data from this study can be used to evaluate the importance of ebullition as a mechanism of gas exchange in the study stream. In traditional models of gas exchange in natural water bodies, a key process is the diffusion of the compound of interest through water at the air:water interface; hence, a compound's aqueous diffusion coefficient is a key parameter. However, a different mode of gas exchange could be important for streams having complex channel geometries (such as the stream in this study), where flow takes place over small waterfalls and around irregularly shaped objects. Flow through such a complex channel is highly turbulent, and small bubbles of air may be forced into the stream in some places. A continual input of air bubbles might effectively strip dissolved

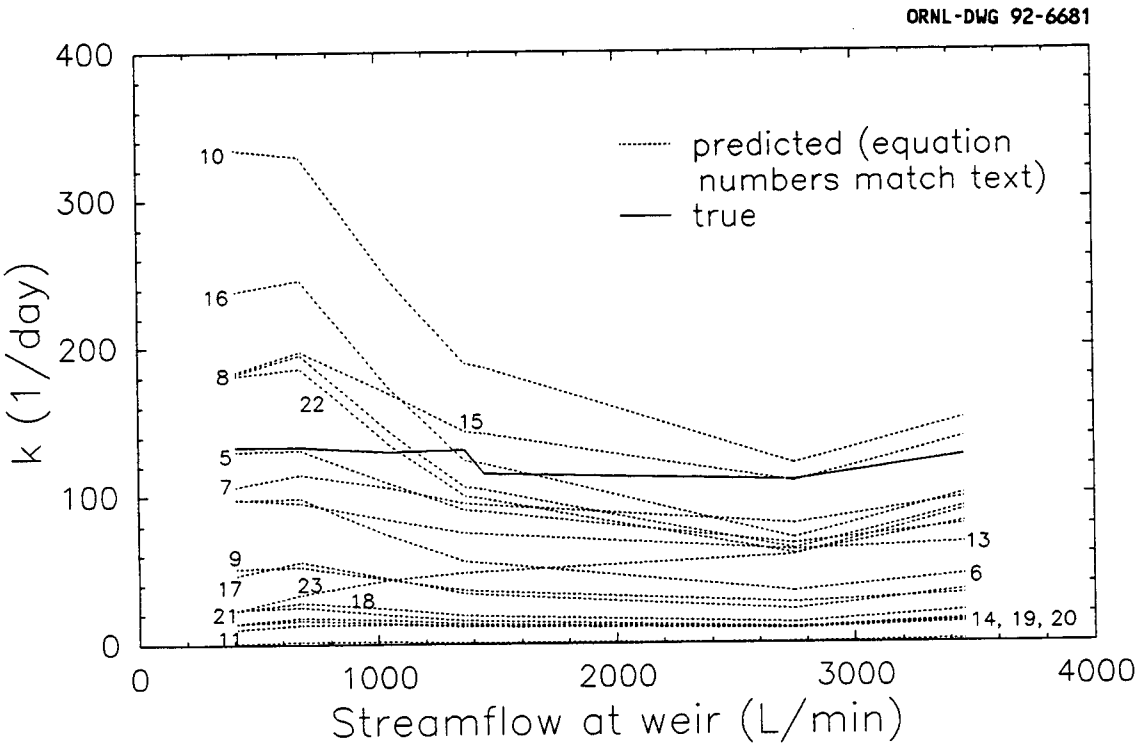

Figure 6. Comparison of predicted and true values of k_{O2} for reach 2 (WB242-WB170) for seven of our experiments. Predicted values were generated by using 19 previously published empirical equations which relate k_{O2} to stream hydraulic characteristics; each dashed line represents a different empirical equation. True values were obtained by using the two methods described above in the text to convert measured k_p values to k_{O2} values and then averaging the two k_{O2} values obtained for each experiment.

gases from the streamwater, since these bubbles could rapidly acquire volatile compounds and transport them to the stream surface where they would be released to the air as the bubbles break. In a stream dominated by this mode of gas exchange, with injected air bubbles rapidly equilibrating with the streamwater, the ratio k_e/k_p would be more closely related to H_e/H_p (where H is the compound's Henry's Law constant) than to D_e/D_p or $(D_e/D_p)^{0.5}$. The ratio H_e/H_p is about 0.82 at 20°C [Hayduk, 1982; Hayduk, 1986]; thus, measured values of k_e/k_p are much closer to D_e/D_p and $(D_e/D_p)^{0.5}$ than to H_e/H_p, suggesting that stripping of dissolved gases by air bubbles is not a significant means of gas exchange for the study stream.

6. Summary and Conclusions

The steady-state tracer gas method was found to be an excellent way of determining gas exchange rate constants for a first order stream on Walker Branch Watershed. A steady injection of chloride (in a concentrated NaCl solution) from a Marriotte bottle was a convenient and effective means of accounting for lateral inflow of water to the study stream. Gas exchange rate constants for propane (k_p) were found to be about 100 day^{-1}, with little temporal or spatial variability; rate constants for ethane (k_e) were about 117 day^{-1}.

In general, if two tracers of different volatility are injected from a single tank, and the tank pressure is high enough that some liquid is present, the injection may be significantly unsteady for at least one of the tracers. In this study, unsteadiness in the ethane injection resulted in only a few experiments being

acceptable for k_e determination. This problem could be eliminated by using a separate injection apparatus for each gaseous tracer.

Based on previously published results [Rathbun et al., 1978] of the relative gas exchange rates of propane and O_2, k_{O2} (the gas exchange rate constant for O_2) would average about 139 day^{-1} for the study stream. The k_{O2} estimate obtained from $k_{O2} = k_p(D_{O2}/D_p)^{0.7}$ is 118 day^{-1} (based on the D_{O2}/D_p value of Wise and Houghton [1966]). These rate constants are roughly 8-400x larger than those found in rivers and large streams.

Existing empirical equations for prediction of k_{O2} from stream hydraulic characteristics performed poorly when applied to reach 2 (WB242-WB170) of our study stream. Over a narrow range of flow, a few of the equations predict k_{O2} values which are close to our experimental values, but none of the equations are accurate predictors over a wide range of flow. This underscores the importance of field-measured gas exchange rates in studies of gas transport and fate in small streams.

An experiment conducted on 11/1/89 revealed the importance of leaf fall in controlling gas exchange in the study stream. With approximately half the stream surface covered with floating leaves, propane gas exchange was cut in half. Leaves were able to accumulate in and on the stream only because of the low streamflow rate (about 350 L/min). The leaves remained in the channel until 11/16/90, when most were flushed downstream or concentrated along the channel margins by the high streamflow (>4000 L/min) associated with a large storm. Thus, forest type

(deciduous vs. coniferous) and productivity (specifically, litter fall), in combination with channel geometry and the rate of streamflow, determine the extent to which leaves may accumulate in the channel, and hence the extent to which gas exchange may be lowered. The duration of any decrease in gas exchange also depends on streamflow, and hence on the local hydrologic regime (precipitation and watershed characteristics). These processes illustrate the complex relationships which may exist among forest type and productivity, hydrology, and gas exchange in forested ecosystems. We would expect these seasonal dynamics to be a common feature in other temperate zone deciduous forests, where streamflow is often relatively low at the time of leaf fall.

Our best estimate of the exponent in the relationship $k_e/k_p = (D_e/D_p)^n$ was found to be about 0.7, a result falling about midway between the predictions of the surface renewal and stagnant boundary layer models of gas exchange (these models predict n=0.5 and n=1, respectively). Though the uncertainties in k_e/k_p and D_e/D_p were only about 5% (one s.d.), both ratios being very close to 1 results in a large uncertainty in n ($\pm$0.9). The fact that H_e/H_p is much lower (0.82) than k_e/k_p (1.17) and D_e/D_p (1.24) suggests that stripping of dissolved gases by air bubbles is not an important mode of gas exchange for the study stream, in spite of its apparently highly turbulent flow. To our knowledge, this study contains the first published results from the simultaneous use of two volatile tracers in a small natural stream. Multi-tracer experiments, already common in laboratory systems [e.g., Jähne et al., 1984], would be useful in natural streams as well (especially if done with tracers

that are more different from each other, with respect to diffusion coefficient and Henry's Law constant, than ethane and propane).

Acknowledgements

The authors gratefully acknowledge the invaluable and generous assistance of many people at Oak Ridge National Laboratory, especially Patrick Mulholland who cleared numerous administrative and bureaucratic hurdles for us, provided thoughtful discussions of results, and helped carry carboys of salty water in the field. Several others besides Pat (Amy Rosemond, Bonnie Lu, Amanda Hood, and Lisa Au) provided important help in the field. Tim Tschaplinski generously allowed us the use of his gas chromatograph. The hard work of Bonnie Lu in analyzing all the chloride samples for this study is greatly appreciated. This work was sponsored by the U.S. Geological Survey (contract no. 14-08-0001-G-1725) and the National Science Foundation (contract no. BCS-8906032). The first author also acknowledges his fellowship support from Oak Ridge Associated Universities, and support from the Walker Branch Watershed Project funded by the Ecological Research Division, Office of Health and Environmental Research, U.S. Department of Energy, under contract DE-AC05-84OR21400 with Martin Marietta Energy Systems Inc.

Bibliography

Baird, M.H.I., and J.F. Davidson. 1962. Annular jets II - Gas absorption. Chemical Engineering Science 17: 473-480.

Bansal, M.K. 1973. Atmospheric reaeration in natural streams. Water Research 7(5): 769-782, Pergamon Press, Oxford, England.

Bennett, J.P., and R.E. Rathbun. 1972. Reaeration in Open Channel Flow. USGS Professional Paper 737.

Cadwallader, T.E., and A.J. McDonnell. 1969. A multivariate analysis of reaeration data. Water Research 3: 731-742.

Churchill, M.A., H.L. Elmore, and E.A. Buckingham. 1962. The prediction of stream reaeration rates. American Society of Civil Engineers, Journal of the Sanitary Engineering Division 88(SA-4): 1-46.

Dobbins, W.E. 1965. Closure to "BOD and oxygen relationship in streams". American Society of Civil Engineers, Journal of the Sanitary Engineering Division 91(SA-5): 49-55.

Duran, A.P., and H.F. Hemond. 1984. Dichlorodifluoromethane (Freon-12) as a tracer for nitrous-oxide release from a nitrogen enriched river. In: W. Brutsaert and G.H. Jirka (eds.), Gas Transfer at Water Surfaces, p.421-429, D. Reidel Pub. Co., Hingham, MA.

Elmore, H.L., and W.F. West. 1961. Effect of water temperature on stream reaeration. Proc. of the ASCE, Journal of the Sanitary Engineering Division 87(SA6): 59-71.

Genereux, D.P., and H.F. Hemond. 1990. Naturally occurring radon-222 as a tracer for streamflow generation: steady state methodology and field

example. Water Resources Research 26(12): 3065-3075.

Hayduk, W. (ed.). 1982. Ethane, volume 9 of Solubility Data Series, Pergamon Press, New York.

Hayduk, W. (ed.). 1986. Propane, Butane, and 2-Methylpropane, volume 24 of Solubility Data Series, Pergamon Press, New York.

Isaac, W.P., and A.F. Gaudy. 1968. Atmospheric oxygenation in a simulated stream. American Society of Civil Engineers, Journal of the Sanitary Engineering Division 94(SA-2): 319-344.

Jähne, B., T. Wais, and M. Barabas. 1984. A new optical bubble measuring device: a simple model for bubble contribution to gas exchange. In: W. Brutsaert and G.H. Jirka (eds.), Gas Transfer at Water Surfaces, p. 237-246, D. Reidel Pub. Co., Hingham, MA.

Johnson, D.W., and R.I. van Hook (eds.). 1989. Biogeochemical Cycling in Walker Branch Watershed: A Synthesis of Research Results, Springer-Verlag, New York.

Kilpatrick, F.A., R.E. Rathbun, N. Yotsukura, G.W. Parker, and L.L. Delong. 1987. Determination of Stream Reaeration Coefficients by Use of Tracers. USGS Open File Report 87-245.

King, C.J. 1980. Separation Processes, 2nd ed., McGraw-Hill, New York.

Kline, S.J. 1985. The purposes of uncertainty analysis. J. Fluids Engineering 107: 153-160.

Krenkel, P.A., and G.T. Orlob. 1963. Turbulent diffusion and the reaeration

coefficient. American Society of Civil Engineers Transactions, Paper 3491, 128: 293-334.

Langbein, W.B., and W.H. Durum. 1967. The aeration capacity of streams. U.S. Geological Survey Circular 542.

Lau, Y.L. 1972. Prediction equations of reaeration in open-channel flow. American Society of Civil Engineers, Journal of the Sanitary Engineering Division 98(SA-6): 1063-1068.

Lietzke, D.A. 1990. Soils of Walker Branch Watershed. ORNL/TM-11724, Oak Ridge National Laboratory, Oak Ridge, Tennessee.

Mémery, L., and L. Merlivat. 1984. Contribution of bubbles to gas transfer across an air:water interface. In: W. Brutsaert and G.H. Jirka (eds.), Gas Transfer at Water Surfaces, p. 247-253, D. Reidel Pub. Co., Hingham, MA.

Merlivat, L., and L. Mémery. 1983. Gas exchange across an air:water interface: Experimental results and modelling of bubble contribution to transfer. J. Geophysical Research 88: 707-724.

Metzger, I. 1968. Effects of temperature on stream aeration. Proc. of the ASCE, Journal of the Sanitary Engineering Div. 94(SA6): 1153-1159.

Negulescu, M., and V. Rojanski. 1969. Recent research to determine reaeration coefficients. Water Research 3(3): 189-202, Pergamon Press, Oxford, England.

O'Connor, D.J., and W.E. Dobbins. 1958. Mechanisms of reaeration in natural streams. American Society of Civil Engineers Transactions 123: 641-684.

Owens, M., R.W. Edwards, and J.W. Gibbs. 1964. Some reaeration studies in streams. International Journal of Air and Water Pollution 8(8/9): 469-486, Oxford, England.

Padden, T.J., and E.F. Gloyna. 1971. Simulation of Stream Processes in a Model River. Report EHE-70-23, CRWR-72, University of Texas, Austin, Texas.

Parker, G.W., and F.B. Gay. 1987. A procedure for estimating reaeration coefficients for Massachusetts streams. USGS Water Resources Investigations Report 86-4111.

Parkhurst, J.D., and R.D. Pomeroy. 1972. Oxygen absorption into streams. American Society of Civil Engineers, Journal of the Sanitary Engineering Division 98(SA-1): 101-124.

Peters, G.P., J.M. Hayes, and G.M. Hieftje. 1974. Chemical Separations and Measurements: Theory and Practice of Analytical Chemistry. W.B. Saunders Co., Philadelphia, Pennsylvania.

Rathbun, R.E., D.W. Stephens, D.J. Shultz, and D.Y. Tai. 1978. Laboratory studies of gas tracers for reaeration. Proc. of the ASCE, Journal of the Environmental Engineering Division 104(EE2): 215-229.

Thackston, E.L., and P.A. Krenkel. 1969. Reaeration prediction in natural streams. American Society of Civil Engineers, Journal of the Sanitary Engineering Division 95(SA-1): 65-94.

Tsivoglou, E.C., and L.A. Neal. 1976. Tracer measurement of reaeration, part 3: Predicting the reaeration capacity of inland streams. Journal of the Water

Pollution Control Federation 48(12): 2669-2689.

Unver, A.A., and D.M. Himmelblau. 1964. Diffusion coefficients of CO_2, C_2H_4, C_3H_6, and C_4H_8 in water from 6° to 65°C. Journal of Chemical and Engineering Data 9: 428-431.

U.S. EPA. 1983. Methods for chemical analysis of water and wastes. EPA-600/4-79-020, Environmental Monitoring and Support Laboratory, Cincinnati, Ohio.

Wanninkhof, R., P.J. Mulholland, and J.W. Elwood. 1990. Gas exchange rates for a first order stream determined with deliberate and natural tracers. Water Resources Research 26(7): 1621-1630.

Weast, R.C. (ed.). 1976. Handbook of Chemistry and Physics, 56th edition, Chemical Rubber Co. Press, Cleveland, Ohio.

Wise, D.L., and G. Houghton. 1966. The diffusion coefficients of ten slightly soluble gases in water at 10°-60°C. Chemical Engineering Science 21: 999-1010.

Witherspoon, P.A., and L. Bonoli. 1969. Correlation of diffusion coefficients for paraffin, aromatic, and cycloparaffin hydrocarbons in water. Industrial and Engineering Chemistry Fundamentals 8: 589-561.

Yotsukura, N., D.A. Stedfast, R.E. Draper, and W.H. Brutsaert. 1983. An Assessment of Steady-State Propane-Gas Tracer Method for Reaeration Coefficients - Cowaselon Creek, New York. USGS Water Resources Investigations Report 83-4183.

CHAPTER 3

Spatial Variability in Streamflow Generation on the West Fork of Walker Branch Watershed

David P. Genereux, Harold F. Hemond, and Patrick J. Mulholland

Abstract

Spatially intensive measurements of streamflow were used to document the spatial variability in streamflow generation on the West Fork of Walker Branch Watershed, a 38.4 ha forested catchment in Oak Ridge, Tennessee. The study focused on a 300 m section of a first order stream, and covered a wide range of flow conditions (Q_{weir}, streamflow at the basin outlet, varied from about 350 to 3500 L/min). There was enormous spatial variability in the stream inflow, down to the finest scale investigated (reaches 20 m in length). Lateral inflow to longer reaches (60-130 m) was linearly correlated with Q_{weir} over the full range of flows studied, making it possible to estimate the spatial pattern of stream inflow from measurement of Q_{weir} alone. The heterogeneous nature of the karstic dolomite bedrock was the dominant control on the observed spatial variability in streamflow generation. This thesis is consistent with the results of field investigations using natural tracers, reported in Chapter 4. Bedrock structure and lithology may affect streamflow generation directly (via water movement through fractured rock), and indirectly (by influencing the slope and thickness of the overlying soil). While the West Fork contains all the topographic and surface hydrologic features of larger basins (ridge tops, valleys, hollows, spurs, ephemeral and perennial stream channels), it covers an area which is relatively small with respect to the bedrock heterogeneity. Therefore, while the hydrologic processes observed on the West Fork are no doubt typical of those occurring elsewhere in karst terrain, the particular patterns of spatial and temporal variability are clearly unique to the study site.

1. Introduction

The study of streamflow generation is an important topic in environmental science, both because of its direct relevance to the hydrologic cycle and because the water quality of streams is directly affected by the nature of the flowpaths supplying water to the streams. Consideration of spatial variability is a necessary component of streamflow generation studies, both in the field and on the computer. Since the number of sites at which measurements can be made is always limited in practice, it is useful to identify areas of high streamflow production so that measurements may be concentrated in those areas. In addition, it is essential to have some idea how representative a measurement is if it will be used to infer the behavior of the surrounding area.

Also, comparison of the spatial pattern of stream inflow with that of other watershed parameters can elucidate the controls on streamflow generation. For a study site in southern England, Anderson and Burt [1978] found that all stream reaches of high lateral inflow were adjacent to hillslopes with concave, hollow-shaped topography. Concave topography led to convergent drainage pathways, which in turn led to saturated conditions and higher overall streamflow production in the hollows.

Spatial variability in streamflow generation is also a concern in modelling. Wood et al. [1988] proposed the notion of a "Representative Elementary Area" (REA), the smallest basin size for which the variance of a basin output or response (e.g., volume of storm runoff for a particular rain event) is a minimum. The REA

would be "a fundamental building block for catchment modelling" [Wood et al., 1988, p.31] since at this scale the particular pattern of heterogeneity in the study basin becomes unimportant, and the basin response can be analyzed in terms of the statistics of the underlying parameter distributions. Thus, an estimate of the REA would be useful in deciding the appropriate basin size for a modelling study.

This paper describes measurements of the spatial variability in streamflow generation on the West Fork of Walker Branch Watershed, a forested watershed in Oak Ridge, Tennessee. Chemical dilution stream gauging was used to determine streamflow at a number of points in the first order stream draining the study site, over a wide range of flow conditions. Chapter 4 reports the results of simultaneous work with natural tracers.

2. Study Site

The West Fork of Walker Branch has an area of 38.4 ha and an elevation range of 78 meters (Fig. 1). Precipitation is measured with two weighing-type rain gauges on the ridgetop; average annual precipitation is 140 cm. Streamflow at the basin outlet is monitored by means of a 120° V-notch weir with automatic stream stage recording (5 minute interval). Vegetation is dominated by oak and hickory, with scattered pines on the ridges and mesophytic hardwoods such as tulip poplar and beech near the stream channels.

The West Fork is located on the southeast slope of Chestnut Ridge, one of many NE-SW trending subparallel ridges in this area of the southern Appalachians.

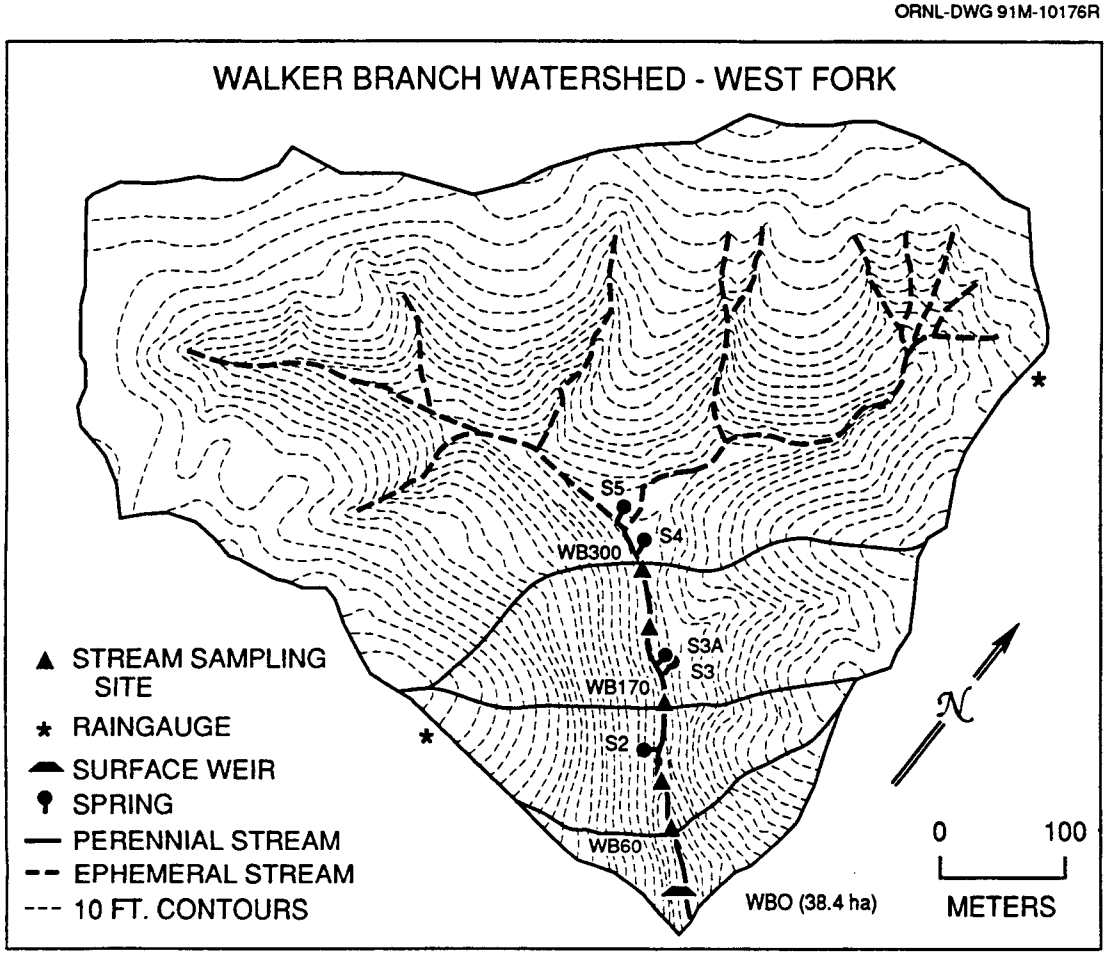

Figure 1. Contour map of the study site. Major stream sampling sites are indicated by triangles; stream sites are designated with the prefix "WB" followed by their distance upstream of the weir in meters (e.g., WB300 is the point 300 meters upstream of the weir). The two unlabeled triangles represent WB100 and WB242. Solid lines normal to the elevation contours and passing through WB60, WB170, and WB300 indicate the boundaries of "apparent contributing areas" (ACAs) for the stream reaches they define (that is, contributing areas defined in the usual way, on the basis of topography).

Bedrock consists of highly fractured dolomite (with some chert beds) of the Knox Group. Strata dip to the southeast at about 35° and strike along the long axis of Chestnut Ridge (roughly N 55° E), approximately normal to the study stream on the West Fork [Crider, 1981; Lee et al., 1984]. The West Fork is underlain by three different formations of the Knox; from oldest to youngest (i.e., going southeast along the perennial stream towards the weir) they are the Chepultepec, the Longview, and the Kingsport dolomites (Fig. 2). The Longview is much thinner than the other two formations and is more resistant to weathering because of its significantly higher chert content [Lietzke et al., 1989; Lietzke, 1990]. All three formations are highly fractured; a study involving measurement of 210 fractures in outcrops on Walker Branch (the West Fork and the adjacent 59.1 ha East Fork) found that fractures cluster in two common orientations, roughly perpendicular to and parallel to the local bedrock strike [Crider, 1981]. In addition to being more numerous, fractures with these orientations were also found to be the only fractures "solutionally enlarged to conduits in outcrops on the West Fork" [Crider, 1981, p.85]. As discussed below, these fractures are hydrologically significant in allowing groundwater movement across surface topographic divides.

Soils on the West Fork are mainly Ultisols (mostly of the Paleudult suborder), with one small band (<5% of the watershed area) of Alfisols (suborder Hapludalf) along the east side of the lower 150 m of the perennial stream [Lietzke, 1990]. Both Ultisols and Alfisols show the effects of clay translocation: an eluvial E horizon from which clay has been removed overlies an argillic Bt horizon where

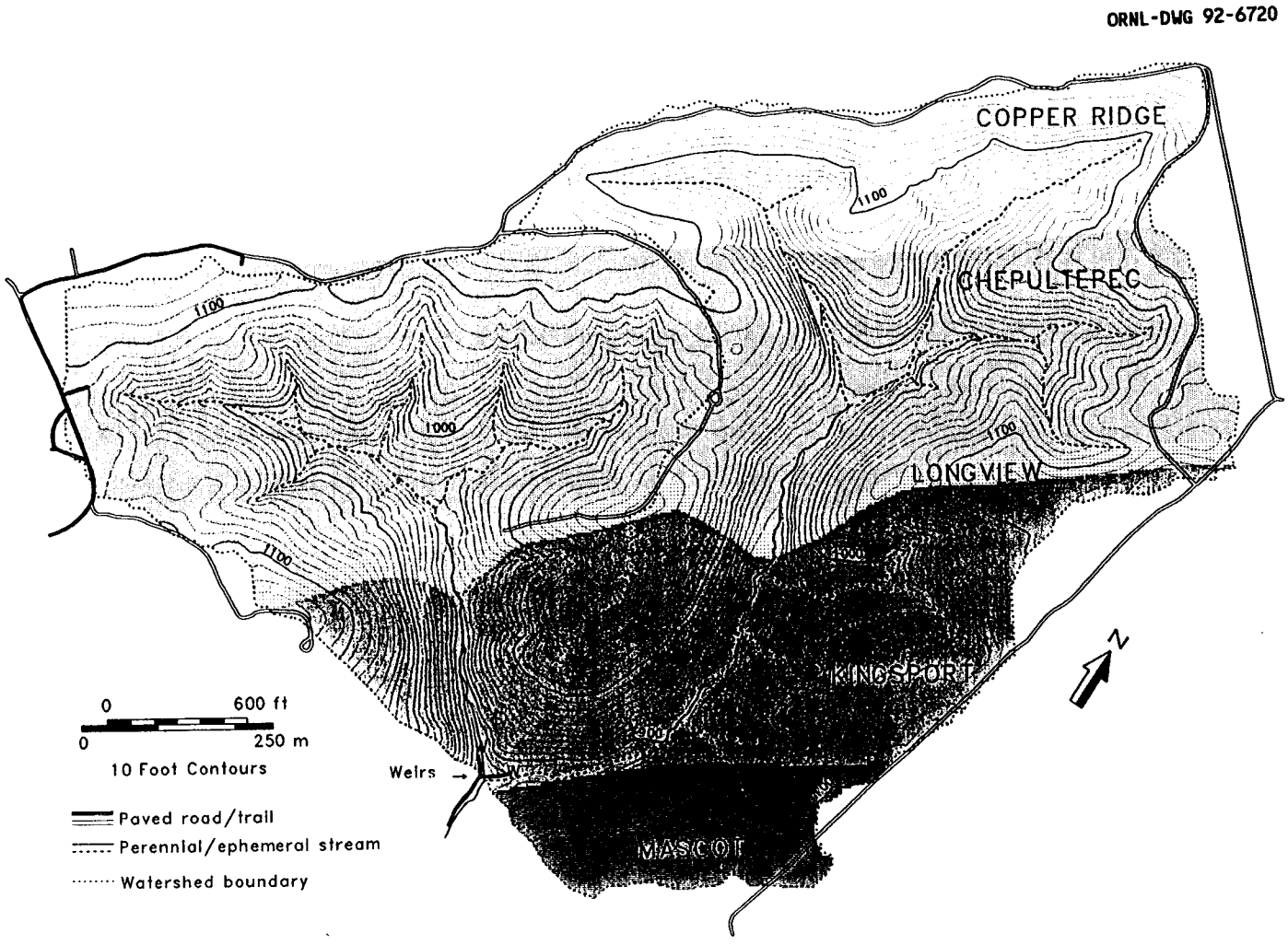

Figure 2. Map of Walker Branch Watershed showing the different bedrock formations. The West Fork catchment shown in Fig. 1 is the triangular basin occupying the left side of this map (the East Fork, on the right, makes up the rest of Walker Branch).

the clay particles have been deposited [Soil Conservation Service, 1975]. The dominant clay mineral on the West Fork is kaolinite (10-40% of the clay fraction), with vermiculite and mica present in smaller amounts (5-20% of the clay fraction). The primary distinctions between Ultisols and Alfisols are chemical and mineralogical, rather than structural or physical. According to Fanning and Fanning [1989, p.264], "Most Alfisols differ from Ultisols in having a naturally higher base saturation [the percent of cation exchange capacity accounted for by base cations as opposed to H^+; >35% for the former, <35% for the latter] - thus, commonly higher pH values - generally lower chromas and yellower hues for the well-drained counterparts, and clay usually containing less 1:1 and more 2:1 layer silicate minerals." Narrow zones of Entisols, soils which lack distinct pedogenic horizons, are found along the stream channels (both ephemeral and perennial).

In many places on the West Fork a thick layer of saprolite (residual clayey material formed in place by weathering of the bedrock) lies between the 1-2 m thick forest soil and the bedrock. This saprolite consists mainly of kaolinite (30-55%), mica (10-25%), vermiculite (5-20%), and iron oxide (2-8%) [Lee et al., 1984]. Chert fragments are common, in places where a chert bed in the original bedrock has partially weathered but the surrounding dolomite has completely weathered to saprolite. In places on the western and northern ridgetops around the West Fork, the saprolite is nearly 30 m thick. Over much of the eastern side of the perennial stream valley (the same general area covered by Alfisols), there appears to be little or no saprolite (small rock outcrops can be seen running

upslope from the stream channel; well points have been driven to refusal within 2 m of the ground surface). The saprolite thickness is unknown or poorly known for much of the watershed. Previous studies have shown that a perched saturated zone often develops above the soil/saprolite interface during storms [e.g., Wilson et al., 1990].

While the saprolite may be much thicker than the overlying soil in some places, it has a much lower maximum potential transmissivity than the soil ("maximum potential transmissivity" refers to the transmissivity of the layer saturated over its entire thickness). The hydraulic conductivity of saprolite was measured in three different depth intervals (2.5-3 m, 6-12 m, and 21-30 m) at a site about 6 km west of the West Fork on Chestnut Ridge [Ketelle and Huff, 1984]. Geometric mean conductivities were 6.1×10^{-8} m/s at 2.5-3 m (21 field measurements), 2.0×10^{-8} m/s at 6-12 m (19 field measurements), and 6.3×10^{-10} m/s at 21-30 m (8 lab measurements). Assigning these three conductivity values to three somewhat arbitrarily chosen layers (1.5-4.5 m, 4.5-16 m, and 16-30 m below ground surface) gives an estimate of 4.2×10^{-7} m^2/s for the maximum potential transmissivity of the saprolite. Even if the laboratory measurements of hydraulic conductivity for the deepest layer underestimate the field scale value by a factor of 10 (which is possible), the effect on overall transmissivity is minor (it increases to 5×10^{-7} m^2/s). An overlying soil consisting of a 1 m thick B horizon (hydraulic conductivity of 10^{-5}-10^{-4} m/s [Luxmoore et al., 1981]) and a 0.5 m thick A horizon (hydraulic conductivity of about 10^{-4} m/s [Peters et al., 1970]) would have a

maximum potential transmissivity of 6×10^{-5} to 1.5×10^{-4} m^2/s, 140-360 times larger than that of the 28.5 m thick saprolite.

Streamflow and rainfall data for the West Fork indicate that the watershed receives subsurface inflow from outside its topographic boundary. For the 12 years from 1969 through 1980, the average difference between annual rainfall and annual runoff at the weir was 34 cm (s.d.=16 cm, n=12). The best estimates of annual evapotranspiration (based on the average difference between rainfall and runoff for a number of watersheds in the Oak Ridge area) are about 73 cm [McMaster, 1967; TVA, 1972]. Thus, the West Fork stream seems to be receiving about 1.5×10^5 m^3 of water each year (39 cm times 38.4 ha) from outside the West Fork boundary. Solutionally enlarged fractures and cavities in bedrock are the most likely conduits for this interbasin transfer.

3. Methods

Chemical dilution gauging was used to determine the streamflow rate at a number of sites in the perennial stream channel; experiments spanned the range of Q_{weir} (streamflow at the weir) from 350 to 3500 L/min. The five main sites for streamflow determination are indicated with triangles in Figure 1. The sites, each named with the prefix "WB" followed by its distance upstream of the weir in meters, are WB300, WB242, WB170, WB100, and WB60. A flume installed in the stream channel at WB300 allowed us to check (or, occassionally, forego) chemical dilution streamflow measurements at that site. In addition to these five main sites,

measurements were occassionally made at six other sites (WB280, WB260, WB220, WB140, WB120, and WB80) in order to get more detailed information on the spatial structure of stream inflow.

The chemical dilution methodology involves a one dimensional steady state analysis [e.g., Genereux and Hemond, 1990]. A 50-liter Marriotte bottle was used to inject a concentrated (2.7-3 M) NaCl solution into the stream at a steady rate. The injection site varied, but was always 12-17 m upstream of the nearest measurement site. Since the channel was laterally well mixed (no vertical or horizontal tracer gradients), the streamflow Q at a stream measurement site was given by the simple steady state relationship:

$$Q = Q_i C_i / C \qquad (1)$$

where Q_i and C_i are the injection rate and concentration of the NaCl tracer solution, respectively, and C is the steady state tracer Cl^- content of the streamwater at the site.

C values were estimated by two different means: field measurement of the specific conductance (γ) of the streamwater, and laboratory measurement of the Cl^- content (S) of the streamwater. Before beginning the NaCl injections the background specific conductance of the streamwater (γ_b) was determined at each measurement site. A battery powered hand-held conductivity meter with a gold dip cell (Cole-Parmer Instrument Co.) was used; the meter automatically corrected the measured conductance to an equivalent value at 25°C. Measurements were

generally taken 30 seconds apart for several minutes in order to determine if there was any drift in γ_b. Prior to the three highest flow experiments γ_b was slowly drifting upward at WB170, WB100, and WB60. The γ_b drift rate at the three sites was noted and used to extrapolate γ_b forward in time to when γ_s (the steady state plateau γ value) was measured, in order to better estimate the background specific conductance under the plateau. The drift in γ_b was associated with a slow decrease in Q_{weir} (maximum rate of Q_{weir} decrease was -1.7% per hour, during the highest flow experiment on 3/18/90). Strictly speaking, the chemical dilution methodology employed here requires that the streamflow be steady. In practice, the small drop in streamflow observed during the highest flow experiments introduces a relatively small uncertainty into the calculated Q values (see appendix). After measuring γ_b at a particular site, water samples (usually 2-3) were collected for analysis of background Cl^- content (S_b). We did not attempt to measure drift in S_b because both S_b (about 0.02 mM) and changes in S_b associated with changes in streamflow (<0.01 mM; Mulholland et al. [1990]) were much smaller than the amount of tracer chloride added (0.5-5.0 mM).

Salt injections were started after γ_b measurements were made and background water samples were collected. The specific conductance at each measurement site rose and eventually leveled off during the injection (Fig. 3). Steady state was generally considered to have been attained when a constant γ reading (within the instrument resolution of 1 μS/cm) was obtained for ≥10 minutes (or γ on the plateau was drifting at the same rate as γ_b). After the specific con-

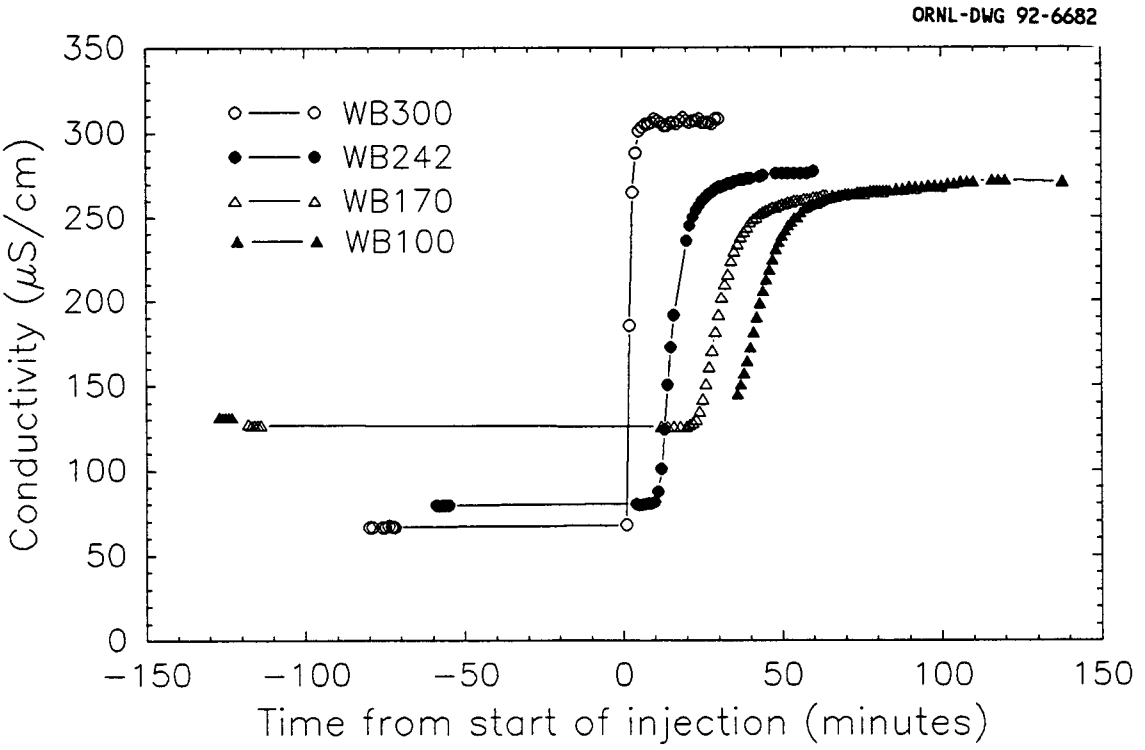

Figure 3. Specific conductance data for the experiment of October 4, 1989. The steady NaCl injection was begun at time zero.

ductance reached steady state, three or four water samples were collected for Cl^- analysis (S_s). Both S_s-S_b and γ_s-γ_b were used as measures of C in calculating Q values with Eqn. 1.

Q_i values for use in Eqn. 1 were measured in the field with a stopwatch and graduated cylinder; C_i for each tracer solution was determined from the known amounts of NaCl and water used to prepare the solution. In determining the uncertainty in Q, the uncertainties in Q_i and C_i were negligible compared to the uncertainty in C (see appendix).

Chloride concentrations (both S_s and S_b) were measured with an automated ferricyanide method (U.S. EPA [1983]), using a Technicon TRAACS 800 auto-analyzer. The steady state (S_s) samples were diluted with doubly distilled water prior to analysis, to bring their Cl^- contents into the range spanned by the calibration standards. The difference S_s-S_b was calculated and used directly as C in Eqn. 1.

In using γ_s-γ_b values in Eqn. 1 to determine Q values, it is necessary to convert the γ_s-γ_b value from at least one measurement site to an equivalent Cl^- concentration. Measuring the specific conductance of the tracer solution (γ_i) and expressing the tracer injection rate as $Q_i\gamma_i$ (instead of Q_iC_i) would not suffice because the relationship between γ and NaCl concentration is not linear over the full range from γ_i (roughly 1.7×10^5 μS/cm) to γ_s-γ_b (typically 100-400 μS/cm); therefore $Q_i\gamma_i \neq Q(\gamma_s-\gamma_b)$. Data from Jones [1912] was used to convert the γ_s-γ_b value from the first measurement site (that farthest upstream; either WB300 or

WB242) to a Cl^- concentration. A linear regression of Jones' five data points (at 25°C) in the range $29<\gamma<880$ μS/cm gave the following relationship:

$$C=8.91\times10^{-6}\gamma-2.97\times10^{-5} \qquad (r=0.99997) \qquad (2)$$

where C is concentration in moles per liter and γ is specific conductance in μS/cm. After using Eqn. 2 to convert the γ_s-γ_b value from the first site to a Cl^- concentration, and using Eqn. 1 to calculate Q, streamflow values at the other sites downstream were calculated by using γ_s-γ_b values directly in Eqn. 1:

$$Q_j=Q_1(\gamma_s-\gamma_b)_1/(\gamma_s-\gamma_b)_j \qquad (3)$$

where the subscripts 1 and j refer to the measurement site farthest upstream and a site downstream of it, respectively. This is possible because the conductance-concentration relationship for aqueous NaCl solutions is highly linear over the relatively small range of γ_s-γ_b values (100-400 μS/cm) spanned by the stream sites (see Eqn. 2).

Lateral inflow to a given stream reach was determined as the difference in streamflow rates at the upstream and downstream ends of the reach. There are two estimates of Q for each measurement site during each experiment (one based on γ data, the other on S data), and hence two estimates of the lateral inflow to each reach during each experiment (except for the 3/6/90 experiment, when S data were not collected). In general, the lateral inflow determinations based on γ data were in good agreement with those based on S data, and the two were simply averaged. The few exceptions (marked by asterisks in Table 1) were cases in which

the γ data gave unrealistic results at high flow. For example, γ data gave lateral inflow rates of about 400 L/min for WB170-WB100 and WB100-WB60 when Q_{weir} was 2749 L/min, much higher than the lateral inflow to these reaches at Q_{weir}=3457 L/min. Specific conductance data also suggested a lateral inflow rate of about 13 L/min for WB300-WB242 at Q_{weir}=3457, a value roughly 10 times lower than that indicated by the S data for the same experiment, and by both the γ and S data when Q_{weir} was 2749 L/min. These few seemingly anomalous results could be due in part to the random noise associated with calculating a small difference between two much larger numbers. However, the fact that all the anomalous numbers are based on γ data at high flow, which is known to be potentially problematic because of drift in γ_b, suggests there is an important non-random aspect to the observed behavior. Perhaps the γ_b measurements prior to the start of the injections did not accurately characterize the γ_b drift occurring later in the experiments, near steady state. Because of these anomalies, lateral inflow values were based on S data alone for six cases.

4. Results

4.1. Variability

There was considerable spatial variability in streamflow generation on the West Fork at all spatial scales investigated (reaches from 20 to >100 m in length). Figure 4 shows lateral inflow to the perennial channel between WB300 and the weir on three different days with different Q_{weir} values. The reach between WB220

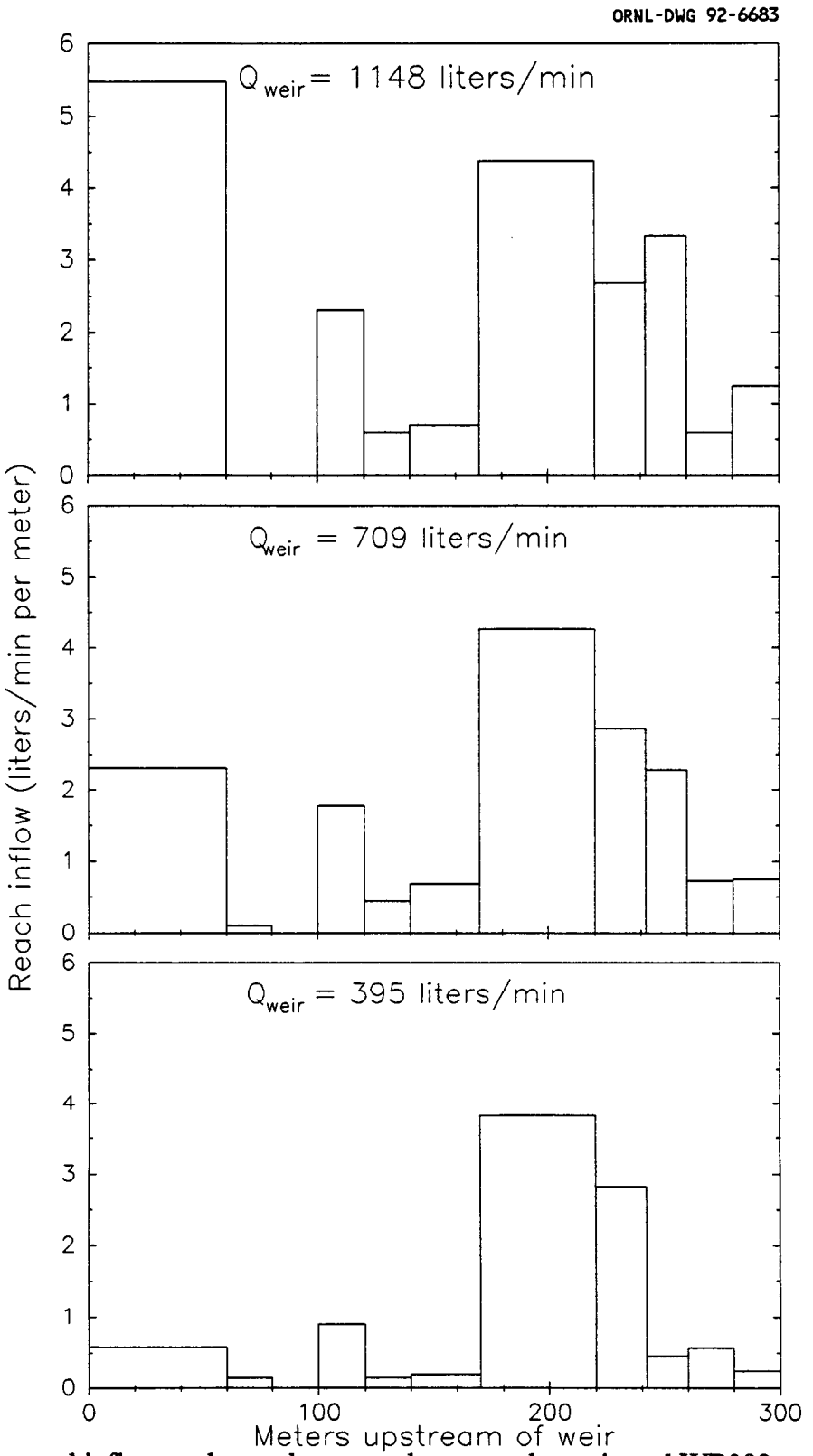

Figure 4. Lateral inflow to the study stream between the weir and WB300 on three different days with different Q_{weir} values.

and WB170 stands out as an important contributor, especially at low flow. Most of the inflow in this reach is due to two springs (S3 and S3A) at the base of a large hollow on the east slope.

Perhaps the most dramatic feature of these data is the dynamic behavior of lateral inflow between WB60 and the weir. While relatively unimportant at low flow, lateral inflow to this 60 m reach increases rapidly and eventually becomes the largest contributor to inflow in the perennial stream channel. Data from Huff et al. [1982] also show the importance of this reach, though this was not discussed in their paper. Their study involved the release of 9.75 mCi of ^3H (as tritiated water) to the stream. Streamflow was determined at several sites from WB181 to WB66; Q_{weir} was 371 L/min. Figure 5 is similar to a graph in Figure 1 of Huff et al. [1982], but is redrawn to include the lateral inflow between WB66 and the weir (using the Q_{weir} value given in their paper). There is more lateral inflow in this 66 m reach (98 L/min) than in their 115 m study reach, WB181-WB66 (82 L/min).

Data covering a wider range of flow at a somewhat coarser spatial resolution (40-70 m reaches) are given in Table 1. Reach lateral inflow correlated well with Q_{weir}. Treating the channel section between WB300 and WB60 as two reaches instead of four removes some of the random scatter associated with calculating a small lateral inflow as the difference in two large streamflow numbers. Figure 6 shows linear regressions of lateral inflow vs. Q_{weir} for four stream reaches comprising the entire West Fork surface drainage system: above WB300, WB300-WB170, WB170-WB60, and WB60-WB0 (WB0 is the weir). Table 2 gives the

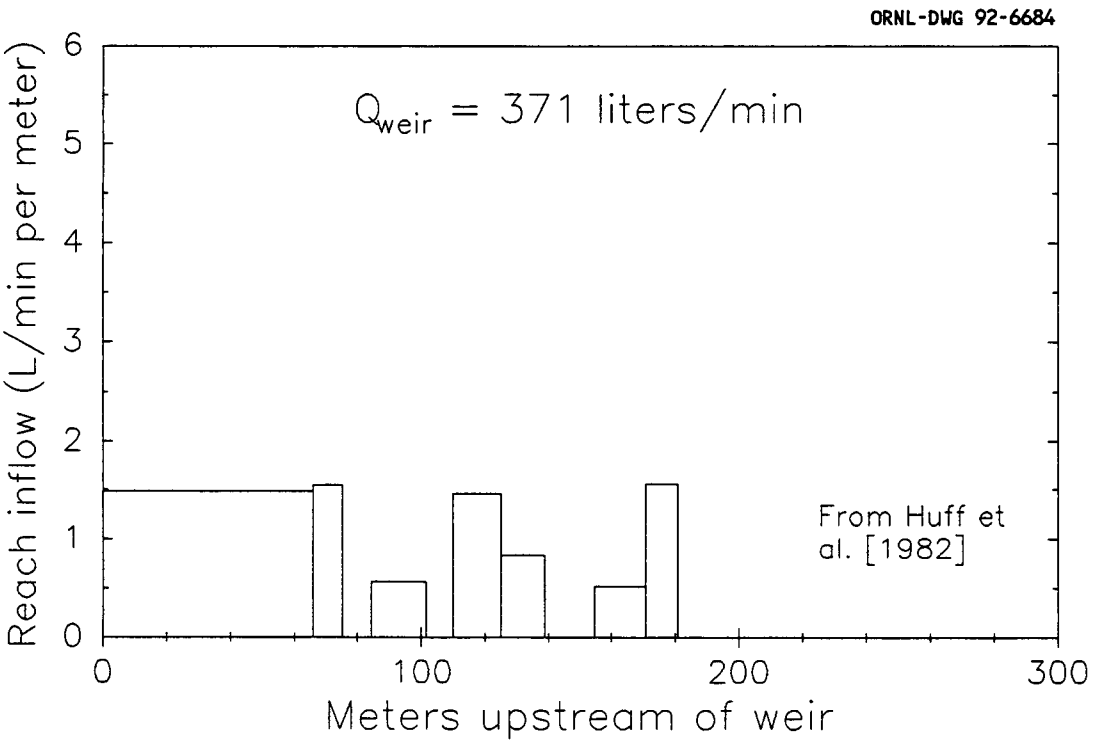

Figure 5. Lateral inflow data of Huff et al. [1982] between WB181 and the weir.

Q_{weir}		Lateral Inflow (liters/min)					
(L/min)	Date	1	2	3	4	5	6
302	9/8/89				13		
354	11/1/89	37	39	203	54	14	21
395+	7/20/90	53	33	248	23	13	26
411	8/28/90	60	30	204	29	7	78
680	4/13/90	161	37	249	56	11	166
709+	4/12/90	162	70	276	65	2	138
722	4/8/90	178	55	251	71	20	150
1050	3/7/90	350	46	304	87	5	260
1148+	3/6/90	380	97	278	79	0	326
1368	10/4/89	526	110	254	15	[468]	
1447	5/7/90	537	105*	323	54	55	403
2749	11/17/89	1055	122	323	97*	82*	1081
3457	3/18/90	1640	125*	466*	61*	151	1007

Table 1. Lateral inflow to six reaches of the study stream during thirteen chemical dilution experiments. Plus symbols (+) mark the experiments represented in Fig. 4, during which measurements were made at additional sites. Asterisks mark lateral inflow values which are based on S data alone (γ data are not considered reliable here; see text). Stream reaches 1-6 are as follows: 1=>WB300, 2=WB300-WB242, 3=WB242-WB170, 4=WB170-WB100, 5=WB100-WB60, and 6=WB60-WB0. No measurements were made at WB60 on 10/4/89; a total lateral inflow value for WB100-WB0 is given in parentheses for that day.

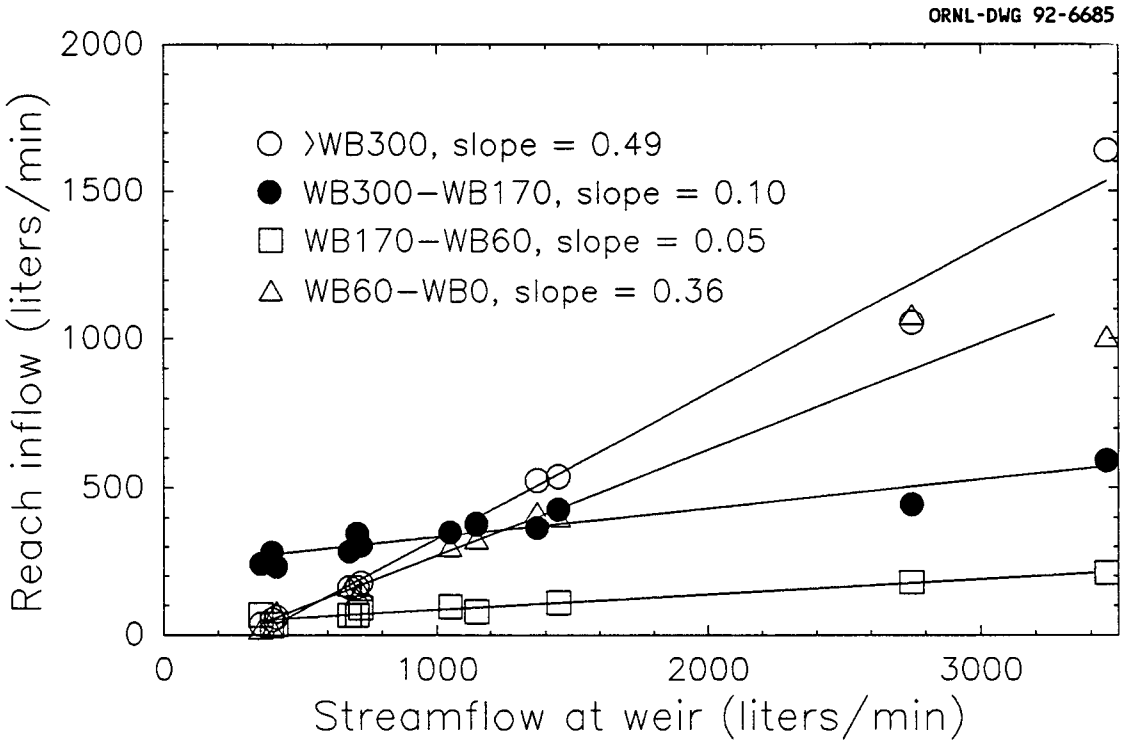

Figure 6. Linear regressions of lateral inflow vs. Q_{weir} for four stream reaches on the West Fork. Regression parameters are given in Table 2.

Reach	Regression Parameters			
	Slope	Intercept	Corr. Coef.	n
>WB300	0.4912	-162.9	0.9937	12
WB300-WB170	0.0973	236.5	0.9442	12
WB170-WB60	0.0529	31.5	0.9724	11
WB60-WB0	0.3575	-89.9	0.9786	11

Table 2. Parameters for linear regressions of lateral inflow vs. Q_{weir} for four reaches; n is the number of points used in the regression.

parameters for these regressions. An important limitation to keep in mind is that the lateral inflow data were collected during times of steady flow, or slowly decreasing flow on the falling limbs of hydrographs. The relationships in Table 2 and Fig. 6 would not necessarily hold during the rising limbs of hydrographs.

The relationships between lateral inflow and Q_{weir} were highly linear over a wide range of flow. The regression parameters (slope and intercept) are of interest because they contain the basic information about where streamflow is generated on the watershed. The intercepts of the lines in Fig. 6 show that at low flow typical of the late summer (~350 L/min), most of the streamflow leaving the West Fork is generated between WB300 and WB170 (much of that in springs S3 and S3A). The slopes of the lines show that as Q_{weir} increases, 49% of any increase is generated above WB300 (mainly in the ephemeral channel system), 10% is generated between WB300 and WB170, 5% between WB170 and WB60, and 36% between WB60 and the weir.

A dramatic demonstration of spatial variability is provided by using the regressions in Fig. 6 and the streamflow data from the weir to estimate the "apparent runoff" from the "apparent contributing areas" (ACAs) delineated in Fig. 1. For the period 9/1/89-8/31/90 the total amount of streamflow passing the weir was 132 cm, or 965 L/min averaged over the 12 month period; precipitation was 168 cm. (These data suggest an interbasin transfer into the West Fork, equal to total streamflow plus average evapotranspiration minus rainfall, of about 37 cm for the 12 month period.) Using this average Q_{weir} of 965 L/min in the regression lines

of Fig. 6 gives an estimate of the average lateral inflow rate to each stream reach for the 12 month study period. Dividing the average volumetric lateral inflow rate for each reach by the size of its ACA yields an estimate of the depth of "apparent runoff" from each ACA. Since flows under the rising limbs of hydrographs account for a small proportion of the year's total flow, results should not be greatly affected by possible hysteresis in the spatial distribution of stream inflows (i.e., by the possibility that the spatial distribution of stream inflows during rising flow is not accurately represented by data in Fig. 6).

Results show tremendous variability (Table 3), with the bulk of the watershed (upstream of WB300) apparently generating only 55 cm of streamflow and the small area just above the weir seemingly producing an amount of streamflow equivalent to about 6.5 times the total depth of precipitation. These apparent runoff values, and the regression equations from which they were calculated, clearly reflect the movement of subsurface water across surface topographic divides. Some of the streamflow generated downstream of WB300 may be due to groundwater movement across the downstream boundary of the >WB300 ACA, within the West Fork. However, the overall water balance for the West Fork indicates that much of the stream inflow must be due to groundwater movement into the West Fork from outside.

4.2 Controls

Streamflow data at different spatial scales indicate the importance of

ACA	Area (ha)	Runoff (cm)
whole watershed	38.4	132
>WB300	29.5	55
WB300-WB170	4.47	389
WB170-WB60	3.15	138
WB60-WB0	1.24	1080

Table 3. "Apparent runoff" from four "apparent contributing areas" (ACAs), 9/1/89-8/31/90. Precipitation during this 12 month period totaled 168 cm.

groundwater movement across surface topographic divides, including a net transfer into the West Fork from outside. It is much more likely that such transfers take place within the bedrock than in the overlying regolith (soil plus saprolite). Significant water movement through the saprolite is unlikely given its low transmissivity. The overlying 1-2 m thick soil mantle has a much higher transmissivity, but it obviously follows the topography and hence is not a logical candidate for a medium in which there are significant water fluxes across topographic divides.

On the other hand, the permeable karst nature of the bedrock is well established, by observations both in outcrop within the West Fork [Crider, 1981] and in boreholes outside the West Fork but within Chestnut Ridge [e.g., Ketelle and Huff, 1984]. Of 20 boreholes drilled into bedrock on west Chestnut Ridge (about 6 km west of the West Fork, in the same Knox Group rocks), most penetrated some weathered, cavitose bedrock, and seven penetrated more than 30 m of cavitose bedrock (vertical dimensions of cavities were 0.3-5 m) without encountering sound, unweathered rock [Ketelle and Huff, 1984]. Thus, direct physical observations of geologic media at the study site suggest that the bedrock carries the bulk of the interbasin transfer, a substantial volume of water corresponding to ~37 cm of runoff during the 12 month study period. It is of course possible that some of the groundwater moving through the bedrock as fracture flow fell as precipitation on the West Fork (all the bedrock groundwater flow need not be interbasin transfer, though it is likely that nearly all the interbasin

transfer is bedrock groundwater flow). Tracer data are used to pursue this point in Chapter 4.

Groundwater movement to the study stream in bedrock fractures should affect the spatial variability as well as the magnitude of stream inflows. Relative to a case with no bedrock groundwater inputs, the spatial variability of stream inflows would be increased by water inputs from irregularly spaced fractures. Springs S3 and S3A are examples of this effect. S3 and S3A are large perennial springs with relatively constant flow (about 100 and 50 L/min, respectively), constant chemistry (the water is saturated with respect to dolomite), and constant temperature (approximately equal to the mean annual air temperature, 14.5°C). These characteristics indicate that S3 and S3A are almost certainly sites where bedrock groundwater discharges into the study stream. Additional evidence for the bedrock origin of outflow from S3 and S3A comes from the lack of a soil saturated zone near the springs. Five well points were driven into the soil (four to refusal) between S3 and S3A, along a line roughly parallel to and about 3 m from the streambank. No water table was ever found in the downstream three; the two farthest upstream were installed side by side near S3A (one 87 cm deep, at refusal, the other 40 cm deep), and the deeper well showed saturated conditions on 4 days during the study period (11/16/89, 3/17/90, 5/4/90, and 5/5/90), and the shallow well only one (3/17/90). The general lack of a soil saturated zone near S3 and S3A is consistent with a bedrock source for these two large springs. Thus, the bedrock groundwater inputs are responsible for one of the most prominent features of the

spatial variability (springs S3 and S3A), and probably other features as well (such as the WB60-WB0 inflow, most of which is clearly due to groundwater movement across the boundaries of the ACA for this reach (Table 3), and perhaps some of the smaller inflow features shown in Fig. 4).

Bedrock fractures and cavities are important in bringing water to the study stream (probably from both within and outside of the West Fork), and in influencing the spatial pattern of stream inflow. Other factors must also be considered in looking for controls on the observed patterns of stream inflow. By comparing the spatial distributions of various watershed parameters that might have an effect on streamflow generation with the distribution of stream inflow, one can assess whether heterogeneity in these parameters plays an important role in producing the observed heterogeneity in stream inflow. A parameter whose spatial distribution bears no relationship to that of stream inflow can not be an important control on the variability in streamflow generation.

Perhaps the most logical parameter to consider first is spatial variability in the dominant water input, precipitation. During the years 1969-1980, five weighing type rain gauges were continuously operated in small clearings on Walker Branch (Fig. 7). Yearly total precipitation (I) was very similar at the five gauges. The average of the five I values for a given year ($\bar{I}$) had a standard deviation (σ_I) of 0.7-5.0% (average σ_I was 2.2% for the 12 years of record). There is generally small variability in the total depths of individual storms (i) as well. Average total storm precipitation for the five gauges ($\bar{i}$) and standard deviation (σ_i) were compiled for

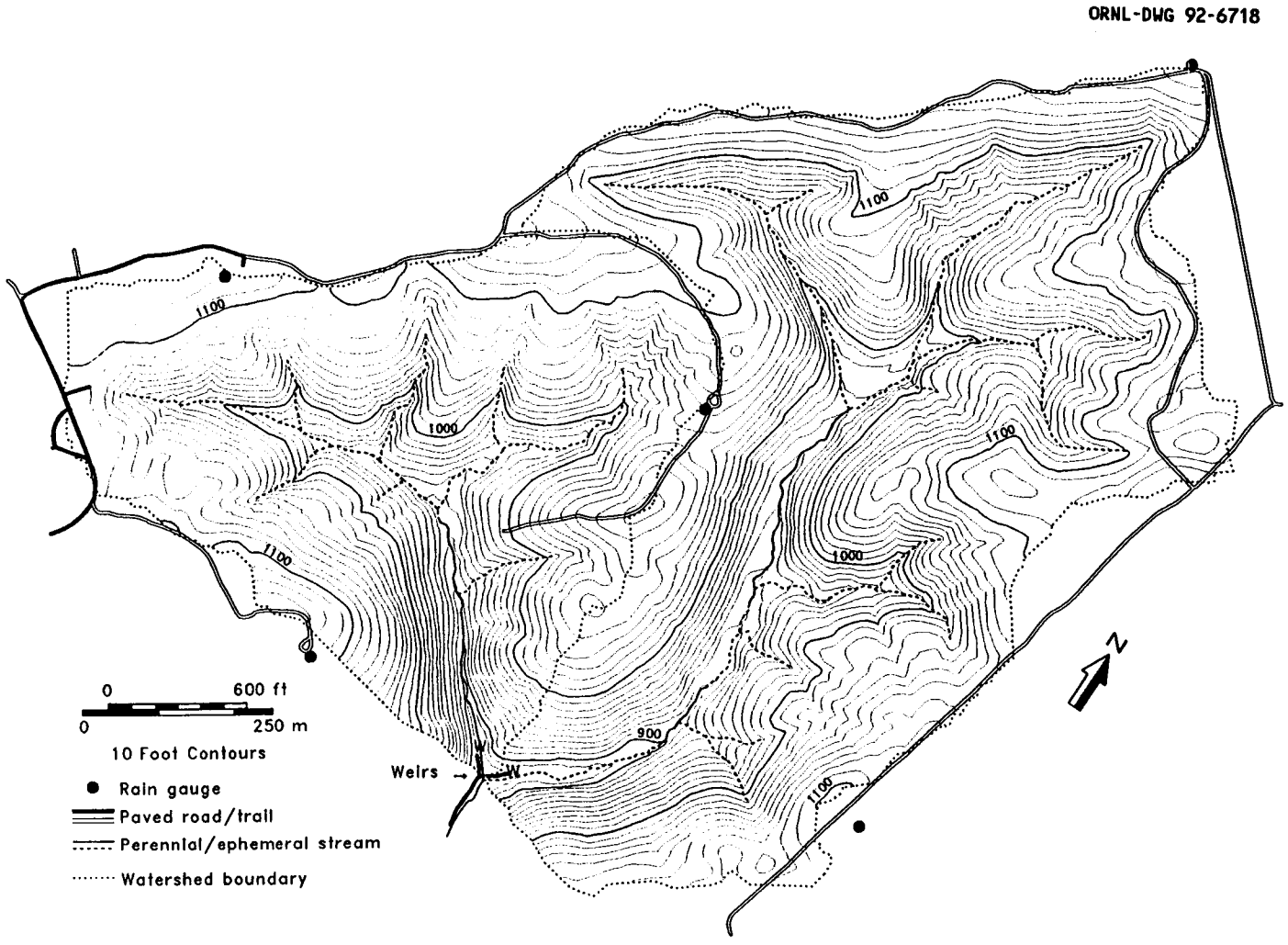

Figure 7. Map of Walker Branch showing the stream channel system for the entire watershed and the locations of five rain gauges.

129 storms from three years: 1969 (drier than average), 1971 (average rainfall), and 1973 (wetter than average). Results (Table 4 and Fig. 8) show that σ_i was typically about 5%. Thus, precipitation is generally very homogeneous over Walker Branch; this is consistent with the fact that the typical horizontal length scale for thunderstorms (the smallest type of precipitation systems) is 2-20 km [Orlanski, 1975], 2-20 times the horizontal dimension of Walker Branch.

A study of yearly total precipitation at a somewhat larger scale also indicated that variability at the scale of Walker Branch should be negligible. McMaster [1967] analyzed data from 11 rain gauges in the "Oak Ridge area" (i.e., within about 30 km of the study site) for the period 1936-1960. His contour map of mean annual rainfall for the area shows precipitation generally increasing toward the northwest, with a gradient normal to the contours of about 0.8 cm of precipitation per km of horizontal distance. With such a gradient, the change in annual rainfall across Walker Branch (from southeast to northwest) would be 0.5 cm or less.

Throughfall measurements give a more direct indication of the atmospheric water flux to the ground surface. Forest canopies (including that on the West Fork) can be highly heterogeneous over very short distances, and throughfall collectors separated by several meters or more often show differences of 10-30% in total storm depth collected (e.g., Genereux, unpub. data). However, in a study involving use of 96 collectors spaced 11 m or more apart, throughfall on Walker Branch was found to be extremely homogeneous, even across forest types

Year	# storms	Average σ_i (%)
1969	39	2.8
1971	45	5.1
1973	45	7.1

Table 4. Number of storms with $\bar{i}$>1 cm and the average σ_i (see text for definitions) for each of three years on Walker Branch.

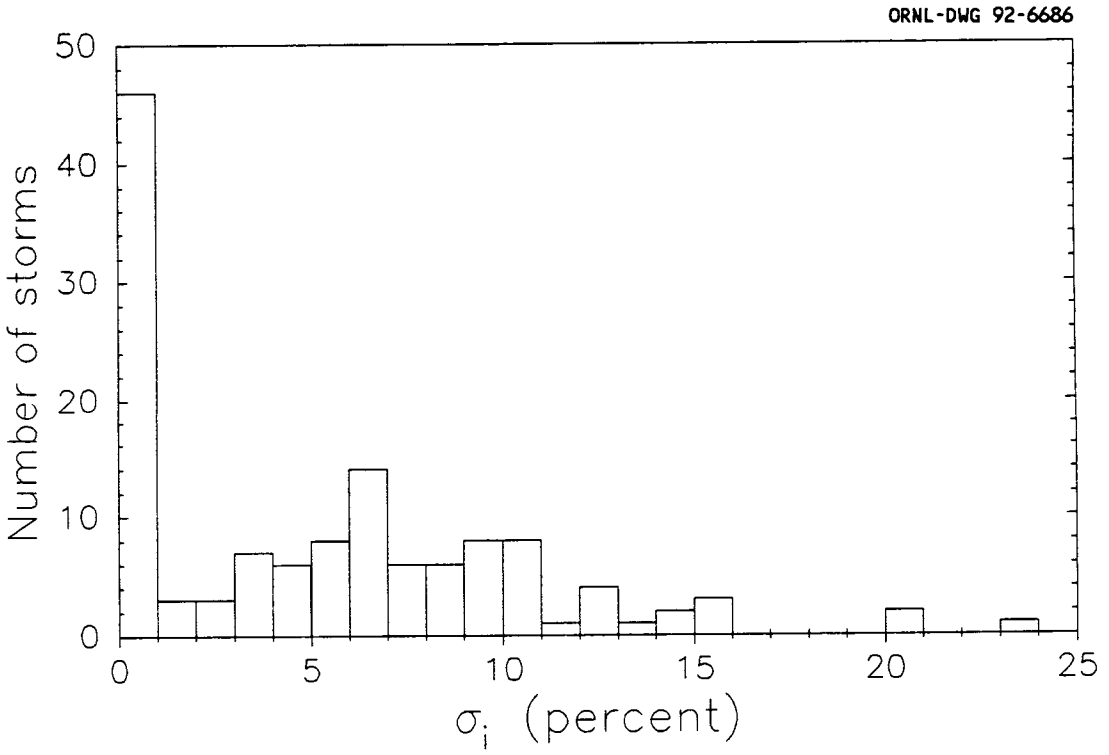

Figure 8. Histogram showing the number of storms in each 1% σ_i (see text for definition) interval. The 129 storms are all those totalling more than 1 cm in the years 1969, 1971, and 1973. The large number of storms showing $\sigma_i<1\%$ (actually, $\sigma_i=0$) is due to the fact that precipitation at each gauge was recorded to the nearest tenth of an inch; because of this relatively low sensitivity, i values from all five gauges were often exactly the same.

[Henderson et al., 1977]. Thus, the length scales for variability in the precipitation and throughfall fields seem to be much larger and much smaller, respectively, than the dimensions of the study area (though clearly the throughfall must also have a larger scale variability tied to that of the rainfall). Spatial variability in rainfall or throughfall can be ruled out as an important factor influencing the observed spatial variability in streamflow generation (especially when one considers that the rainfall/throughfall pattern required to produce the observed pattern of stream inflow would be alternating bands of high and low rainfall/throughfall, normal to the stream channel and in some cases 20 m wide or less).

Spatial variability in vegetation could be reflected in soil moisture and soil structure (e.g., number and type of biogenic macropores). While there is varibility in the forest composition on the West Fork, it does not coincide with the pattern of stream inflow. Most of the east slope of the perennial stream valley is under oak and hickory, while beech and tulip poplar dominate at least the lower two thirds of the west slope [Johnson, 1989]. Thus, each stream reach has an adjacent "oak-hickory" hillslope section (to the east) and an adjacent "beech-poplar" hillslope section (to the west). Since each stream reach lies between one oak-hickory slope and one beech-poplar slope, vegetation can not be an important contributor to the spatial variability in streamflow generation.

Previous research on the West Fork has shown that there is no spatial correlation of hydraulic properties for either surface soil [Wilson and Luxmoore, 1988] or B2t horizon subsoil [Wilson et al., 1989] for separation distances of 4 m

or greater. Since any possible correlations exist at distances <4 m, and the length scale for each ACA (for even the smallest reaches, 20 m long) is much greater than 4 m, it is likely that each ACA samples enough of the soil hydraulic conductivity field to ensure that all the ACAs have approximately the same average hydraulic conductivity. Also, as noted earlier, the primary soil difference (Alfisol vs. Ultisol) is based on chemical and mineralogical criteria rather than physical characteristics or hydraulic properties. While the regolith thickness varies widely on the West Fork (1-30 m), the transmissivity probably does not vary similarly. As described earlier, the transmissivity of the soil is much greater than that of the underlying saprolite. Since the transmissivity of the regolith is controlled by that of the soil, it probably does not vary greatly from one ACA to another. Thus, hydraulic properties of the regolith (hydraulic conductivity, transmissivity) do not seem to be an important control on the observed variability in streamflow generation. One possible exception to this, which may apply to areas of thin soil (e.g., the east slope of the perennial stream valley downstream of ~WB150), is discussed in the following section.

A parameter whose importance can not be ruled out is topography. The importance of topography on a watershed in Somerset, England was well illustrated by Anderson and Burt [1978], who found that hollows (concave hillslope sections) produced more runoff per unit area than spurs (convex hillslope sections) or straight hillslopes. On the West Fork, the association between hillslope concavity and large stream inflow seems to hold for the large hollow centered at roughly

WB200, near springs S3 and S3A. However, as already discussed, the high stream inflow here is almost certainly due to flow in bedrock fractures; it would be misleading to suggest a cause and effect relationship (such as that described by Anderson and Burt [1978]) between concave topography and high stream inflow for this hollow on the West Fork. Differences in topography can not account for the small scale variability shown in Fig. 4, since many of these reaches (e.g., WB120-WB100 and WB100-WB80) have ACAs of nearly identical topography.

One might expect that an index of "responsiveness" (e.g., the slope of the reach inflow vs. Q_{weir} regression) to be related to topography, even if the absolute amount of reach lateral inflow (reflected in both the slope and intercept of the inflow regression) is not. However, this would require that inputs of bedrock groundwater be steady. While these inputs may vary more slowly than those from soil, there is some evidence to suggest that they are not truly steady. For example, output from springs S3 and S3A does vary (though relatively slowly). Inflow to WB60-WB0, which must be strongly controlled by bedrock, varies rapidly. Thus, while the importance of topography can not be ruled out, it can not be directly evaluated because of the confounding influence of bedrock fracture flow (and especially unsteadiness in that flow). Table 5 summarizes the conclusions of this section with respect to controls on the observed variability in streamflow generation.

Parameter	Variable at ACA scale?	Variability oriented parallel to stream channel?
rainfall	no (larger)	
throughfall	no (smaller and larger)	
soil hydraulic properties	no (smaller, perhaps larger)	
vegetation	yes	no (normal to channel)
topography	yes	yes
bedrock fractures	yes	yes

Table 5. Summary of the importance of various watershed parameters in controlling spatial variability in streamflow generation. The second column indicates whether the scale of spatial variability in a given parameter is similar to the dimensions of "apparent contributing areas" (tens of meters). The third column shows whether a parameter which is variable at the ACA scale has variability oriented parallel to the perennial stream channel (a necessary but not sufficient condition for the parameter to be partially responsible for the observed variability in stream inflow). Results show that only topography and bedrock fractures can not necessarily be considered unimportant.

5. Discussion

The hydrologic importance of bedrock makes the West Fork somewhat unusual among small watersheds where streamflow generation has been studied. Since a significant amount of water moves to the study stream through fractured bedrock, traditional hillslope hydrometric methods (e.g., grids of tensiometers or piezometers in the soil) would be poorly suited for determining water flux to the study stream. This is one of the main reasons why channel based methods (spatially intensive stream gauging, the tracer work reported in chapter 4) were used extensively in this study.

While some of the bedrock groundwater reaching the study stream must be interbasin transfer into the West Fork, the source areas for this transfer remain unknown. It is possible that some of the water moving into the West Fork in the subsurface is from the stream on the East Fork, the 59.1 ha basin adjacent to the West Fork. As Figure 7 shows, there are two places where streamwater infiltrates the stream bed and is lost from the main channel on the East Fork; this leads to two reaches with ephemeral flow lying downstream of reaches with perennial flow. The upstream point of loss in the East Fork stream lies at an elevation of 280 m, the downstream point at 274 m (elevations are above mean sea level, and are plus or minus about 0.5 m). On the West Fork, springs S3 and S3A lie at about 277 m, while WB60-WB0 covers an elevation range of about 268-271 m. Thus, each of the two points where water is lost from the East Fork stream is roughly 3 m higher in elevation than one of the two prominent inflow features associated with bedrock

on the West Fork stream. Also, the sites of water loss on the East Fork are displaced mainly along strike (with a small component of displacement normal to strike) from S3/S3A and WB60-WB0; as noted earlier, parallel to strike is a prime direction for solutional enlargement of fractures and cavities [Crider, 1981]. Tests with injected tracers might establish whether streamwater from the East Fork contributes to streamflow on the West Fork.

In addition to directly affecting streamflow generation by transmitting water through cavities, the bedrock may also exercise indirect control over streamflow generation. Bedrock may affect water flow in the soil by influencing the shape of the soil mantle in places where there is little or no saprolite. Figure 9 is a schematic vertical cross section normal to strike, through a site with tilted karst carbonate strata. On the West Fork, a similar cross section might be found on the east slope of the perennial stream valley, parallel to the stream channel; as noted earlier, small outcrops that just break the soil surface can be traced upslope in this area, and there appears to be little or no saprolite between the bedrock and overlying Alfisols. Between the edges of the more resistant beds which outcrop at the ground surface lie bands of deeper soil covering the ends of the less resistant beds. Thus, differential weathering leads to a pattern in which bands of relatively deep soil alternate with outcrops or bands of shallow soil (the bands being parallel to strike and, on the West Fork, normal to the perennial stream channel). This variability in soil thickness could be partially responsible for the difficulty in locating saturated conditions in the soil, even near the stream bank (saturated conditions

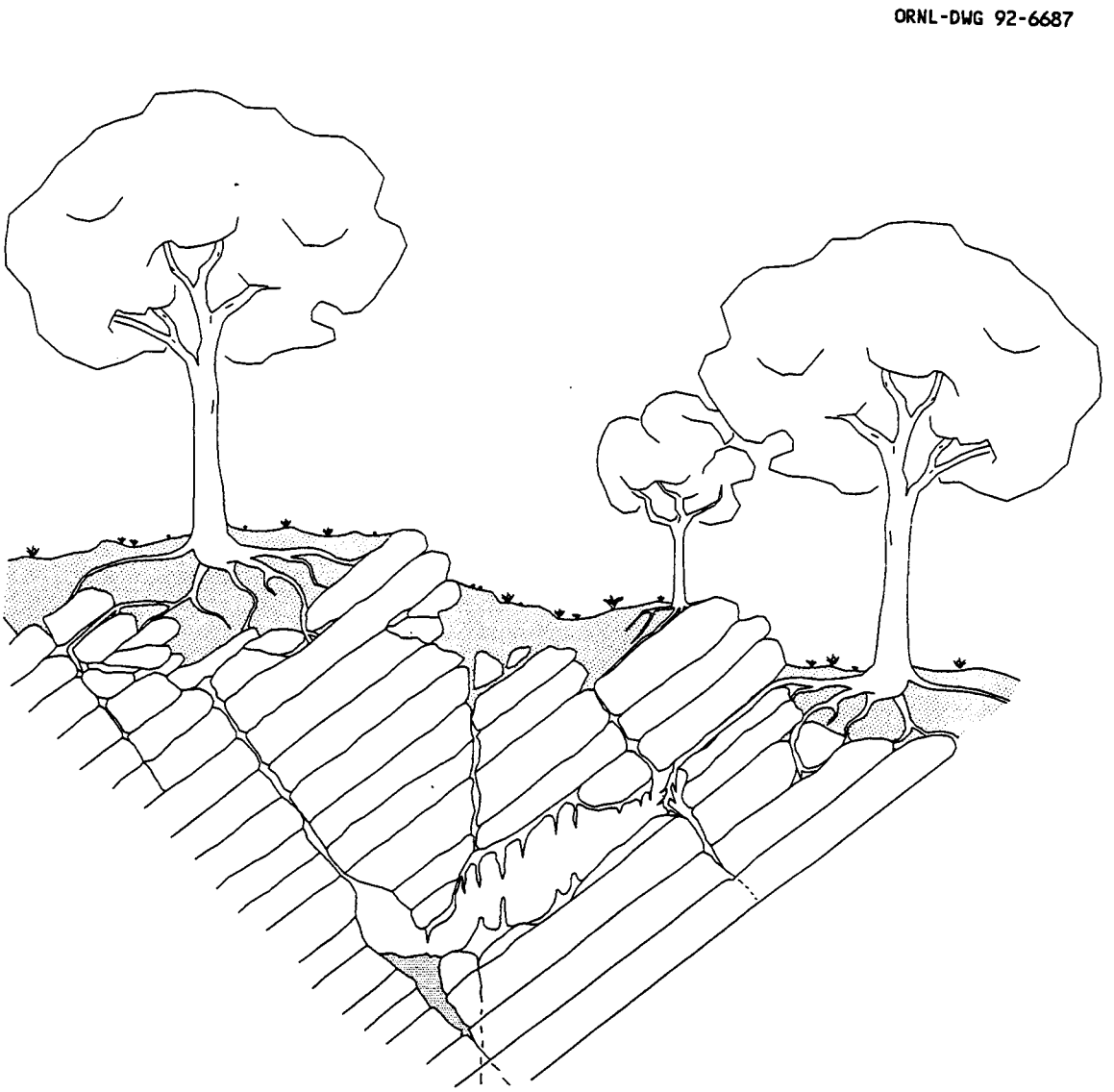

Figure 9. Schematic vertical cross section normal to bedrock strike in karst terrain. After Fanning [1970].

may be restricted to the areas of deeper soil much of the time). Such variability in saturated conditions (and in soil moisture in general) could be responsible for some of the observed spatial variability in stream inflow since, other factors being equal, bands of deeper, wetter soil would be associated with stream reaches of higher inflow. This is one restricted sense in which variability in soil thickness (and therefore in maximum potential transmissivity) could be partially responsible for the spatial variability in streamflow generation.

WB120-WB100 is an example of a reach where this phenomenon may be at work. This reach has significantly higher inflow than the adjacent reaches (Fig. 4) and there are rock outcrops which can be traced upslope from the stream channel at approximately WB120 and WB90. A well point was driven to a depth of 1.5 m about 2 m from the stream bank on the east slope, at WB110; the well was used for groundwater sampling, and yielded water year-round. Attempts at driving well points a few meters upstream and downstream met with refusal at <1 m, in the unsaturated zone. Thus, this reach of "locally" high inflow is centered on a band of relatively deep soil (on at least the east slope) which is perennially saturated below 1.5 m and which thins towards the outcrops that lie on either side.

A third way (one which operates on all watersheds) in which bedrock geology can affect streamflow generation in through its influence on topography. Some beds are more erodable than others because of differences in lithology (e.g., on the West Fork, lower chert content) and/or structure (e.g., greater density of fractures), and these beds weather more deeply to produce convergent, hollow

shaped topography. Springs S3 and S3A and their environs (WB242-WB170) provide an interesting example of the relationships among erodability, topography, and water flux to the study stream. For reasons discussed in the previous section, the association between high water inflow to this reach and adjacent convergent topography is not due to convergent drainage from the soil mantle (the process responsible at the study site of Anderson and Burt [1978]). Instead, three independent lines of evidence (steady water flow, chemical and temperature characteristics, and general lack of a significant soil saturated zone) indicate that most of the inflow to WB242-WB170 is from the bedrock groundwater system. Thus, rather than high stream inflow being due to convergent topography, the high inflow and convergent topography are probably both due to a highly fractured, highly erodable zone in the lower Kingsport Formation. There are no direct observations of the bedrock which point to a greater fracture density in the vicinity of WB242-WB170. However, this hypothesis does tie together a variety of hydrogeologic observations in a reasonable manner.

In a somewhat trivial sense, one could use the water balance data to argue that the West Fork is not a "representative" basin for this region (clearly, not every basin in a region can receive a net interbasin transfer of 30-40 cm per year). In addition, the West Fork is probably not "representative" in the more specific sense suggested by Wood et al. [1988]. They suggested the existence of a "Representative Elementary Area" (REA), which "is strictly analogous to the concept of the Representative Elementary Volume (REV) in porous media"; the REA would be

"a critical area at which implicit continuum assumptions can be used without knowledge of the patterns of parameter values" [Wood et al., 1988, p.31]. While our data do not allow quantitative estimation of the REA following a method similar to that of Wood et al. [1988], the lack of repetition in data such as those in Fig. 4 suggests that we have not sampled a "Representative Elementary Stream" (RES), and hence, its associated REA. (RES, our own term, is used informally here to refer to the longest stream on a REA. If the REA is determined by sampling in the stream at different scales, as in Wood et al. [1988], then the REA would be inextricably linked to a RES of some kind.) Since our 300 m study reach includes only one example of some reach types (i.e., only one reach like WB242-WB170 where inflow is high at low Q_{weir} and increases moderately with Q_{weir}, and only one reach like WB60-WB0 where inflow is low at low Q_{weir} and increases dramatically with Q_{weir}), the West Fork probably does not contain a representative sample of the different reach behaviors which would constitute a RES (REA) in this terrain. The REA (if it can be defined for this landscape) is probably significantly larger than a first order basin (~50 ha), the basin size used in this and in most field studies of streamflow generation. Though a first order basin includes all the topographic and surface hydrologic features of the landscape (valley bottoms, ridge tops, hollows, spurs, ephemeral and perennial stream channels), it does not fully sample the bedrock heterogeneity. Thus, while hydrologic processes on the West Fork are probably typical for karst terrain, the West Fork is probably not "representative" in the particular sense suggested by Wood et al. [1988].

6. Summary

Chemical dilution stream gauging was used to determine the lateral inflow to stream reaches of various sizes (down to 20 m in length) on a 300 m section of a first order stream draining the West Fork of Walker Branch Watershed. For reaches of 60-130 m, the relationships between lateral inflow and Q_{weir} (streamflow at the basin outlet) were highly linear over a wide range of flow ($350<Q_{weir}<3500$ L/min). These relationships can be used to estimate the spatial pattern of stream inflow at a given time from a single Q_{weir} measurement. Tremendous spatial variability was evident at all scales (reaches of 20-130 m); the permeable karst nature of the dolomite bedrock is the dominant control on the observed variability. This control is probably exerted directly, by water movement through the bedrock, and indirectly, through the effects of geology on topography, and the shape and thickness of the soil mantle. Many of the traditional hillslope hydrometric methods which focus solely on measurement of water flux and/or storage in the soil would be of limited utility in this complex hydrogeologic environment. For this reason, use of natural tracers has been an important part of the research on the West Fork. While this chapter has focused on the amount of water entering the study stream at different places and times (strictly speaking, different places and Q_{weir} values), Chapter 4 describes the use of natural tracers in partitioning the stream inflow into water drainage from three hydrogeologic reservoirs.

Appendix

As described in section 3, two different methods were used to calculate streamflow (Q) values:

Method 1: The specific conductivity change at the measurement site farthest upstream, $(\gamma_s-\gamma_b)_1$, was converted to a NaCl concentration (C_1) using data from Jones [1912]. Q at this station was then determined from the equation $Q_1 = Q_0C_0/C_1$, where Q_0 and C_0 are the injection rate and NaCl concentration, respectively, of the tracer solution. Q values at sites farther downstream (Q_j) were calculated using the flow and specific conductivity data at the first site: $Q_j = Q_1(\gamma_s-\gamma_b)_1/(\gamma_s-\gamma_b)_j$.

Method 2: The chloride content of background and plateau samples (S_b and S_s, respectively) was measured in the lab, and streamflow values were calculated from the expression $Q_j = Q_0C_0/(S_s-S_b)_j$.

Uncertainty in Q_0 and C_0 is directly relevant for both methods. Q_0 was measured in the field by capturing the flow from the Marriotte bottle in a graduated cylinder for a period of time (20-30 seconds) measured with a stopwatch; replicate measurements were always nearly (and often exactly) identical. The flow from a properly functioning Marriotte bottle is extremely steady, and replicate measurements sufficed to establish Q_0 to within ~1% (all the uncertainties mentioned in this section refer to 95%, ~2σ, confidence limits).

S_0 was determined from the known weights of reagent grade NaCl (>99% pure) and distilled water used to prepare the tracer solution. The mass of NaCl

(m_s) was determined by weighing out 3-4 aliquots of NaCl (each up to 2500 g, weighed to the nearest 0.2 g); the uncertainty in m_s was negligible (much less than 1%). The NaCl was placed in a 50 L carboy, and the carboy was then weighed on a balance with a 50 g resolution. The carboy was filled with distilled water and reweighed on the same balance, and the amount of water (m_w) determined by difference. The mass of water was generally about 40 kg, plus or minus about 100 g. The parameter A, defined as $100m_s/(m_s+m_w)$, was calculated for the tracer solution. A linear regression of M (molarity, moles NaCl per liter of solution) vs. A was calculated using nine data points from Weast [1976, p.D-253] between A=12 and A=17 (tracer solutions had A values of 14-15). The resultant straight line (with a correlation coefficient of 0.999949) was used to convert the A value for each tracer solution to a molarity. The uncertainty in the final molarity was very small, about 0.01 M (<1%). Thus, the uncertainty in Q_0 and C_0 introduced a negligible uncertainty in the measured streamflow values. The uncertainty associated with streamwater tracer concentrations (explored below for both methods of calculating Q) accounted for most of the uncertainty in the streamflow values.

Method 1

The uncertainty in γ_s-γ_b values was generally plus or minus 0.4-2 μS/cm; the larger uncertainties were obtained when there was significant γ_b drift, and when γ_b and/or γ_s were $\geq$200 μS/cm (γ values in this range could only be measured with a

resolution of ±1 μS/cm, instead of the ±0.1 μS/cm resolution obtained for lower values). Using data from Jones [1912], $(\gamma_s-\gamma_b)_1$, (the $\gamma_s-\gamma_b$ value at the site farthest upstream) was converted to an equivalent NaCl concentration (C_1). Standard statistical methods (Zar [1984], p.275, equation 17.28) were used to estimate the uncertainty in C_1 (it was plus or minus 0.04-0.06 mM, depending on the value of C_1). The uncertainties in Q_0, C_0, and C_1 were propagated according to equation B.4 of Kline [1985] to determine the uncertainty in Q_1; this uncertainty, along with those of $(\gamma_s-\gamma_b)_1$ and $(\gamma_s-\gamma_b)_j$, was propagated to determine the uncertainty in other streamflow values (Q_j). Total uncertainty in streamflow values calculated by Method 1 averaged 5%, and ranged from 1-11%.

Method 2

The uncertainty in S_s-S_b values was a function of the number of replicate samples and their variability, and the uncertainty in the calibration line on the TRAACS 800 auto analyzer. Usually, 3-4 samples were collected at steady state, 1-2 at background. The number of steady state samples was greater because S_s was generally much greater than S_b (0.5-5.0 mM, compared to 0.02 mM), hence the uncertainty in S_s-S_b was controlled by uncertainty in S_s (the fact that S_b might be 0.02 plus or minus 25-50% was relatively unimportant). Calibration lines were prepared by running five NaCl standards on the TRAACS 800; the standards had concentrations of 2, 4, 6, 8, and 10 mg/L of NaCl (0.0564-0.282 mM Cl^-). As noted earlier, S_s samples were diluted with doubly distilled water to bring their Cl^-

concentrations into the range spanned by the standards. The average uncertainty in S_s-S_b values was 6% (the range was 2-17%), leading to an average uncertainty of 7% (the range was 2-18%) in streamflow values determined by Method 2.

Lateral inflow

The lateral inflow to a given reach was generally much less than the streamflow at either end of the reach; as a result, a small relative uncertainty in the streamflow values led to a much larger relative uncertainty in lateral inflow. For example, if the lateral inflow to a reach is 10% of the streamflow at the upstream end, and the streamflow at each end has an uncertainty of ±5%, the lateral inflow would have an uncertainty of ±74%. Thus, there is a trade-off between spatial resolution and relative uncertainty, with the choice of reach length being determined largely by the intended use of the data. While there is a large relative uncertainty in the lateral inflow to the short reaches shown in Fig. 4 (plus or minus 50-100%, except for WB220-WB170 and WB60-WB0), these data are useful in demonstrating the general spatial pattern of stream inflow and the extent of variability. Aggregating the data to larger reaches allowed development of highly linear correlations with Q_{weir} (see Fig. 6) which can be used in a predictive mode over a wide range of flows. Table A.1 gives lateral inflow and uncertainty data for three of the reaches shown in Fig. 6. The uncertainty in WB60-WB0 inflow was calculated assuming a 4% uncertainty in Q_{weir} measurements. The relative uncertainties cover a much wider range than the absolute uncertainties,

Q_{weir} (L/min)	Lateral inflow (L/min)		
	WB300-WB170	WB170-WB60	WB60-WB0
354	242 ± 11 (4.5%)	68 ± 17 (24%)	21 ± 19 (91%)
395	281 ± 15 (5.2%)	36 ± 22 (63%)	26 ± 20 (76%)
411	234 ± 11 (4.6%)	36 ± 16 (43%)	78 ± 20 (26%)
680	286 ± 20 (7.0%)	67 ± 31 (47%)	166 ± 36 (22%)
709	346 ± 22 (6.3%)	67 ± 34 (51%)	138 ± 38 (28%)
722	306 ± 23 (7.7%)	91 ± 47 (51%)	150 ± 50 (33%)
1050	350 ± 21 (6.1%)	92 ± 40 (41%)	260 ± 54 (21%)
1148	375 ± 53 (14%)	79 ± 74 (94%)	326 ± 72 (22%)
1368	364 ± 38 (10%)	[482 ± 89 (18%)]	
1447	428 ± 40 (9.3%)	109 ± 62 (57%)	403 ± 76 (19%)
2749	445 ± 123 (28%)	179 ± 179 (100%)	1081 ± 267 (25%)
3457	591 ± 122 (21%)	212 ± 159 (75%)	1007 ± 175 (17%)

Table A.1. Lateral inflow 95% confidence limits for three reaches of the study stream. No measurements were made at WB60 on 10/4/89; the value given in brackets is for WB170-WB0.

from 5-10% for much of the WB300-WB170 data to over 90% for some of the very small lateral inflows to the other two reaches. The highly uncertain values represent small differences between two much larger numbers (e.g., the 79 L/min value in the eighth row of the WB170-WB60 column is the difference between 822 and 743 L/min).

There were very small decreases in streamflow during most of the experiments; the maximum rate of decrease in Q_{weir} (1 L/min per minute) was observed during the highest flow experiment (3/18/90; average Q_{weir} during the two hour experiment was 3457 L/min). The magnitude of the change in lateral inflow to a given reach can be estimated with the linear regressions in Fig. 6 and the observed rate of decrease in Q_{weir}. For example, the slope of the lateral inflow vs. Q_{weir} regression for WB60-WB0 indicates that any change in Q_{weir} is associated with a change 36% as large in the lateral inflow to this reach. Thus, the WB60-WB0 lateral inflow would have been decreasing at about 0.36 L/min per minute during the 3/18/90 experiment, leading to a drop in the lateral inflow rate of 38 L/min during the 105 minute experiment. This decrease of 38 L/min in the lateral inflow rate of ~1000 L/min represents a change of 3.8%. This is much smaller than the lateral inflow uncertainty which is due to uncertainty in streamwater tracer concentrations (±17% for this reach during this experiment), and unsteadiness in lateral inflow was even less important for other reaches and other experiments. Thus, ignoring the slightly unsteady nature of the stream inflow during our experiments introduces only a very small error which is dwarfed by the uncertainty

in the tracer measurements.

Acknowledgements

The helpful advice of Phil Gschwend and Peter Eagleson at MIT is gratefully acknowledged. The authors are also thankful for the assistance provided by several staff scientists and students at Oak Ridge National Lab. Michael Huston and David Lietzke provided useful discussions of soils, topography, and other aspects of the study site. The field work would not have been possible without the timely help of Amy Rosemond, Bonnie Lu, Amanda Hood, and Lisa Au. Bonnie also analyzed all the chloride samples. This work was sponsored by the U.S. Geological Survey (contract no. 14-08-0001-G-1725) and the National Science Foundation (contract no. BCS-8906032). The first author acknowledges his fellowship support from Oak Ridge Associated Universities, as well as support from the Walker Branch Watershed Project funded by the Ecological Research Division, Office of Health and Environmental Research, U.S. Department of Energy, under contract DE-AC05-84OR21400 with Martin Marietta Energy Systems Inc.

Bibliography

Anderson, M.G., and T.P. Burt. 1978. The role of topography in controlling throughflow generation. Earth Surface Processes 3:331-344.

Crider, D.V. 1981. Structural and Stratigraphic Effects on Geomorphology and Groundwater Movement in Knox Dolostone Terrain. M.S. Thesis,

University of Tennessee, Knoxville, Tennessee.

Fanning, D.S. 1970. Cave features: Information concerning the nature and genesis of soils. Soil Science Society of America Proceedings 34:98-104.

Fanning, D.S., and M.C.B. Fanning. 1989. Soil: Morphology, Genesis, and Classification. John Wiley and Sons, New York.

Fennessey, N.M., P.S. Eagleson, W. Qinliang, and I. Rodriguez-Iturbe. 1986. Spatial Analysis of Storm Depths from an Arizona Raingage Network. Ralph M. Parsons Laboratory Report No. 306, Dept. of Civil Engineering, MIT, Cambridge, Massachusetts.

Henderson, G.S., W.F. Harris, D.E. Todd Jr., and T. Grizzard. 1977. Quantity and chemistry of throughfall as influenced by forest type and season. Journal of Ecology 65:365-374.

Huff, D.D., R.V. O'Neill, W.R. Emanuel, J.W. Elwood, and J.D. Newbold. 1982. Flow variability and hillslope hydrology. Earth Surface Processes and Landforms 7:91-94.

Johnson, D.W. 1989. Site description, in Analysis of Biogeochemical Cycling Processes on Walker Branch Watershed, D.W. Johnson and R.I. van Hook (eds.), p.6-20, Springer-Verlag, New York.

Jones, H.C. 1912. The Electrical Conductivity, Dissociation and Temperature Coefficients of Conductivity from Zero to Sixty-Five Degrees of Aqueous Solutions of a Number of Salts and Organic Acids. Carnegie Institution of Washington, Washington D.C.

Ketelle, R.H., and D.D. Huff. 1984. Site Characterization of the West Chestnut Ridge Site. ORNL/TM-9229, Oak Ridge National Laboratory, Oak Ridge, Tennessee.

Kline, S.J. 1985. The purpose of uncertainty analysis. Journal of Fluids Engineering 107:153-160.

Lee, S.Y., O.C. Kopp, and D.A. Lietzke. 1984. Mineralogical Characterization of West Chestnut Ridge Soils. ORNL/TM-9361, Oak Ridge National Laboratory, Oak Ridge, Tennessee.

Lietzke, D.A., R.H. Ketelle, and R.R. Lee. 1989. Soils and Geomorphology of the East Chestnut Ridge Site. ORNL/TM-11364, Oak Ridge National Laboratory, Oak Ridge, Tennessee.

Lietzke, D.A. 1990. Soils of Walker Branch Watershed. ORNL/TM-11724, Oak Ridge National Laboratory, Oak Ridge, Tennessee.

Luxmoore, R.J., T. Grizzard, and M.R. Patterson. 1981. Hydraulic properties of Fullerton cherty silt loam. Soil Science Society of America Journal 45:692-698.

Luxmoore, R.J., and D.D. Huff. 1989. Water, in Analysis of Biogeochemical Cycling Processes in Walker Branch Watershed, D.W. Johnson and R.I. van Hook (eds.), p.164-196, Springer-Verlag, New York.

McMaster, W.M. 1967. Hydrologic Data for the Oak Ridge Area, Tennessee. U.S. Geological Survey Water Supply Paper 1839-N, U.S. Government Printing Office, Washington D.C.

Mulholland, P.J., G.V. Wilson, and P.M. Jardine. 1990. Hydrogeochemical response of a forested watershed to storms: Effects of preferential flow along shallow and deep pathways. Water Resources Research 26(12):3021-3036.

Orlanski, I. 1975. A rational subdivision of scales for atmospheric processes. Bulletin of the American Meteorological Society 56(5):527-530.

Peters, L.N., D.F. Grigal, J.W. Curlin, and W.J. Selvidge. 1970. Walker Branch Watershed Report: Chemical, Physical, and Morphological Properties of the Soils of Walker Branch Watershed. ORNL/TM-2968, Oak Ridge National Laboratory, Oak Ridge, Tennessee.

Soil Conservation Service. 1975. Soil Taxonomy: A Basic System of Soil Classification for Making and Interpreting Soil Surveys. Agriculture Handbook No.436, U.S. Department of Agriculture, Washington, D.C.

TVA. 1972. Upper Bear Creek Experimental Project: A Continuous Daily Streamflow Model. Research Paper No.8, Tennessee Valley Authority, Knoxville, Tennessee.

U.S. EPA. 1983. Methods for Chemical Analysis of Water and Wastes. EPA-600/4-79-020 (350.1-1 to 350.1-6), Environmental Monitoring and Support Laboratory, Cincinnati, Ohio.

Weast, R.C. 1976. Handbook of Chemistry and Physics, 56th Edition. Chemical Rubber Co., Cleveland, Ohio.

Wilson, G.V., and R.J. Luxmoore. 1988. Infiltration, macroporosity, and

mesoporosity distributions on two forested watersheds. Soil Science Society of America Journal 52:329-335.

Wilson, G.V., J.M. Alfonsi, and P.M. Jardine. 1989. Spatial variability of saturated hydraulic conductivity of two forested watersheds. Soil Science Society of America Journal 53:679-685.

Wilson, G.V., P.M. Jardine, R.J. Luxmoore, and J.R. Jones. 1990. Hydrology of a forested watershed during storm events. Geoderma 46:119-138.

Wood, E.F., M. Sivapalan, K. Beven, and L. Band. 1988. Effects of spatial variability and scale with implications to hydrologic modelling. Journal of Hydrology 102:29-47.

Zar, J.H. 1984. Biostatistical Analysis. Prentice-Hall, Englewood Cliffs, New Jersey.

CHAPTER 4

Use of Calcium and ^{222}Rn as Tracers in a Three-End-Member Mixing Model for Streamflow Generation on Walker Branch Watershed, Tennessee

David P. Genereux, Harold F. Hemond, and Patrick J. Mulholland

Abstract

Measurements of naturally occurring ^{222}Rn and Ca in a variety of different waters on the West Fork of Walker Branch suggest that a simple three-end-member mixing model is appropriate for streamflow generation over a wide range of flow conditions. The three end members are vadose zone water, soil groundwater, and bedrock groundwater. Bedrock groundwater was distinguished from the soil end members on the basis of its high Ca content; ^{222}Rn concentration was the basis for the distinction between vadose zone water (low ^{222}Rn) and soil groundwater (high ^{222}Rn). The behavior of the end members with changing flow was consistent with a wide variety of environmental observations, including temperature and flow variations at springs, water table responses, the general lack of saturated zones on hillslopes and even near the stream in some places, and the importance of water movement through bedrock. Variability in the chemistry of the end members precluded using other solutes (Na, K, and SO_4) to test the mixing fractions derived from ^{222}Rn and Ca data; during those times of year when the soil temperature is most different from that of the underlying bedrock (late summer and late winter), temperature may be a useful tracer for distinguishing between water from the soil end members and that from bedrock. The mixing model provides a simple framework for analyzing the essential features of streamflow generation in this highly heterogeneous terrain.

1. Introduction

Naturally-occurring isotopic and chemical tracers are important tools in the study of streamflow generation. Such tracers are often applied in the context of simple mixing models which attempt to separate the relative contributions to streamflow from different hydrologic reservoirs. A well-known example is the use of ^{18}O or ^{2}H to separate storm streamflow into "new" water (storm precipitation) and "old" water (prestorm subsurface water) [e.g., Sklash et al., 1976, 1986; Hooper and Shoemaker, 1986]. These studies place important constraints on the nature of streamflow generation during storms, by demonstrating that usually more than half (and often ≥80%) of storm streamflow is old water. As with any natural tracer, there are limitations on the utility of ^{18}O and ^{2}H. The two-component old-new distinction is relevant only during stormflow, and the principle criterion for a useful old-new separation (that the difference in isotopic composition between the old and new water be large relative to the sum of the analytical uncertainty of the isotope measurements plus any isotopic variability within the two components) is not met by every storm. Spatial and/or temporal variability in the isotopic composition of old and new water leads to complications with the simple two-component model [Hooper and Shoemaker, 1986; DeWalle et al., 1988; McDonnell et al., 1990]. DeWalle et al. [1988] used a three-component (channel precipitation, soil water, and groundwater) mixing model for stormflow in order to account for spatial variability in the ^{18}O content of old water on their study site (soil water was isotopically heavier than groundwater). While this framework could

potentially be useful when old water isotopic composition is heterogeneous, it is not without its own complications [Genereux and Hemond, 1990a].

Others have formulated three-component mixing models based on major ion concentrations. Hooper et al. [1990] found that when a variety of water samples (soil water, groundwater, and streamwater) from Panola Mountain Watershed in Georgia were plotted on a graph showing the concentration of one solute vs. that of another (e.g., SO_4 vs. Ca, Si vs. Mg), the streamwater samples generally fell within the triangular space bounded by three subsurface waters of extreme (very high or very low) concentration. These three subsurface waters, referred to as "end members", were found to be "organic" horizon water (water draining the organic soil horizon), "hillslope" water (from a hillslope well in the upper part of the watershed), and "groundwater" (from a floodplain well near the basin outlet). Streamwater chemistry was explained by viewing streamwater as a mixture of the three end members, with the end members having approximately constant chemical concentrations and the temporal variability in streamwater chemistry being due to changes in the end member mixing proportions (i.e., the fraction of streamflow accounted for by each end member). Christophersen et al. [1990] followed the same approach for the Birkenes (southern Norway) and Plynlimon (Mid-Wales) catchments, but were not able to identify three subsurface end members which bounded streamwater chemistry.

This approach takes advantage of the differences in water chemistry among subsurface horizons to show how important the different water sources (end

members) are to streamflow generation. It also has the advantage of being applicable to both baseflow and stormflow. One possible disadvantage is the lack of information regarding the rate at which water moving from one zone to another in the subsurface will acquire the chemical signature of the zone it enters. For example, nearly all the "hillslope" water and "groundwater" at Panola Mountain must have infiltrated through the organic surface soil (except for rain falling on a patch of bare bedrock in the upper part of the watershed), and hence they were once "organic" water. The chemistry of drainage from the organic zone obviously changes as it moves into the underlying mineral soil (otherwise the streamwater at Panola would be ~100% "organic" water), and the rate at which this occurs is one of the controls on how much of the streamflow is due to the "organic" end member. Thus, the mixing proportions calculated are influenced by how far "organic" water can move through mineral soil (or, how much time it can spend in mineral soil) before acquiring "hillslope" or "groundwater" chemistry. The same applies to water moving between other zones (e.g., "hillslope" to "groundwater", "hillslope" to "organic", etc.). Knowledge of these chemical transformation rates would help clarify what the end members actually represent, in cases where water moves through subsurface zones corresponding to more than one end member.

^{222}Rn can be useful in distinguishing between saturated zone water and vadose (unsaturated) zone water, since the former often has a much higher ^{222}Rn content than the latter [Genereux and Hemond, 1990b]. Water in unsaturated zones may lose much of its ^{222}Rn to the atmosphere by diffusion through soil gas,

while water in saturated zones generally retains most of its ^{222}Rn. Vadose zone water which enters a saturated zone begins to accumulate ^{222}Rn (i.e., to acquire the ^{222}Rn signature of soil groundwater) at a rate controlled by the radioactive decay rate of ^{222}Rn (0.181 day^{-1}). Thus, when the distinction between vadose zone water and soil groundwater is based on ^{222}Rn, water having been in a saturated zone for several days or more is considered "soil groundwater" [Genereux and Hemond, 1990b]. Since the rate at which vadose zone water acquires the ^{222}Rn signature of soil groundwater depends on a well-known constant, the end members in a ^{222}Rn-based separation are in some sense more easily interpreted than those in the ^{18}O-based separation of DeWalle et al. [1988] or the major-ion-based separation of Hooper et al. [1990].

In this paper we report results from the application of ^{222}Rn as a tracer for separating vadose zone water and soil groundwater contributions to streamflow on the West Fork of Walker Branch Watershed in eastern Tennessee. There is a substantial body of evidence (see Chapter 3) which suggests that a third water source (groundwater from fractured bedrock) is also important to streamflow generation on the West Fork. Following a suggestion from some earlier work on the West Fork [Mulholland et al., 1990], we used naturally-occurring Ca as a second tracer to distinguish bedrock water from vadose zone water and soil groundwater. Water having significant contact with the dolomite bedrock on the West Fork acquires a much higher Ca content than water contacting only the Ca-poor soil. Thus, our study involved measuring ^{222}Rn and Ca concentrations in

various waters on the West Fork (vadose zone water, soil groundwater, springwater, and streamwater) in order to determine whether ^{222}Rn and Ca concentrations in streamwater and springwater could be explained by viewing these waters as mixtures of subsurface waters, and, if so, whether the mixing model was hydrologically reasonable.

2. Study Site and Methods

2.1. Sampling sites

The West Fork is a 38.4 ha forested watershed in Oak Ridge, Tennessee. Data on the magnitude and spatial variability of stream inflows are given in Chapter 3; these data indicate that the heterogeneous nature of the karst bedrock is an important control on streamflow generation. A detailed description of the West Fork is also given in Chapter 3.

Each stream sampling site in Figure 1 is labeled with the prefix "WB" followed by its distance (in meters) upstream of the weir at the basin outlet (i.e., WB0 is the weir itself, WB60 is the site 60 m upstream of the weir, etc.). The three main stream sampling sites were WB242, WB170, WB60. Water from four springs (S2, S3, S3A, and S4) and two shallow groundwater wells (4B and 8) was also sampled. Small fiberglass flumes were used to measure flow rates at springs S3, S3A, and S4. Wells 4B and 8 consisted of a narrow (4 mm ID) steel pipe inside a larger (about 2.5 cm OD) steel pipe with a stainless steel well screen (7.5 cm long, 2.5 cm OD) at the bottom. The annulus between the inner and outer

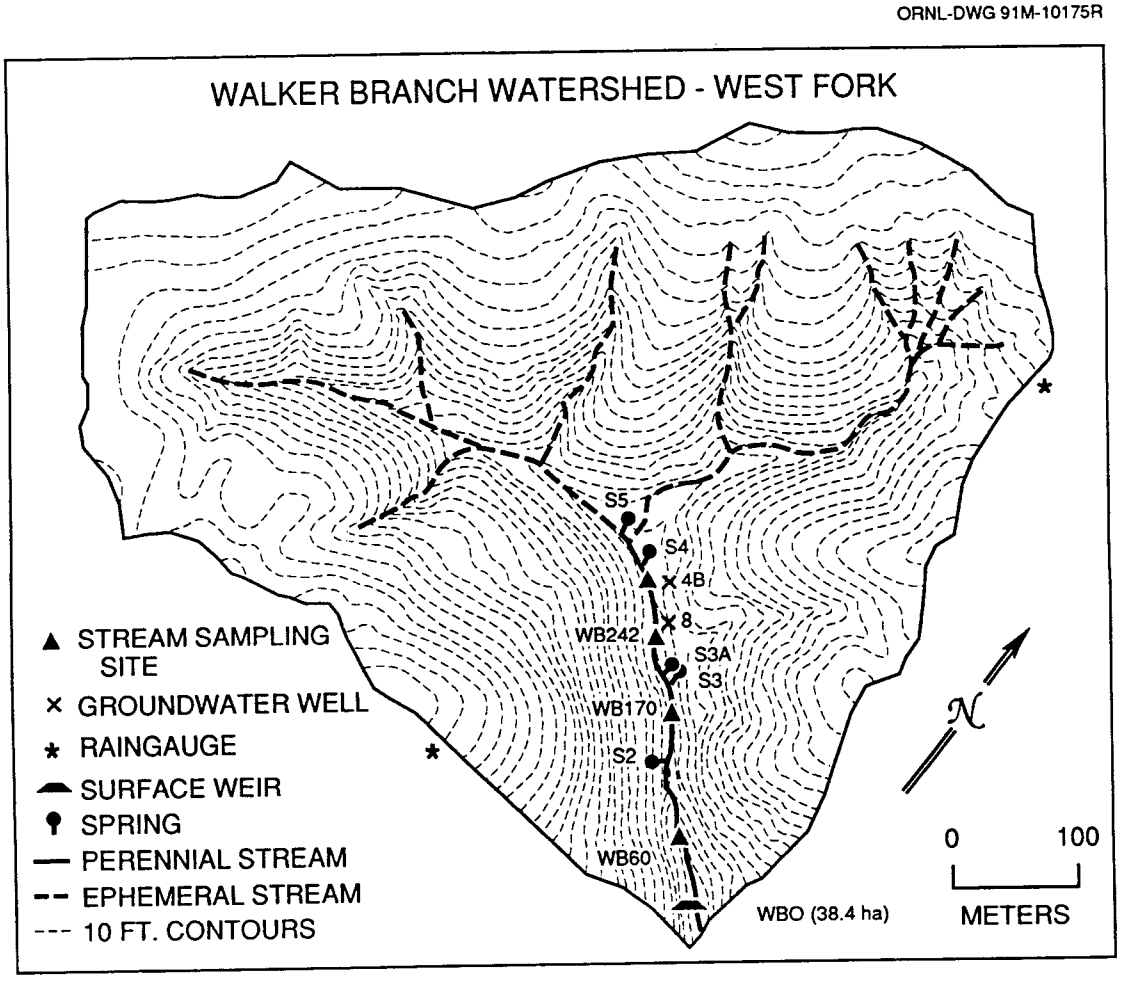

Figure 1. Map of the study site.

steel pipes was sealed off at the bottom (and top), so water entering the well screen could rise into only the narrow inner pipe. A narrow inner pipe was used to decrease the "dead volume" in the wells, an important concern when sampling for volatiles like ^{222}Rn; the larger outer pipe was used only because it was sturdy enough to be hammered into the soil to provide an easy pathway for installation of the narrow pipe. Wells 4B and 8 were 140 and 53 cm deep, respectively (ground surface to center of well screen). Well 4B yielded water continuously throughout the study period (October 1989 to November 1990), while well 8, installed in April 1990, yielded water only until August.

The ^{222}Rn content of vadose zone water was inferred by measuring the ^{222}Rn content of soil gas and assuming local equilibrium partitioning of ^{222}Rn between soil gas and soil water [Genereux and Hemond, 1990b, 1991]. Soil gas was collected from 12 narrow diameter sampling tubes installed in mid- to lower-slope locations between WB300 and WB60 on both sides of the perennial stream valley; the tubes were of the same construction as wells 4B and 8. At least seven of the 12 tubes were installed in (i.e., their screens lay in) the B horizon, three were installed very near the A/B interface (just above or below, or possibly straddling the interface), and two were installed in the dense clay saprolite below the B horizon (soils are discussed in detail in chapter 3). The Ca content of vadose zone water was not measured in this study, since it was already well known from previous work. Dale Johnson and coworkers made monthly measurements of the Ca concentration of B horizon vadose zone water from five plots on the West Fork between May 1983

and May 1986 [Johnson and Todd, 1990; Johnson, unpub. data]. Soil water was drawn from four lysimeters at each plot; the lysimeters were installed at a depth of about 100 cm.

2.2. Sampling program

The ^{222}Rn content of streamwater, [Rn], is strongly affected by volatilization to the atmosphere, and this must be accounted for in using [Rn] data to elucidate the subsurface water sources important in streamflow generation. The method used in this study was identical to that of Genereux and Hemond [1990b]. Steady simultaneous injections of NaCl and propane were made into the study stream upstream of WB242. Steady state plateau concentrations of Cl^- and propane were then measured at WB242, WB170, and WB60. The injected Cl^- allowed determination of the rate of lateral inflow of water to the study reaches (WB242-WB170 and WB170-WB60), and the propane data allowed determination of the amount of ^{222}Rn lost by volatilization from the study reaches. In accord with the results from previously published laboratory experiments, propane and ^{222}Rn were considered to have identical volatilization rates; this is discussed in detail in Appendix B of Chapter 1. Measuring [Rn] at the same three sampling sites allowed us to solve a ^{222}Rn mass balance around each study reach and calculate the ^{222}Rn concentration in the lateral inflow ($[Rn]_q$):

$$[Rn]_q = \frac{Q_2[Rn]_2 - Q_1[Rn]_1 + \tau k Q_{avg}[Rn]_{avg}}{q\Delta x} \qquad (1)$$

where Q = volumetric streamflow rate

q = lateral inflow rate of water, volume/time per unit length of channel

Δx = length of stream reach

τ = travel time of water through stream reach

k = first order volatilization rate constant for ^{222}Rn in the stream reach ($time^{-1}$)

[Rn] = ^{222}Rn content of streamwater

$Q_{avg} = (Q_1 + Q_2)/2$

$[Rn]_{avg} = ([Rn]_1 + [Rn]_2)/2$

and subscripts 1 and 2 designate the upstream and downstream ends of the reach, respectively. Eqn. 1 can be formulated in terms of the six tracer concentrations actually measured (those of the injected tracers Cl^- and propane, and the natural tracer ^{222}Rn, at the upstream and downstream ends of the reach):

$$[Rn]_q = \frac{[Rn]_2}{1-\frac{C_2}{C_1}} - \frac{[Rn]_1}{\frac{C_1}{C_2}-1} + \frac{([Rn]_1+[Rn]_2)(\frac{C_2}{C_1}+1)F}{4(1-\frac{C_2}{C_1})} \qquad (2)$$

where $F = \ln(G_1C_2/G_2C_1)$, and G represents the concentration of the gaseous tracer (propane) and C the concentration of the conservative tracer (Cl^-). $[Rn]_q$, the ^{222}Rn

content of lateral inflow as it arrives at the stream channel, contains information about the water sources contributing to streamflow generation. The background for this methodology, including mathematical derivations, is given by Genereux and Hemond [1990b].

Eight injected tracer experiments were performed on the West Fork from October 1989 to August 1990. The 8 days selected cover a wide range of flow conditions, from Q_{weir} = 354 L/min (Q_{weir} is the streamflow rate at the V-notch weir at the basin outlet) to Q_{weir} = 3457 L/min. Four additional injections of Cl^- (without propane) were also done in order to further study the spatial structure of lateral inflow. The results from the 12 Cl^- injections are discussed in Chapter 3; the propane volatilization data are discussed in Chapter 2.

Ca data were collected at the same stream sampling sites during 5 of the 8 injected tracer experiments, allowing calculation of $[Ca]_q$ (the Ca content of lateral inflow) for both study reaches during the 5 experiments. Analogous forms of Eqns. 1 and 2 for Ca are:

$$[Ca]_q = \frac{Q_2[Ca]_2 - Q_1[Ca]_1}{q\Delta x} \qquad (3)$$

$$[Ca]_q = \frac{\frac{[Ca]_2}{C_2} - \frac{[Ca]_1}{C_1}}{1 - \frac{C_2}{C_1}\left(\frac{C_1}{C_2} - 1\right)} \qquad (4)$$

Springwater and soil groundwater samples were also collected for Ca analysis on

these same 5 days. Measurements of ^{222}Rn in vadose zone water, soil groundwater, and springwater were also made on the days of injected tracer experiments. Springwater was generally collected <1 m from where it first emerged from the ground. Volatilization over this short distance was generally insignificant, and no volatilization correction was applied to the ^{222}Rn springwater data. However, some of the data shown in Section 3 suggest that ^{222}Rn volatilization from springwater may be important at times of very low flow.

In order to determine $[Rn]_q$ and $[Ca]_q$ values for days other than those of the 8 injected tracer experiments, correlations were developed between the parameters derived from the injected tracers (streamflow, lateral inflow, and amount of volatilization) and Q_{weir}. By using these correlations along with the continuously recorded Q_{weir} data, it was possible to estimate Q, $q\Delta x$, and τk values for any day for use in Eqns. 1 and 3. Values of these parameters were estimated for 21 different days on which ^{222}Rn and Ca data were collected, and $[Rn]_q$ and $[Ca]_q$ values were calculated for both study reaches for all of these days. In this manner, injected tracer data collected on 8 days (12 for Cl^-) were used to help provide $[Rn]_q$ and $[Ca]_q$ values for 21 additional days. The particular correlations used are given in Section 3.

The temperature of streamwater and springwater was measured during injected tracer experiments and on other sampling days from 5/11/90 through the end of the study. Subsurface temperature measurements were made at the bottoms of wells 4B and 8 and the vadose zone sampling tubes during the last 3

months of the study.

2.3. Field and laboratory methods

Water samples for ^{222}Rn analysis were collected in ground glass syringes; two samples were collected at each stream site, one sample at other sites. About 300 ml of groundwater were flushed from each well before sample collection (this volume was several times the "dead volume" inside the wells). Samples were filtered through 0.8 μm Nuclepore filters; streamwater and springwater samples were filtered as they were drawn into the syringe in the field, groundwater samples were filtered as they were expelled from the syringe in the lab. At the lab, 16.0 ml of water from each syringe was expelled into a 20 ml (nominal) glass scintillation vial containing 6.0 ml of Opti-Fluor-O™ scintillation cocktail (the actual volume of "20 ml" vials was about 24 ml). Vials were quickly and tightly capped and inverted to reduce the potential for ^{222}Rn leakage around the caps. Since the scintillation cocktail and water were immiscible, each vial contained three phases (16 ml of water at the bottom, 6 ml of scintillation cocktail floating on the water, and about 2 ml of room air headspace). To facilitate equilibration of ^{222}Rn partitioning among the three phases, vials were gently swirled and rotated and then allowed to sit for at least 16 hours before counting on a Packard Instrument Co. 4640 liquid scintillation counter. This waiting period was more than long enough to allow the short-lived radioactive daughters of ^{222}Rn to grow into secular equilibrium with the parent ^{222}Rn (this requires only about 3-4 hours). In this condition, the decay rates

of the daughters (^{218}Po, ^{214}Pb, ^{214}Bi, and ^{214}Po) are equal to that of the parent ^{222}Rn; since some of the daughter decay events are counted along with those of ^{222}Rn, overall counting efficiencies (counts per minute for each decay per minute of ^{222}Rn) can be well over 100% [e.g., Genereux and Hemond, 1991].

Calibration was achieved by counting standards containing known amounts of ^{226}Ra (^{222}Rn's parent radionuclide). A ^{226}Ra solution was prepared by careful dilution (with 1 M HCl) of an aliquot of N.B.S. Standard Reference Material 4950E, and different amounts of the solution were added to seven scintillation vials. Additional 1 M HCl was added to bring the total aqueous volume in each vial up to 16 ml. Six ml of Opti-Fluor-O™ were then added to each vial, and the vials were capped and inverted. Thus, each standard vial contained the same three phases (water, Opti-Fluor-O™, and air) in the same proportions as the sample vials. Standards were set aside for 4 weeks to allow ^{222}Rn to grow into secular equilibrium with its parent ^{226}Ra; in this condition, the decay rate of ^{222}Rn in each vial was exactly equal to the known decay rate of ^{226}Ra in the vial. The seven standards were counted (along with an eighth ^{222}Rn-free background standard) in the same manner as samples, on 23 separate occasions during the study. No drift was found in instrument performance, so the 23 count per minute (cpm) values for each standard were averaged and used along with the known ^{222}Rn concentrations (decays/minute per liter, or dpm/L) to generate the following calibration line:

$$dpm/L = 20.11cpm - 108.0 \qquad (n=8, r=0.99988) \qquad (5)$$

After using this calibration line to convert a measured cpm value for a sample to a dpm/L value, a decay correction was applied to account for ^{222}Rn decay during the time between sample collection and counting.

The ^{222}Rn content of soil gas was also measured by liquid scintillation counting, following the method of Genereux and Hemond [1991] and incorporating the changes in the "Improvements" section of that paper. Soil gas samples (each ~20 ml) were collected in ground glass syringes (~150 ml of soil gas were flushed from each tube before sample collection). At the lab 6 ml of Opti-Fluor-O™ were introduced into each syringe and the syringes were gently shaken for about 30 minutes to allow ^{222}Rn partitioning to reach equilibrium. The scintillation cocktail was then ejected into scintillation vials containing 16 ml of distilled water, and the vials were quickly and tightly capped and inverted. This processing resulted in soil gas samples being in vials of an identical nature (16 ml water, 6 ml Opti-Fluor-O™, ~2 ml of air) to water samples, allowing use of the same standards for calibration. If the dpm/L values for the standards are multiplied by their aqueous volume (0.016 L), a calibration line relating total dpm of ^{222}Rn in the vials to cpm is obtained:

$$dpm = 0.3221cpm - 1.732 \qquad (6)$$

Knowing the total dpm of ^{222}Rn in the scintillation vial, it was possible to calculate the ^{222}Rn concentration in the soil gas, $[Rn]_g$ [Genereux and Hemond, 1991].

As noted earlier, we assumed local equilibrium between soil gas and soil water with respect to ^{222}Rn partitioning. Thus, the ^{222}Rn content of vadose zone water, $[Rn]_{vzw}$, was calculated as:

$$[Rn]_{vzw}=[Rn]_g/K \qquad (7)$$

where K is the dimensionless Henry's Law constant (dpm/L in air over dpm/L in water) for radon. Data on K as a function of temperature are given by Clever [1979]. Temperature values for our sampling sites were measured directly during the last 3 months of the study by inserting a narrow thermistor down to the bottom of each sampling tube after sample collection. For days on which measurements of soil temperature were not made, soil temperatures were estimated from unpublished historical data collected about every 5 days at 4 PM from October 1975 to October 1977. Soil temperature measured at a depth of 30 cm was used for the three shallow sampling tubes, and temperature measured at 110 cm was used for the other tubes. From the estimate (or measurement) of soil temperature, the data of Clever [1979] were used to find K, and $[Rn]_{vzw}$ was calculated with Eqn. 5.

Water samples for Ca analysis were collected in 30 or 60 ml polyethylene bottles. These samples were filtered with 0.8 μm Nuclepore filters; previous work by Mulholland et al. [1990] showed no significant difference in the Ca content of the filtrate when different aliquots of the same sample were passed through 0.45 versus 1.0 μm glass fiber filters. Samples were acidified with Ultrex™ HNO_3 after filtering. Ca was measured by inductively coupled plasma (ICP) emission

spectroscopy. Samples from 3/7/90, 3/18/90, and 4/13/90 were analyzed by a commercial lab at the University of Georgia; all other samples were analyzed on a Thermo-Jarrell-Ash Atom-Scan 25.

Chloride concentrations were determined by both field measurements of specific conductivity and laboratory measurements of Cl^- with a Technicon TRAACS 800 Auto-Analyzer. Details are given in Chapter 3.

Propane concentrations were measured using a headspace equilibration technique. Streamwater samples were collected in ground glass syringes, and a small amount of He (6-7 ml) was introduced into each syringe at the lab. After allowing 2-3 hours for equilibration, 1.0 ml of the He headspace (which contained most of the propane) was injected via a sample loop onto a packed column in a Perkin Elmer 3920B gas chromatograph equipped with a flame ionization detector. Details of the procedure are given in Chapter 2.

3. Results and Discussion

3.1. End member mixing model

We begin the presentation of results with the one essential fact on which the interpretation of all the tracer data is based: when a wide variety of water samples from the West Fork are plotted on a diagram of ^{222}Rn concentration vs. Ca concentration, they fall within the triangular space defined by three waters of extreme (very high or very low) concentrations. This fact is illustrated in Fig. 2, where the water composition of samples from four springs, two wells, two stream

reaches, and the vadose zone is plotted in "^{222}Rn-Ca space". At the corners of the triangle lie the three waters of extreme composition (hereafter referred to as "end members", as in Hooper et al. [1990]). Other water samples have Ca and ^{222}Rn concentrations which can be explained by viewing these other waters as mixtures of the three end members. The remainder of this paper is devoted to a discussion of this three-end-member mixing model (whether it is hydrologically reasonable, how it can be tested, etc.).

The three end members indicated on Fig. 2 may be designated vadose zone water, soil groundwater, and bedrock groundwater. Soil groundwater and bedrock groundwater were defined by water from well 4B and spring S3, respectively. The ^{222}Rn content of vadose zone water was defined by 531 samples from 10 vadose zone sampling tubes (data from the two tubes screened in saprolite were not used because, as discussed in Chapter 3, water flow through the clay saprolite is not considered important). The Ca content of vadose zone water was defined as the average Ca content of soil water sampled during a previous study [Johnson and Todd, 1990]. The mixing triangle in Fig. 2 was drawn to surround the extremes of end member composition, thereby enclosing as many samples as possible; the corners lie at the following coordinates:

vadose zone water: $[Rn]_{vzw}$ = 100 dpm/L, $[Ca]_{vzw}$ = 0.04 mM

soil groundwater: $[Rn]_{sgw}$ = 4300 dpm/L, $[Ca]_{sgw}$ = 0.065 mM

bedrock groundwater: $[Rn]_{bgw}$ = 1070 dpm/L, $[Ca]_{bgw}$ = 0.87 mM.

An important point to note is that the three end members are exactly what

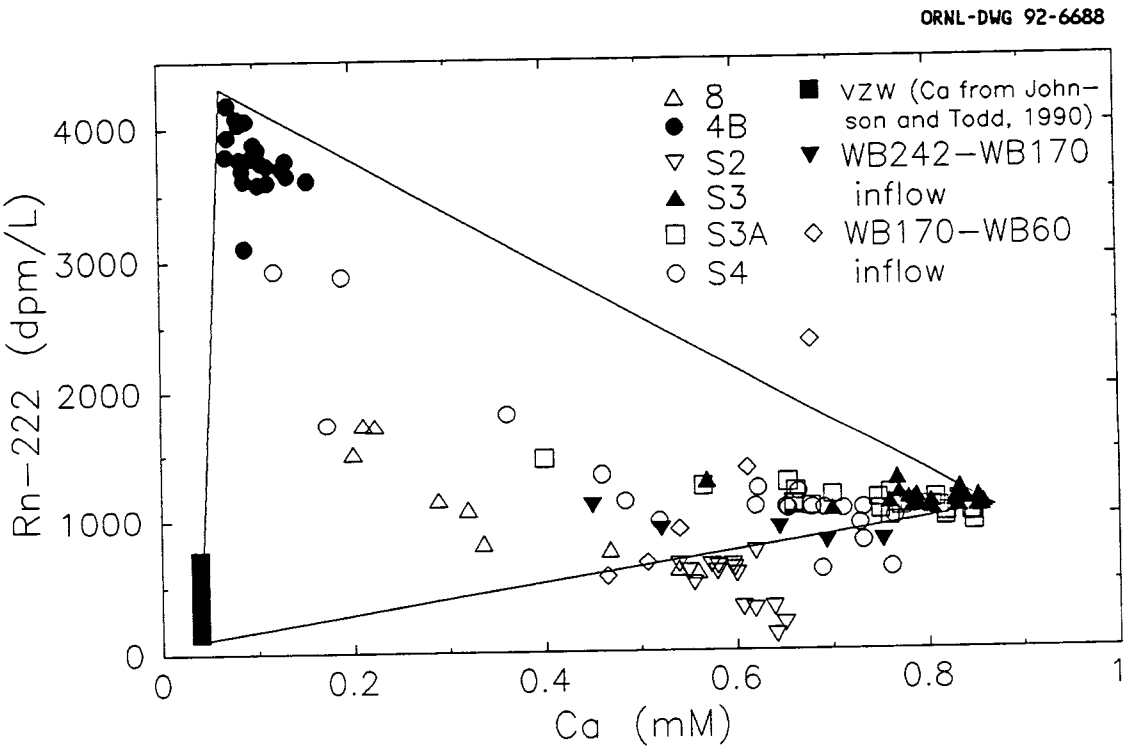

Figure 2. Plot of ^{222}Rn concentration vs. Ca concentration for a variety of water samples (vadose zone water, soil groundwater, springwater, and lateral inflow to two stream reaches) from the West Fork. The "mixing triangle" bounds the space which could be occupied by samples that are mixtures of solutions represented by the corners of the triangle. These diagrams are referred to as "mixing diagrams" in the text.

one would predict based on the tracer characteristics described in the introduction. ^{222}Rn was used as a tracer because of the large concentration difference that often exists between vadose zone water and groundwater in the same soil. This concentration difference is evident along the left side of the triangle in Fig. 2, where vadose zone water plots below soil groundwater from well 4B. Also, there is a large contrast in Ca content between the soil end members and the bedrock end member. Spring S3 has a very steady perennial flow, nearly constant temperature (equal to the mean annual air temperature of 14.5 °C), and constant chemistry (the water is saturated with respect to dolomite, the bedrock material). These characteristics, along with other information (Chapter 3) indicate that outflow from spring S3 is almost certainly bedrock groundwater from a fracture flow system. Thus, the end members that would be predicted from knowledge of the subsurface distributions of ^{222}Rn and Ca are exactly those identified by plotting a variety of West Fork waters in ^{222}Rn-Ca space.

3.2. Variability within end members

Variability in the ^{222}Rn and Ca concentrations of the end members is a prime concern with the end member mixing model. Variability within the end members will generally control the accuracy with which a mixture may be separated into contributions from vadose zone water, soil groundwater, and bedrock groundwater. For the model to be conceptually and practically useful, each end member must be very different, with regard to at least one tracer, from the other

end members. Any attempt to decide whether the tracer concentration in one end member is "very different" from that in another must consider the variability within each end member. In the model proposed here, there are six tracer concentrations (two tracers in three end members) which could exhibit both temporal and spatial variability; thus, there are 12 domains of variability which need be considered. The information used to assess each of these 12 is indicated in Table 1, and summarized briefly below.

As noted earlier, our $[Ca]_{vzw}$ value (0.04 mM) is based on 3 years of data from a previous study [Johnson and Todd, 1990; Johnson, unpub. data]. Soil water was collected monthly from 4 B-horizon lysimeters on each of five study plots. The five plots were chosen largely on the basis of vegetation; each plot had a different dominant tree specie [Johnson and Todd, 1990]. In general, it was found that temporal variability at a given lysimeter or plot was significantly smaller than the spatial variability among the five plots. Concentrations from the four lysimeters on each plot were averaged to give a monthly average value for each plot, and the monthly average values were then averaged over the 3 years of data to give a "global" average value for each plot (thus, the five global averages included temporal and within-plot spatial variability). Finally, the five global plot averages (0.0065, 0.028, 0.035, 0.052, and 0.075 mM) were averaged to give $[Ca]_{vzw}$ = 0.040 ± 0.026 mM (plus or minus one s.d.). While this is a large relative variability (± 65%), it is small compared to the much larger difference between $[Ca]_{vzw}$ and $[Ca]_{bgw}$ (0.04 vs. 0.87 mM).

End Member	Type of Variability	Tracer	
		^{222}Rn	Ca
VZW	temporal	repeated sampling at 10 tubes	3 years of data, 5 plots
	spatial	sampling at 10 tubes	sampling from 4 lysimeters on each of 5 plots
SGW	temporal	repeated sampling at well 4B	repeated sampling at well 4B
	spatial	not addressed	not addressed, but likely -same as for vadose zone water
BGW	temporal	repeated low-flow sampling, 3 West Fork springs	repeated low-flow sampling, 3 West Fork springs
	spatial	low-flow sampling, 3 springs in West Fork, 8 others nearby	low-flow sampling, 3 springs in West Fork, 8 others nearby

Table 1. Twelve possible domains of variability for the end member ^{222}Rn and Ca concentrations, and the sampling used to address each. VZW = vadose zone water, SGW = soil groundwater, and BGW = bedrock groundwater.

The mean and standard deviation (which reflects both spatial and temporal heterogeneity) of the 531 samples used in drawing the ^{222}Rn range of the vadose zone water field in Fig. 2 were 460 ± 310 dpm/L; Fig. 3 shows the distribution of ^{222}Rn concentrations in these samples.

There are no direct measurements available for assessing spatial variability in the soil groundwater end member. Groundwater was sampled from two wells screened in soil (4B and 8), but groundwater from well 8 is best interpreted as a mixture of the three end members (see Fig. 2, and discussion below) rather than as groundwater which, along with that from well 4B, demonstrates spatial variability in the soil groundwater end member. It is likely that spatial variability in $[Ca]_{sgw}$ is similar to that in $[Ca]_{vzw}$, since both are based on Ca measurements in the B-horizon soil (the former in saturated soil, the latter unsaturated).

Temporal variability in $[Ca]_{sgw}$ was assessed through repeated sampling at well 4B. The Ca content of groundwater from well 4B varied between 0.06 and 0.13 mM (Fig. 2). This variability (a factor of ~2 between the lowest and highest values) was similar to the temporal variability in the Ca content of vadose zone water [Johnson, unpub. data], and much smaller than the difference between $[Ca]_{sgw}$ and $[Ca]_{bgw}$ (Fig. 2).

Temporal variability in $[Rn]_{sgw}$ was also assessed by repeated sampling of groundwater from well 4B; 76 samples from 4B were analyzed for ^{222}Rn (55 for ^{222}Rn alone, 21 for ^{222}Rn and Ca). Fig. 4 shows the distribution of ^{222}Rn concentration for all 76 samples and for the 21 on which Ca was also measured

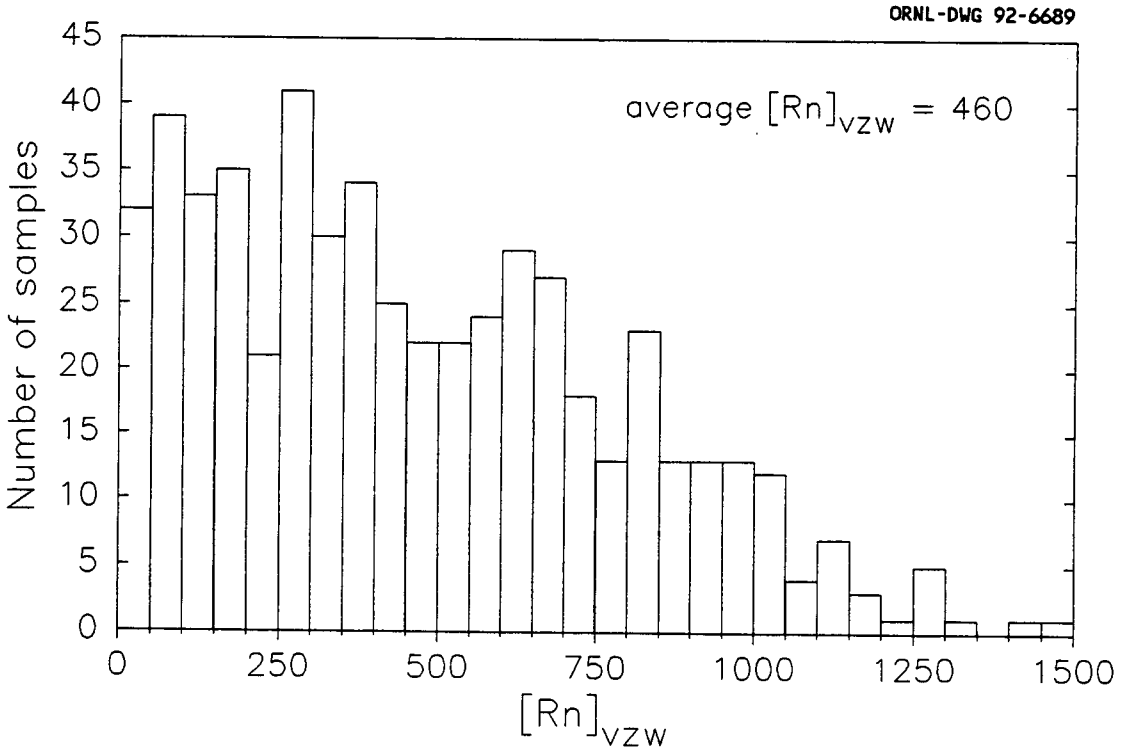

Figure 3. Histogram showing ^{222}Rn concentration for 531 vadose zone water samples from ten vadose zone sampling tubes on the slopes of the perennial stream valley.

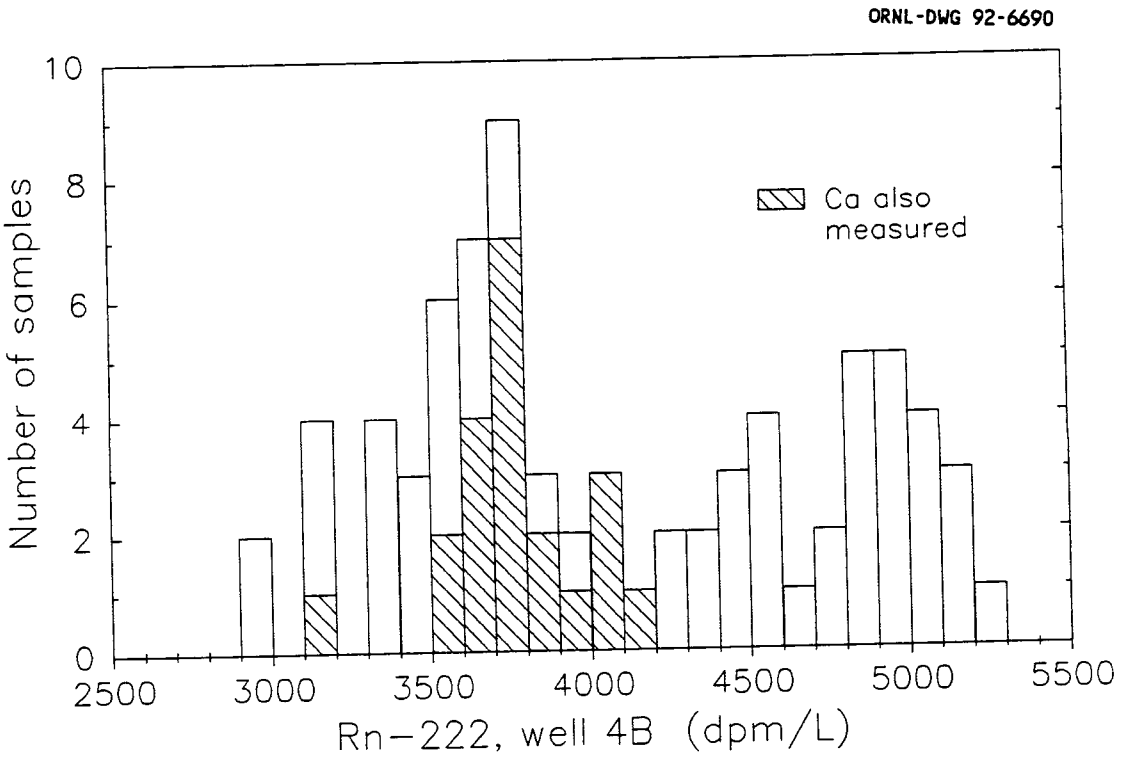

Figure 4. Histogram showing ^{222}Rn concentration for groundwater samples from well 4B. Hatching indicates samples for which Ca was also measured (i.e., the 4B samples plotted in Fig. 2).

(e.g., the 21 plotted in Fig. 2). Fig. 4 gives the impression that there was a bimodal distribution of ^{222}Rn concentrations in groundwater from well 4B. However, the peak at 4900-5000 dpm/L is an artifact of the large number of samples (17) collected during April 1990, when ^{222}Rn concentration was significantly higher than during the rest of the year. As Fig. 5 shows, the sampling frequency in April was ~3 times the average for the study (six samples per month). The sampling frequencies in March and May, the two months showing the next-highest ^{222}Rn concentrations, were also somewhat higher than average.

Figure 5 suggests there was seasonality to the ^{222}Rn concentration of groundwater at well 4B. Water storage and temperature may both affect ^{222}Rn transport in the subsurface, and both may have played a role in producing the pronounced springtime maximum (the ^{222}Rn maximum occurred at just about the time when hydrologic fluxes and storages were at their maximum and subsurface temperature was near its minimum). While the exact causes of this seasonality are beyond the scope of this study, the variability in ^{222}Rn concentration of groundwater from well 4B does have implications for the end-member mixing model. It is necessary to decide what value would be best assigned to $[Rn]_{sgw}$ (the mean of the concentration distribution at well 4B? the upper limit? some other value?). For purposes of this study, it is probably best to adhere to the empirical notion of an end member as a subsurface water of extreme chemistry which, along with other such waters, bounds the chemistry of surface waters. This is especially so when much of the apparent variability in an end member can be viewed as the result of

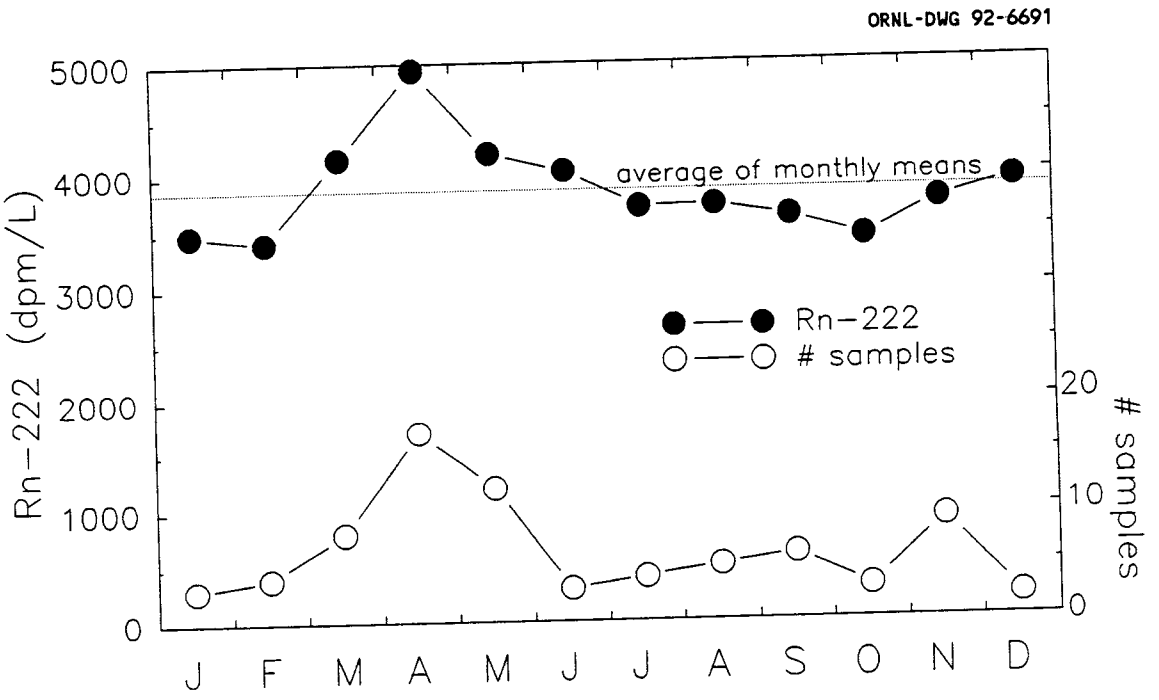

Figure 5. Number of groundwater samples collected from well 4B in each month, and average ^{222}Rn concentration of the samples collected in each month. The peak in ^{222}Rn concentration coincided with the peak in sampling frequency.

"contamination" with small amounts of the other end members. For example, the 4B points plotted in Fig. 2 fan out toward the interior of the mixing triangle when the values 0.065 mM and 4300 dpm/L are chosen as the end member Ca and ^{222}Rn concentrations. This can be viewed as the result of mixing of small amounts of vadose zone water and bedrock groundwater with the soil groundwater, rather than a manifestation of variable soil groundwater. From this perspective, well 4B is simply an imperfect sampling site for soil groundwater, since it samples water which is mostly, but not necessarily completely, soil groundwater (where soil groundwater is defined by the extreme chemistry at the corner of the mixing triangle).

As Fig. 4 shows, ^{222}Rn concentrations at 4B do go above 4300 dpm/L (though it is only in April when they go well above this). However, the Ca content of these high ^{222}Rn samples was not measured, so they can not be plotted on Fig. 2. Even if this high ^{222}Rn water had a Ca content similar to that of other 4B samples, it would be questionable whether a ^{222}Rn concentration found during only 4 weeks of the year should be used to represent $[Rn]_{sgw}$ throughout the year. Though the end member tracer concentrations are considered, to a first approximation, to be temporally invariant, they could in practice be allowed to vary seasonally in the mixing model. This was not done since only a few of the samples plotted in Fig. 2 were collected during the time of highest ^{222}Rn concentration at 4B and these samples do not depart from the trends exhibited by the other samples. Seasonally-varying values for $[Rn]_{sgw}$ or other end member tracer concentrations might be useful with more extensive data sets having finer spatial

and temporal resolution.

Thus, for all these reasons, 4300 dpm/L seems to be the most appropriate value for $[Rn]_{sgw}$. This value was originally arrived at by drawing a triangle, with one corner near the 4B data, to include most of the points in Fig. 2. 4300 dpm/L serves well as an extreme or limiting value for at least 11 months of the year (April excluded). The value of $[Rn]_{vzw}$ was chosen in the same way (as a limiting, low value for the concentration distribution). Coincidentally, the $[Rn]_{sgw}$ and $[Rn]_{vzw}$ values are each almost exactly equal to the means of their distributions plus (for soil groundwater) or minus (for vadose zone water) one standard deviation. The mean and standard deviation of the 531 vadose zone water samples was 460 ± 310 dpm/L; the mean of the 12 monthly means for well 4B groundwater was 3870 ± 430 dpm/L. (The average of the 12 monthly means was used for the well 4B samples because, for reasons mentioned earlier, the seasonal variability in ^{222}Rn concentration and the uneven sampling frequency would give undue weight to the springtime samples in a direct average of all 76 samples from well 4B. Sampling frequency for vadose zone water was also somewhat uneven, but this was not an issue because there was no pronounced seasonal variability among the 10 vadose zone sampling tubes.) $[Rn]_{sgw}$, 4300 dpm/L, was identical to 3870 + 430 dpm/L, and $[Rn]_{vzw}$, 100 dpm/L, was nearly identical to 460 - 310 dpm/L. Thus, the mean of each distribution, shifted away from the other end member by one standard deviation, was essentially the same as the end member tracer concentration that was derived graphically for $[Rn]_{sgw}$ and $[Rn]_{vzw}$.

Since the variability in $[Rn]_{sgw}$ and $[Rn]_{vzw}$ is important in controlling the accuracy with which water mixtures may be separated into the end members, documentation of this variability is crucial to a full accounting of the uncertainty associated with such separation calculations (see appendix). In spite of the observed variability, it appears that there is a large enough ^{222}Rn concentration difference between vadose zone water and soil groundwater to make ^{222}Rn useful in the end member mixing model. This can be better seen by plotting the data in Figs. 3 and 4 on a single graph (Fig. 6).

In comparison to the soil end members, bedrock groundwater is somewhat removed from the more dynamic aspects of near surface hydrology and probably has a longer residence time in the subsurface. These characteristics are likely responsible for the relatively small temporal and spatial variability in bedrock groundwater chemistry. At times of low flow, when the relative contributions from the soil end members are lowest, Ca concentrations at springs S3 and S3A converge to similar values (about 0.85 mM). Along with the Ca data, measurements of Mg, bicarbonate, and pH [Mulholland, unpub. data] show that these waters are saturated with respect to dolomite, the bedrock material. (Water from S4 has a slightly lower Ca content (0.77 mM) at low flow, and seems to be slightly undersaturated with respect to dolomite.) Since the processes controlling the ^{222}Rn content of groundwater in fractured rock are more complicated than the simple dissolution equilibrium apparently controlling the Ca content of bedrock groundwater at the study site, one might expect that $[Rn]_{bgw}$ would show greater

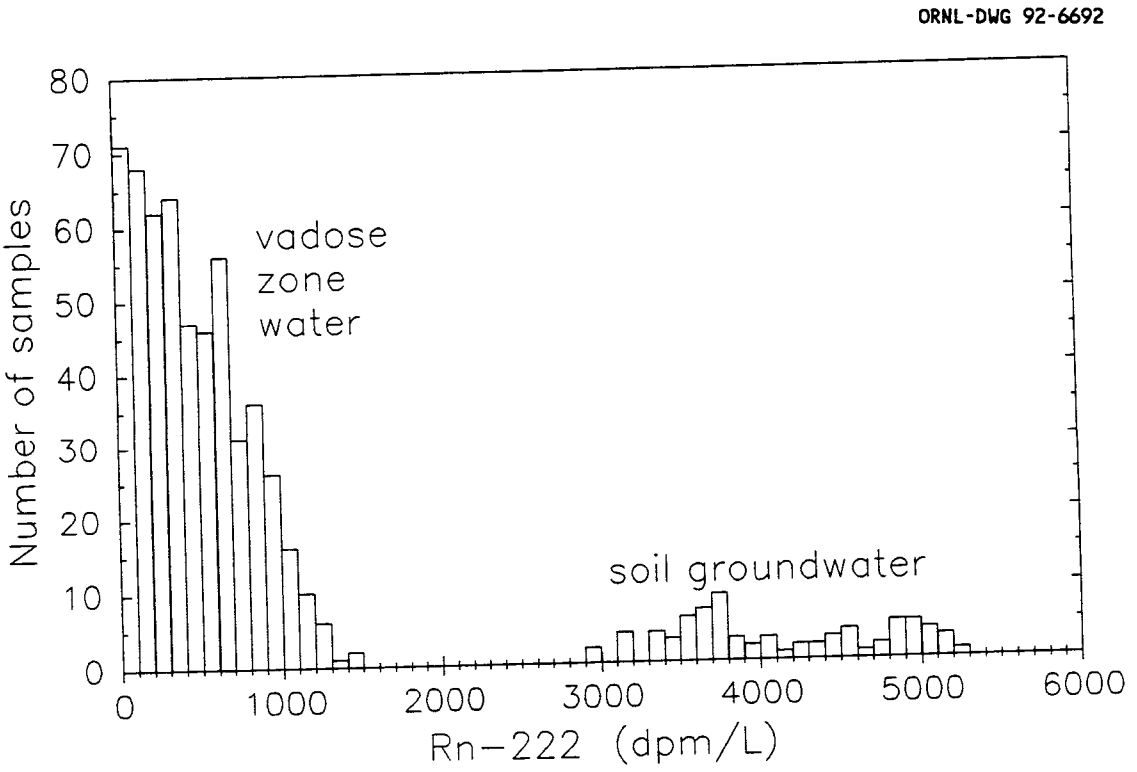

Figure 6. Data from Figs. 3 and 4 combined on a single plot.

spatial variability than $[Ca]_{bgw}$. However, the ^{222}Rn content of water at springs S3, S3A, and S4 also converges at low flow, to about 1100 dpm/L.

Low flow ^{222}Rn and Ca concentrations at springs outside the West Fork, but on the same ridge (Chestnut Ridge) and the same Knox Group dolomite bedrock, cluster around the same values found at springs within the West Fork. Water samples were collected at eight such sites, all within about 5 km of the West Fork, on November 1 and 2, 1990. The eight seepage points are referred to as springs because they were sustaining flow at the dryest, lowest-flow time of year and hence may be assumed to be perennial. In addition, we hypothesize that, like springs within the West Fork, they are fed almost exclusively by bedrock groundwater at times of lowest flow. The springs were identified by simply walking along first and second order streams on Chestnut Ridge and looking for obvious, significant points of seepage. The average Ca content at the eight springs was 0.84 ± 0.09 mM, and the average ^{222}Rn content for seven of them was 1060 ± 340 dpm/L (errors are one s.d.; the ^{222}Rn number at one spring was excluded because the flow was clearly exposed to the atmosphere before it emerged from under a rock ledge, leading to an unknown and potentially large loss of ^{222}Rn from the water by volatilization, the likely cause of the low ^{222}Rn concentration of 490 dpm/L). While the scatter in bedrock groundwater tracer concentrations appears to be greater when the whole of Chestnut Ridge is considered, the means are nearly identical to those found within the West Fork.

Thus, spatial variability in $[Rn]_{bgw}$ and $[Ca]_{bgw}$ was assessed by sampling

springs both within and near the West Fork. Temporal variability was investigated by repeated sampling of the springs within the West Fork. We interpret much of the variability as the result of having imperfect sampling sites for bedrock groundwater rather than having truly variable bedrock groundwater. For example, as flow increased the chemistry of water at spring S3 evolved toward the soil end members and away from the bedrock end member (see Fig. 2 and discussion in Section 3.4.1). Defining $[Rn]_{bgw}$ and $[Ca]_{bgw}$ as the average ^{222}Rn and Ca concentrations from all the samples (high and low flow) would involve an implicit assumption that the bedrock groundwater chemistry was changing on storm event time scales. It is hydrologically more reasonable to ascribe the observed changes at S3 to the increased importance of water flow from the soil adjacent to S3 under the wetter conditions (i.e., water from the soil end members mixing with bedrock groundwater at or near the spring outlet on the streambank). Thus, spring S3 was not a perfect sampling site for bedrock groundwater under all flow conditions, and water collected at low flow best represented the end member composition. Also, the relatively larger scatter in low-flow ^{222}Rn and Ca concentrations at springs outside the West Fork is not necessarily due to spatially variable bedrock groundwater. It could be the result of changes to originally homogeneous bedrock groundwater caused by the characteristics of water flow just before the spring outflow points (e.g., bedrock groundwater traveling a short distance as free surface flow, or through a saturated soil zone). In summary, available data suggest that variability in tracer concentrations within bedrock groundwater is substantially

smaller than variability in the other end members, and hence is relatively unimportant.

3.3. Use of other solutes in validating the end-member mixing model

In general, an excellent test of the three-end-member mixing model would be comparison of predicted and measured concentrations of solutes other than ^{222}Rn and Ca in mixtures (e.g., stream lateral inflow and springwater). For example, the ^{222}Rn and Ca contents of lateral inflow to a stream reach could be used, along with the ^{222}Rn and Ca concentrations of the end members, to determine the mixing fractions for the lateral inflow (i.e., the fraction of the total which is from each end member). This is done by solving the following system of three simultaneous equations (mass balances for water, ^{222}Rn, and Ca) for the three unknown fractions on the left side of the first equation:

$$f_{vzw}+f_{sgw}+f_{bgw}=1 \qquad (6a)$$

$$[Rn]_{vzw}f_{vzw}+[Rn]_{sgw}f_{sgw}+[Rn]_{bgw}f_{bgw}=[Rn]_q \qquad (6b)$$

$$[Ca]_{vzw}f_{vzw}+[Ca]_{sgw}f_{sgw}+[Ca]_{bgw}f_{bgw}=[Ca]_q \qquad (6c)$$

where f_{vzw} is the fraction of the mixture (lateral inflow, in this case) which is vadose zone water and f_{sgw} and f_{bgw} are analogous fractions for the soil groundwater and bedrock groundwater end members. With known mixing fractions (the three f values) one could, for example, predict the concentration of Na in the lateral

inflow, $[Na]_q$, if the Na concentrations of the end members were known ($[Na]_{vzw}$, $[Na]_{sgw}$, and $[Na]_{bgw}$). The closeness of fit between predicted and measured $[Na]_q$ values (or values for other solutes) would give an indication of whether the end member mixing model captured the major hydrogeochemical features of the study site.

Unfortunately, on the West Fork no other major solute exhibits concentration differences between end members which are large relative to the spatial and/or temporal variability within the end members. (The one exception to this is Mg, whose distribution on the watershed mirrors that of Ca. However, because the behavior of Mg and Ca is so similar, Mg can not offer a very strong test of mixing fractions determined in part with Ca data. In fact, Ca concentration alone is an excellent predictor of the Mg content of water on the West Fork [Mulholland et al., 1990], underscoring the fact that Mg provides essentially no information beyond that provided by Ca.) For example, $[SO_4]_{sgw} = 0.032 \pm 0.009$ mM (12 samples from well 4B, $\pm$ 2 s.d.), $[SO_4]_{bgw} = 0.025 \pm 0.002$ mM (12 samples from spring S3, $\pm$ 2 s.d.), and $[SO_4]_{vzw}$ ranges from 0.002 to 0.153 mM (volume weighted average concentrations for two of the five vadose zone sampling plots; the other three had average concentrations of 0.038, 0.113, and 0.121 mM). Analogous concentrations for Na are $[Na]_{sgw} = 0.025 \pm 0.005$, $[Na]_{bgw} = 0.020 \pm 0.002$, and $0.016 < [Na]_{vzw} < 0.023$. Temporal variability within the five vadose zone sampling plots further widens the vadose zone concentration ranges given above. For example, $[Na]_{vzw}$ ranges from 0.016 ± 0.008 mM on the lowest Na plot to 0.023

± 0.005 on the highest Na plot (uncertainties are ±1 s.d.), or from 0.008 to 0.028 overall. This large variability within end members makes Na, SO_4, K, and Cl (the solutes for which significant amounts of data are available) ill-suited for use in the three-end-member mixing model, precluding what would potentially be an excellent means of model validation.

In general, variability in the soil is also a problem in using temperature as a tracer, though temperature may be useful, like Ca, in separating soil end members from bedrock groundwater at those times of year when soil temperatures are most different from those in the bedrock (i.e., late summer and late winter). The temperature of the bedrock aquifer is nearly constant and approximately equal to the mean annual air temperature, 14.5°C; this is evident from, for example, the temperature record at spring S3. The soil temperature is of course more temporally variable, being colder than bedrock in winter and warmer in summer. There is also significant spatial variability in soil temperature, variability which depends on depth, slope aspect (soil on the southwest-facing slope of the perennial stream valley was found to be warmer in summer than soil on the opposite northeast-facing slope), proximity to heat sources or sinks (during summer, the coolest soil was that in the immediate vicinity of springs S3 and S3A), and perhaps shading by vegetation. The temperature of vadose zone water and soil groundwater were not significantly different; but during late summer the soil temperature, though it was spatially variable, was significantly higher than that of the bedrock, allowing temperature to be used in a manner analogous to Ca.

We do not have adequate data to close the heat budget around a stream reach and calculate T_q, the temperature of lateral inflow to the reach. However, it is possible to apply temperature to a spring, making the same assumption made for the ^{222}Rn sampling at springs: the water sampled at springs has, with few exceptions, not lost ^{222}Rn to the air, or exchanged heat with the air. Table 2 shows that, during September and early October 1990, temperature and Ca give similar estimates of bedrock groundwater contributions to flow at spring S4. Simple mixing calculations based on temperature generally support the Ca-based separations at springs. Temperature would be most useful as a tracer during those times of year when soil temperature is most different from that of bedrock (i.e., late summer and late winter). However, even at these times, the temperature contrast between soil and bedrock end members is not as large as the contrast in Ca concentration, making Ca a more useful tracer at all times.

While the major ions investigated can not provide adequate tests of the end-member-mixing model, and temperature has a very limited utility, comparisons with hydrologic data not involving natural tracers can provide a check on the behavior of the mixing model. While such comparisons can not provide explicit tests of the mixing fractions of different end member mixtures, they can provide a good indication of whether the end members behave in a reasonable and consistent manner. Several different sites (springs, stream reaches, and shallow wells) are considered below in turn.

Date	T_{soil}	T_{S4}	$f_{bgw}(T)$	$f_{bgw}(Ca)$
9/2/90	19.3±1.2	16.2	0.64	0.58
9/9/90	19.2±1.4	16.2	0.64	0.70
9/16/90	18.6±1.2	15.9	0.66	0.74
9/27/90	16.6±0.9	14.9	0.83	0.82
10/5/90	16.8±0.7	14.9	0.83	0.83

Table 2. Comparison of temperature and Ca as tracers for determining the proportion of bedrock groundwater (f_{bgw}) in outflow at spring S4. The temperature and Ca content of bedrock groundwater were taken to be 14.5°C and 0.87 mM, respectively; both values are based on measurements as spring S3. T_{soil} is the average temperature of the soil at the bottom of 12 ^{222}Rn sampling tubes (wells 4B and 8, and the 10 vadose zone tubes); uncertainty is one standard deviation.

3.4. Relationship between the end-member mixing model and hydrologic observations

3.4.1. Springs S3 and S3A

Springs S3 and S3A are located about 200 and 210 m upstream of the weir, respectively. The late summer flow at S3 was about 75 L/min, and that at S3A was about 40 L/min. The characteristics indicating a bedrock groundwater origin for S3 were noted in Section 2, and in Chapter 3. The direction of evolution of water composition at S3 and S3A with increasing flow is toward the left in Fig. 7; thus, as one would expect, the soil end members account for a progressively larger proportion of the spring outflow as flow increases. Except at very low flow, outflow at S3A seemed to contain a greater proportion of the soil end members than outflow at S3 on the same day. One would therefore expect S3A to exhibit greater excursions in flow on both seasonal and storm event time scales, since flow from the soil was more dynamic on all time scales than that from bedrock. This is indeed observed [Mulholland et al., 1990; Mulholland, unpub. data]. One would expect a similar situation for temperature: the soil is more variable (on all time scales) than the bedrock, and hence outflow from S3A should be more variable than that from S3. This too was observed, as water at S3A underwent larger temperature changes after storms and through the 6 months from May to November 1990 (Fig. 8). Finally, a greater contribution to S3A from the soil end members is also consistent with the few observations of soil saturation in the vicinity of S3 and S3A. As noted in Chapter 3:

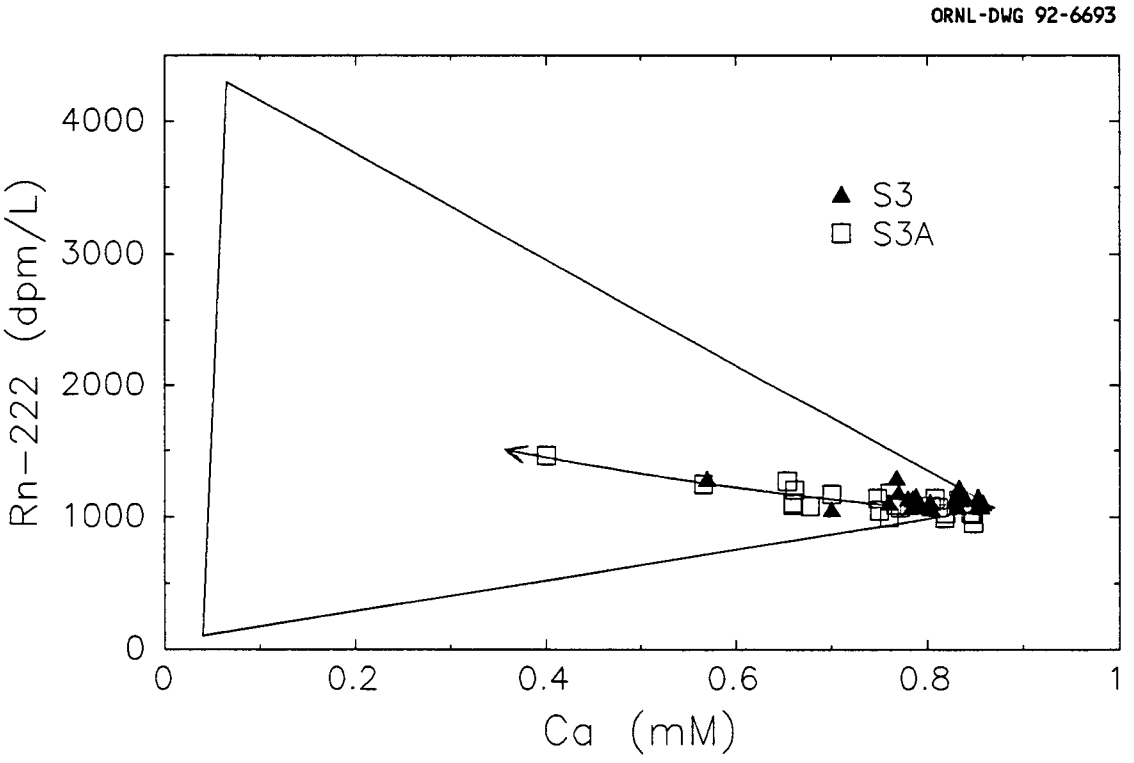

Figure 7. Mixing diagram showing samples from springs S3 and S3A. The triangle plotted here (and in all such subsequent figures) is identical to that in Fig. 2. Arrow indicates direction of increasing flow.

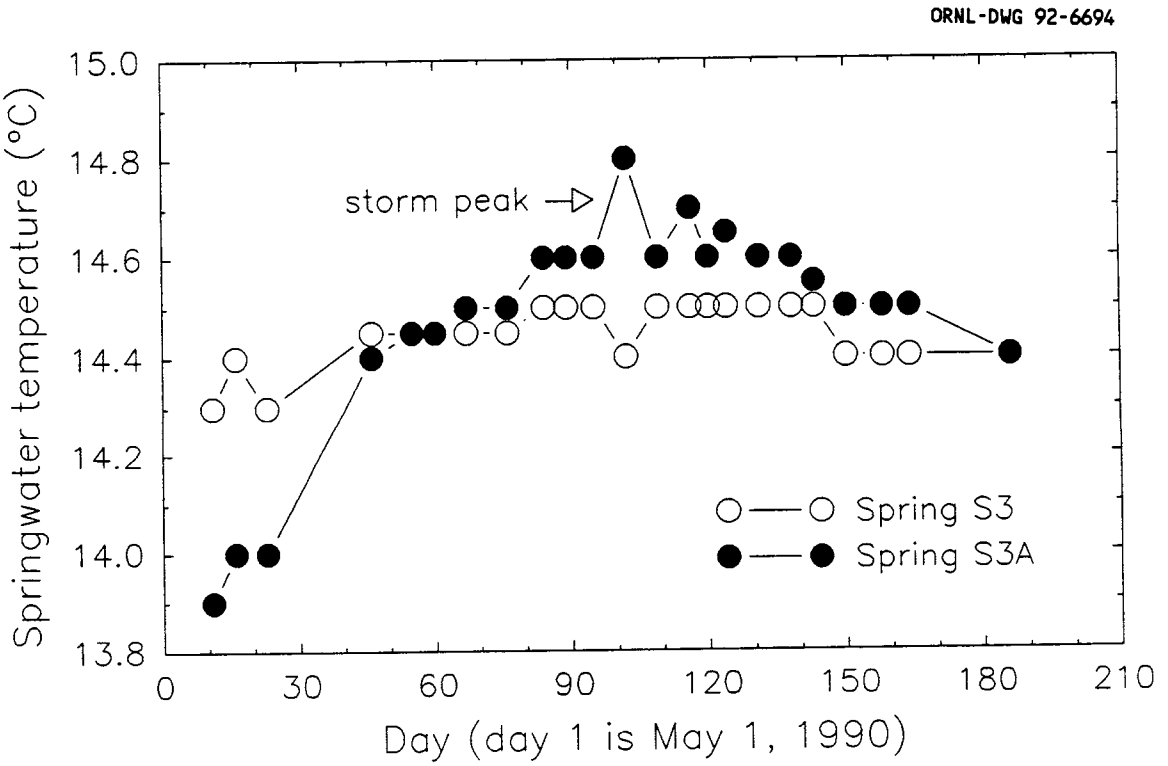

Figure 8. Temperature of outflow at springs S3 and S3A. The transient temperature increase at S3A labeled "storm peak" was associated with an increase in flow due to a large (6.7 cm) rain event.

Five well points were driven into the soil (four to refusal) between S3 and S3A, along a line roughly parallel to and about 3 m from the stream bank. No water table was ever found in the downstream three; the two farthest upstream were installed side by side near S3A (one 87 cm deep, at refusal, the other 40 cm deep), and the deeper well showed saturated conditions on 4 days during the study period (11/16/89, 3/17/90, 5/4/90, and 5/5/90), the shallow well only one (3/17/90).

Thus, in addition to the fact that water compositions at the two springs evolve in a consistent and hydrologically reasonable manner with increasing flow, the difference between the two (i.e., the greater importance of soil end members at S3A) is consistent with the wetter soil conditions near S3A, and the more responsive and variable temperature and flow rate at S3A.

3.4.2. Spring S4

Water composition at S4 evolves toward the soil end members, especially soil groundwater, as flow increases (low flow points are on the right in Fig. 9). S4 is located near the limit of perennial flow and the confluence of the two ephemeral stream valleys. The small area of low slope surrounding S4 is hydrologically very responsive. Flow increases associated with storms are much larger at S4 than at S3 and S3A; large rises in the nearby water table elevation (50-100 cm in one well) are also common during storms [Mulholland et al., 1990]. Occassionally the water

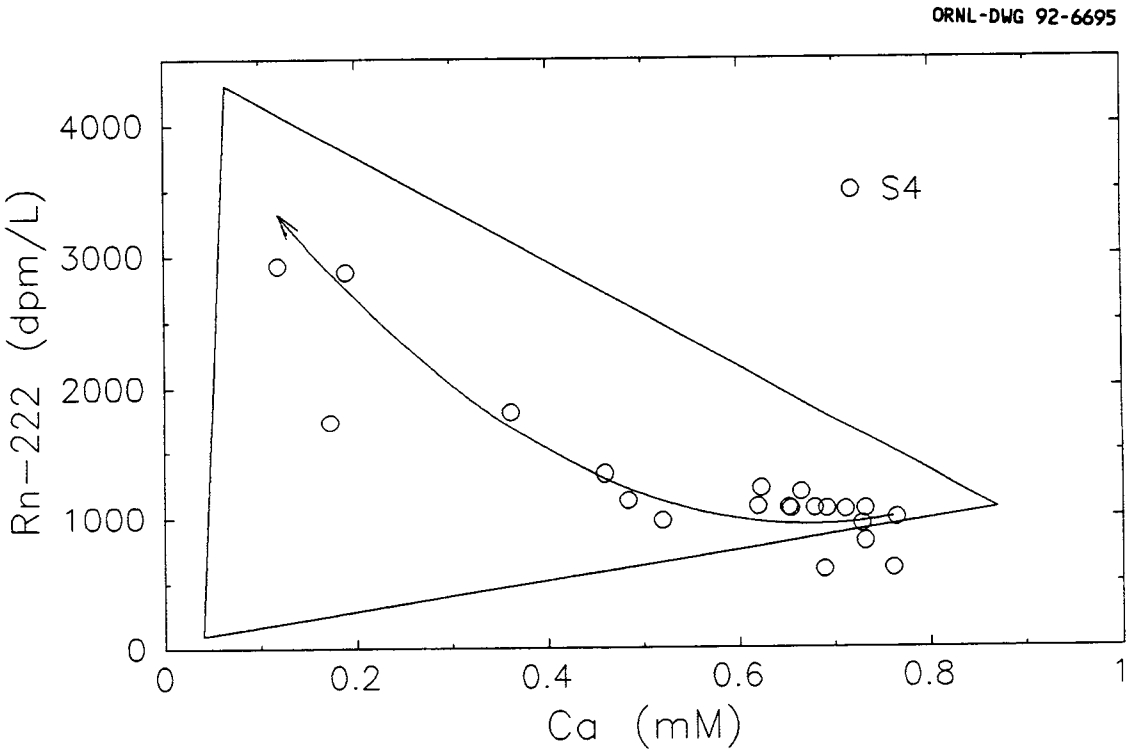

Figure 9. Mixing diagram showing samples from spring S4. Arrow indicates direction of increasing flow.

table reaches the ground surface and overland flow occurs in this area. Thus, hydrologic observations (highly responsive flow conditions at S4 and in the surrounding soil, superimposed on a low flow of at least 20 L/min maintained throughout the year) suggest a dramatic shift in flowpaths and water sources supplying S4 as flow increases. The ^{222}Rn and Ca data indicate exactly this, with water at S4 shifting from mostly bedrock groundwater at low flow to mostly soil groundwater at high flow.

Confidence limits (±95%) on the ^{222}Rn values for the two points plotting below the mixing triangle (Fig. 9) are about ±70 dpm/L, indicating the points do fall a significant distance below the mixing triangle. These two lowest flow points illustrate a phenomenon described earlier for one of the springs outside the West Fork. At low flow, the water flow at S4 appears to be in contact with the atmosphere for at least a short distance before emerging from the ground. This results in some ^{222}Rn being lost from the water before the water emerges to where a sample can be collected (samples were collected in a small pool at the spring outlet, just several cm from the outflow point). This ^{222}Rn loss became significant at low flow because the travel time of water in the short free surface rivulet upstream of the sampling point was longer, and the water depth was shallower, allowing a greater fraction of the dissolved ^{222}Rn to volatilize from the water. This phenomenon seemed to be confined to the very lowest flow times at S4 (the 2 samples falling outside the mixing triangle were collected during early November 1990, the lowest flow time of the year). The samples plotting below the mixing

triangle could also be explained by contributions from a fourth water source with moderately high Ca (~0.7 mM) and very low ^{222}Rn (0-100 dpm/L). It's conceivable that water with this composition could exist in a very well ventilated (i.e., very thin) soil layer over a bedrock outcrop. The only bedrock outcrops are in the lower reaches of the perennial stream valley, far downstream of spring S4. Thus, given what is known about Ca and ^{222}Rn distributions on the watershed, it is more reasonable to explain the two S4 samples falling below the mixing triangle by ^{222}Rn loss from a mixture of the known, sampled waters, rather than by the sudden importance at low flow of a hypothetical, unsampled end member.

3.4.3. Spring S2

Spring S2 is a small (smaller than S3A) ungauged seepage point about 130 m upstream of the weir. Unlike the other springs which discharge at about stream level, the outflow point for S2 is about 3 m above the local stream level. Water emerges from a hole (about 10 cm in diameter) in the lower part of the hillslope and runs downhill toward the stream. Essentially all of this outflow from S2 infiltrates soil on the lower hillslope and streambank before reaching the stream. The flow at S2 is in contact with the atmosphere before it reaches its outflow point (the mouth of the soil hole, where samples were collected). Most of the data from S2 plot approximately on a mixing line between vadose zone water and bedrock groundwater (Fig. 10). However, the five samples collected under the lowest flow conditions (late Sept. through early Nov., 1990) plot significantly below this line.

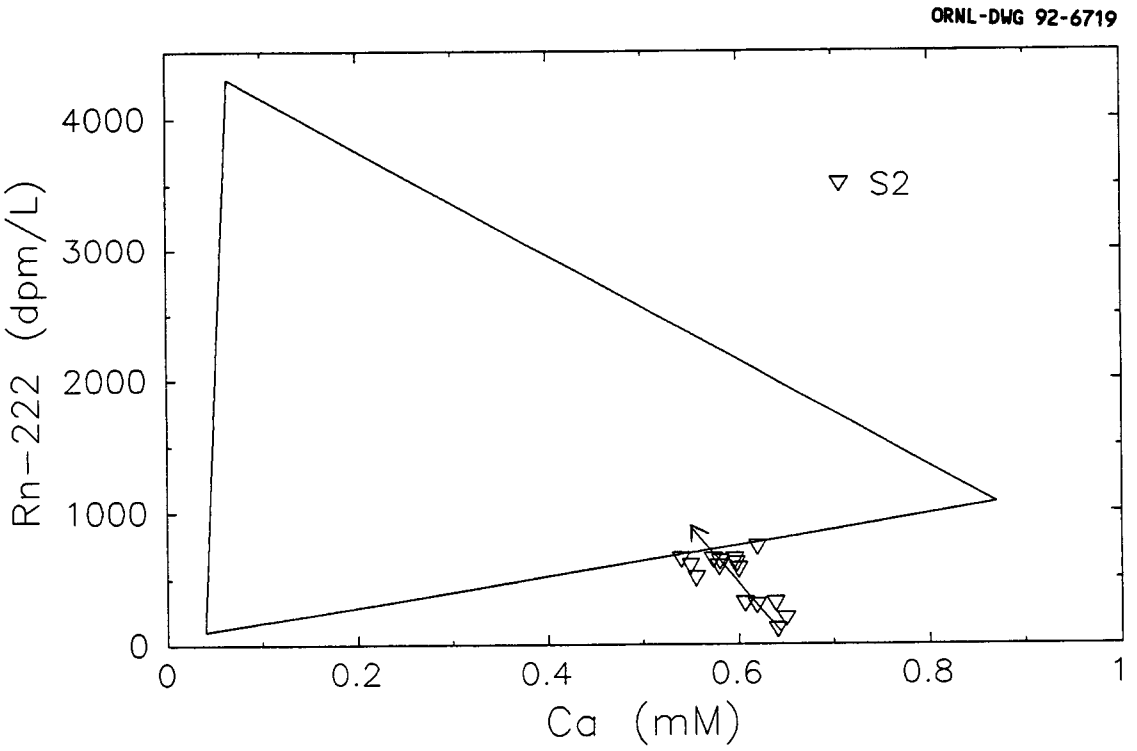

Figure 10. Mixing diagram showing samples from spring S2. Arrow indicates direction of increasing flow.

This could be due to ^{222}Rn volatilization from the springwater; as noted in the discussion of S4, this volatilization loss should be larger at lower flows.

While there were no hydrometric observations made in the immediate vicinity of S2, the apparent lack of significant soil groundwater contributions is generally consistent with the lack of saturated soil zones on the hillslopes. Several shallow wells installed in the B horizon on the slopes of the perennial stream valley showed only transient perched saturation above the soil/saprolite interface in response to storms. Also, a trench (or "subweir" [Mulholland et al., 1990]) dug across slope and down to the soil/saprolite interface in the upper part of the western ephemeral stream valley showed outflow from its 0.5 ha drainage area only for short periods (generally less than a day) following storms [Mulholland et al., 1990; Wilson et al., 1990].

3.4.4. Stream reach WB242-WB170

Fig. 11 shows ^{222}Rn and Ca concentrations for the lateral inflow to the stream reach between WB242 and WB170. The five solid points represent values for five of the injected tracer experiments, calculated with Eqns. 2 and 4 (see section 2). $[Rn]_q$ was also determined during three other injected tracer experiments, though $[Ca]_q$ was not (Table 3). For the other 21 points in Fig. 11, [Rn] and [Ca] were measured directly at WB242 and WB170 but injected tracers were not used; $[Rn]_q$ and $[Ca]_q$ were calculated with Eqns. 1 and 3, respectively, with Q_1, Q_2, Q_{avg}, $q\Delta x$, and F determined by empirical regression equations based

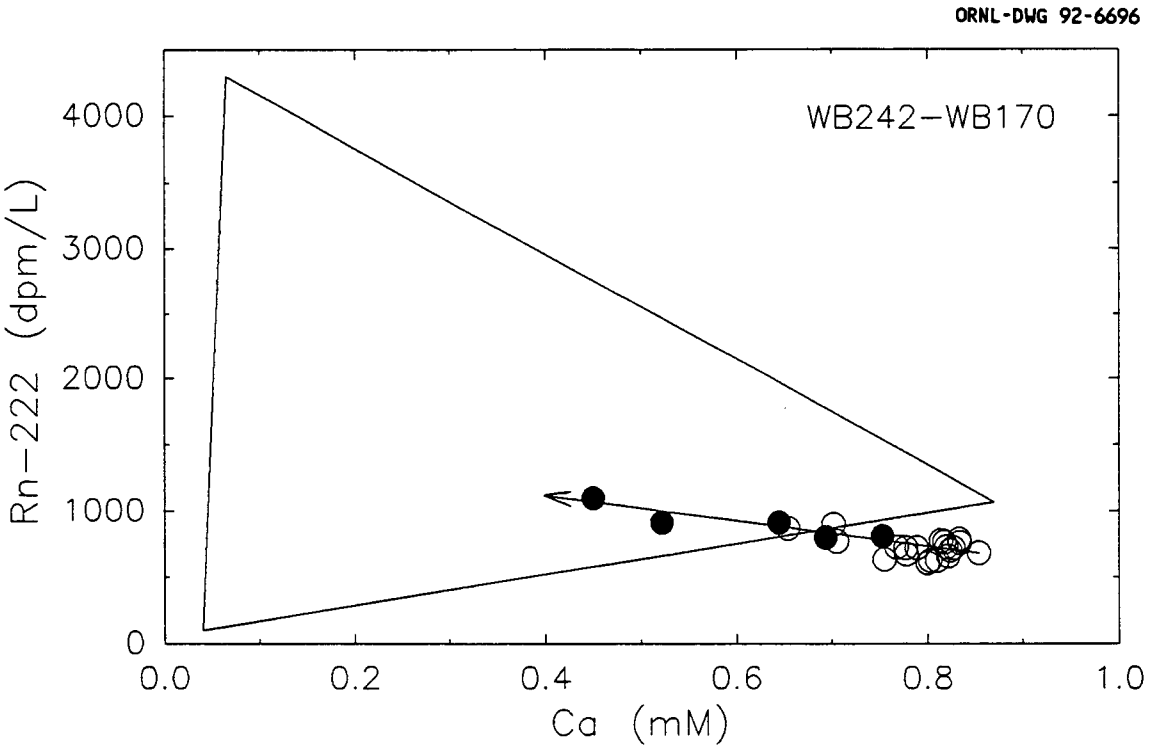

Figure 11. Mixing diagram showing lateral inflow to stream reach WB242-WB170. Open circles are regression-based points (see text). Arrow indicates direction of increasing flow.

Q_{weir}	Date	$[Rn]_q$	$[Ca]_q$
354	11/1/89	700	
411	8/28/90	810	0.75
680	4/13/90	800	0.69
1050	3/7/90	910	0.65
1368	10/4/89	920	
1447	5/7/90	930	
2749	11/17/89	910	0.52
3457	3/18/90	1100	0.45

Table 3. Q_{weir}, date, $[Rn]_q$, and $[Ca]_q$ for injected tracer experiments, WB242-WB170.

on Q_{weir} (which is continuously recorded). These 21 points are hereafter referred to as "regression based points".

First, Q_1 (i.e., for WB242-WB170, Q_{242}) and $q\Delta x$ (both in L/min) were determined from the following equations:

$$Q_{242}=0.524Q_{weir}-132 \qquad (n=12, r=0.99481) \qquad (11)$$

$$q\Delta x=0.0650Q_{weir}+203 \qquad (n=12, r=0.8989) \qquad (12)$$

The 12 points in these regressions were from the 12 steady Cl^- injections. Q_2 (in this case, Q_{170}, equal to $Q_{242} + q\Delta x$) and Q_{avg} (equal to $Q_{242} + \frac{1}{2}q\Delta x$) were then calculated. For calculation of $[Rn]_q$, the product $\tau k \equiv F$ was then determined from a regression against Q_{avg} (Fig. 12):

$$lnF=-0.563lnQ_{avg}+3.75 \qquad (n=7, r=0.99402) \qquad (13)$$

The seven points in the regression came from the eight propane-plus-Cl^- injections (one of the injections was not used in the regression because, as noted in Chapter 2, it was done when a large portion of the stream surface was covered with floating leaves, leading to a much lower volatilization rate than would be found at the same flow under more typical conditions). Finally, $[Rn]_q$ was calculated with Eqn. 1, and $[Ca]_q$ with Eqn. 3. This approach is hereafter referred to as the "regression method".

As noted in Chapter 3, the lateral inflow data were collected during times of steady flow, or slowly decreasing flow on the falling limbs of hydrographs.

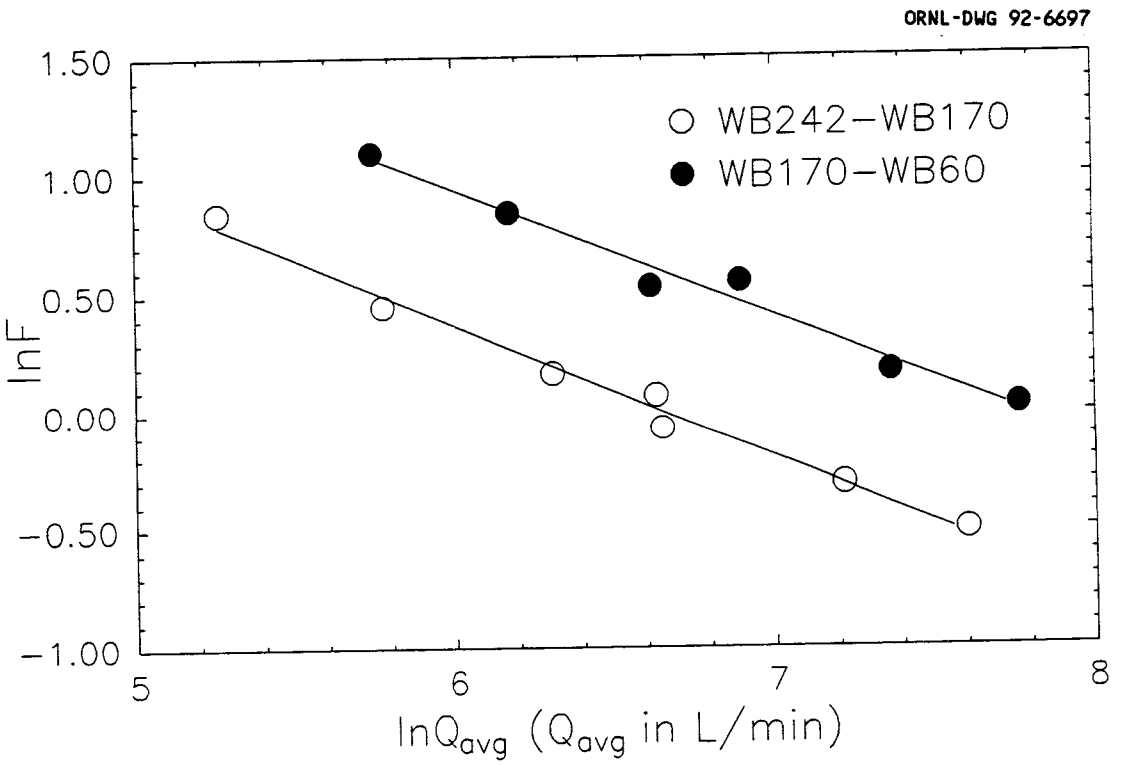

Figure 12. Natural log of F ($F=\tau k$) vs. natural log of reach-average streamflow for WB242-WB170 and WB170-WB60.

Relationships such as Eqns. 11 and 12 would not necessarily hold as well on the rising limbs of hydrographs (and they were not applied to such flow conditions in this tracer work).

Data from the 12 Cl^- injections and from the flumes at S3 and S3A show that flow from these two springs accounted for 50-75% of the lateral inflow to WB242-WB170 (Fig. 13). Thus, one would expect there to be a strong relationship between the chemistry of the springwater and that of the total lateral inflow to WB242-WB170. The composition of the lateral inflow does evolve in the same manner as that at S3 and S3A with increasing flow (toward the left in Fig. 11). Relative to the springs, the total lateral inflow to the reach is consistently offset to lower ^{222}Rn and Ca values (i.e., the lateral inflow contains a higher proportion of vadose zone water than does the spring outflow, as one would expect).

As Fig. 11 shows, most of the regression based points fall just below the end member mixing triangle. These points represent days of low to moderate baseflow (300-600 L/min at the weir). ^{222}Rn loss from S3A springwater as it flows to the stream channel could be partially responsible. Water from S3A runs down a narrow, shallow rivulet about 5 m long from the main S3A outflow point (where S3A samples were collected) to the perennial stream channel. ^{222}Rn volatilization occurring in this small rivulet is not accounted for by the volatilization correction applied to the main channel. Thus, a portion of the lateral inflow to WB242-WB170 (40-50 L/min out of 200-240 L/min total) had an opportunity to lose some of its ^{222}Rn before reaching the stream. No direct measurements of volatilization

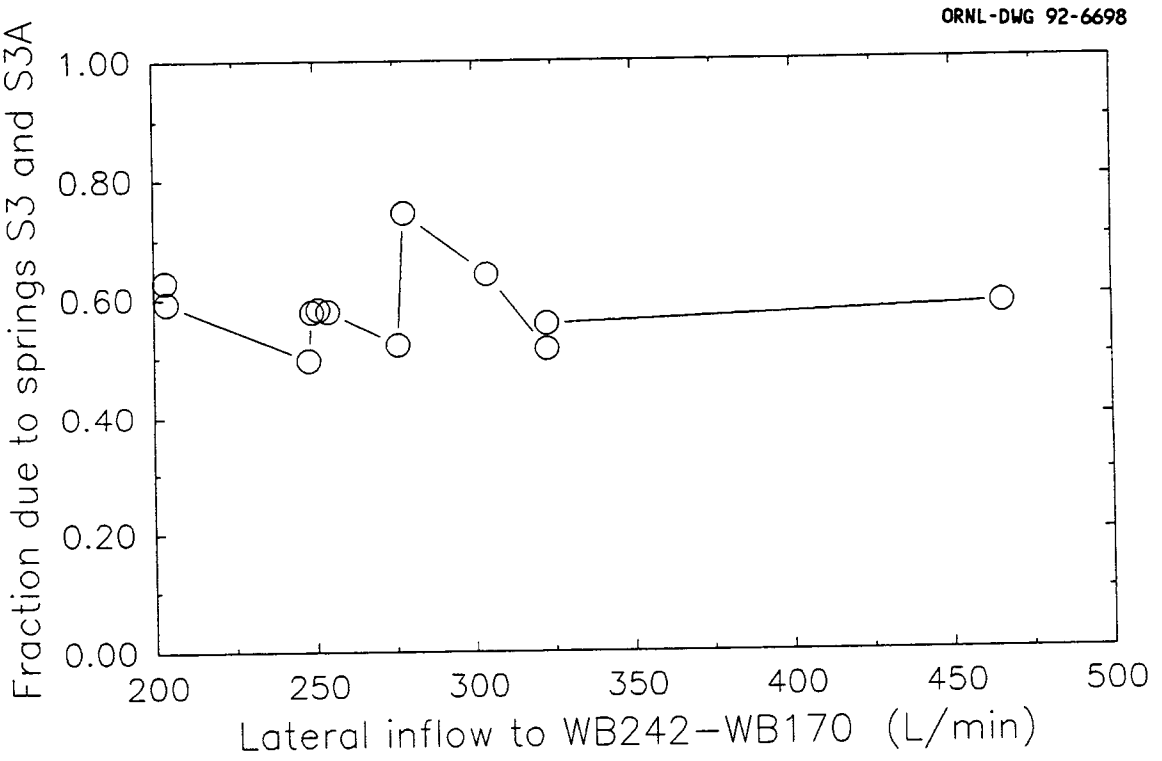

Figure 13. Fraction of lateral inflow to WB242-WB170 accounted for by flow (measured in flumes) from springs S3 and S3A.

rate were made in the small rivulet connecting S3A to the stream. However, using data from the propane gas exchange experiments in the perennial stream and applying a correction to account for the shallower depth, we estimate that the $[Rn]_q$ values in question would be no more than 50-60 dpm/L higher after accounting for ^{222}Rn loss from the S3A rivulet. This in itself is not quite enough to bring the points within experimental uncertainty of the mixing triangle in Fig. 11.

It is possible that one or more of the regressions used (Eqns. 11, 12, and 13) contains some bias error which prevents it from accurately representing the behavior of its dependent variable in the flow range $300<Q_{weir}<600$ L/min, resulting in slight systematic underprediction of $[Rn]_q$ or overprediction of $[Ca]_q$ (either of which could move points from the bottom of the mixing triangle to just below it). Having accurate measurements of streamflow on each day [Rn] was measured would have been preferable to using Eqns. 11 and 12 (use of Eqn. 13 or a similar empirical relationship could not have been avoided unless a gas exchange experiment was done on every sampling day, a practical impossibility). We did estimate streamflow using stream stage measurements and stage-discharge relationships (rating curves) obtained by measuring stage during the Cl^- injections. We compared these two methods (calculating $q\Delta x$, $[Rn]_q$, and $[Ca]_q$ based on stage measurements, rating curves, and, for $[Rn]_q$, Eqn. 13, vs. calculating $q\Delta x$, $[Rn]_q$, and $[Ca]_q$ based on Eqns. 11, 12, and 13) by comparing their predicted $q\Delta x$, $[Rn]_q$, and $[Ca]_q$ values to directly measured values from the injected tracer experiments. The results (Table 4) show that all three parameters were better predicted by the

regression method (Eqns. 11, 12, and 13) than by the method involving rating curves. The likely cause of this was inaccuracy in the rating curves caused by changes in channel geometry over the course of the study. Our stage measurement sites were in the natural channel, not carefully constructed and maintained flow control cross-sections. Changes in channel geometry due to sediment transport had a greater effect than was anticipated (one rather compelling illustration of this phenomenon occurred after a particularly large storm, when stage measurement rods that had been driven into the stream bed were found "high and dry", not moved but surrounded by large masses of newly deposited sediment forming a new streambank).

In summary, the behavior of lateral inflow to WB242-WB170, within the context of the end member mixing model, is generally consistent with hydrologic observations (i.e., the previously mentioned lack of saturated soil zones, leading to low f_{sgw}) and with the behavior of the two springs (S3 and S3A) which account for over half the lateral inflow. Most of the regression based points in Fig. 11 fall slightly below the mixing triangle. Having accurate measurements of streamflow at the ends of the reach on each sampling day would have been preferable to using Eqns. 11 and 12. However, considering the potential uncertainties involved in the regression method (see appendix), and the additional small uncertainty due to ^{222}Rn loss from S3A springwater, the regression method seems to perform reasonably well as a means of extending the usefulness of injected tracer data by allowing calculation of $[Rn]_q$ and $[Ca]_q$ on days when only [Rn], [Ca], and Q_{weir} were

	$q\Delta x$	$[Rn]_q$	$[Ca]_q$
average Δregress. (%)	11	9.6	5.0
average Δr.c. (%)	25	13.3	8.2

Table 4. Comparison of two different methods for calculating $q\Delta x$, $[Rn]_q$, and $[Ca]_q$ for WB242-WB170 on days when only [Rn], [Ca], and stream stage measurements were available. The two methods differ only in how Q and $q\Delta x$ values are calculated. The regression method makes use of empirical relationships given in the text, and the rating curve method uses rating curves and measurements of stream stage (see text for details). The two methods were evaluated by applying both to the eight injected tracer experiments, when "true" values of $q\Delta x$, $[Rn]_q$, and $[Ca]_q$ were calculated directly from the injected tracer data (using Eqn. 2). The difference between these "true" values and values obtained with the regression method was designated "Δregress."; the difference between "true" values and those from the rating curve method was designated "Δr.c.". The average Δregress. and Δr.c. values, as a percentage of the "true" values, are given above for $q\Delta x$, $[Rn]_q$, and $[Ca]_q$ (the values are averages of eight values, one from each injected tracer experiment). Results show that the regression method predicts all three parameters significantly better than the rating curve method.

measured. Regression based $[Rn]_q$ and $[Ca]_q$ data are consistent with the hydrologic pattern exhibited by the other data of bedrock groundwater dominance at low flow with increased importance of soil end members as flow increases.

3.4.5. Stream reach WB170-WB60

Data for WB170-WB60 are plotted in Fig. 14. Solid dots represent the days of injected tracer experiments, open dots were calculated with the regression method. Equations used for the regression method for this reach were:

$$Q_{170}=0.592Q_{weir}+64.4 \qquad (n=13, r=0.99266) \qquad (14)$$

$$q\Delta x=0.0529Q_{weir}+31.5 \qquad (n=11, r=0.97236) \qquad (15)$$

$$lnF=-0.528lnQ_{avg}+4.11 \qquad (n=6, r=0.98916) \qquad (16)$$

Considering the uncertainty in the points, all of them (even the three falling just to the right of the mixing triangle) can be accounted for by mixing of the three end members (uncertainty is discussed in the appendix). In addition, the solid points show a trend to the left with increasing flow (with one insignificant reversal: the solid point farthest to the left represents the experiment done at Q_{weir} = 2749 L/min, while the solid point just to the right of it represents the Q_{weir} = 3457 L/min experiment). The regression based points do not exhibit this same trend. However, the uncertainty in these points is significantly larger than in the five points that were determined directly (see appendix), mainly because use of Eqn.

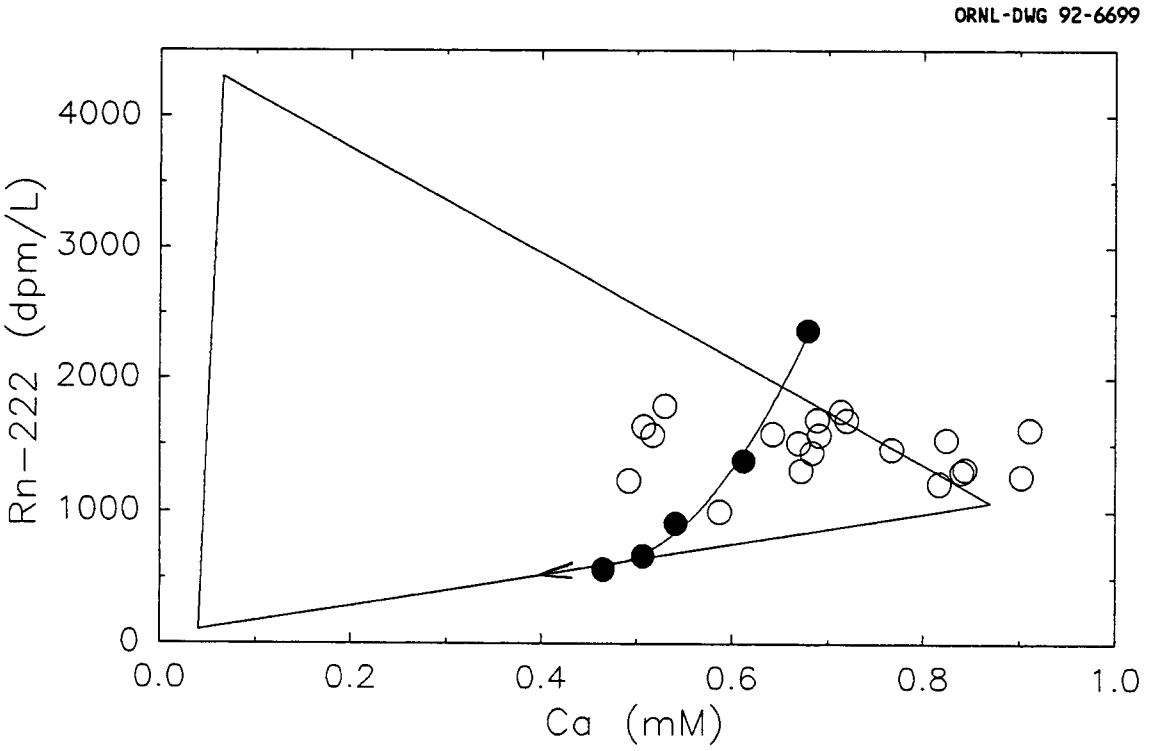

Figure 14. Mixing diagram showing lateral inflow to stream reach WB170-WB60. Open circles are regression-based points (see text). Arrow indicates direction of increasing flow.

14, though it is a tight correlation, leads to Q_{170} values significantly more uncertain than those measured directly.

The trend exhibited by the five solid points in Fig. 14 is slightly different from the trends at other sampling sites in that it is down and to the left (clearly toward vadose zone water) instead of up and to the left (toward soil groundwater or a mixture of soil groundwater and vadose zone water). This trend can be understood in terms of the nature of subsurface flow on the adjacent hillslopes and the distinction between vadose zone water and soil groundwater. As lateral inflow to WB170-WB60 increases, additional flow is generated by perched saturated flow on the adjacent hillslopes. This saturation typically persists only several hours or less, as Fig. 15 shows. This phenomenon would seem to be inconsistent with the trend indicated by the end member mixing model since the perched saturation is soil groundwater. However, as noted earlier, when the distinction between soil groundwater and vadose zone water is drawn on the basis of ^{222}Rn content, only groundwater having been in a saturated zone for several days or more is considered "soil groundwater". (In fact, hydrological and logical considerations suggest that any attempt to separate vadose zone water and soil groundwater contributions to streamflow by any method whatsoever should contain a criterion for how long water must reside in a saturated zone before being considered "soil groundwater". Such a criterion is called for by either one of the two following facts: all vadose zone water passes through a saturated zone, even if only very briefly, before draining to a stream, and virtually all water in the saturated zone was at one time

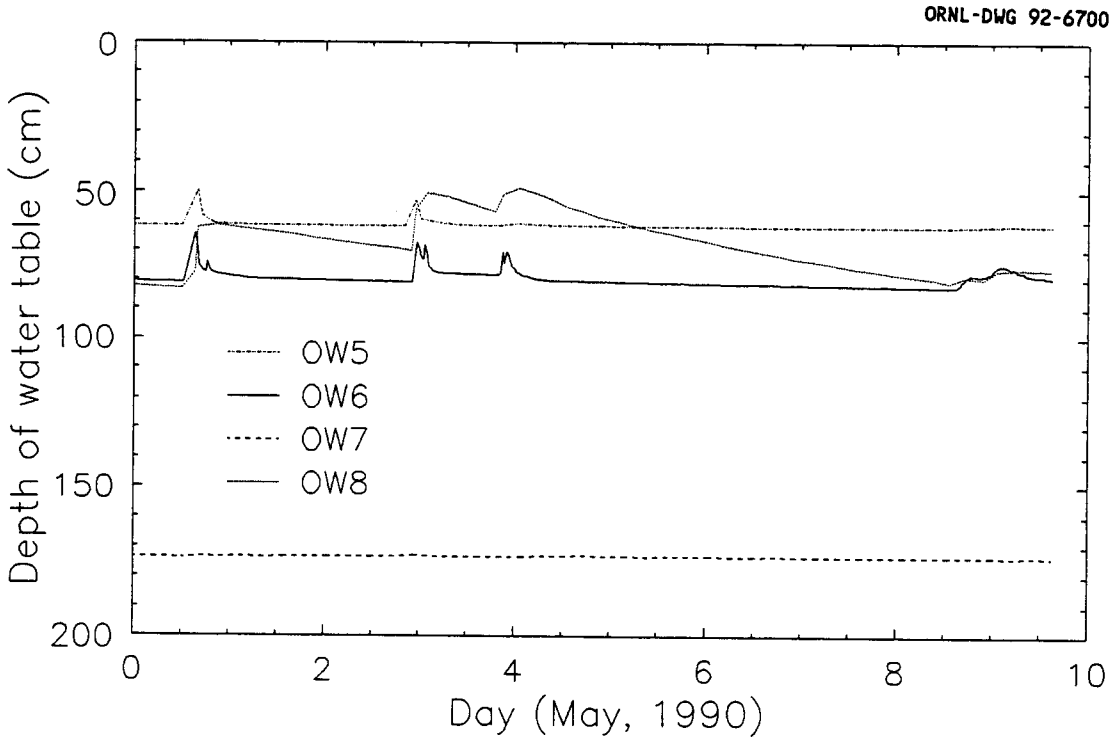

Figure 15. Depth to water table at four observation wells during the first 10 days of May, 1990. OW5 is located at the foot of the hillslope, just across the stream from spring S2. OW6 and OW7 are located straight upslope about 50 m (horizontally) from OW5. OW8 is located about 50 m (horizontally) from the stream channel, in the small hollow which intersects the streambank at about WB175. A few cm of water trapped in the bottom of each well are responsible for the horizontal segments on each record. Wells OW6 and OW7 are side by side, the latter screened below the soil/saprolite interface, the former above it. The storm responses clearly show the development of very short-lived perched saturation above the clayey saprolite at these two wells. Such short-lived saturation was also found at OW5, only 2 m from the stream channel. The much slower water table recession at OW8 could be the result of convergent flow supporting more lasting saturation in the hollow.

in the vadose zone. The time criterion for a ^{222}Rn-based separation is inextricably linked to the radioactive half-life of ^{222}Rn, 3.82 days. This point was also discussed by Genereux and Hemond [1990b].) Thus, the short-lived perched saturation observed on hillslopes adjacent to WB170-WB60 would be considered vadose zone water from the standpoint of the end member mixing model. While the perched saturation is short-lived, its effects might be felt for a few days if it displaces true soil groundwater from the small near-channel saturated zone and then drains to the stream over the next few days. Differences in mixing fractions between the two study reaches are discussed in more detail in Section 3.6.

Thus, the general trend exhibited by the five non-regression-based points is consistent with the hydrologic observations of perched saturation. The regression based points fall within the mixing triangle (Fig. 14) but show a relatively large amount of scatter and do not follow the trend exhibited by the other points. Replacing use of Eqn. 14 with accurate measurements of streamflow on each sampling day might provide a significantly less "noisy" signal that could confirm the trend indicated by the five "best" points.

While spring S2 is adjacent to this reach, the water from S2 re-infiltrates before reaching the stream channel, giving this water an opportunity to have its ^{222}Rn and Ca concentrations altered by further interaction with soil before reaching the stream. Thus, there is no reason to suspect a close relationship between WB170-WB60 lateral inflow and S2 outflow chemistry.

3.4.6. Well 8

Well 8 is located about 255 m upstream of the weir and only ~1 m from the stream, on a small patch of relatively level ground between the stream channel and the foot of the hillslope. The center of its screen lies at a depth of about 53 cm (40-45 cm below the level of the stream). Water from well 8 was clearly drawn from a saturated zone in the soil, and hence could be considered "soil groundwater" in a purely physical sense. However, this water (like that in perched saturated zones) appears to have retained a "chemical memory" long enough so that something can be learned of its origin. As Fig. 16 shows, samples from well 8 do not plot at the soil groundwater end member. At low flow, well 8 water falls along the mixing line between bedrock groundwater and vadose zone water. As flow increased water composition at well 8 moved to the left in Fig. 16, toward soil groundwater and vadose zone water, as one would expect. High-Ca bedrock groundwater would likely exchange some Ca with soil when it moves into a saturated soil zone. Likewise, the ^{222}Rn content of vadose zone water will begin to change (increase) when the water reaches a saturated zone. Fortunately, under the flow conditions investigated, water from well 8 retained the chemical signatures of its precursors, allowing identification of the waters mixing in the streambank to produce the small saturated zone there.

3.5. Additional considerations; modelling

While much of the foregoing has focused on some practical limitations of

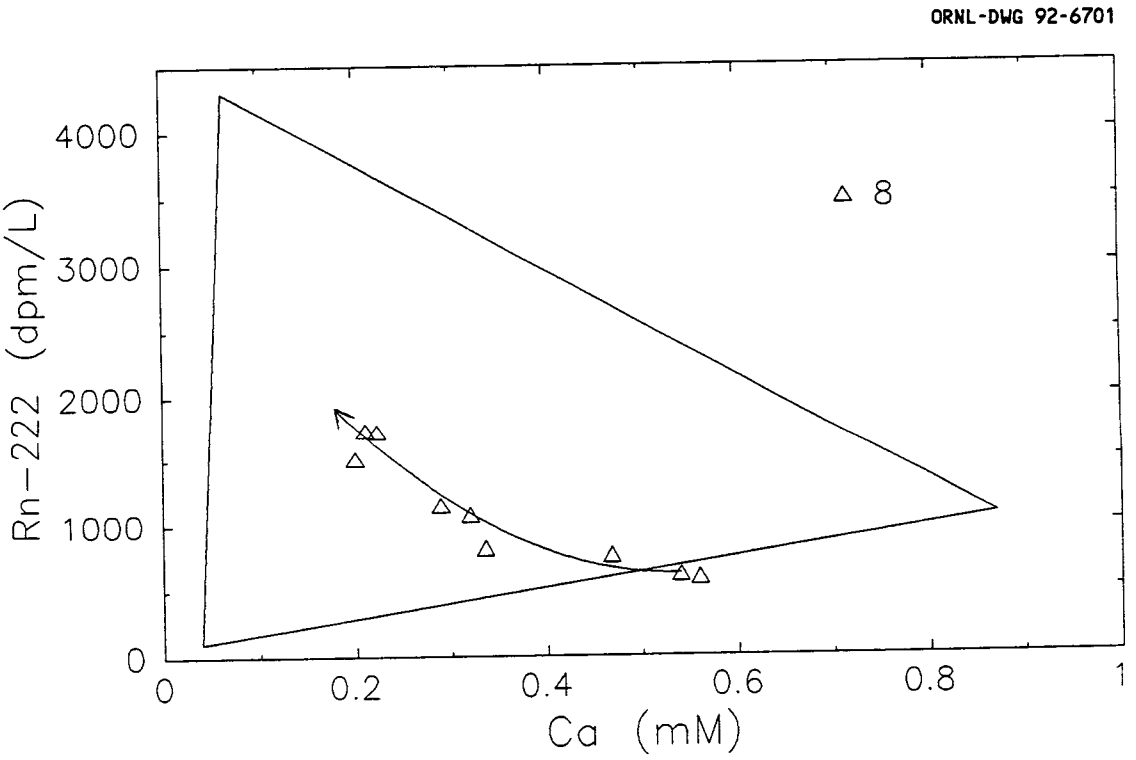

Figure 16. Mixing diagram showing samples from well 8. Arrow indicates direction of increasing flow.

the end member mixing model (e.g., variability in end member ^{222}Rn and Ca concentrations, the few samples falling outside the mixing triangle), this should not obscure the powerful unifying nature of this simple conceptual model. The end member mixing model pulls together a diverse body of field measurements (everything from temperature variations at springs S3 and S3A to the appearance of perched saturation on hillslopes between WB170 and WB60) in a hydrologically reasonable and consistent manner, no small accomplishment given the heterogeneous nature of the West Fork as described in Chapter 3 and elsewhere. The use of two naturally occurring tracers with special capabilities allowed identification and analysis of the important hydrologic features of streamflow generation in a way that hydrometric measurements probably could not have. Traditional hillslope methods (trenches, grids of tensiometers, etc.) are generally useful only in soil (not bedrock), are more costly, and probably more destructive of the study site. In addition, using flume measurements of flow at the springs as a measure of bedrock groundwater contributions to the stream could be misleading. As the ^{222}Rn and Ca data show, not all the water flowing from the springs is necessarily bedrock groundwater, and not all the bedrock groundwater reaching the stream enters via a spring (e.g., bedrock groundwater inputs to WB242-WB170 were larger than the sum of S3 and S3A outflow).

As Hooper et al. [1990, p.328] stated, in reference to mixing diagrams such as Fig. 2, "The utility of these plots can hardly be overstated." If it was not possible to identify subsurface waters which bound the chemistry of surface waters on such

a two-solute plot (after accounting for any non-conservative behavior of the solutes), we could conclude that subsurface sampling had missed a hydrologically and chemically important water. Even in this case, the mixing diagram would give an indication of the tracer concentrations that the missing end member should have, and therefore provide some guidance on where it might be found on the watershed. Thus, even in the worst case, two-solute mixing diagrams can suggest what additional measurements are required to apply an end member mixing model.

When end members are successfully identified (as they were in this study), the end member mixing model provides an indication of the appropriate structure for a lumped conceptual model for streamflow generation. Such models are often employed in the study of streamflow generation on small catchments [e.g., Christophersen et al., 1982; Lin and Schnoor, 1986; Villars, 1988]. These models typically generate streamflow as a mixture of outflow from two or more linear reservoirs (reservoirs for which outflow is linearly related to storage). Simple models based on linear reservoirs have been commonplace in the analysis of rainfall/runoff relationships for many years [Bras, 1990]. Our goal here is not to develop and parameterize a particular model; nor is it to propose that the end members in our mixing model should necessarily be treated as linear reservoirs in a lumped hydrologic model. However, if one were to draw the analogy between end members and linear reservoirs in such a model, then ^{222}Rn and Ca could be useful in deriving parameters for the reservoirs. For example, if Q, [Ca], and [Rn] were measured at both ends of a stream reach over the falling limb of a

hydrograph, the lateral inflow to the reach could be separated into contributions from the three end members (if flow was changing rapidly, some additional measurements of channel depth and/or width might be needed to account for changes in channel storage). Such a hydrograph separation would allow estimation of the time constants governing drainage from the three end members (i.e., the three reservoirs). This could be accomplished with linear regressions of $\ln D_i$ (the natural log of the drainage rate D of end member i) vs. t, where D_i is equal to $f_i(q\Delta x)$, the product of the mixing fraction of i and the total lateral inflow to the reach at a given time. The slope of such a regression would give the rate constant r_i in an exponential drainage relationship such as $D_i = D_i^{\circ}\exp(-r_i t)$, the sort of drainage relationship applicable to a linear reservoir [Bras, 1990].

Tracer and lateral inflow data covering a wide range of flow are available and can be used to give rough estimates of the drainage rate constants (r_i) of the end members. This was done for the two main channel stream reaches (WB242-WB170 and WB170-WB60); the following procedure was applied to two of the storms (those in March and June, 1989) studied by Mulholland et al. [1990]:

1. For each reach, f_i was plotted against Q_{weir} using data from the injected tracer experiments (Figs. 17 and 18).

2. The falling limbs of lateral inflow hydrographs were generated using Eqns. 12 and 15, and the Q_{weir} hydrographs given by Mulholland et al. [1990] for the March and June storms. About 10 points were chosen on each falling limb. Figs. 17 and 18 were used to obtain f_i values for the same

points. In this way, each of ~10 points on the falling limb of each Q_{weir} hydrograph was associated with a $q\Delta x$ value and f_i values for each reach. These values were then multiplied to give D_i values (e.g., $D_{vzw} = f_{vzw}q\Delta x$) in both reaches for about 10 points on the falling limb of each hydrograph.

3. Linear regressions of $\ln D_i$ vs. t were prepared for each end member in each reach during each storm (12 regressions in all; Figs. 19-22).

The use of two empirical relationships (f_i vs. Q_{weir}, $q\Delta x$ vs. Q_{weir}) developed with data collected over the course of the study guarantees that this method captures average or "composite" behavior; the actual separations for the two storms may be somewhat different from those estimated here, depending on the particular values of rainfall intensity, antecedent moisture, etc. This method could be applied to springs as well; a spring hydrograph measured with a flume and a plot of f_i vs. spring outflow (e.g., Fig. 23) would be needed.

Not surprisingly, Figs. 19 and 20 show that drainage rate constants for the bedrock groundwater feeding WB242-WB170 (~0.02 day^{-1}) are one tenth or less of those for vadose zone water (0.2-0.4 day^{-1}) and soil groundwater (0.8-1.7 day^{-1}). The soil groundwater constants are about four times larger than those for vadose zone water. This could be at least partially due to saturated hydraulic conductivities being higher than unsaturated conductivities because of the larger pores involved in saturated flow. Previous work has described the importance of macropores in transmitting saturated flow on the West Fork [Wilson et al., 1990]. The soil groundwater recession constants are intermediate between those of the

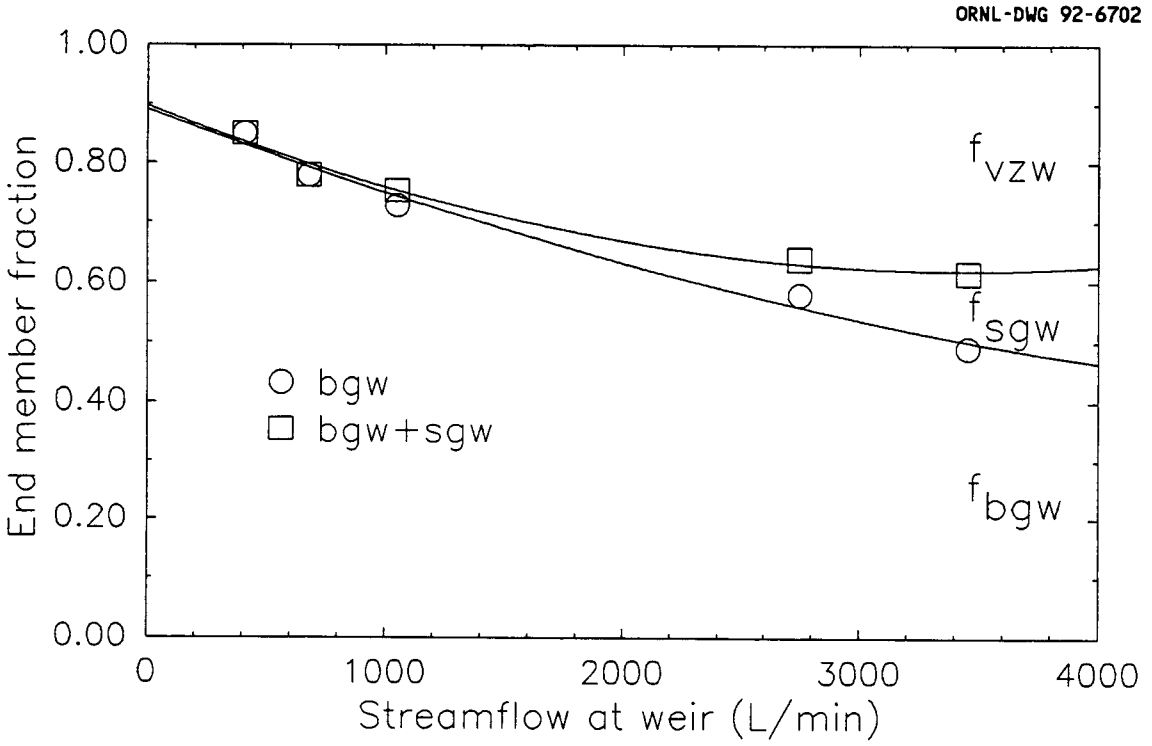

Figure 17. Plot of f_i (mixing fraction of end member i) vs. Q_{weir} for stream reach WB242-WB170. The five points are from injected tracer experiments.

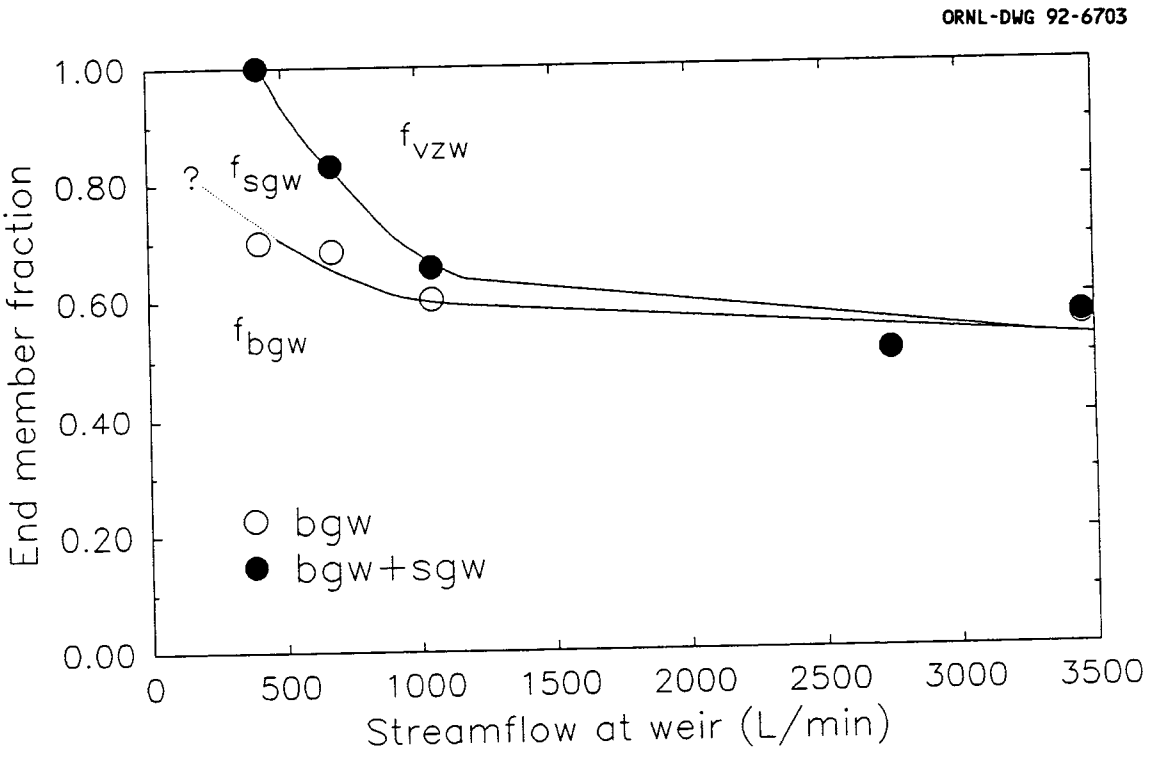

Figure 18. Plot of f_i vs. Q_{weir} for stream reach WB170-WB60. The five points are from injected tracer experiments.

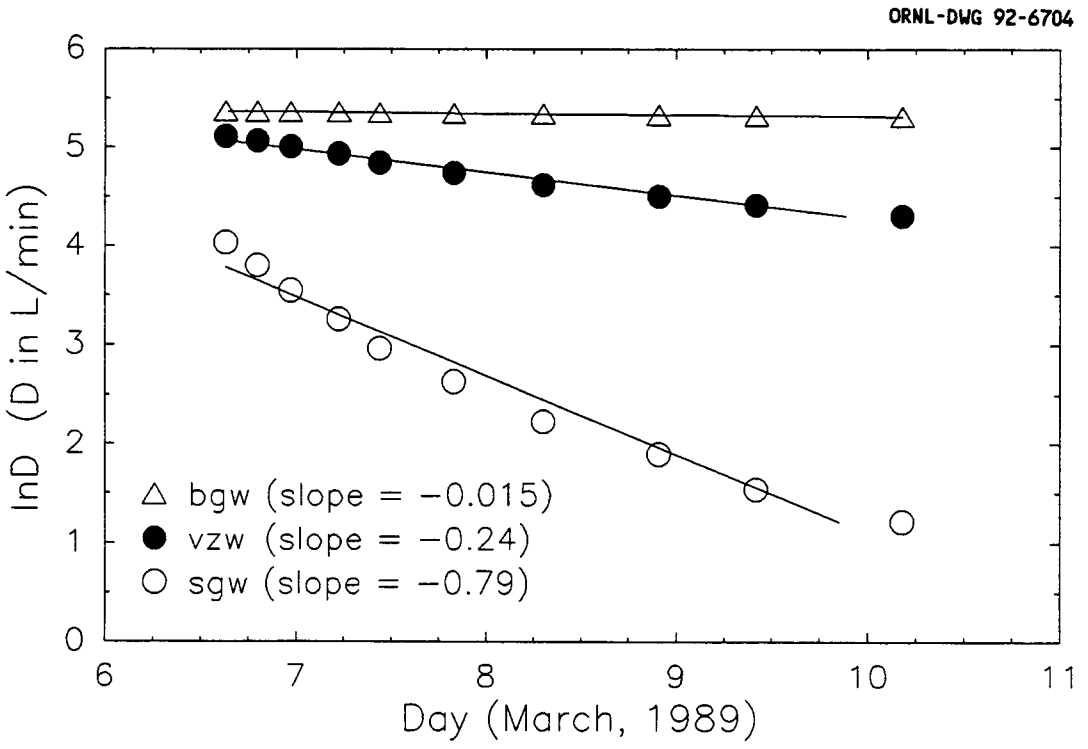

Figure 19. Natural log of D_i (drainage rate of end member i) vs. time for falling limb of estimated lateral inflow hydrograph, WB242-WB170, March 1989 storm.

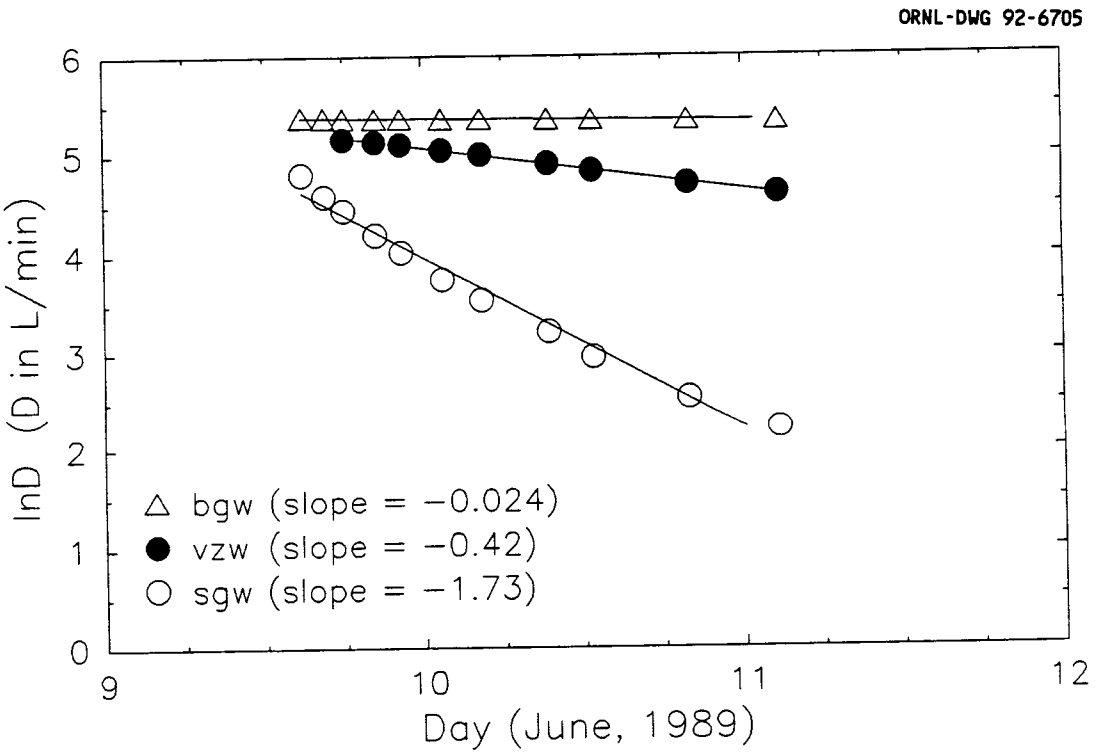

Figure 20. Natural log of D_i vs. time for falling limb of estimated lateral inflow hydrograph, WB242-WB170, June 1989 storm.

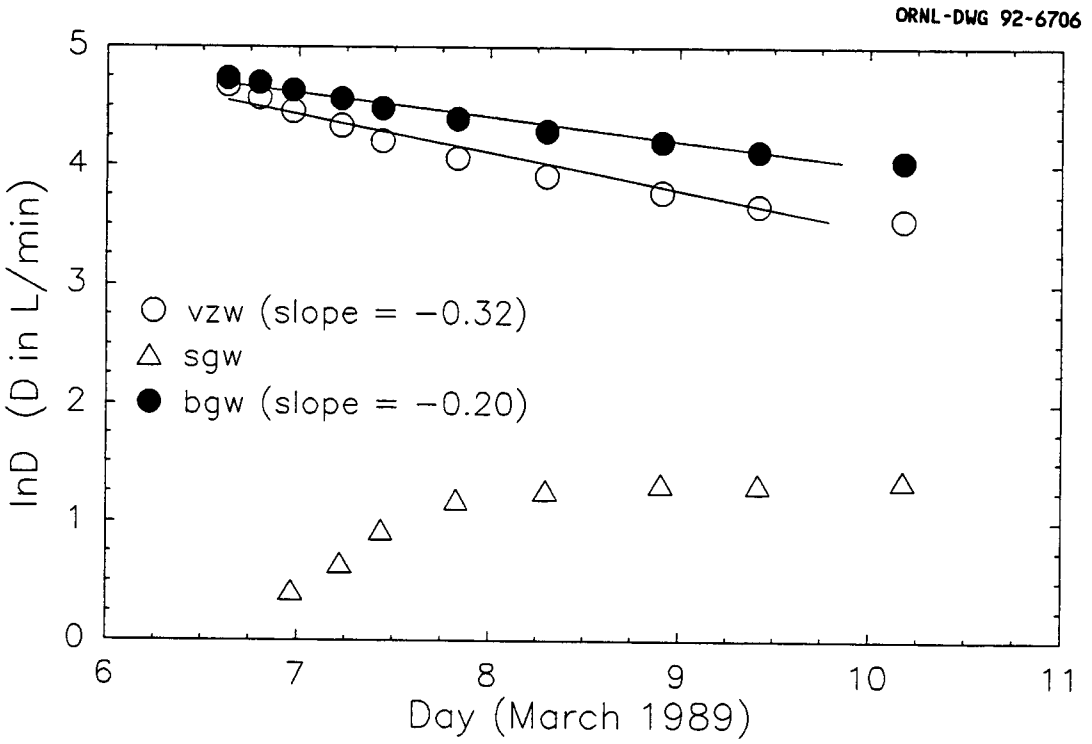

Figure 21. Natural log of D_i vs. time for falling limb of estimated lateral inflow hydrograph, WB170-WB60, March 1989 storm.

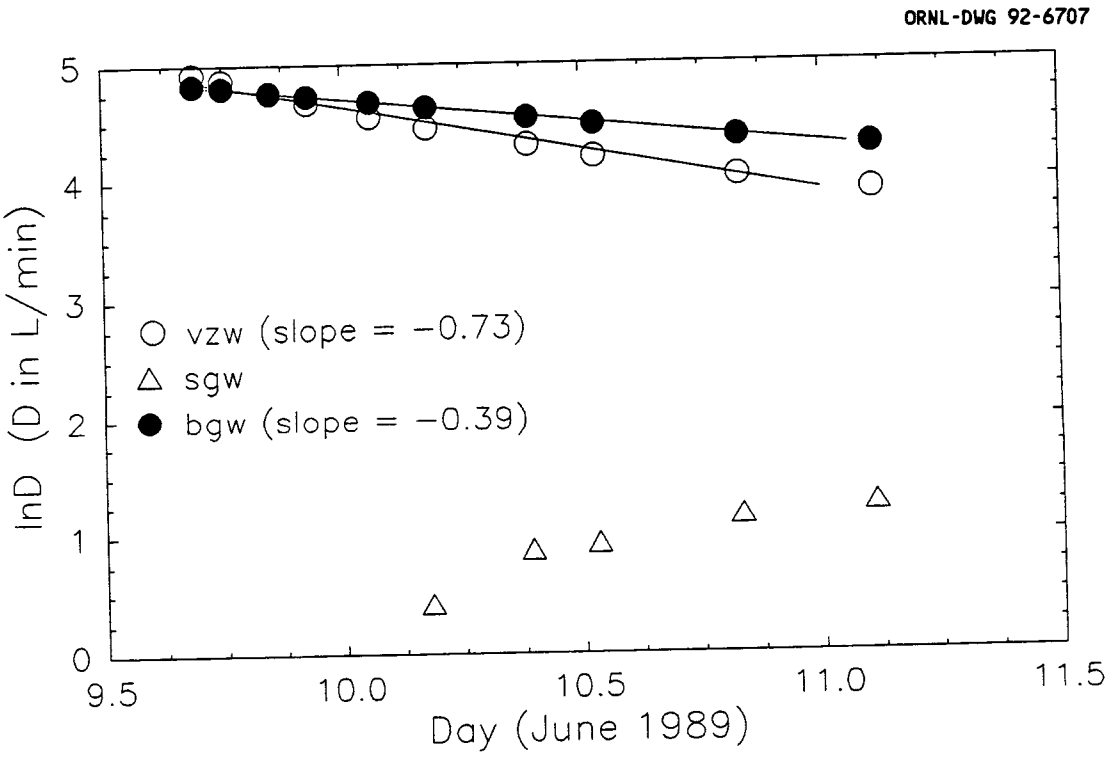

Figure 22. Natural log of D_i vs. time for falling limb of estimated lateral inflow hydrograph, WB170-WB60, June 1989 storm.

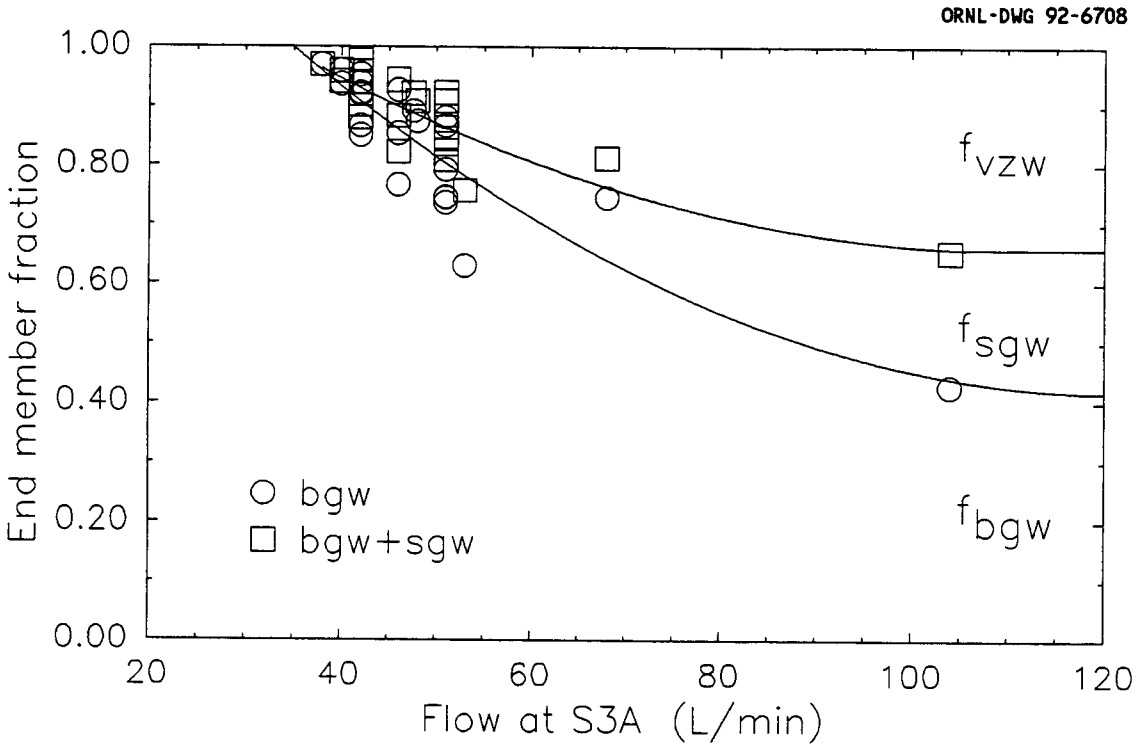

Figure 23. Plot of f_i vs. Q_{weir} for spring S3A.

saturated zones sampled by wells OW6 (about 20 day^{-1} for storms in Fig. 15) and well OW8 (about 0.2 day^{-1} for the same storms). Soil groundwater drainage as measured in the lateral inflow to a stream reach may average across some of the small scale local variability in the drainage of saturated zones in these heterogeneous soils.

The separations for WB170-WB60 are more complex and do not fit the simple picture of exponential flow regression with time; this is due largely to the nature of Fig. 18, with f_{sgw} decreasing with increasing flow. As noted earlier, this seemingly anomalous behavior can be understood in terms of the very rapid drainage of perched saturation and the somewhat slower acquisition of the soil groundwater ^{222}Rn signature by newly-created saturated zones. Thus, Figs. 21 and 22 show soil groundwater flow actually *increasing* with time, as the lateral inflow to the reach decreases. Had there been longer hydrograph recessions for these storms (more rain fell a few days after each storm), it might have been possible to evaluate r_{sgw}. Fig. 18 and Eqn. 15 show that D_{sgw} peaks and begins to fall as Q_{weir} drops below ~425 L/min, though Q_{weir} did not drop this low for the hydrographs in question. Use of this fairly crude technique leads to problematic results for WB170-WB60, where drainage of perched saturated zones seems to be faster than the ingrowth of ^{222}Rn to newly created saturated zones. This issue would perhaps best be pursued with actual measurements of lateral inflow and tracer concentrations on the falling limbs of hydrographs.

3.6. Differences between the two study reaches

By focusing on individual springs and stream reaches, we have captured some of the spatial information that would have been lost by sampling only at the basin outlet. One of the most interesting contrasts revealed was that between the two study reaches. As Figs. 17 and 18 show, soil groundwater contributions to the study reaches were quite different. During baseflow, a significant portion of the very small lateral inflow to WB170-WB60 was due to soil groundwater. As noted earlier, spring S2 discharges about 3 m above the stream level, and its outflow infiltrates the lower slope and streambank as it runs downhill, maintaining an area of wet soil which could be partially responsible for some of the soil groundwater flow to WB170-WB60. (This possibility, which essentially involves adding ^{222}Rn to spring S2 outflow by routing it through a soil saturated zone before it becomes WB170-WB60 lateral inflow, is lent credence by the fact that a water composition like that of low-flow lateral inflow to WB170-WB60 can indeed be obtained by adding ^{222}Rn to spring S2 outflow; see Fig. 2.) Additional small saturated zones contributing soil groundwater to WB170-WB60 could be found in bands of relatively thick soil lying normal to the stream. Evidence for the existence of one such band was given in Chapter 3, along with a discussion of the geological conditions giving rise to such bands (e.g., see Fig. 9 of Chapter 3) and the hypothesis that other such bands may exist. We hypothesize that these saturated zones (that maintained by spring S2 and those potentially lying in bands of thick soil) are small enough that they are effectively flushed out and overwhelmed by

inputs from shallow perched saturation (which, for reasons discussed earlier, carries the ^{222}Rn signature of vadose zone water) as flow increases. Thus, there is an increase in f_{vzw} and a decrease in f_{sgw} with increasing lateral inflow to WB170-WB60.

The lower baseflow contribution of soil groundwater to WB242-WB170 can be viewed as a result of the absence of the two factors mentioned above as contributors to soil groundwater flow in WB170-WB60. Springs feeding WB242-WB170 discharge at stream level, and do not maintain significant saturated soil zones on the streambanks of this reach. Also, the depth to bedrock is probably greater on slopes between WB242 and WB170 than on slopes between WB170 and WB60 (presumably because of thicker saprolite). Our data on depth to bedrock are somewhat patchy, but rock outcrops are seen running up the southwest-facing slope only downstream of WB170, not upstream. With soil lying over saprolite instead of the irregular bedrock surface, there would not be bands of relatively thick soil running upslope between WB242 and WB170. Thus, between WB242 and WB170, there is no evidence of the conditions (springs above stream level, bedrock-controlled bands of thick soil) which seem to maintain small saturated soil zones between WB170 and WB60; hence, at baseflow, f_{sgw} was near zero for WB242-WB170.

Convergent flow in the hollow-shaped topography on the southwest-facing slope between WB242 and WB170 may have aided in the development of saturated zones long-lived enough to produce the observed increase in f_{sgw} with flow. As noted earlier, data from well OW8 (Fig. 15) show that saturated zones in a small

hollow receded very slowly (with a rate constant of ~0.2 day^{-1}), giving this water ample time to acquire the ^{222}Rn signature of soil groundwater. Thus, there are saturated zones in hollows that are much longer-lived than the shallow perched saturation observed in wells OW5 and OW6, and we believe these longer-lived saturated zones are responsible for the observed increase in f_{sgw} with increasing flow in WB242-WB170. More extensive monitoring of saturated soil zones would be useful in assessing these ideas on why soil groundwater contributions to the two study reaches are so different. Discovery of these differences between the two reaches points out the strength of a reach-based approach in capturing spatial information lost when tracer sampling is done only at the basin outlet.

4. Summary and Conclusions

Measurements of naturally occurring ^{222}Rn and Ca in vadose zone water, soil groundwater, springwater, and streamwater suggest that a simple three-end-member mixing model is appropriate for streamflow generation over a wide range of flow conditions on the West Fork. The behavior of the end members (vadose zone water, soil groundwater, and bedrock groundwater) with changing flow was consistent with a variety of environmental observations, including temperature and flow variations at springs, water table responses, the general lack of soil saturated zones on hillslopes and even near the stream in many places, and the importance of water movement through the bedrock (see Chapter 3). Focusing on individual springs and stream reaches allowed us to capture spatial information that would

have been lost by sampling only at the basin outlet; this information revealed important differences in the behavior of the various springs and stream reaches.

At low flow, f_{vzw} and f_{bgw} were significantly larger than f_{sgw} for the springs and WB242-WB170 (though f_{sgw} at WB170-WB60 was as high as 0.3 at low flow). This suggests that baseflow to the stream is maintained largely by a combination of the two predominant baseflow generation mechanisms identified in the literature: groundwater inputs from a regional aquifer (i.e., bedrock groundwater) [e.g., Kazmann, 1972, p. 67-68] and unsaturated lateral drainage of soil on the hillslopes (i.e., vadose zone water) [Hewlett and Hibbert, 1963; Weyman, 1970, 1973; Mosely, 1979].

Variability in the natural chemistry of the end members precluded use of other solutes (Na, K, SO_4) to test the mixing fractions predicted from ^{222}Rn and Ca, though temperature may be a useful tracer for distinguishing the soil end members from bedrock groundwater during late summer and late winter (when soil and bedrock temperatures differ most). The simple mixing model provides a framework for focusing future data collection and modeling efforts on the broad essential features of streamflow generation in this highly heterogeneous system. Topics for further study include direct analysis of more unsteady flows, collection of more detailed information on the size and drainage rates of saturated soil zones, and assessment of spatial variability in the ^{222}Rn content of soil groundwater.

Appendix: Uncertainty Analysis

A1. Natural Tracers

A1.1. ^{222}Rn in water samples

The uncertainty in aqueous ^{222}Rn concentrations was the sum of radioactive counting uncertainty and the uncertainty associated with the calibration line, Eqn. 5. Counting uncertainty is directly related to sample activity and counting time (the standard deviation of the counting uncertainty for a sample giving N counts is the square root of N). The calibration uncertainty is also related to sample activity, but more weakly. The calibration uncertainty was smallest at ~1150 dpm/L, and increased slightly toward higher and lower ^{222}Rn concentrations. Analysis of calibration uncertainty was based on standard methods [Zar, 1984, chapter 17]; all the uncertainties given in this appendix correspond to one standard deviation (1 s.d.).

Figure 24 shows the relationship between ^{222}Rn concentration and uncertainty. In calculating the counting uncertainty curve, ^{222}Rn concentrations given by Eqn. 5 were multiplied by $\exp(7.549 \times 10^{-3}\ hr^{-1})(34\ hr)$ to account for ^{222}Rn decay during the time between sample collection and counting (34 hours was roughly the average duration of this time). The solid and dotted curves in Fig. 24 show the absolute (dpm/L) and relative (%) uncertainty, respectively, of ^{222}Rn concentrations based on having no replicates (i.e., one sample per site per sampling time, or n=1); the dashed line shows the absolute uncertainty a ^{222}Rn concentration would have if it were based on two samples (n=2). In sampling streamwater, replicates were always collected in order to achieve greater accuracy

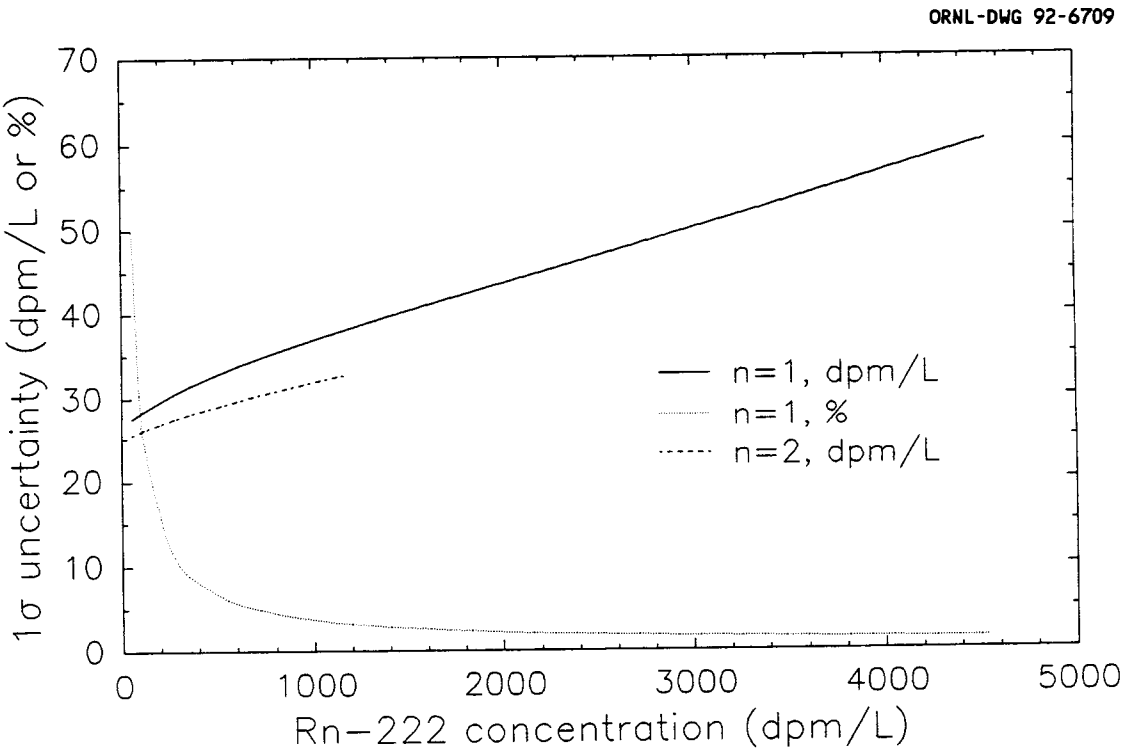

Figure 24. Uncertainty (1 s.d.) in ^{222}Rn concentration for water samples. The solid and dotted curves give the absolute (dpm/L) and relative (%) uncertainty, respectively, for values based on a single sample. The dashed curve gives the absolute uncertainty associated with values based on two samples.

for these relatively low activity samples (especially WB60, which generally had ^{222}Rn concentrations of 50-150 dpm/L).

A1.2. Vadose zone water (soil gas) samples

Uncertainty in vadose zone water ^{222}Rn concentrations is shown in Figure 25. Uncertainty was ±6% for samples having ≥400 dpm/L. The uncertainty analysis was very similar to that of Genereux and Hemond [1991], with some minor differences to account for the different calibration method used in the present study.

A1.3. Calcium

One Ca standard (1.25 mM) was used to calibrate the ICP, while a second (0.499 mM) was analyzed to see how well its known Ca content would be predicted by the ICP. Based on repeated analyses (n=46) of the second standard, its predicted concentration was 0.514 ± 0.006 mM. Combining the apparent small positive bias (0.015 mM) and the precision error (0.006 mM) in root-mean-square fashion [e.g., Kline, 1985] leads to an uncertainty of ±0.016 mM for the Ca measurements.

A2. Injected Tracers

A2.1. Propane

As Eqn. 2 shows, only ratios of propane concentrations were needed (not

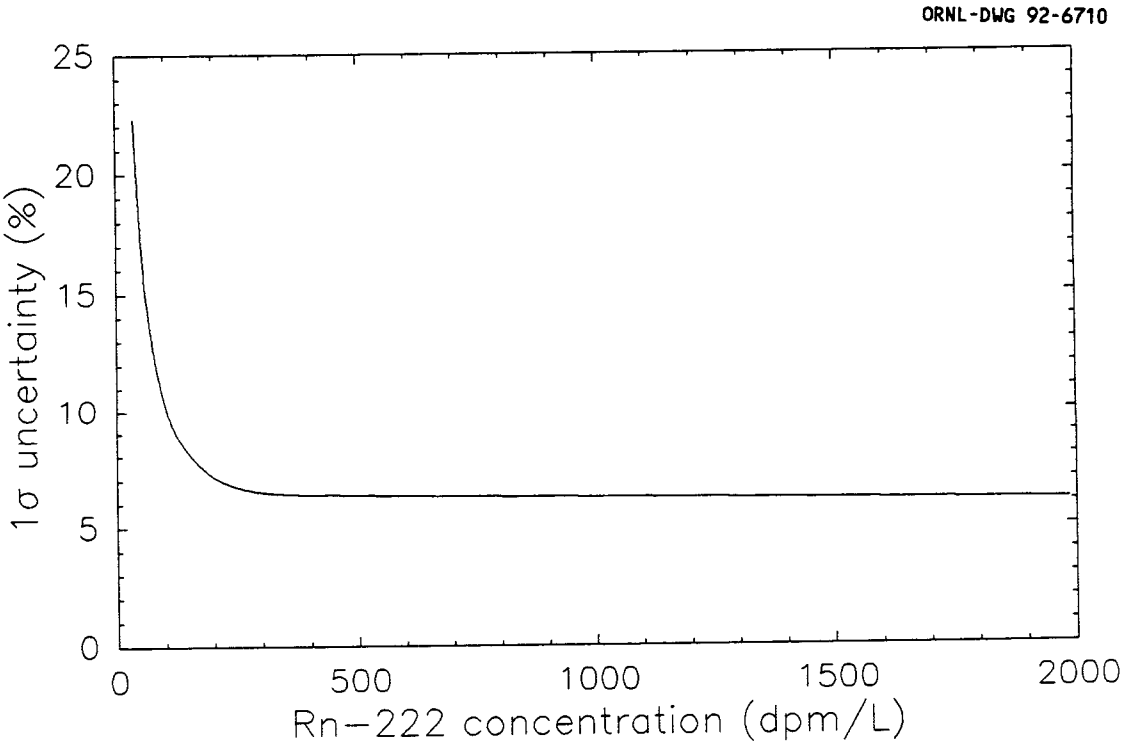

Figure 25. Uncertainty in the ^{222}Rn concentration of vadose zone water samples.

absolute concentration values). Thus, the only relevant aspects of uncertainty are those of linearity and precision, not absolute accuracy. Since flame ionization detectors have a linear dynamic range of 10^5-10^8 [Peters et al., 1974, p.576], linearity was not an issue (propane concentrations spanned a range of ~$5x10^2$, and were well above the limit of detection). Generally, 4 samples for propane analysis (occasionally, only 3) were collected at each stream site during the injected tracer experiments. The standard deviation for these replicates was typically 3-4%.

A2.2. Specific conductance (γ) and chloride (C)

In determining lateral inflow concentrations for ^{222}Rn and Ca the only relevant uncertainty issues for specific conductance (γ) and Cl^- measurements (C) were linearity and precision. Of the two concerns, precision was by far the largest source of uncertainty (the response of the auto-analyzer used for Cl^- measurements, and the relationship between γ and Cl^- concentration, are both highly linear over the ranges encountered in this study). The typical relative standard deviation of Cl^- estimates (from both the field γ measurements and laboratory Cl^- measurements) was about 2%.

For determination of streamflow at the stream measurement sites, and lateral inflow between these sites, accuracy of the Cl^- determinations was also important. Chapter 3 contains a detailed uncertainty analysis for the Cl^- determinations, including absolute uncertainty and the implications for uncertainty of the streamflow and lateral inflow values.

A3. Stream Lateral Inflow Concentrations

A3.1. Values calculated directly from injected tracer data

The uncertainties in $[Rn]_1$, $[Rn]_2$, C_1, C_2, G_1, and G_2 were propagated using standard methods [Kline, 1985, Eqn. B.4] to determine the uncertainty in $[Rn]_q$ values calculated with Eqn. 2. One s.d. uncertainties in $[Rn]_q$ averaged ±150 dpm/L for WB242-WB170, and ±500 dpm/L for WB170-WB60. The same procedure was applied to determine the uncertainty in $[Ca]_q$ values calculated with Eqn. 4. Average uncertainty was ±0.06 mM for WB242-WB170 and ±0.26 mM for WB170-WB60.

The much larger uncertainty associated with tracer concentrations in WB170-WB60 lateral inflow was due mainly to the relatively small streamflow increase across this stream reach. The flow increase (lateral inflow rate divided by streamflow rate at the upstream end of the reach) was 350-28% for WB242-WB170, but only 24-10% for WB170-WB60. In general, the approach of solving mass balance equations around individual reaches does not perform well when there is a small (less than ~15%) increase in streamflow across the reach. However, if one's goal is an understanding of the whole system, it is at least somewhat helpful that a reach where uncertainty in large must be a relatively minor component of the system.

A3.2.Values calculated by the "regression method"

Standard methods [Zar, 1984; Kline, 1985] were also used to determine the

uncertainty in $[Rn]_q$ and $[Ca]_q$ values calculated by the "regression method" (see section 3.4.4.). Uncertainty in $[Rn]_q$ was about ±120 dpm/L for WB242-WB170, and ±600 dpm/L for WB170-WB60. The uncertainty for the regression-based $[Rn]_q$ values for WB242-WB170 is slightly smaller than the uncertainty in values from the injected tracer experiments only because the regression based values were taken at a lower average flow (and hence larger flow increase across the reach). A $[Rn]_q$ value determined directly from injected tracer data is less uncertain than a regression-based value at the same flow rate. Uncertainty in regression-based $[Ca]_q$ values was ±0.06 mM for WB242-WB170 and ±0.3 mM for WB170-WB60.

Bibliography

Bras, R.L. 1990. Hydrology: An Introduction to Hydrologic Science. Addison-Wesley, Reading, Massachusetts.

Christophersen, N., H.M. Seip, and R.F. Wright. 1982. A model for streamwater chemistry at Birkenes, Norway. Water Resources Research 18: 977-997.

Christophersen, N., C. Neal, R.P. Hooper, R.D. Vogt, and S. Andersen. 1990. Modelling streamwater chemistry as a mixture of soilwater end members: a step towards second-generation acidification models. Journal of Hydrology 116: 307-320.

Clever, H.L. (ed). 1979. Solubility Data Series: Volume 2, Krypton, Xenon, and Radon. Pergammon Press, New York, NY.

DeWalle, D.R., B.R. Swistock, and W.E. Sharpe. 1988. Three-component tracer

model for stormflow on a small Appalachian forested catchment. Journal of Hydrology 104: 301-310.

Genereux, D.P., and H.F. Hemond. 1990a. Three-component tracer model for stormflow on a small Appalachian forested catchment: Comment. Journal of Hydrology 117: 377-380 (with Corrigendum in Journal of Hydrology 122: 429, 1991).

Genereux, D.P., and H.F. Hemond. 1990b. Naturally occurring ^{222}Rn as a tracer for streamflow generation: steady state methodology and field experiment. Water Resources Research 26(12): 3065-3075.

Genereux, D.P., and H.F. Hemond. 1991. Measurement of the ^{222}Rn content of soil gas by liquid scintillation counting. Isotope Geoscience, in press.

Hewlett, J., and A. Hibbert. 1963. Moisture and energy conditions within a sloping soil mass during drainage. Journal of Geophysical Research 68(4): 1081-1087.

Hooper, R.P., and C.A. Shoemaker. 1986. A comparison of chemical and isotopic streamflow separation. Water Resources Research 22(10): 1444-1454.

Hooper, R.P., N. Christophersen, and N.E. Peters. 1990. Modelling streamwater chemistry as a mixture of soilwater end members: an application to the Panola Mountain catchment, Georgia, U.S.A. Journal of Hydrology 116: 321-343.

Johnson, D.W., and D.E. Todd. 1990. Nutrient cycling in forest of Walker Branch Watershed, Tennessee: roles of uptake and leaching in causing soil changes.

Journal of Environmental Quality 19(1): 97-104.

Kazmann, R. 1972. Modern Hydrology. Harper and Row, New York.

Kline, S.J. 1985. The purposes of uncertainty analysis. Journal of Fluids Engineering 107: 153-160.

Lin, J.C., and J.L. Schnoor. 1986. Acid precipitation model for seepage lakes. ASCE Journal of the Environmental Engineering Division 112: 677-694.

McDonnell, J.J., M. Bonell, M.K. Stewart, and A.J. Pearce. 1990. Deuterium variations in storm rainfall: Implications for stream hydrograph separation. Water Resources Research 26(3): 455-458.

Mosely, M.P. 1979. Streamflow generation in a forested watershed, New Zealand. Water Resources Research 15(4): 795-806.

Mulholland, P.J., G.V. Wilson, and P.M. Jardine. 1990. Hydrogeochemical response of a forested watershed to storms: effects of preferential flow along shallow and deep pathways. Water Resources Research 26(12): 3021-3036.

Peters, D.G., J.M. Hayes, and G.M. Hieftje. 1974. Chemical Separations and Measurements: Theory and Practice of Analytical Chemistry. W.B. Saunders Co., Philadelphia, Pennsylvania.

Sklash, M.G., R.N. Farvolden, and P. Fritz. 1976. A conceptual model of watershed response to rainfall, developed through the use of oxygen-18 as a natural tracer. Canadian Journal of Earth Science 13: 271-283.

Sklash, M.G., M.K. Stewart, and A.J. Pearce. 1986. Storm runoff generation in

humid head-water catchments. 2. A case study of hillslope and low order stream response. Water Resources Research 22: 1273-1282.

Villars, M.T. 1988. Modeling flowpaths and streamflow generation at the Bickford Watershed: Applications to acid deposition modeling. M.S. Thesis, Dept. of Civil Engineering, MIT, Cambridge, Massachusetts.

Weyman, D.R. 1970. Throughflow on hillslopes and its relation to the stream hydrograph. Int. Assoc. Sci. Hydrol. Bull. 15: 25-33.

Weyman, D.R. 1973. Measurements of the downslope flow of water in a soil. Journal of Hydrology 20: 267-288.

Wilson, G.V., P.M. Jardine, R.J. Luxmoore, and J.R. Jones. 1990. Hydrology of a forested hillslope during storm events. Geoderma 46: 119-138.

Zar, H. 1984. Biostatistical Analysis. Prentice-Hall, Englewood Cliffs, New Jersey.

APPENDIX 1

Measurement of the Radon-222 Content of Soil Gas by Liquid Scintillation Counting

David P. Genereux and Harold F. Hemond

Isotope Geoscience, 1991

Abstract

A method is described for measuring the ^{222}Rn content of soil gas using a conventional liquid scintillation counter. Gas samples, collected in wetted ground glass syringes, are equilibrated with a scintillation cocktail which is then expelled into a scintillation vial and counted. The method is straightforward and relatively fast (5-6 minutes of operator's time per sample), and yields results having 95% confidence limits of about $\pm$ 10% for samples containing $\geq 2 \times 10^4$ Bq/m^3 of ^{222}Rn. The method is applied to a watershed near Bickford Reservoir in Massachusetts, where soil gas ^{222}Rn content is found to be reasonably constant horizontally, but strongly and systematically increasing with depth, to over 5×10^4 Bq/m^3 at soil depths of about 1 m.

1. Introduction

Transport of ^{222}Rn in soils is a topic of central importance to studies of both basic radon geochemistry and the health effects of radon. Studies of gas-phase transport of ^{222}Rn often rely on measurement of the ^{222}Rn content of soil-gas, [Rn]. Methods of obtaining time-averaged, in-situ [Rn] values (with averaging periods of about 1 week to 1 month) have been described by Fleischer and Mogro-Campero [1978], and Wadach and Hess [1985], among others. For soil-gas samples withdrawn from the subsurface, most measurements of [Rn] are made by gas-phase alpha counting techniques (e.g., Kraner et al. [1964]; Schery et al. [1984]; Rose et al. [1988]). These techniques make use of scintillation cells ("Lucas cells") which vary in size from 100 ml [Schery et al., 1984] to 450 ml [Kraner et al., 1964], and which are manually placed onto and taken off of photomultiplier tubes for counting. The counting efficiencies of such cells are typically 70-80% per alpha particle (e.g., Lucas [1957]; Broecker and Peng [1971]; Broecker et al. [1976]), resulting in overall efficiencies of 200-250% (since the alphas from ^{214}Po and ^{218}Po, short-lived daughters of ^{222}Rn, are counted along with those of the parent radon).

Fukui [1987] has described a method for measuring [Rn] by liquid scintillation counting. The method involves bubbling soil gas through a series of three vials containing scintillation cocktail. The field sampling required a pump (and hence a power supply), a pyrostat, vials of scintillation cocktail, and the associated tubing and connectors. Bubbling times of 30-60 minutes were required to reach equilibrium.

In this paper, we describe an alternate technique for the measurement of [Rn] using liquid scintillation counting. The method is intended to serve as an alternative to gas-phase alpha counting for those situations in which large numbers of samples are required (the sample-changing and programming capabilities of most liquid scintillation counters make them well-suited for large numbers of samples), and/or in which a somewhat larger overall uncertainty in the final [Rn] values (10-20%) can be tolerated. The method is more convenient than that of Fukui (1987) since less field equipment is required (only one glass syringe per sample and a single short piece of tubing to connect the syringes to sampling tubes installed in the soil). Also, far less time is required (5-6 minutes per sample, about 15 seconds of which is field sampling time). The method is described below, along with some results from its application at the Bickford watershed in central Massachusetts.

2. Methodology

2.1. Overview

Soil-gas samples were collected in wetted ground-glass syringes, and a known volume of scintillation cocktail was drawn into each syringe. Once the cocktail:air ^{222}Rn partitioning reached equilibrium, the cocktail was expelled into a glass scintillation vial, and the vial was quickly and tightly capped. Vials were allowed to stand for at least 3 hours before counting, to allow the short-lived radioactive progeny of ^{222}Rn (^{218}Po, ^{214}Pb, ^{214}Bi, and ^{214}Po) to grow into secular equilibrium with

the parent ^{222}Rn.

Six calculations were performed to obtain the [Rn] value for each sample from the measured counts per minute (cpm):

1. subtracting the background count rate (BG) and multiplying by the counting efficiency (E) to relate the measured net cpm to m_4, the number of Bequerels (Bq) of ^{222}Rn in the scintillation cocktail at the time of counting;

2. calculating the cocktail:air partitioning of ^{222}Rn in the scintillation vial to determine m_3, the total number of Bq of ^{222}Rn in the vial at the time of counting;

3. correcting for ^{222}Rn decay (and leakage) during the time between capping and counting the vial to determine m_2, the total number of Bq of ^{222}Rn brought into the scintillation vial with the cocktail;

4. calculating the cocktail:air partitioning of ^{222}Rn in the syringe to determine m_1, the total number of Bq of ^{222}Rn in the syringe at the time the cocktail was transferred to the vial;

5. correcting for ^{222}Rn decay during the time between collecting the sample and capping the vial to determine m_0, the total number of Bq of ^{222}Rn in the sample at the time of collection; and

6. calculating [Rn] from m_0 and the volume of the soil gas sample.

Nine pieces of information are needed to obtain [Rn] for a given sample:

1. the efficiency of the liquid scintillation counter in counting the decays of interest (E)
2. the count rate for the sample (cpm)
3. the background cpm in the counting window used (BG)
4. the true total volume of the liquid scintillation vial (V_t)
5. the volume of the soil-gas sample (V_g)
6. the volume of cocktail used (V_c)
7. the time between collecting the sample and capping the vial (t_2)
8. the time between capping and counting the vial (t_1)
9. the cocktail:air partition coefficient for radon (K), at the temperature of the sample (K is the radon concentration in cocktail divided by the radon concentration in air, both in Bq/m^3).

The discussion below describes how each of these nine items was determined and used.

2.2. Details of Procedure

Soil-gas samples were collected in wetted ground-glass syringes. Both 30 ml and 50 ml syringes were used; the former had 1-ml volume markings, the latter 2-ml. A three-way nylon Luer-Lok™ valve was affixed to the end of each syringe, to close the syringe off after sampling. Sample size (V_g) varied from 15-32 ml, and was determined from the volume markings on the syringe barrels. At the lab, 10 ml of scintillation cocktail was drawn into each syringe, through a hypodermic needle attached to the Luer-Lok™ valve. The cocktail consisted of toluene with 4 g/L PPO and 0.04 g/L M_2-POPOP. V_c values were determined from the volume markings on the syringes. Corrections were applied to V_g and V_c to account for the small volume (about 0.5 ml) inside the syringe tip.

The syringes were then gently shaken with a mechanical wrist-action shaker. Equilibration was found to be rapid, reaching completion in a few minutes. This was determined by running a series of samples with roughly the same [Rn] (within about 10%), and equilibrating them for different periods of time (five minutes to three hours). The results, shown in Fig. 1, suggest that equilibration times of a few minutes are adequate. However, to ensure that equilibrium was reached, most samples were allowed to equilibrate for 30-35 minutes. Since K was about 12.7 (see discussion below), 80-90% of the ^{222}Rn in each sample was extracted into the

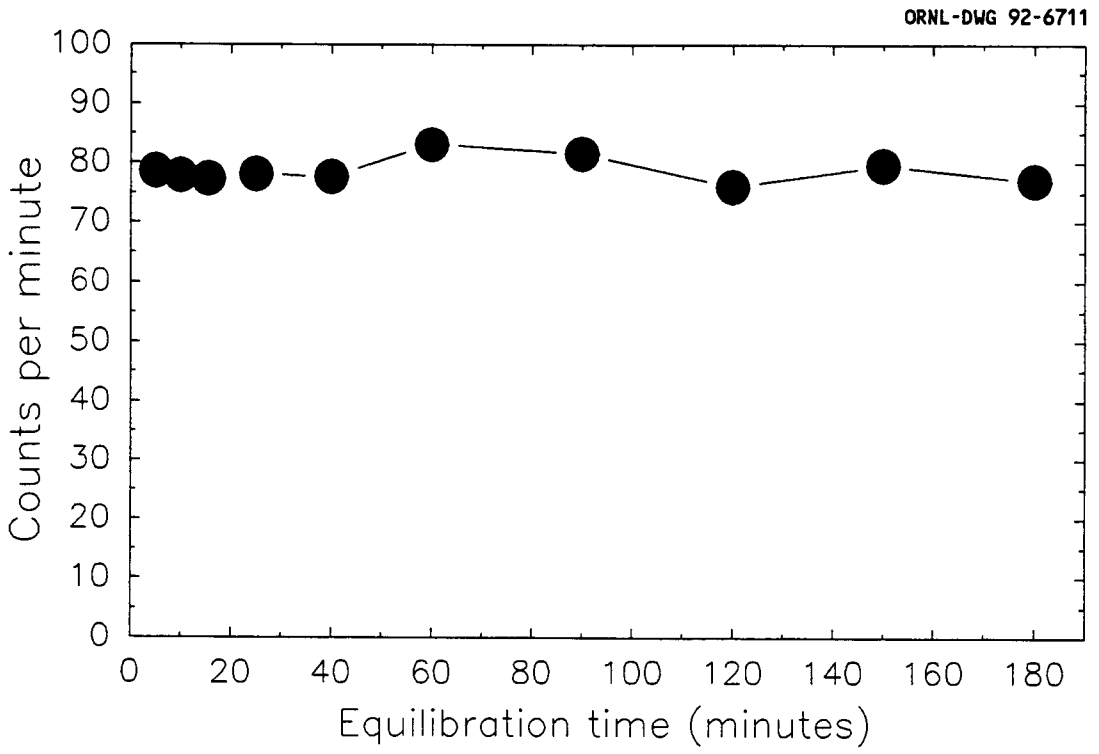

Figure 1. Cpm (corrected for decay and leakage) vs. equilibration time (length of time the cocktail and soil-gas were in contact in the syringe) for a series of 30-ml samples collected from tube 22 on July 8, 1987. Other data have shown that successive samples from tube 22 have the same ^{222}Rn content (within about 10%), so each cpm value plotted here may be compared directly to the others in the series in assessing the effect of varying equilibration time. It appears that equilibration occurs in less than five minutes.

cocktail.

After equilibration, the cocktail was ejected from the syringe into a 20 ml (nominal) glass scintillation vial. Glass vials were used instead of plastic because radon may diffuse into and through many types of plastic. The vial was then quickly and tightly capped, and the time noted. The difference between this time and the time of sample collection (usually 2-10 hours) was designated t_2, and was used to correct for decay of ^{222}Rn which occurred in the syringe.

The true volume of "20 ml" scintillation vials was determined by weighing several vials empty, filling them with water, and reweighing them. The average volume of these vials was found to be 23.9 ml (s.d.=0.1, n=7), and this value of V_t was used for all samples.

Since a toluene-based cocktail was used, K was taken to be the toluene:air partition coefficient of radon. Data on K as a function of temperature was obtained from Schulz (1920). A linear regression of Schulz's five data points between 9°C and 30°C gave the following expression:

$$\log K = (750/T) - 1.456 \qquad (r=0.99908, n=5) \qquad (1)$$

where T is the temperature in kelvin. Using this expression, the value of K at 20°C (the approximate temperature of the laboratory) was found to be 12.7; this value was used for all samples.

As indicated above, each vial was allowed to sit for at least three hours between capping and counting. This allowed the short-lived ^{222}Rn daughters to

grow into secular equilibrium with the parent ^{222}Rn. During this time period (t_1), ^{222}Rn was lost from vials by both leakage (the vial caps were not perfectly gas-tight) and radioactive decay. (Leakage of ^{222}Rn from the ground-glass syringes was not considered important, since these syringes were demonstrably gas-tight when properly wetted.) The average rate of ^{222}Rn leakage from the vials was established through repeated counting of selected samples. Observation of the decrease of count rate with time for 54 samples showed that L_T = 10.1 x 10-3 hr^{-1} (s.d. = 2 x 10^{-3}) where $L_T = L + L_L$, L_T = total rate of decrease of cpm-BG, L = radioactive decay constant for ^{222}Rn (7.55 x 10-3 hr^{-1}), and L_L = rate constant for ^{222}Rn leakage from the vials. Thus, the ^{222}Rn loss from leakage was about 1/3 that due to radioactive decay. The correction for ^{222}Rn loss between capping and counting was based on the measured overall loss rate, L_T.

All samples were counted for 50 minutes on a Beckman 150 liquid scintillation counter. The counting window used was between channels 440 and 1000. Setting the lower discriminator at 440 increased the signal-to-noise ratio by excluding the high-background, low-energy channels. The background count rate (about 17 cpm) was determined from 50-minute counts of blank vials (glass vials containing 10 ml of radon-free cocktail). At least two blank vials were counted with each set of samples.

As noted earlier, samples were counted only after ^{222}Rn and its short-lived daughters were in secular equilibrium. In this condition, every ^{222}Rn alpha decay is accompanied by two other alpha (^{218}Po and ^{214}Po) and two beta (^{214}Pb and ^{214}Bi)

decays. Thus, there are five total Bq for every ^{222}Rn Bq. This fortuitous situation results in overall counting efficiencies of over 400%, since the alpha decays are counted with nearly 100% efficiency [Horrocks, 1973] and the two beta decays with >50% efficiency.

The overall counting efficiency (E) for this procedure was determined by analyzing gas samples of known ^{222}Rn content. The gas was obtained from a sealed flow-through type source made by Pylon Electronic Development Co. of Ottawa, Canada. The source consists of about 4.88×10^5 Bq of Ra-226 in a metal can, through which air is pumped at a known rate (about 1030 ml/min for our purposes). The ^{222}Rn content of air in the source was determined by exposing small cannisters of activated charcoal to the air, and then analyzing the ^{222}Rn content of the charcoal. This procedure was performed by Stephen Shefsky of Niton, Inc., in Lexington, MA (Niton uses this same charcoal-cannister method to determine the ^{222}Rn content of indoor air). The ^{222}Rn content of air from the source was found to be $(6.11 \pm 0.15) \times 10^4$ Bq/m^3 (uncertainty is the standard deviation of the mean for six charcoal samples). This value agreed well with the estimate of $(5.96 \pm 0.30) \times 10^4$ obtained from the manufacturer's estimate of the Ra-226 content of the source ($\pm$ 4%) and the measured flow-rate of air through the source ($\pm$ 2%). Four gas samples were taken from the source, two of 20 ml and two of 10 ml. The 10 ml samples were diluted with lab air (containing a negligible ^{222}Rn content of <30 Bq/m^3), one by a factor of 2 (to 3.05×10^4 Bq/m^3), the other by a factor of 3 (to 2.04×10^4 Bq/m^3). All four samples were then carried

through the same procedure used for soil-gas samples, and the known [Rn] values were used to back-calculate E values. The value of E was found to be 276 $\pm$ 12 cpm per Bq of ^{222}Rn (uncertainty is the standard deviation of the mean of the E values for the four samples). This could also be expressed as 4.6 cpm per disintegration/minute of ^{222}Rn, or 460%.

Using the variables defined above, the six calculation steps described in the previous section may be written as follows:

1. $m_4 = (cpm - BG)/E$
2. $m_3 = m_4[1 + (V_t/V_c - 1)/K]$
3. $m_2 = m_3 exp(L_T t_1)$
4. $m_1 = m_2(1 + V_g/KV_c)$
5. $m_0 = m_1 exp(Lt_2)$
6. $[Rn] = m_0/V_g$

As is apparent from Eqn. 1, we assumed that ^{222}Rn decay events in the vial headspace, and the daughter decay events that they lead to, did not contribute to the measured cpm value. It is likely that some small fraction (f) of these decays were counted, but determination of f would be difficult (f would depend on the fraction of ^{222}Rn daughters attached to aerosol particles in the headspace, the relative rates of settling, coagulation, and diffusion for the different sized aerosols, the rate of diffusion of the unattached daughters, etc.). If one assumes that diffusion dominates, then f = 0.17 (the ratio of the area of the air:cocktail interface to the total surface area of the vial headspace), and the [Rn] values obtained by

including the assumed headspace contribution differ by only about 1% from those obtained by assuming no headspace contribution. Therefore, in the absence of a compelling, quantitative reason to do otherwise, the possible contribution of headspace decay events was ignored in calculating [Rn].

A potential concern with this method was the volatilization of ^{222}Rn from the cocktail during and immediately after the cocktail transfer, in the 3-4 seconds before the vial was capped. Prichard and Gesell [1977] gave data on the rate of volatilization of ^{222}Rn from scintillation cocktail ejected from syringes into vials which were left uncapped. Their experiment (which only accounted for volatilization taking place from the open vials after the cocktail transfer, not volatilization during the cocktail transfer) suggests that loss during the first 10 seconds is negligible. Therefore, this loss was ignored (except in the sense that efforts were made to minimize it, by filling the vials quickly but smoothly, with a minimum of turbulence, and by capping them rapidly, within 3-4 seconds after the start of the cocktail transfer).

Also of concern was the potential for interference from ^{220}Rn daughters. ^{220}Rn and ^{222}Rn may be present in soil gas in similar activities [e.g., Rose et al. [1988]). The half-life of ^{220}Rn is 56 seconds, so within about five minutes of collecting a soil-gas sample, all the ^{220}Rn in the sample has decayed to ^{212}Pb (which has a 10.6 hour half-life). ^{212}Pb decays to ^{212}Bi (1 hour half-life), which decays to ^{212}Po (3 x 10-7 second half-life); ^{212}Po decays to stable ^{208}Pb. ^{212}Pb, ^{212}Bi, and ^{212}Po could interfere with our procedure (i.e., contribute to the measured cpm) if ^{212}Pb

was washed off the inner walls of the syringes by the scintillation cocktail. However, experiments showed that soil-gas samples collected and held in a syringe for five minutes, and then transferred to another syringe for analysis (thus leaving the ^{212}Pb behind on the walls of the first syringe) generally had the same count rates as replicates run as described earlier, without transfer to a second, ^{212}Pb-free syringe. This is perhaps not suprising, considering that the total activity of the three daughters produced from a given amount of ^{220}Rn will be <0.5% of the activity of the original ^{220}Rn (because the half-life of ^{212}Pb is much longer than that of ^{220}Rn). Thus, if a sample has roughly equal amounts of ^{220}Rn and ^{222}Rn when it is collected, within five minutes the activity of the ^{220}Rn daughters will be a tiny fraction of the activity of the ^{222}Rn and its daughters.

3. Results: Bickford Watershed

Soil-gas samples from the Bickford watershed were collected and analyzed for their ^{222}Rn content from August to November, 1986. The Bickford watershed has been discussed elsewhere (Hemond and Eshleman [1984]; Eshleman and Hemond [1985]; Benoit and Hemond [1987]; Eshleman and Hemond [1988]), and is in many respects typical of forested watersheds in Massachusetts. All samples were taken from the West Road catchment, a section of the watershed having thin (about 1 m) rocky Spodosol soils and mixed hardwood (beech, oak, and maple) and coniferous (mainly hemlock) vegetation. The West Road catchment lies on the west slope of Mount Wachusett, a large granite monadnock.

All samples were withdrawn from the subsurface through permanently installed sampling tubes. The tubes consisted of metal pipe (1/4" nominal black steel pipe, having a 7 mm ID) with a piece of copper screening (30 mesh) crimped over the end and held on with a stainless steel hose clamp. A section of clear PVC tubing about 10 cm long was affixed to the top of each sampling tube, and held in place with another hose clamp. A multi-position tubing clamp was used to pinch the plastic tubing shut when the sampling tube was not in use. A tubing connector was fitted into the end of the plastic tubing, and a small rubber cap (fashioned from a serum stopper) was placed over the connector to keep rain and debris out of the plastic tubing.

All sampling tubes were installed in holes (3 cm diameter) augered in the soil. Sieved sand (approximate grain diameters of 0.08-0.8 cm) was placed in the bottom of each hole, around the screened end of the sampling tube; the height of the sand in the hole was generally 8-10 cm. The remainder of the hole was backfilled with concrete. Liquid scintillation analyses similar to those described by Wadach and Hess [1985] revealed that the sand and concrete were not significant sources of ^{222}Rn.

Of the sixteen sampling tubes used, seven tubes were about 30 cm deep, six were about 60 cm deep, and three were roughly 90 cm deep. Sampling tubes were installed in "nests" made up of at least one tube 30 cm deep and one 60 cm deep, with another one at about 90 cm if soil depth allowed. No two tubes in a nest were more than 4 m apart horizontally; most were about 1-2 m apart. About 400 ml

of soil gas were flushed from each tube prior to sample collection.

Figure 2 shows that horizontal heterogeneity in [Rn] was generally small at the 30 cm depth. Differences among the 30 cm tubes were generally smaller than the differences between the 30 and 60 cm tubes (Fig. 3). The one exception to this was tube 11, which showed higher [Rn] than the other 30 cm tubes. The average [Rn] value at 30 cm (excluding tube 11) was about 7200 $\pm$ 2800 Bq/m^3.

Values from most of the 60-cm tubes clustered between 8000 and 2.5 x 10^4 Bq/m^3, with the nest 1 tube (tube 12) being significantly higher (Fig. 3). Although the high [Rn] at nest 1 could be due in part to higher ^{222}Rn production by soils at that location (we have no data on ^{222}Rn production rates), we suspect the elevated values were caused in part by higher soil moisture at nest 1 (Gordesky, 1987). Nest 1 is in a small topographic depression immediately upslope of a narrow dirt road, and the higher soil moisture here may play a role in lowering the ^{222}Rn loss to the atmosphere from these soils. The average [Rn] for the 60 cm tubes (excluding tube 12) was about (1.6 $\pm$ 0.5) x 10^4 Bq/m^3.

The average [Rn] at 90 cm is about (6.2 $\pm$ 0.8) x 10^4 Bq/m^3 (Fig. 4).

Vertical heterogeneity (variation of [Rn] with depth in the soil) may be shown by plotting profiles of [Rn] vs. depth for individual nests. Figure 5 shows profiles obtained from nest 2 on three different days. Samples were drawn from 36, 41, 61, and 92 cm below the ground surface (tubes 21a, 21b, 22, and 23b respectively).

While no analyses by another method are available for comparison, the [Rn]

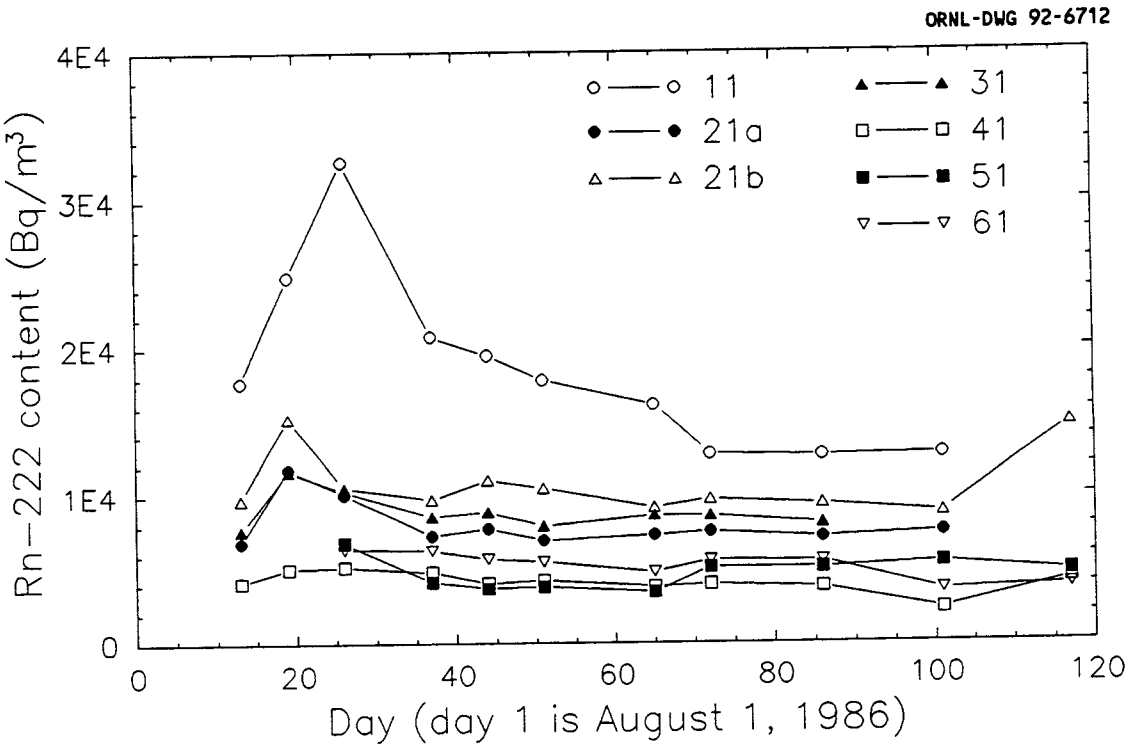

Figure 2. [Rn] (Bq/m^3) for soil-gas from seven sampling tubes about 30 cm deep, August-November, 1986. The numbering system adopted for sampling tubes was as follows: tube XYn was a tube in nest X whose approximate integer depth in feet was Y; n was a lower-case letter used when a nest contained more than one tube of approximately the same depth. For example, sampling tubes 21a and 21b were located in nest 2, and were each about one foot deep (36 and 41 cm, respectively).

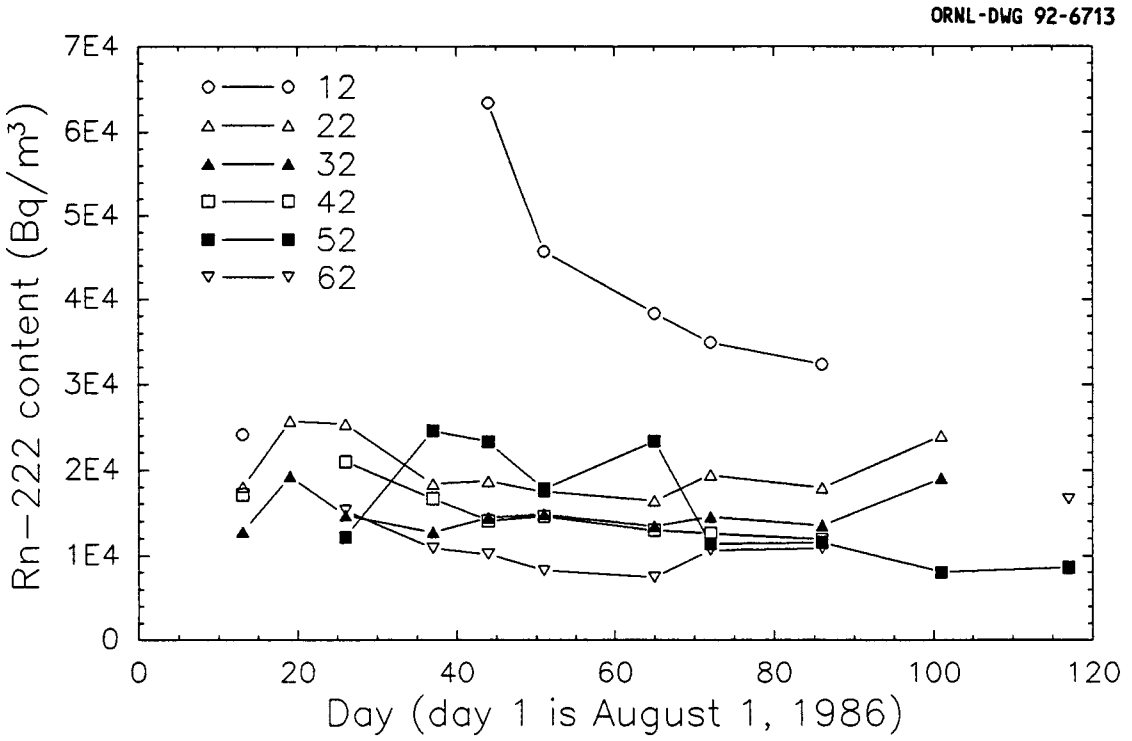

Figure 3. [Rn] (Bq/m^3) for soil-gas from six sampling tubes about 60 cm deep, August-November, 1986.

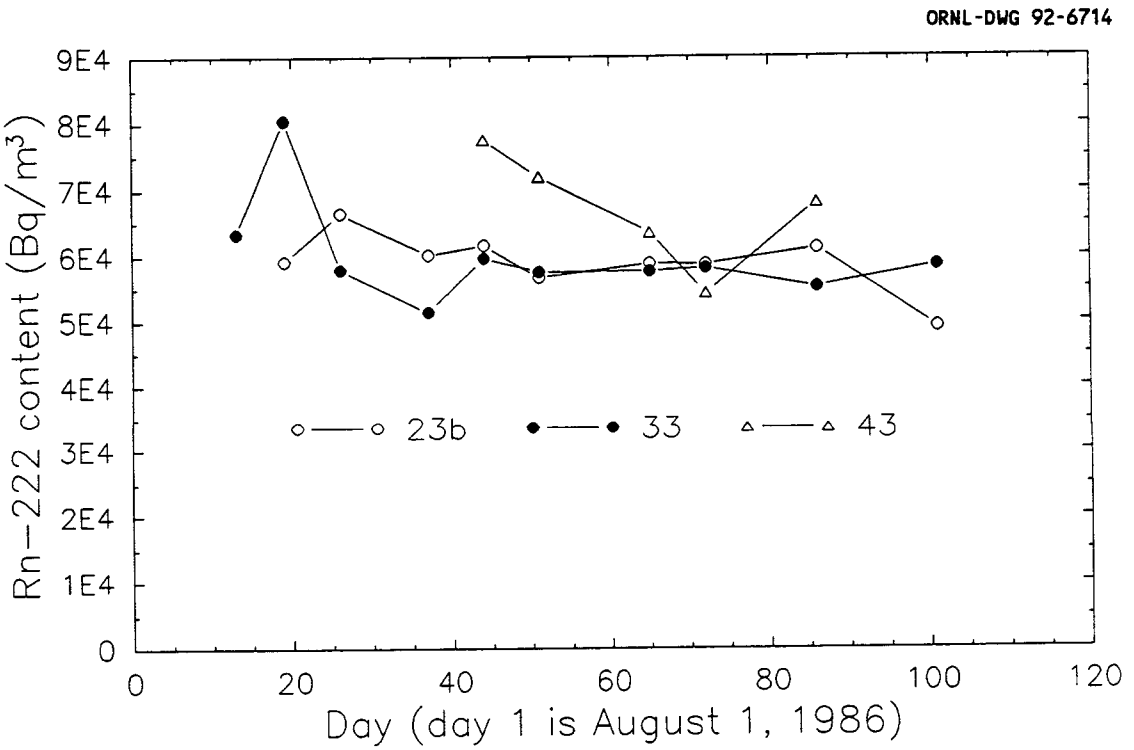

Figure 4. [Rn] (Bq/m^3) for soil-gas from three sampling tubes about 90 cm deep, August-November, 1986.

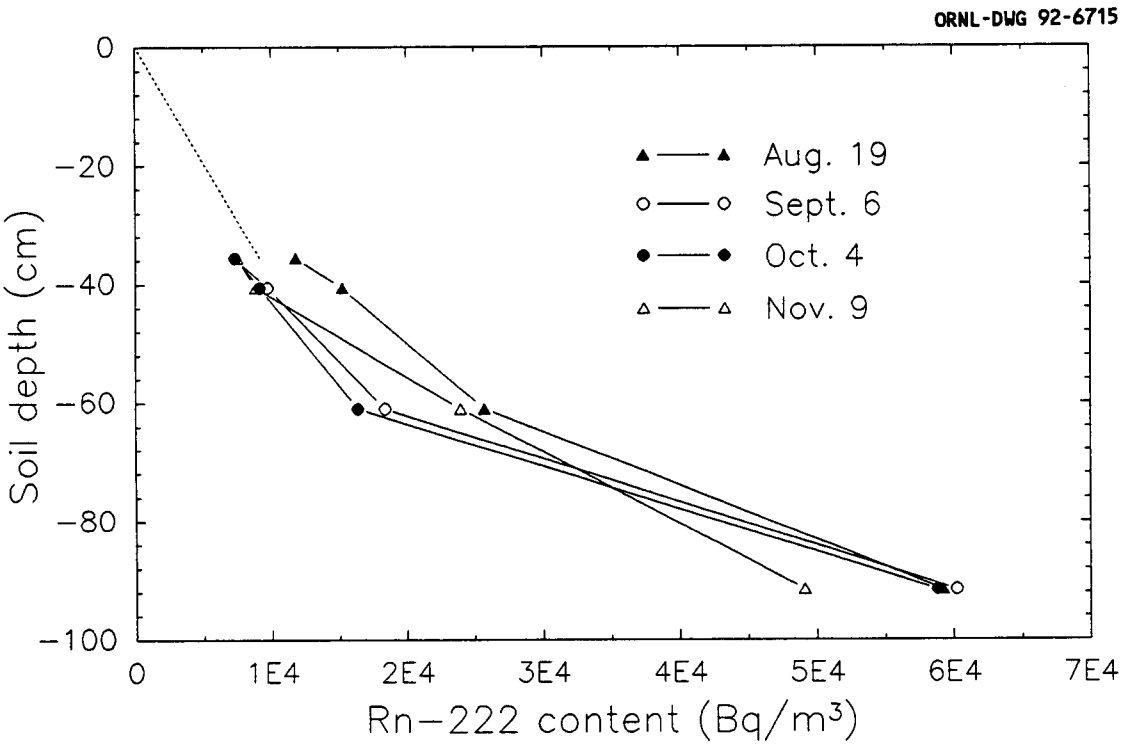

Figure 5. [Rn] as a function of depth for tube nest 2 on four different days. The four tubes sampled were 21a (36 cm), 21b (41 cm), 22 (61 cm), and 23b (91 cm).

values determined appear reasonable. The agreement between replicate samples (samples collected a few minutes apart at the same tube) was excellent, as Table 1 shows. Confidence in the reproducibility of the method is enhanced by the fact that [Rn] values from tubes located near one another varied in a coherent manner. For example, the ratio of the [Rn] values for tubes 21a and 21b was virtually constant for the study period (21a/21b = 0.77 $\pm$ 0.08, n=11).

Date	Tube	$[Rn]_1$	$[Rn]_2$	% difference
8/13/86	31	3550	3370	5.2
	32	5750	5780	0.5
	33	27800	29300	5.2
8/19/86	21a	12200	11400	6.8
	22	26200	25200	3.9
	23b	60800	57700	5.2
	33	78800	82300	4.3

Table 1. Replicate samples. The first column gives the date of sample collection, the second column the sampling tube. The third and fourth columns give the [Rn] values (Bq/m^3) for the two replicate samples; the second sample in each pair was collected about two minutes after the first. The fifth column gives the difference (as a percentage) between the [Rn] values of the two replicates.

The overall uncertainty in the [Rn] values was estimated by propagating the 2σ uncertainty in each parameter (cpm, BG, E, V_g, etc.) through the six calculation steps described in the previous section. Uncertainty propagation was based on Eqn. B4 of Kline [1985]. Figure 6 is a graph showing the percent error in the final [Rn] value as a function of [Rn]. Curves are shown for two different sample sizes, 15 ml (samples from 60 and 90 cm depths) and 30 ml (samples from 30 cm depth). This figure reflects the fact that differences in uncertainty among samples of the same volume were mainly due to differences in statistical counting error (i.e., the error in cpm). Uncertainty in the other terms (V_g, V_c, V_t, K, E) was exactly or very nearly the same for all samples of a given volume.

4. Improvements

Inverting the scintillation vials after capping, and counting them in this upside-down position, may eliminate all or most of the ^{222}Rn leakage. This is a potentially important improvement, since the decay+leakage correction may introduce a significant amount of uncertainty for those samples that are not counted soon (within a day or so) after sampling. However, if a vial containing only cocktail is turned upside-down, some of the cocktail will fill the neck of the vial, and photons from radioactive decays occurring in that portion of the cocktail may be blocked by the sides of the vial cap; thus, some loss of counting efficiency may occur.

One way of correcting this is to add 5-15 ml of distilled water to each vial,

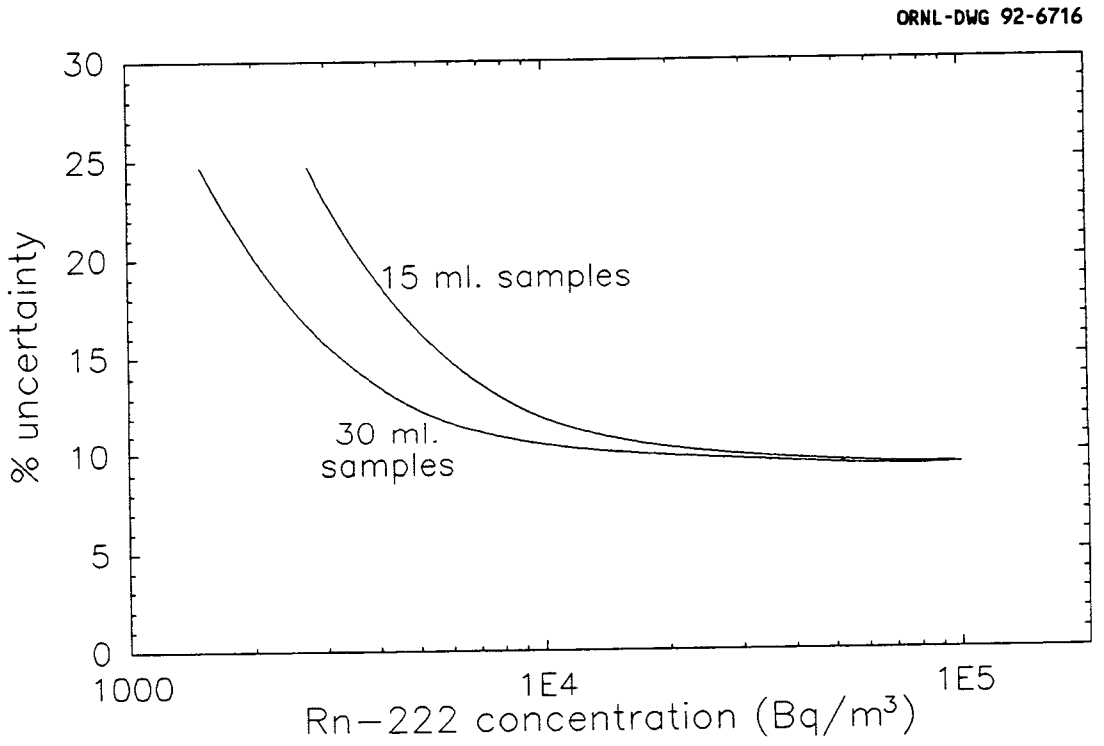

Figure 6. Estimated relative uncertainty (U) in [Rn]. For a given point ($[Rn]_i$, U_i) on one of the curves, there is a 95% probability that the true [Rn] value falls within $[Rn]_i \pm U_i$. At low [Rn] values, uncertainty is dominated by the statistical counting error in the cpm values; at high [Rn] values, uncertainty is controlled by the error in E, K, and the measured volumes.

before adding the sample cocktail. Since the cocktail will float on the water, the water serves to lift the cocktail upward toward the center of the vial, where radioactive decay events can be counted more effectively.

An additional benefit of the added water is the increased partitioning of ^{222}Rn into the cocktail, since adding 10 ml of distilled water to a vial reduces the headspace volume by 10 ml. The net effect is to force more of the ^{222}Rn in the vial into the cocktail, thus increasing counting efficiency, and reducing statistical counting error (for a constant counting time).

A third benefit of the inverted-vial technique is the potential for an alternative means of determining counting efficiency. The method described in the previous section would work as well for this modified technique. However, since the samples are counted with water in the vials, one could prepare a counting standard by substituting an aqueous Ra-226 solution for the distilled water which would be used with samples. Such a standard would have a known m_3 and hence a known m_4 value (see Eqn. 2), allowing calculation of E with Eqn. 1. This mode of standardization would be especially convenient to those investigators who are also measuring the ^{222}Rn content of water samples by liquid scintillation, since such standards could be used for those analyses as well (e.g., Wadach [1983]).

Another possible improvement would be the substitution of a low-vapor-pressure, "environmentally-benign" scintillation cocktail for the toluene-based cocktail. This would be helpful in decreasing the exposure of laboratory personnel to aromatic solvents. Experiments in our lab indicate that at least one of the

currently-available environmentally-benign cocktails has radon-partitioning characteristics very similar to those of xylene, at room temperature. Thus, the xylene:air partition constant for radon (e.g., Clever [1980]) could be used with this "benign" cocktail, with only a small error.

5. Summary

We have described a simple technique for measuring the ^{222}Rn content of soil gas by liquid scintillation. The technique gives results which are highly reproducible ($\pm$ about 5%), and which have 95% confidence limits of about 10-20%. There is a great deal of flexibility inherent in this method, as one may adjust any or all of four independent parameters (V_g, V_c, counting time, and, for those liquid scintillation counters that accept different sized vials, V_t) to meet a wide range of counting precision requirements. The method is well suited for large numbers of samples since preparation time is about 5-6 minutes per sample, far less than the time required by other published methods for measuring the ^{222}Rn content of soil gas. The accuracy and precision of the technique may be enhanced by adding several ml of water to the vials and counting them upside-down, to eliminate ^{222}Rn leakage.

Acknowledgements

We thank Steven Shefsky for providing use of his ^{222}Rn gas standard. Financial support for this work was provided by the USGS (Grant # 14-08-0001-G-

1725), the National Science Foundation (Grant # BCS-8906032), and by New England Power Service Co., American Electric Power Service Co., and Empire State Electric Energy Research Corp.

Bibliography

Benoit, G. and H.F. Hemond. 1987. A biogeochemical mass balance of Pb-210 and Po-210 in an oligotrophic lake with seasonally anoxic hypolimnion. Geochimica et Cosmochimica Acta 51:1445-1456.

Broecker, W.S., and T.H. Peng. 1971. The vertical distribution of radon in the Bomex area. Earth and Planetary Science Letters 11:99-108.

Broecker, W.S., J. Goddard, and J.L. Sarmiento. 1976. The distribution of Ra-226 in the Atlantic Ocean. Earth and Planetary Science Letters 32:220-235.

Clever, H.L. 1980. IUPAC Solubility Data Series: Volume 2: Krypton, Xenon, and Radon. Pergammon Press, New York, NY.

Eshleman, K.N., and H.F. Hemond. 1985. The role of organic acids in the acid-base status of surface waters at Bickford Watershed, Massachusetts. Water Resources Research 21(10):1503-1510.

Eshleman, K.N., and H.F. Hemond. 1988. Alkalinity and major ion budgets for a Massachusetts reservoir and watershed. Limnology and Oceanography 33(2):174-185.

Gordesky, B.T. 1987. Soil water pathways in a forested watershed in central Massachusetts. M.S. Thesis, Dept. of Civil Engineering, M.I.T.

Fleischer, R.L., and A. Mogro-Campero. 1978. Mapping of integrated radon emanation for detection of long-distance migration of gases within the Earth: Techniques and principles. J. Geophysical Research 83(B7):3539-3549.

Fukui, M. 1987. Soil water effects on concentration profiles and variations of ^{222}Rn in a vadose zone. Health Physics 53(2):181-186.

Hemond, H.F., and K.N. Eshleman. 1984. Nitrate processing and watershed acid sensitivity. Water Resources Research 20(11):1718-1724.

Horrocks, D.L. 1973. Measurement of radioactive noble gases by liquid scintillation techniques. In: Stanley, R.E, and A.A. Moghiessi (eds.), Noble Gases, USERDA CONF-730915.

Kline, S.J. 1985. The purposes of uncertainty analysis. J. of Fluids Engineering 107:153-160.

Kraner, H.W., G.L. Schroeder, and R.D. Evans. 1964. Measurements of the effects of atmospheric variables on radon-222 flux and soil-gas concentrations. In: The Natural Radiation Environment, Univ. of Chicago Press, Chicago, IL, p. 191-215.

Lucas, H.F. 1957. Improved low-level alpha-scintillation counter for radon. The Review of Scientific Instruments 28(9):680-683.

Prichard, H.M., and T.F. Gesell. 1977. Rapid measurements of ^{222}Rn concentrations in water with a commercial liquid scintillation counter. Health Physics 33:577-581.

Rose, A.W., J.W. Washington, and D.J. Greeman. 1988. Variability of radon with depth and season in a central Pennsylvania soil developed on limestone. Northeastern Environmental Science 7(1):35-39.

Schery, S.D., D.H. Gaeddert, and M.H. Wilkening. 1984. Factors affecting exhalation of radon from a gravelly sandy loam. Journal of Geophysical Research 89(D5):7299-7309.

Schulz, A. 1920. Uber die Loslichkeit der Radiumemanation in organischen Flussigkeiten. Zeitschr. fur physik. Chemie 95:257-279.

Wadach, J.B. 1983. Detection of radon concentration in air, water, and soil using Track Etch™ detectors and liquid scintillation. M.S. Thesis, Univ. of Maine at Orono.

Wadach, J.B., and C.T. Hess. 1985. Radon-222 concentration measurements in soil using liquid scintillation and Track Etch™. Health Physics 48(6):805-808.

APPENDIX 2

Walker Branch ^{222}Rn and Ca Data

^{222}Rn Concentrations (dpm/L) in Soil Groundwater (marked with *) and Vadose Zone Water from 12 Sampling Tubes

Date	1A	2	3A	3B	4A	4B*	5A	6A	6B	7A	8*	9
9/1/89						2980						
9/8	340						560					
10/4	193	150	570	120	700	2960	810					
10/11	110	100	280	120	570							
11/1	39	86	330	50	700							
11/9		87	850			3727						
11/14						4286						
11/15						4600						
11/16				1230*		3120						
11/17	23	44	190	22	810	3130						
11/21	39	110	360	33	820	3550						
11/28	350	320	1030	660	970	3990						
12/1						3460						
12/5						4410						
1/9/91						3390						
1/12						3540						
1/26						3540						

Date	1A	2	3A	3B	4A	4B*	5A	6A	6B	7A	8*	9
2/5						3170						
2/20						3340						
2/23						3520						
2/24	34	62	290	250	690	3610	280					
3/3	61	170	550	150	1130	4540	590	180	1280	200		
3/6	210	220	600	460	910	3710	470	44	1270	180		
3/13	430	800	1180	620	1020	4340	330	42		430		
3/17	420	540	1850*	2020*	920	3630	250	99	1250	430		
3/18						3450						
3/23						3660						
3/24	34	120	540	120	700		490	280	1260	290		
3/30						4920						
3/31	180	390	950	1000	820	5020	480	96	1460	330		
4/1	190	260	1060	830	890	4950	460	94	1444	400		
4/2	190	180	1010	590	880	5100	440	110	1350	420		
4/3	21	62	370	34	1030	5120	510	240	1270	180		
4/4	78	130	230	280	960	5260	530	160	1110	160		
4/5	84	110	310	320	810	5040	500	76	1120	160		

Date	1A	2	3A	3B	4A	4B*	5A	6A	6B	7A	8*	9
4/6	45	100	420	24	810	4900	480	300	1190	260		
4/7	16	39	120	25	1000	5000	410	210	800	82		
4/8	28	80	160	37	930	4900	360	260	680	110		
4/10	260	320	660	540	730	4820	430	31	1140	350		
4/11	38	77	460	96	810	5120	490	220	1160	250		
4/13	73	86	260	280	910	4920	410	89	950	140		
4/18	15	87	240	25	1100	4980	420	330	1050	210		
4/21	400	740	910	590	840	5130	340	56	1220	420		
4/24		690										
4/25	360	590	830	670	760	4550	310	61	1020	300		
4/28						4800					1680	
4/29	200	190	650	540	840	4890	380	170	1140	420	1760	670
4/30						4600					1640	
5/1	390	810	930	550	860	4720	330	70	1130	340	1570	230
5/1	340	620	410	860	840	4740					2000	240
5/2	390	790	910	810	890	4530	350	140	1050	370	2580	370
5/2	390	850	960	620	830	4450					2400	220
5/3	360	890	1010	560	780	4350					2490	290

Date	1A	2	3A	3B	4A	4B*	5A	6A	6B	7A	8*	9
5/4	350	1020	950	1180*	770	3900					2440	390
5/5	350	840	950	1640*	830	3460					2510	500
5/6	32	70	310	65	910	3310					1990	510
5/7	150	210	370	420	690	3390					1740	280
5/11	140	120	400	380	750	4220					1990	510
5/16	500	640	860	500	680	4490	300	49	990	350	1700	180
5/23	260	280	770	640	700	4870					1540	570
6/15	290	620	700	470	490	4180	370	75	710	580	1080	120
6/24	290	690	560	610	380	4060	400	140	860	640	760	200
6/29	300	600	630	540	310	3880	350	81	680	540	620	89
7/6	280	600	630	500	390	3770	400	83	640	590	590	89
7/15	290	720	810	780	560	3790	530	170	1010	650	1510	220
7/22	280	640	690	620	390		530	120	878	655		95
7/23						3720						
7/28	280	180	620	690	340	3590		110	840	660		120
8/3	270	600	570	670	300	3750	430	160	720	640		76
8/10	320	700	650	560	440	3100	540	150	960	660	1730	210
8/13	300	550	950	640	500		490	74	980	650		88

Date	1A	2	3A	3B	4A	4B*	5A	6A	6B	7A	8*	9
8/17	270	560	880	740	510	4040	490	110	1000	650	1160	110
8/24	260	550	790	720	530	3680	440	100	1000	660	1740	160
8/28	240	520	760	600	470	4080	470	85	920	630	820	92
9/1	290	560	740	720	390	3940	530	230	920	710		98
9/8	280	550	620	680	320	3610	390	190	750	640		78
9/15	210	130	390	280	370	3780	550	260	880	440		300
9/20	410	480	630	830	310	3840	590	120	880	720		80
9/27	260	170	260	290	270	3600	470	98	680	310		180
10/5	190	120	400	300	360	3700	560	160	820	360		220
10/11	44	50	310	140	620	3650	630	370	850	370		180
11/2	50	75	260	120	450	3610	520	220	740	150		150
11/16	150	82	340	270	560	3750	500	79	760	200		210

^{222}Rn Concentrations (dpm/L) in Streamwater at Six Sites in the Perennial Channel and Springwater at Four Springs

Date	WB317	WB300	WB242	WB170	WB100	WB60	S4	S3	S3A	S2
8/24/89								1100		
9/8				240	74					
10/4		1170	520	280	120					
10/11	310	580	340	250	110		810	1120	920	
11/1			390	250	120	68				
11/9		1710	900	460	250	150		1220	1180	
11/14	620	1240	550	380	150	79	2150	1150	1050	
11/15	890	1380	540	350	130	75	2360	1060	1230	
11/16	660	700	560	390	250	170	1220	1150	1480	
11/17		990	610	370	220	120	1380	1030	1030	
11/21	1420	1500	590	311	132	67	2120	1180	1110	
11/28	1740	1690	700	340	170	90	3210	1170	1380	
12/1	1550	1470	650	340	150	71	2940	1170	1110	
12/5	770	1130	420	280	110	67	2210	1230	1220	
1/9/90	1480	1470	880	490	250	170	2380	1330	1350	
1/12	1580	1620	720	360	160	81	3120	1230	1200	
1/26	1840	1660	840	390	190	96	2960	1190	1130	

Date	WB317	WB300	WB242	WB170	WB100	WB60	S4	S3	S3A	S2
2/5	850	870	660	450	280	170	1470	1300	1380	
2/20	1500	1380	810	430	230	130	2100	1160	1190	
2/23	2080	1860	940	460	220	130	2970	1450	1270	
3/3	1800	1840	780	380	190	94	3460	1300	1200	
3/7	1680	1820	730	330	150	83	3020	1060	1110	
3/12	1860	1880	740	340	180	93	3610	1150	1340	
3/17	480	580	510	440	340	240	1460	1480	1770	
3/18	660	790	590	450	290	170	1490	1290	1460	
3/23	1650	1620	650	320	170	80	3040	1190	1250	
3/30	1330	1340	520	330	110	76	2600	1220	1320	
4/1	1270	1230	450	280	115	79	2740	1180	1400	
4/2	1160	1090	460	260	120	55	2910	1120	1280	
4/3	1030	1010	380	250	110	69	2820	990	1240	
4/4	750	830	390	250	120	44	2310	1140	1080	
4/5	850	820	380	250	86	65	2100	1130	1260	
4/6	900	980	420	280	110	65	2790	1170	1210	
4/7	780	880	410	270	91	60	3610	1110	1230	
4/8	800	1020	410	270	110	54	3270	1050	1050	

Date	WB317	WB300	WB242	WB170	WB100	WB60	S4	S3	S3A	S2
4/10	1240	1470	470	290	130	59	3750	1210	1180	
4/11	1360	1460	500	270	120	62	4170	1110	1210	
4/12		1180	470	290	91	58		1100	1140	
4/13	790	1000	430	260	100	61	3120	1100	1170	
4/18	650	890	410	260	85	55	2480	1110	1140	
4/21	1010	1250	490	300	130	68	3370	1230	1250	
4/25	1410	1660	590	310	140	89	3750	1232	1370	
4/28	1020	1270	470	300	130	64	3340	1180	1320	
4/29	910	1270	450	250	120	46	2910	1230	1260	
4/30	790	1090	460	290	130	69	3230	1220	1210	
5/1	650	1030	450	290	130	66	2320	1210	1200	
5/1	990	1110	560	390	200	110	2730	1320	1300	
5/2	1560	1520	650	420	150	91	3380	1300	1510	
5/2	1680	1650	660	360	200	100	3600	1240	1280	
5/3	1770	1710	640	410	200	110	3430	1250	1400	
5/4	1030	1240	820	570	320	190	2930	1344	1830	
5/4		1110	770	460	250	190				
5/5	910	970	700	490	280	180	1650	1390	1680	

Date	WB317	WB300	WB242	WB170	WB100	WB60	S4	S3	S3A	S2
5/5		1090	710	490	250	210				
5/6	1270	1340	750	430	210	160	1900	1170	1270	
5/7	1540	1470	680	370	210	130	2340	1190	1140	
5/11	1730	1720	620	310	140	63	3550	1250	1330	
5/16	940	1150	410	300	140	79	2360	1190	1160	
5/23	530	970	430	260	92	59	2270	1200	1350	
6/15	230	670	350	230	100	63	1340	1110	1090	
6/24	210	560	330	240	88	55	1220	1170	1180	
6/29	190	500	310	260	100	46	1200	1140	1070	
7/6	130	450	320	270	110	59	1070	1080	1090	
7/15	1270	1300	470	230	110	62	2880	1300	1270	
7/20	220	540	330	220	85	50	1080	1150	1130	
7/23	120	490	310	250	81	48	1080	1090	1070	
7/28	90	450	300	250	89	49	1070	1150	1140	610
8/3	91	420	320	270	89	51	1060	1130	1080	570
8/10	1120	1100	510	300	130	86	1740	1190	1250	640
8/17	920	960	340	230	90	52	1820	1150	1090	630
8/24	1220	1360	500	280	120	80	2930	1220	1200	580

Date	WB317	WB300	WB242	WB170	WB100	WB60	S4	S3	S3A	S2
8/28	870	590	320	240	82	54	1130	1160	1080	500
9/1	270	470	290	230	81	57	980	1150	1050	640
9/8	110	440	310	250	98	61	1090	1090	1000	590
9/15	60	390	290	220	75	48	1070	1140	1140	640
9/20	86	340	290	220	69	57	1070	1120	1120	730
9/27	150	340	300	210	59	36	820	1140	1030	310
10/5	120	360	290	220	62	37	950	1080	1000	300
10/11	98	340	310	230	71	33	1000	1080	960	310
11/2	240	260	330	240	77	47	610	1110	1030	190
11/16	200	290	350	280	89	46	600	1080	1030	110

Ca Concentration (μM) in Streamwater at Six Sites in the Perennial Channel, Springwater at Four Springs, and Groundwater at Wells 4B and 8

Date	WB317	WB300	WB242	WB170	WB100	WB60	S4	S3	S3A	S2	4B	8
11/17/89		130	157	235	248	259						
3/7/90		223	271	433	449	446		700	664			
3/18		112	141	214	233	238		573	397			
4/13		355	403	565	566	571						
6/15	499	482	497	676	651	654	462	756	656		73	324
6/24	565	621	642	769	776	777	623	838	761		92	468
6/29	575	641	657	777	790	785	665	838	772		100	540
7/6	585	668	677	795	799	783	679	831	781		85	560
7/15	347	264	299	492	492	492	193	768	654		71	201
7/23	546	631	647	784	775	767	652	852	811		113	
7/28	559	663	686	796	788	780	692	853	808	598	104	
8/3	570	699	719	813	791	794	711	828	804	600	107	
8/10	277	252	290	406	426	425	173	770	566	596	89	223
8/17	390	360	422	634	638	639	362	829	767	581	84	289
8/24	303	249	300	478	510	502	119	833	662	580	88	211
8/28	447	474	510	679	690	679	484	788	678	556	82	336
9/1	467	529	554	729	689	696	521	783	751	541	73	

Date	WB317	WB300	WB242	WB170	WB100	WB60	S4	S3	S3A	S2	4B	8
9/8	474	581	596	753	704	719	616	788	763	551	89	
9/15	514	616	640	734	739	739	654	785	748	574	96	
9/20		663		789	791	808	732	803	832	620	104	
9/27	518	676	710	788	795	806	732	785	819	607	114	
10/5	519	665	687	787	802	796	729	784	818	619	129	
10/11	574	701	727	808	832	813	765	856	848	639	134	
11/2	581	746	766	846	853	813	762	858	847	650	155	
11/16	501	666	696	801	799	788	689	803	845	641	133	

APPENDIX 3

Longitudinal Dispersion Coefficients for the

Study Stream on Walker Branch

During the steady NaCl injections to the study stream on Walker Branch, the rise in specific conductance (γ) with time was often recorded; Fig. 3 in Chapter 3 shows an example of the type of data obtained. The amount of time required for specific conductance to rise from background (γ_b) to steady-state (γ_s) contains information about longitudinal dispersion in the study stream. Assuming a simple Gaussian model for longitudinal dispersion [e.g., Fischer et al., 1979, p.40], and keeping in mind that a steady injection can be viewed as the sum of many closely-spaced "slug" or instantaneous injections, longitudinal dispersion coefficients were calculated from the following:

$$D_L = \sigma^2/2t_{0.5}$$

$$\sigma = \tfrac{1}{2}V(t_{0.84} - t_{0.16})$$

where D_L = longitudinal dispersion coefficient (m^2/s)

σ = standard deviation of hypothetical γ vs. time curve for a slug injection of NaCl, determined from the equation above for our steady injections; multiplying by the stream velocity (V) converts σ from time (s) to length (m)

$t_{0.5}$ = time to half-height (i.e., time when $\gamma = \gamma_b + 0.5(\gamma_s-\gamma_b)$) from start of injection (t=0), in seconds

$t_{0.84}$ = time to 84% height from start of injection (s)

$t_{0.16}$ = time to 16% height from start of injection (s)

V = velocity of streamflow (m/s).

This simple method was used to calculate D_L values at WB300, WB242, WB170,

and WB100. When V was known for stream reaches on both sides of a measurement site, the values for the two reaches were averaged to obtain a V value for the site (e.g., V at WB170 was taken to be the average of the velocity over WB242-WB170 and WB170-WB100). When a velocity value from only one adjacent reach was available, that value was used for the site (e.g., the velocity over WB170-WB100 was used for WB100). Most of the calculated D_L values fall between 0.05 and 0.3 m^2/s, with higher values at higher flow (Table A3). Newbold et al. [1983] report an approximate D_L value of 0.1 m^2/s at a velocity of about 0.04 m/s for the same stream on Walker Branch, in good agreement with the values given here.

Date	WB300		WB242		WB170		WB100	
	V	D_L	V	D_L	V	D_L	V	D_L
9/8/89					0.042	0.014	0.042	0.058
8/28/90			0.037	0.052	0.042	0.079	0.045	0.061
4/13/90			0.055	0.11	0.055	0.11		
3/7/90			0.071	0.053	0.070	0.13	0.069	0.017
10/4/89	0.073	0.064	0.076	0.21	0.085	0.43	0.090	0.40
5/7/90	0.078	0.050	0.078	0.33				
11/17/89	0.10	0.12	0.10	0.48	0.098	0.70	0.099	0.44
3/18/90			0.15	0.25	.015	0.33		

Table A3. Streamwater velocity (V, m/s) and longitudinal dispersion coefficient (D_L, m^2/s) for four sites in the perennial stream on Walker Branch.

References

Fischer, H.B., E.J. List, R.C.Y. Koh, J. Imberger, and N.H. Brooks. 1979. Mixing

in Inland and Coastal Waters. Academic Press, New York.

Newbold, J.D., J.W. Elwood, R.V. O'Neill, and A.L. Sheldon. 1983. Phosphorus dynamics in a woodland stream ecosystem: A study of nutrient spiralling. Ecology 64(5): 1249-1265.

INTERNAL DISTRIBUTION

1. L. D. Bates
2. J. B. Cannon
3. R. B. Clapp
4. L. W. Cooper
5. J. H. Cushman
6. T. A. Fontaine
7. D. E. Fowler
8. C. W. Gehrs
9. S. G. Hildebrand
10. M. A. Huston
11. P. Kanciruk
12. G. K. Moore
13-17. P. J. Mulholland
18. D. E. Reichle
19. F. E. Sharples
20. D. S. Shriner
21. D. K. Solomon
22. S. H. Stow
23. L. E. Toran
24. R. S. Turner
25. R. I. Van Hook
26. Central Research Library
27-41. ESD Library
42-43. Laboratory Records Dept.
44. Laboratory Records, ORNL-RC
45. ORNL Patent Section
46. ORNL Y-12 Technical Library

EXTERNAL DISTRIBUTION

47. J. F. Franklin, Bloedel Professor of Ecosystem Analysis, College of Forest Resources, University of Washington, Anderson Hall (AR-10), Seattle, WA 98195
48-52. D. Genereux, Department of Civil Engineering, Bldg. 48, Room 419, Massachusetts Intitute of Technology, Cambridge, MA 02139
53. R. C. Harriss, Institute for the Study of Earth, Oceans, and Space, Science and Engineering Research Building, University of New Hamphire, Durham, NH 03824
54. H. Hemond, Department of Civil Engineering, Bldg. 48, Room 419, Massachusetts Intitute of Technology, Cambridge, MA 02139
55. G. M. Hornberger, Professor, Department of Environmental Sciences, University of Virginia, Charlottesville, VA 22903
56. G. Y. Jordy, Director, Office of Program Analysis, Office of Energy Research, ER-30, G-226, U.S. Department of Energy, Washington, DC 20545
57. C. R. Olsen, 10101 Grosvenor Place, Apt. 116, Rockville, MD 20852

58. R. H. Olsen, Professor, Microbiology abnd Immunology Department, University of Michigan, Medical Science Building II, #5605, 1301 East Catherine Street, Ann Arbor, MI 48109-0620
59. A. Patrinos, Acting Director, Environmental Sciences Division, Office of Health and Environmental Research, ER-74, U.S. Department of Energy, Washington, DC 20585
60. F. J. Wobber, Environmental Sciences Division, Office of Health and Environmental Research, ER-74, U.S. Department of Energy, Washington, DC 20585
61. Office of Assistant Manager for Energy Research and Development, U.S. Department of Energy Oak Ridge Field Office, P.O. Box 2001, Oak Ridge, TN 37831-8600
62-71. Office of Scientific and Technical Information, P.O. Box 62, Oak Ridge, TN 37831